Inaugural dissertation

for

obtaining the doctoral degree

of the

Combined Faculty of Mathematics, Engineering and Natural Sciences

of the

Ruprecht - Karls - University

Heidelberg

Presented by

M.Sc. Sarah Janice Hörner

born in: Heidelberg

Oral examination: 11/07/2023

Optimized differentiation of hiPSC-derived Schwann cells

and their integration into 2D and 3D neuromuscular tricultures

Referees: Prof. Dr. Christoph Schuster

Prof. Dr. Rüdiger Rudolf

Acknowledgements

First of all, heartfelt thanks to Rüdiger Rudolf, for enabling me to work on this project. Thank you for all advice and encouragement, productive discussions to shape ideas, and for providing me with a great degree of freedom and trust in pursuing my ideas. Likewise, many thanks to Mathias Hafner, for input in discussions, opening new opportunities – and the occasional aquarists' talk. My sincere thanks to Christoph Schuster, for taking up the role of examiner and committee chair, and accompanying this project through valuable Thesis Advisory Committee meetings. To Hilmar Bading for kindly agreeing to join my committee and assess this thesis, and to Thorsten Lau for instrumentally contributing to TAC meetings and help with setting up the project when I first started. Thank you all for your investment and insight. Also, I would like to thank Philipp Koch for the opportunity to stay as a guest in his lab, as well as all members at the Hector Institute for Translational Brain Research, for taking me in and supporting me so kindly in my first year.

Thank you, wonderful people of the Rudolf/Hafner lab, present and past members, for the outstanding work atmosphere we have. I enjoy working with every one of you. Thank you also to everyone else at the MZB institute, for making this a great place to work, do research, and have good times together. Special thanks to Tatjana, Patrick, Max, and Matteo, who have welcomed me so warmly when I started and for the fun times together in the lab. Elina – we have shared all the important things: highs, lows, music, food, and writing sessions… and it made everything better. "My" students, Daniele and Madleine, it was a pleasure both to teach you and to work with you, and you have both contributed markedly to this work – thank you. Nathalie, I am so happy you have joined me in this endeavor – looking forward to many more lunch meetings!

Furthermore, I want to thank two personal role models and mentors who both have helped me a lot during different times of my academic education: Katharina Janssen and Maïwen Caudron-Herger. Both of you have helped me to grow as a person and scientist. Thank you for your time and valuable advice.

An meine Familie, danke Euch allen für all Eure Unterstützung. Mama, danke für verständnisvolles Zuhören und Ermutigen. Liebe Oma – ich hab mei Schul' feddich! Sassi und Nana, ich bin unendlich glücklich, Euch als Schwestern zu haben, ich hoffe, ihr seid stolz auf mich. Papa, danke dass du mir so vieles beigebracht und ermöglicht hast, und mich immer unterstützt. Christopher, alles ist besser mit Dir an meiner Seite, danke für Geduld, Motivation, Ablenkung, und so vieles mehr…

Table of contents

Acknowledgements ..... **i**
Abbreviations ..... **v**
List of Figures ..... **vii**
List of Tables ..... **ix**
Abstract ..... **x**
Zusammenfassung ..... **xi**
1 Introduction **1**
1.1 The neuromuscular junction 1
1.1.1 Components and function of the neuromuscular junction 1
1.1.2 Neuromuscular junction development 4
1.2 Schwann cells 5
1.2.1 Schwann cell subtypes in vivo 5
1.2.2 Schwann cells at the neuromuscular junction 6
1.2.3 Development of Schwann cells 9
1.2.4 Sources and culture of Schwann cells in vitro 13
1.3 Human induced pluripotent stem cells 15
1.3.1 Introduction to hiPSC properties and applications 15
1.3.2 Differentiation of hiPSC into motoneurons 17
1.3.3 Differentiation of hiPSC into Schwann cells 18
1.4 Neuromuscular cell culture models 20
1.4.1 Purpose and categories of in vitro neuromuscular models 20
1.4.2 Short overview of the historic development of neuromuscular cocultures 22
1.4.3 hiPSC-derived cells in neuromuscular in vitro models 23
1.5 Aims of this thesis 24
2 Material and methods **25**
2.1 Cell culture 25
2.1.1 Cell lines 25
2.1.2 General cell culture methods, reagents, and materials 25
2.1.3 hiPSC culture and expansion 31
2.1.4 Differentiation of hiPSC-derived motoneurons 34
2.1.5 Differentiation of hiPSC-derived Schwann cells 37
2.1.6 C2C12 culture 39
2.1.7 2D cocultures 40
2.1.8 3D cultures in gelatin mesh 41
2.1.9 3D-bioprinting 42
2.2 Immunofluorescence stainings 47
2.2.1 Immunofluorescence stainings of 2D cultures 47

2.2.2 Immunofluorescence stainings of 3D cultures ... 48
2.2.3 Materials for immunofluorescence stainings ... 49
2.3 Microscopy ... 53
2.4 Data analysis ... 54
2.4.1 Differentiation marker protein expression of motoneurons and Schwann cells ... 54
2.4.2 Schwann cell maturation analysis ... 55
2.4.3 2D coculture analysis ... 56
2.4.4 Statistical analysis ... 57
2.4.5 Other software ... 57
3 Results ... 58
3.1 Differentiation of motoneurons and Schwann cells from hiPSC ... 58
3.1.1 Motoneurons can be derived from hiPSC robustly using a published protocol with small modifications ... 58
3.1.2 Motoneuron precursors can be expanded but exhibit variability with increasing passage number ... 63
3.1.3 Schwann cells can be differentiated from hiPSC using a published protocol, but with low efficiency and robustness ... 65
3.1.4 Tuning of BMP signaling activity to an intermediate level increases robustness and yield of Sox10+ cell differentiation ... 66
3.1.5 Maturation of hiPSC-derived Schwann cells is improved in serum-free media designed for neuromuscular cocultures ... 77
3.2 Neuromuscular cocultures ... 86
3.2.1 2D neuromuscular cocultures can be established in nine days from predifferentiated cells ... 86
3.2.2 hiPSC-derived motoneurons and Schwann cells align, colocalize with nAChR clusters on myotubes, and influence cluster formation ... 90
3.2.3 3D neuromuscular cocultures in hydrogels can achieve spatial organization ... 94
4 Discussion ... 100
4.1 Differentiation of motoneurons from hiPSC ... 101
4.2 Differentiation of Schwann cells from hiPSC ... 103
4.2.1 Evaluation of various parameters for protocol optimization ... 103
4.2.2 Tuning of BMP signaling activity critically improves protocol efficiency and robustness ... 105
4.2.3 Culture passaging and densities influence differentiation efficiency ... 109
4.2.4 BSA and β-ME are not necessary for differentiation and can be omitted ... 110
4.2.5 ROCKi or resveratrol treatments do not show beneficial effects on neural crest differentiation ... 112
4.2.6 Addition of serum is necessary during the Schwann cell precursor stage ... 114
4.2.7 Improvement of Schwann cell maturation in triM is mediated by retinoic and ascorbic acid ... 115
4.3 2D cocultures ... 118
4.3.1 Establishment of a neuromuscular coculture protocol including hiPSC-derived Schwann cells ... 118

4.3.2 Analysis of nAChR clusters in different coculture conditions 120
4.4 3D cocultures 122
4.5 Conclusion and Outlook 125
5 References 127
6 Appendix 157
6.1 Publications 157
6.2 Statement on contributions, copyright and self-plagiarism 157

Abbreviations

a. u.	arbitrary units
ACh	acetylcholine
AChE	acetylcholinesterase
AF	Alexa Fluor
ALS	amyotrophic lateral sclerosis
ATP	adenosine triphosphate
BChE	butyrylcholinesterase
BDNF	brain-derived neurotrophic factor
bFGF	basic fibroblast growth factor
BMP	bone morphogenetic protein
BSA	bovine serum albumin
CAD	computer-aided design
cAMP	cyclic adenosine monophosphate
ChAT	choline acetyltransferase
CNS	central nervous system
cont.	continued
DAPI	4′,6-diamidino-2-phenylindole
DHPR	dihydropyridine receptor
DMEM	Dulbecco's Modified Eagle Medium
DMH1	dorsomorphin homolog 1
DMSO	dimethyl sulfoxide
dok7	downstream of kinase 7
E8 medium	essential 8 medium
ECM	extracellular matrix
EDTA	ethylenediaminetetraacetic acid
EMT	epithelial-to-mesenchymal transition
FACS	fluorescence-activated cell sorting
FBS	fetal bovine serum
G	gauge
GAP-43	growth associated protein of 43 kDa
GDNF	glial cell line-derived neurotrophic factor
GSK-3β	glycogen synthase kinase 3β
(h)ESC	(human) embryonic stem cell
(h)iPSC	(human) (induced) pluripotent stem cell
(h)PSC	(human) pluripotent stem cell (ESC and iPSC)
IGF-1	insulin-like growth factor 1
kDa	kilodalton
LAP	lithium phenyl-2,4,6-trimethylbenzoylphosphinate
Lrp4	low-density lipoprotein receptor-related protein 4
mAChR	muscarinic acetylcholine receptor

Map2	microtubule-associated protein 2
MHC	myosin heavy chain
MMP-3	matrix metalloproteinase-3
MNBM	motoneuron basal medium
MNDM	motoneuron differentiation medium
MSC	mesenchymal stem cell
MuSK	muscle-specific kinase
nAChR	nicotinic acetylcholine receptor
NMJ	neuromuscular junction
Nrg1	neuregulin 1
Olig2	oligodendrocyte transcription factor 2
P0	myelin protein zero
$P2RY_1$	P2Y purinergic receptor 1
p75NTR	p75 neurotrophin receptor
PBS	phosphate-buffered saline
PDGF	platelet-derived growth factor
PMT	photomultiplier tube
PNS	peripheral nervous system
Prph	peripherin
px	pixel
rapsyn	receptor-associated protein of the synapse
ROCK(i)	Rho-associated coiled-coil containing kinases (inhibitor)
ROI	region of interest
RT	room temperature
RyR	ryanodine receptor
SCBM	Schwann cell basal medium
SCM	Schwann cell medium
SCPM	Schwann cell precursor medium
SD	standard deviation
SERCA	sarcoplasmic endoplasmic reticulum calcium ATPase
Shh	sonic hedgehog
SNARE	soluble N-ethylmaleimide-sensitive-factor attachment receptor
SOD1	superoxide dismutase 1
Sph	synaptophysin
TGF-β	transforming growth factor β
triM	triculture medium
Tubb3	class III β-tubulin
UV	ultraviolet
vAChT	vesicular acetylcholine transporter
VGCCs	voltage-gated calcium channels
VGSCs	voltage-gated sodium channels
β-ME	β-mercaptoethanol

List of Figures

Figure 1-1: Components of the NMJ. 1
Figure 1-2: Structure of the NMJ. 2
Figure 1-3: Development of Schwann cells. 11
Figure 1-4: Derivation and applications of hiPSC. 16
Figure 1-5: Differentiation of motoneurons from hiPSC. 18
Figure 1-6: Differentiation of Schwann cells from hiPSC. 19
Figure 1-7: Categories of NMJ cultures. 21
Figure 2-1: hiPSC culture. 32
Figure 2-2: Motoneuron differentiation protocol. 36
Figure 2-3: Schwann differentiation protocol. 39
Figure 2-4: Differentiation of C2C12 myoblasts to myotubes. 40
Figure 2-5: 3D-bioprinting designs. 43
Figure 3-1: Motoneurons can be differentiated from hiPSC via precursor cells. 59
Figure 3-2: Cell density at induction and plate coatings influence differentiation of motoneurons. 61
Figure 3-3: hiPSC-derived motoneurons express typical marker proteins. 63
Figure 3-4: Motoneuron precursors can be expanded and cryopreserved. 64
Figure 3-5: Initial Schwann cell differentiation experiments showed low differentiation yields. 65
Figure 3-6: Heterogeneity between hiPSC-derived Schwann cell batches. 67
Figure 3-7: Different treatments with BMP4 and DMH1 influence cell differentiation and survival. 69
Figure 3-8: BMP4/DMH1 treatment and cell density influence Sox10+ cell yield. 70
Figure 3-9: Addition of BMP4/DMH1 increases Sox10+ cells but addition of BSA/β-ME does not. 72
Figure 3-10: Addition of resveratrol or ROCK inhibitor has no beneficial effects on Sox10+ cell yield. 74
Figure 3-11: Addition of BMP4/DMH1 robustly improves yield of Sox10+ cells. 75
Figure 3-12: Modified Schwann cell differentiation protocol including tuning of BMP activity. 76
Figure 3-13: The protocol allows robust differentiation of Schwann cells from different hiPSC lines... 77
Figure 3-14: Distribution of marker stainings in Schwann cell cultures changes in different media. 79
Figure 3-15: Marker protein distribution and cell morphology depend on medium conditions. 80
Figure 3-16: Cell differentiation is increased in several medium conditions. 81
Figure 3-17: Cell elongation is increased in several medium conditions. 84
Figure 3-18: NT-3 is not beneficial for cell maturation, but serum supplementation is necessary 85
Figure 3-19: C2C12 differentiation can be done serum-free after an induction phase. 87
Figure 3-20: Myotubes, motoneurons, and Schwann cells can be cocultured in a compatible medium...88
Figure 3-21: Tricultures can be established from frozen precursor cells within nine days. 90
Figure 3-22: Motoneurons and Schwann cells colocalize with nAChR on myotubes in tricultures. 91
Figure 3-23: Segmentation of nAChR clusters from image data of different coculture conditions. 93
Figure 3-24: Cocultures influence morphological parameters of nAChR clusters. 94
Figure 3-25: Cell types can be combined in 3D using scaffolds or printed hydrogel chambers. 96
Figure 3-26: C2C12 can be bioprinted and cocultured with neurospheres in 3D. 98

Figure 4-1: Modifications of the Schwann cell differentiation protocol. 104
Figure 4-2: Principle of BMP signaling tuning to achieve an intermediate activity level. 108

List of Tables

Table 1: Culture media compositions 26
Table 2: Components for media preparations 29
Table 3: Small molecules for differentiation media 30
Table 4: Other cell culture reagents 30
Table 5: Materials for 3D-printing and bioprinting 46
Table 6: Antibodies, reagents, and materials for immunostainings. 49
Table 7: Host species and dilutions for antibodies and dyes used for stainings. 52
Table 8: Different BMP activation treatment conditions in Figure 3-7. 68
Table 9: Overview of media compositions for Schwann cell maturation experiments. 78
Table 10: Percentages of cells positive for marker proteins 82
Table 11: Mean signal intensity values for marker proteins 82
Table 12: Contributions from other persons 157

Abstract

Neuromuscular junctions (NMJs) are synapses in the peripheral nervous system where signals are transmitted from spinal motoneurons to skeletal muscle fibers, enabling locomotion. Numerous *in vitro* models for NMJs have been developed to investigate their formation, function, and disease mechanisms. In addition to motoneurons and muscle fibers, the NMJ also consists of other cell types, in particular, glial cells of Schwann cell origin. Although these are critical for all of the aforementioned processes, Schwann cells have not yet been integrated into neuromuscular *in vitro* models in a targeted manner, primarily due to limitations regarding the efficient generation of human Schwann cells *in vitro*. To address this, an optimized protocol for robust and efficient generation of human induced pluripotent stem cell (hiPSC)-derived Schwann cells is presented in this thesis. To achieve this, a number of different modifications to a published differentiation protocol were tested. The activation of BMP signaling to a precisely tuned intermediate level proved to be important for the efficient generation of neural crest cells, which could be differentiated into Schwann cells subsequently. In addition, improved cell maturation was achieved using a defined culture medium, demonstrated by expression of typical Schwann cell marker proteins. This medium also promoted maturation of both hiPSC-derived motoneurons and murine cell line-derived myotubes, and was therefore compatible with neuromuscular tricultures. Using pre-differentiated precursor cells, a protocol was established to combine all three cell types and culture them for several days. In such tricultures, Schwann cells aligned with motoneurons, and both were found to colocalize with nAChR clusters on myotubes and to influence their formation. Additionally, different approaches for multicellular and spatially organized neuromuscular cultures in 3D hydrogels were explored. Overall, this thesis provides the tools for selective integration of hiPSC-derived Schwann cells into neuromuscular cell culture models, which paves the way for future *in vitro* studies of NMJ formation and cell-type specific disease mechanisms.

Zusammenfassung

Die motorische Innervierung der Skelettmuskulatur geschieht durch neuromuskuläre Synapsen, auch motorische Endplatten genannt. An diesen werden Bewegungsreize von den unteren Motoneuronen an die Muskelfasern übertragen. Um die Entwicklung und Funktion von neuromuskulären Synapsen sowie krankheitsbedingte Mechanismen zu untersuchen, wurden bereits zahlreiche *in vitro* Modelle entwickelt. Solche Modelle sind bislang aus Motoneuron-Muskelzell-Kokulturen aufgebaut, während neuromuskuläre Synapsen *in vivo* aus weiteren Zelltypen bestehen, insbesondere spezialisierten Gliazellen aus der Familie der Schwann-Zellen. Obwohl diese an allen der oben genannten Prozesse maßgeblich beteiligt sind, wurden Schwann-Zellen bislang nicht gezielt in neuromuskuläre *in vitro* Modelle integriert. Ein Hauptgrund hierfür liegt in Limitierungen bei der effizienten Generierung humaner Schwann-Zellen *in vitro*. Aus diesem Grund wurde in der vorliegenden Arbeit ein optimiertes Protokoll zum Zweck der robusten und effizienten Differenzierung von Schwann-Zellen aus humanen induzierten pluripotenten Stammzellen (hiPSC) etabliert. Die wesentlichen Verbesserungen beruhen auf präziser Aktivierung von BMP-Signaling durch ein Agonist-Antagonist-System, sowie einem definierten Kulturmedium zur Ausreifung, welches auch mit neuromuskulären Kokulturen kompatibel ist. Die so hergestellten Schwann-Zellen wurden charakterisiert und in ein Protokoll zur gemeinsamen Kultivierung mit hiPSC-Motoneuronen und murinen Muskelzellen integriert. In solchen Kokulturen wurde Kolokalisierung sowohl von Motoneuronen als auch Schwann-Zellen mit Acetylcholinrezeptor-Clustern auf Muskelzellen nachgewiesen, und beide beeinflussten die Ausbildung der Cluster. Darüber hinaus wurden verschiedene Ansätze für multizelluläre und räumlich organisierte neuromuskuläre Kulturen in dreidimensionalen Hydrogelen untersucht. In Summe stellt die vorliegende Arbeit grundlegende Methoden zur selektiven Integrierung von hiPSC-abgeleiteten Schwann-Zellen in neuromuskuläre Zellkulturmodelle bereit, was zukünftige Studien zur Ausbildung von neuromuskulären Synapsen *in vitro* sowie zu zelltyp-spezifischen Krankheitsmechanismen ermöglicht.

1 INTRODUCTION

1.1 The neuromuscular junction

1.1.1 Components and function of the neuromuscular junction

Voluntary body movements are controlled through the transmission of signals from the nervous to the muscular system. This happens at cholinergic synapses of the peripheral nervous system (PNS), termed neuromuscular junctions (NMJs), or motor endplates (Figure 1-1A). Input signals to NMJs are first generated by upper motoneurons, located in the cerebral motor cortex. Those project onto lower (or spinal) α-motoneurons located in the ventral horn of the spinal cord, which innervate skeletal muscle tissue (Figure 1-1A). In adult mammals, each individual muscle fiber – the multinucleated contractile cells which make up skeletal muscle – is innervated by one NMJ. At the same time, one motoneuron can innervate multiple muscle fibers, the sum of which are called a motor unit (Figure 1-1B). The NMJ is formed by the presynaptic motoneuron, rich in acetylcholine (ACh)-containing vesicles, and the postsynaptic muscle fiber membrane, which harbors densely packed nicotinic acetylcholine receptors (nAChR). Further, muscle fibers secrete the basal lamina, a layer of extracellular matrix (ECM), which also extends through the synaptic cleft at the NMJ where it serves as scaffold and anchoring structure for extracellular proteins, but also as diffusion barrier. Classically, NMJs have been denominated as tripartite synapses, i.e., including a third cell type besides neuron and muscle cells: these are called terminal Schwann cells, a specific type of glial cell (Figure 1-2). Those are distinct from the myelinating Schwann cells along the motoneuron axon, and their characteristics and functions are further described in section 1.2.2. In addition to the bona

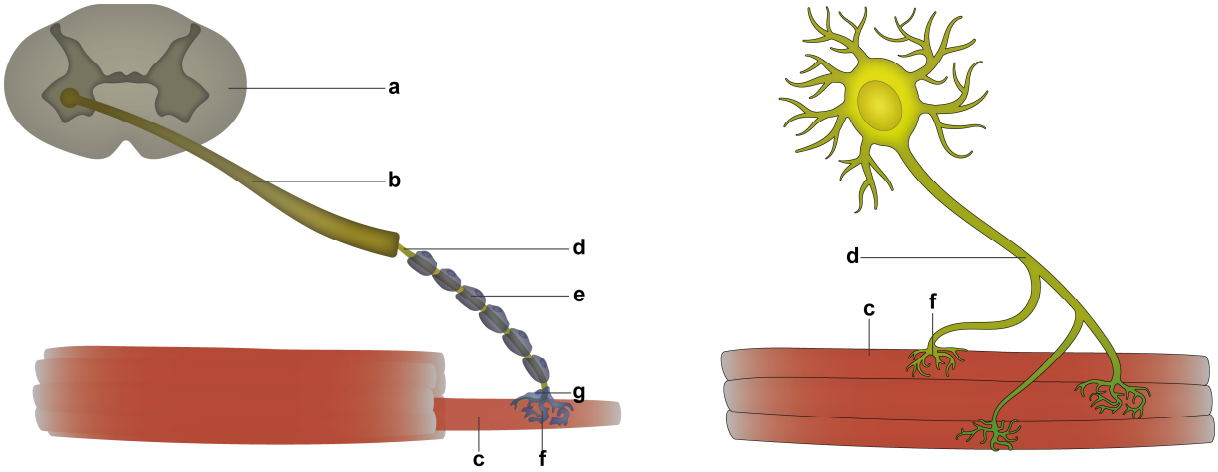


Figure 1-1: Components of the NMJ. Originating from the spinal cord (a), nerves (b) extend throughout the body to reach their targets of innervation, like skeletal muscle fibers (c). Axons of spinal motoneurons (d) are wrapped by myelinating Schwann cells (e) and contact muscle fibers though neuromuscular junctions (NMJs) (f), which are capped by terminal Schwann cells (g). Right: One motoneuron innervates several muscle fibers, which is called a motor unit.

fide tripartite composition, NMJs were recently found to regularly feature usually at least two more cell types, i.e., kranocytes and sympathetic neurons. The fibroblast-like kranocyte is additionally capping the NMJ structure above the Schwann cells (Figure 1-2) [Court et al., 2008]. They might communicate with terminal Schwann cells and seem to play a role in regeneration upon nerve injury, as they rapidly start proliferating and spreading upon denervation [Weis et al., 1991; Court et al., 2008]. Sympathetic neurons have been known to be present throughout muscle tissue, as they regulate vasoconstriction and metabolic activity. With respect to NMJs, some studies in the late 19th and early 20th century observed what seemed to be a co-innervation of NMJs with sympathetic fibers [Bremer, 1882; Boeke, 1909, 1913; Agduhr, 1920]. Although advancements in microscopy confirmed the presence of tyrosine hydroxylase, a marker for sympathetic neurons, at NMJs [Chan-Palay et al., 1982], there was no consensus regarding the question if a sympathetic innervation existed at the NMJ, and in that case, whether it had any functional relevance to NMJs. More recent studies clearly demonstrated sympathetic innervation directly at NMJs (Figure 1-2) [Rudolf et al., 2013; Khan et al., 2016; Straka et al., 2018] and confirmed functional impact on NMJ integrity and signal transmission, acting both pre- and postsynaptically [Khan et al., 2016; Rodrigues et al., 2018; Snyder-Warwick et al., 2018; Rodrigues et al., 2019].

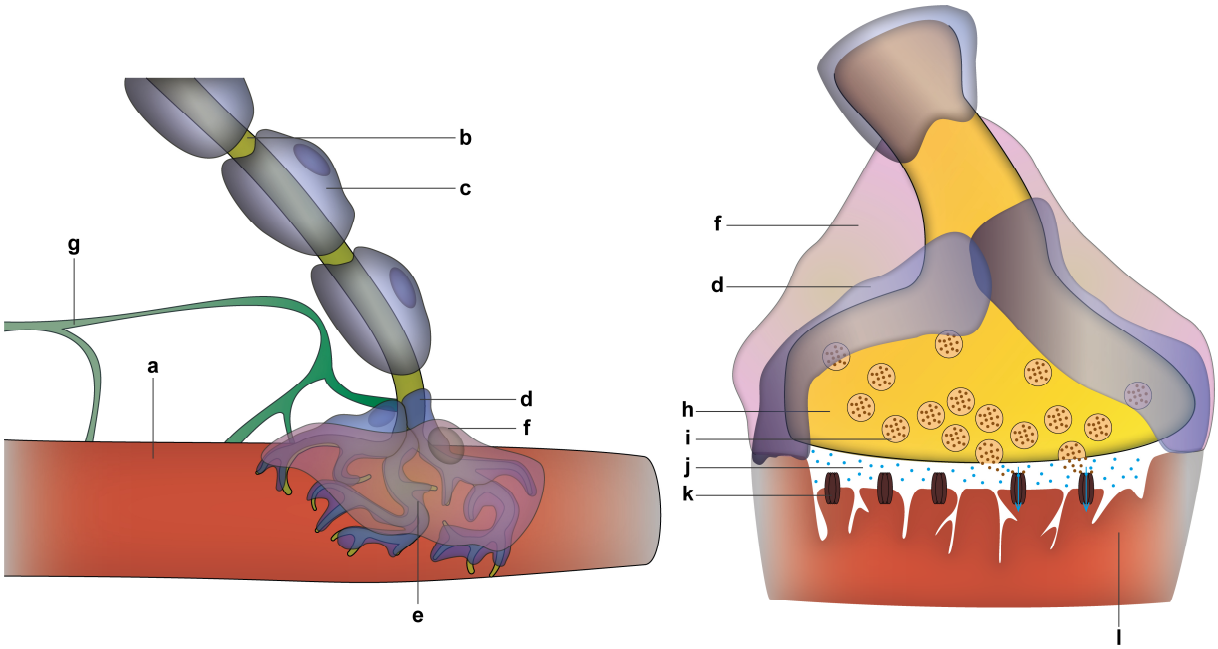


Figure 1-2: Structure of the NMJ. Muscle fibers (a) are innervated by motor axons (b) wrapped by myelinating Schwann cells (c). Non-myelinating terminal Schwann cells (d) cap the NMJ (e), and the whole structure is additionally surrounded by kranocytes (f). Furthermore, muscle fibers are also innervated by sympathetic neurons (g). Upon transmission, the presynaptic nerve terminal (h) releases the neurotransmitter ACh (brown) from synaptic vesicles (i). ACh diffuses through the synaptic cleft (j) and activates nAChR (k) located at the sarcolemma (l), triggering Na^+ (blue) influx and the downstream cascade to induce muscle contraction.

As described, the purpose of NMJs is the signal transmission from motoneurons to muscle fibers to initiate muscle contraction, as briefly explained in the following. The presynaptic nerve terminals are filled with synaptic vesicles loaded with the neurotransmitter ACh (Figure 1-2), which is synthesized in the neuronal cytoplasm by the enzyme choline acetyltransferase (ChAT) and subsequently transferred into vesicles through vesicular acetylcholine transporter (vAChT). Upon arrival of an action potential at the motor nerve terminal, voltage-gated calcium channels (VGCCs) open and allow the influx of Ca^{2+} ions into the presynaptic terminal. This triggers the fusion of synaptic vesicles with the presynaptic membrane mediated by specific SNARE complexes and causes the release of ACh into the synaptic cleft. ACh diffuses across the 50 – 60 nm wide synaptic cleft [Fahim and Robbins, 1982; Kriebel et al., 1986], and binds to the postsynaptic nAChR (Figure 1-2). In the postsynaptic region, these are highly concentrated, with an estimated density of about 10,000 – 20,000 receptors per µm² [Fertuck and Salpeter, 1976; Fambrough, 1979]. Upon binding of two ACh molecules per receptor, nAChR open to allow influx of Na^{+} ions (Figure 1-2), which locally depolarizes the membrane. In the meantime, ACh is hydrolyzed by acetylcholine esterase (AChE) anchored in the synaptic cleft, to clear the neurotransmitter concentration and prevent repetitive activation. While the spontaneous fusion of a single synaptic vesicle, releasing the amount of one vesicle-load of ACh molecules into the synaptic cleft, generates a small postsynaptic potential, called a miniature endplate potential, motoneuronal action potentials lead to the release of tens to hundreds of synaptic vesicles [Wood and Slater, 2001; Hughes et al., 2006] and the induction of bona fide endplate potentials. These reach the threshold for opening of voltage-gated ion channels (mainly VGSCs) in the muscle fiber membrane, and a muscle action potential is triggered which propagates along the muscle fiber via the T-tubule system. This in turn induces the release of internally stored Ca^{2+} ions from the sarcoplasmic reticulum through subsequent activation of voltage-dependent DHPR channels which are located at the T-tubule membrane and physically coupled to RyR1 channels at the sarcoplasmic reticulum, increasing sarcoplasmic Ca^{2+} concentration, which is needed for the binding of actin and myosin in the sarcomeres and therefore, to activate the contractile machinery. Hereby, the force of muscle contraction is steered by the frequency of motoneuronal action potentials, as the neurotransmitter release is happening faster than the postsynaptic excitation-contraction coupling (meaning the translation of the electrical signal into the mechanical contraction response), allowing the accumulation of endplate potentials which lead to muscle action potentials and therefore a larger increase in Ca^{2+} concentration [Jöbsis and O'Connor, 1966; Ridgway and Ashley, 1967]. The increased concentration of Ca^{2+} directly increases the number of cross-bridge cycles between actin and myosin, resulting in stronger muscle fiber shortening and therefore higher contractile force. Muscle contraction continues until cross-bridges are released by removal of Ca^{2+} from the sarcoplasm, which mainly happens by active transport

back into the sarcoplasmic reticulum via a specific ATPase pump (SERCA) [Ebashi et al., 1969; Melzer et al., 1995; Martyn et al., 2009; Frontera and Ochala, 2015].

1.1.2 Neuromuscular junction development

Developmental processes for differentiation of each of the three core cell constituents of the NMJ – muscle fibers, motor axons, and terminal Schwann cells – are spatially and timely organized in coalescence with differentiation of the synapse itself [Sanes and Lichtman, 1999]. First, in a process called pre-patterning, aneural clusters of nAChR are formed on muscle fibers even before nerve terminals arrive [Lin et al., 2001]. Then, motor axons in the developing peripheral nerves grow towards the muscle tissue and establish synaptic contacts with those prepatterned clusters. Schwann cells migrate together with these nerve endings, and they are the first to contact aneural nAChR clusters [Barik et al., 2016]. Although synaptic contacts are also established in the absence of Schwann cells, the latter are crucial for the following synapse stabilization and maturation. The current knowledge on the specific role of terminal Schwann cells in NMJ development will be briefly discussed in section 1.2.2. Once nerve and muscle are in contact, both produce differentiation signals for each other and specifically, for synaptic structures. The key motoneuronal signal is the nerve-specific isoform of the proteoglycan agrin [Gautam et al., 1996], first identified in *Torpedo californica* [Nitkin et al., 1987]. On the postsynaptic membrane, agrin binds to Lrp4, which forms a complex with the receptor tyrosine kinase MuSK and initiates MuSK transphosphorylation, which additionally requires dok7 [Glass et al., 1996; Kim et al., 2008; Zhang et al., 2008; Inoue et al., 2009]. Downstream of MuSK activation, several effects are achieved, most of them not yet well understood [Li et al., 2018]. Importantly, activation of the Lrp4-MuSK complex by agrin regulates synapse-specific gene expression [Lacazette et al., 2003] and clustering of nAChR at the membrane. The latter is mediated by the 43 kDa protein, rapsyn, which anchors nAChR to the cortical cytoskeleton and thereby stabilizes postsynaptic clusters [Tintignac et al., 2015; Xing et al., 2020]. Release of ACh from neurons seems to destabilize nAChR clusters, and it was suggested that aneural clusters, which have not been stabilized through local agrin interaction, are dispersed by this mechanism [Lin et al., 2005; Misgeld et al., 2005; Wu et al., 2010]. Conversely, there are also postsynaptic signals acting on presynaptic differentiation, for example, ECM molecules like laminins and collagens secreted by muscle cells. Molecules which have been shown to play a role in nerve and/or synapse development include laminin β2 [Nishimune et al., 2004; Rogers and Nishimune, 2017], laminin α4 [Patton et al., 2001], and collagen XIII [Härönen et al., 2017]. Notably, the process of synapse development is still going on perinatally. First, synapses show multiple innervation by up to 10 nerve terminals until the process of synapse elimination is taking place (see section 1.2.2) to establish NMJs innervated

by a single axon each. Second, at birth, most nAChR are still of the embryonic subunit composition ($\alpha_2\beta\delta\gamma$) and are getting replaced by adult-type nAChR ($\alpha_2\beta\delta\varepsilon$). In rodents, both of these maturation processes are completed two weeks after birth [Mishina et al., 1986; Tintignac et al., 2015].

1.2 Schwann cells

1.2.1 Schwann cell subtypes in vivo

Schwann cells are glial cells of the PNS, which are mainly known for their myelinating function. Historically, glial cells throughout the nervous system have not been recognized as integral, signaling-active participants in nervous system function. Rather, they were regarded as a scaffolding substance providing structure and support for neurons, reflected in their name: "*γλία*", the Greek word for "glue". When Rudolf Virchow, father of cellular pathology, coined the term "neuroglia" in 1856, he had been looking for a "connective tissue of the brain" underneath the ependyma of ventricles [Virchow, 1858; Chvátal and Verkhratsky, 2018]. However, the term "glia" was then adopted for the entirety of non-neuronal (i.e., not electrically excitable) cells of the CNS and PNS – including Schwann cells. Those were first described as cells associated to both unmyelinated [Remak, 1838] and myelinated [Schwann, 1839] nerve fibers by Robert Remak and Theodor Schwann [Boullerne, 2016], who are both also seen as the founders of animal cell theory together with Virchow. Today, glial cells are considered to be more diverse in function than neurons, and it is evident that they play crucial roles besides neuronal support. For example, certain glia can sense and modulate synaptic transmission: the concept of the tripartite synapse includes astrocytes in the CNS and terminal Schwann cells in the PNS as integral synapse-associated cells [Araque et al., 1999]. In general, Schwann cells are the main glia of the PNS and they exert a variety of functions in different localizations [Bosch-Queralt et al., 2023], which is covered through specialization of several Schwann cell subtypes. The two major, best-known subtypes are the myelinating Schwann cells and the non-myelinating Remak Schwann cells.

Myelinating Schwann cells ensheath peripheral axons with myelin, i.e., membrane lamellae rich in lipids. These enable saltatory conduction of action potentials along the axon by reducing the transverse capacitance of the axonal membrane, thus, increasing the velocity of action potential conduction up to a hundredfold [Purves et al., 2001; Varga and Mravec, 2015]. In contrast to oligodendrocytes in the CNS, each myelinating Schwann cell is exclusively associated with a segment of one individual axon. The length between two gaps in the myelin sheath, known as nodes of Ranvier, can be around 1.5 mm, correlating with axon thickness [Friede et al., 1981]. Remak Schwann cells do not produce myelin, but encase several

unmyelinated, smaller-diameter axons separated in troughs along their surface, called a Remak bundle [Harty and Monk, 2017]. However, non-myelinating Schwann cells are more than mere scaffolding organizers of nerve structure. Instead, they critically contribute to nerve integrity and function, for example by metabolic support of axons, or regulating nociception [Véga et al., 2003; Faroni et al., 2014; Harty and Monk, 2017; Rinwa et al., 2021]. Remak Schwann cells are also usually the first to respond upon denervation [Griffin and Thompson, 2008].

Non-myelinating Remak Schwann cells in peripheral nerves clearly differ from myelinating Schwann cells in expression profiles, morphology, and function; but both share a high plasticity even in the mature stage, and their phenotype seems to be determined by extrinsic, axon-associated signals. Particularly, both subtypes have the ability to de-differentiate upon nerve injury and assume a third subtype, termed repair Schwann cells, which is distinct from all other subtypes [Gomez-Sanchez et al., 2017; Milichko and Dyachuk, 2020]. Such repair Schwann cells are crucial to resolve nerve damage and guide the regeneration response, and they re-differentiate into the other mature subtypes after the repair process is concluded [Jessen and Mirsky, 2016; Boerboom et al., 2017]. This remarkable plasticity of adult Schwann cells is further emphasized by the finding that Schwann cells which had been non-myelinating before can assume a mature myelinating subtype upon re-differentiation, and vice versa [Aguayo et al., 1976; Stierli et al., 2018]. Amazingly, repair Schwann cells were found to even differentiate into non-glial cells occasionally, including melanocytes [Adameyko et al., 2009], enteric neurons [El-Nachef and Bronner, 2020], and dental pulp mesenchymal stem cells [Kaukua et al., 2014]. Such plasticity found in the Schwann cell lineage is connected to its remarkable multipotency in development, which is further discussed in section 1.2.3. Likely, besides myelinating, Remak, repair, and terminal Schwann cells, more specialized Schwann cell subtypes exist which have local functions, that have not been fully characterized yet. Overall, the diversity of peripheral glia is just starting to be appreciated and elucidated [Reed et al., 2021; Tasdemir-Yilmaz et al., 2021; Yim et al., 2022], and many of those probably develop through the immature precursor stages of Schwann cells as well [Kastriti and Adameyko, 2017], for example enteric glia [Uesaka et al., 2021] or the glia cells of cutaneous sensory corpuscles [Etxaniz et al., 2014; Suazo et al., 2022].

1.2.2 Schwann cells at the neuromuscular junction

As introduced in the previous section, the specific subtype of Schwann cells found at NMJs are called terminal Schwann cells, also known as perisynaptic Schwann cells or teloglia. At first described as “arborization nuclei” on the terminal nerve branches by Louis-Antoine

Ranvier [Ranvier, 1878], they were later recognized to be separate cells of Schwann cell origin [Couteaux, 1947, 1955] – initially, not without dispute [Tiegs, 1953]. These cells are crucial for synaptic maturation during development, NMJ stability and maintenance, modulation of synaptic transmission, as well as remodeling and regeneration of NMJs [Reddy et al., 2003; Feng and Ko, 2008; Sugiura and Lin, 2011; Darabid et al., 2014; Ko and Robitaille, 2015; Barik et al., 2016; Alvarez-Suarez et al., 2020]. At the mature NMJ, terminal Schwann cells precisely trace the NMJ structure with their cellular processes to enclose it entirely [Griffin and Thompson, 2008]. They are distinct from myelinating as well as Remak Schwann cells in both, morphology and function [Ko and Robitaille, 2015; Barik et al., 2016]. At the molecular level, terminal Schwann cells express some proteins which are usually associated with myelinating and not expressed in Remak Schwann cells, including myelin protein zero (P0) and myelin-associated glycoprotein (MAG) [Georgiou and Charlton, 1999], but they do not form myelin, and a few subtype-specific markers have been identified also specifically for terminal Schwann cells at mouse [Young et al., 2005; Castro et al., 2020; Jablonka-Shariff et al., 2020] and human [Alhindi et al., 2021b] NMJs.

Terminal Schwann cells are active and principal players at the NMJ which can both sense and modulate synaptic transmission through cholinergic and purinergic signaling. ACh, which is released from the motoneuron presynapse, is not only activating the ionotropic nAChR in the sarcolemma, but also metabotropic muscarinic AChR (mAChR) expressed by terminal Schwann cells [Georgiou et al., 1999; Piovesana et al., 2020]. Furthermore, ATP is co-released with ACh from synaptic vesicles [Smith, 1991] and activates type 2 purinergic receptors (mainly $P2RY_1$) on terminal Schwann cells. Both of these interactions elicit an internal Ca^{2+} response in Schwann cells, which can trigger a direct response through release of gliotransmitters, and influence gene expression [Jahromi et al., 1992; Reist and Smith, 1992; Georgiou et al., 1994; Robitaille, 1995; Rochon et al., 2001; Darabid et al., 2013; Heredia et al., 2018]. Signals which are released by terminal Schwann cells to regulate synaptic activity include glutamate and ATP, but also other molecules [Pinard et al., 2003; Todd et al., 2007; Lindgren et al., 2013; Darabid et al., 2018]. This way, terminal Schwann cells are sensing and decoding synaptic communication, and directly modulate transmission towards depression or potentiation [Todd et al., 2010; Ko and Robitaille, 2015]. Furthermore, terminal Schwann cells anchor butyrylcholinesterase (BChe) at the synaptic cleft, which, like AChE, can hydrolyze ACh. At the terminal Schwann cells, BChE combined with nAChR seem to act as a sensor for ACh spillover, which is recognized and regulated by the Schwann cells [Girard et al., 2007; Petrov et al., 2014; Noronha-Matos et al., 2020]. By this and other processes, e.g., the clearance of perisynaptically accumulationg K^+ ions (thus preventing muscle fatigue), they contribute to NMJ homeostasis [Heredia et al., 2018].

During development, Schwann cells migrate together with sprouting nerve terminals towards the developing muscle, and processes of terminal Schwann cells contact pre-patterned nAChR clusters on muscle fibers before the nerve endings do, suggesting a nerve-guiding role [Flanagan-Steet et al., 2005; Barik et al., 2016]. Yet, if Schwann cells are genetically ablated from peripheral nerves in mice, growing nerve terminals still approach and contact muscle fibers, and the early stages of synaptogenesis including receptor clustering seem to progress normally. However, in the absence of Schwann cells, these immature synaptic contacts do not mature properly and fail to stabilize: presynaptic terminal sprouting and postjunctional fold formation are aberrant. Finally, the nerve terminals retract again and degenerate [Riethmacher et al., 1997; Morris et al., 1999; Woldeyesus et al., 1999; Lin et al., 2000; Wolpowitz et al., 2000; Barik et al., 2016]. Interestingly, this Schwann cell ablation-dependent nerve retraction does not occur if muscle activity is blocked at the same time, either pre- or postsynaptically [Liu et al., 2019]. This suggests that muscle activity might destabilize nerve terminals, and that this is counteracted by terminal Schwann cells [Gould et al., 2019]. Another key role of terminal Schwann cells in NMJ development has emerged regarding synapse elimination [Lee et al., 2017]. In the early stages of innervation, when aneural nAChR clusters are first contacted by nerve terminals, each cluster is approached by several axons, leading to polyneural innervation of muscle fibers. The mature situation, where each muscle fiber receives input from one nerve terminal only, is established about two weeks after birth in rats [Brown et al., 1976]. In the process, called synapse elimination, several axons are competing for the synaptic site, and terminals which lose this competition sequentially withdraw, until one winning terminal is left [Walsh and Lichtman, 2003]. The underlying mechanisms have long been unclear, but they seemed to involve synaptic activity of the competing terminals, and terminal Schwann cell activities [Griffin and Thompson, 2008]. This was confirmed by the findings that terminal Schwann cells are not only able to decode synaptic strengths of the competing nerve terminals [Darabid et al., 2013], but they identify the strongest one and selectively enhance its input, thereby actively driving its selection and elimination of the other terminals [Darabid et al., 2018]. Notably, terminal Schwann cells also phagocytose losing terminals [Bishop et al., 2004; Smith et al., 2013b]. Therefore, terminal Schwann cells are principal mediators of perinatal synapse elimination. In the adult NMJ, terminal Schwann cells function in synaptic maintenance and stability. Indeed, in both frog [Reddy et al., 2003] and mouse [Barik et al., 2016], synaptic function is disturbed and nerve terminals degenerate few days after specific ablation of terminal Schwann cells.

No less important are the roles taken on by Schwann cells upon injury. Overall, the PNS shows an impressive capacity to regenerate when compared to the CNS, which can be attributed pivotally to Schwann cells assuming their repair phenotype throughout the nerve to orchestrate the regeneration process [Jessen and Mirsky, 2016]. At NMJs, terminal Schwann cells fulfill

specific tasks associated with nerve repair upon denervation [Sugiura and Lin, 2011]: they remove axon debris of degenerated neurons [Griffin and Thompson, 2008], extend processes from the denervated site to guide the regenerating nerve terminals, and organize reinnervation [Kang et al., 2014; Jablonka-Shariff et al., 2020]. Considering this manifold importance for synaptic integrity, it is not surprising that terminal Schwann cells – as it is the case for other glial cells – are also increasingly recognized as affected participants in pathological processes of neuromuscular diseases [Santosa et al., 2018]. For example, terminal Schwann cells were shown to be affected in mouse models of amyotrophic lateral sclerosis (ALS) [Arbour et al., 2015; Carrasco et al., 2016; Arbour et al., 2017; Martineau et al., 2020], spinal muscular atrophy (SMA) [Lee et al., 2011; Neve et al., 2016], Duchenne muscular dystrophy [Personius and Sawyer, 2005], or the autoimmune neuropathy Miller Fisher syndrome [Overell and Willison, 2005]. Particularly, for ALS, affected terminal Schwann cells were also described in humans [Bruneteau et al., 2015], and some pathological changes were seen in an *in vitro* model using primary murine Schwann cells [Louit et al., 2022]. More studies are needed along these lines, ideally, using human-cell based model systems. As is true in general for NMJ biology, the major part of knowledge about terminal Schwann cell biology is derived from non-human animal models, primarily frog and rodents. Of course, human biology might diverge from that, and indeed, some differences have already been uncovered which distinguish rodent and human terminal Schwann cells. For example, human terminal Schwann cells are smaller than their murine counterparts [Alhindi et al., 2021b], which matches the overall smaller size of human NMJs [Jones et al., 2017]. But also the positioning seems to differ, as terminal Schwann cells at mouse NMJs usually are rather precisely restricted to the synaptic structure, while human terminal Schwann cells were found to extend to a larger area beyond the synapse perimeter. These and other differences in NMJ and Schwann cell biology between human patients and rodent models call for human-based model systems to generate increasingly relevant data, even more so, as some of the differences found in healthy human NMJs would be considered pathological changes in mouse NMJs [Alhindi et al., 2021b].

1.2.3 Development of Schwann cells

In embryonal tissue, Schwann cells differentiate through several intermediate stages, namely neural crest cells, Schwann cell precursors, and immature Schwann cells [Jessen and Mirsky, 2005; Furlan and Adameyko, 2018; Fledrich et al., 2019; Jessen and Mirsky, 2019; Muppirala et al., 2021; Solovieva and Bronner, 2021]. The neural crest is a unique population of multipotent cells forming at the dorsal neural tube, specific to vertebrate embryonic development. It is derived from the ectoderm through a series of signaling events, which start to induce neural crest already during gastrulation [Basch et al., 2006; Betters et al., 2018].

These inducing signals arise from juxtaposed developing structures: the neural crest is specified from the neural plate border, which is the territory between neural plate and non-neural ectoderm, by signaling from both these structures as well as the mesoderm located underneath (Figure 1-3A). To current knowledge, the most relevant pathways for the induction and specification of neural crest include Wnt, FGF, BMP, and Notch signaling [Prasad et al., 2019]. The initial phase of neural crest induction seems to be orchestrated mainly through Wnt [Ji et al., 2019] and FGF [Lunn et al., 2007; Betters et al., 2018] signals, when the neural plate border is formed, and neural crest-specifying transcription factors are activated subsequently. Furthermore, BMP [Marchant et al., 1998; Anderson et al., 2006; Steventon et al., 2009] and Notch [Morrison et al., 2000; Bellard et al., 2002; Endo et al., 2002; Noisa et al., 2014] signaling are required for several phases of neural crest induction, specification, and differentiation. While it is clearly established that these pathways and importantly, their crosstalk, are primarily regulating the development of neural crest, the picture of their precise spatiotemporal interplay and the roles of other signaling pathways, including Hippo/YAP [Manderfield et al., 2015; Hindley et al., 2016; Kumar et al., 2019; Zhao et al., 2021] and retinoic acid signaling [Martínez-Morales et al., 2011; Rekler and Kalcheim, 2022], remain only partially understood.

Upon invagination and closure of the neural tube, neural crest cells delaminate from adjacent tissue structures of developing epidermis and neural tube (Figure 1-3A), undergoing an epithelial-to-mesenchymal transition (EMT). A portion of these neural crest cells migrate dorsoventrally and associate with early peripheral nerves, which have started to grow towards their innervation targets. Once neural crest cells have entered peripheral nerves, they closely associate with developing axons and are then termed Schwann cell precursors (Figure 1-3B), as this is regarded as a typical property of glial cells [Le Douarin and Teillet, 1974; Jessen and Mirsky, 2005]. The factors driving this process are not entirely known, but crucial roles are attributed to Sox10, Notch, and neuregulin-1 (Nrg1) [Jessen et al., 2015; Fledrich et al., 2019], specifically the isoform Nrg1 type III associated with axons [Dong et al., 1995; Meyer et al., 1997; Leimeroth et al., 2002]. Throughout all of Schwann cell development and behavior, Nrg1 has been found to be a key regulating factor. During the stage of Schwann cell differentiation and migration, it essentially serves as survival factor which is located on axonal membranes and acts on juxtaposed Schwann cell precursors mainly through ErbB2/3 heterodimer receptor tyrosine kinases [Grinspan et al., 1996; Syroid et al., 1996]. Schwann cell precursors are still multipotent and highly migratory. Once they have reached their target tissue by traveling along the peripheral nerves, they can either detach from those and differentiate towards non-glial fates, or they remain associated with axons and differentiate further into post-migratory immature Schwann cells [Jessen et al., 1994; Belle et al., 2017; Furlan and Adameyko, 2018].

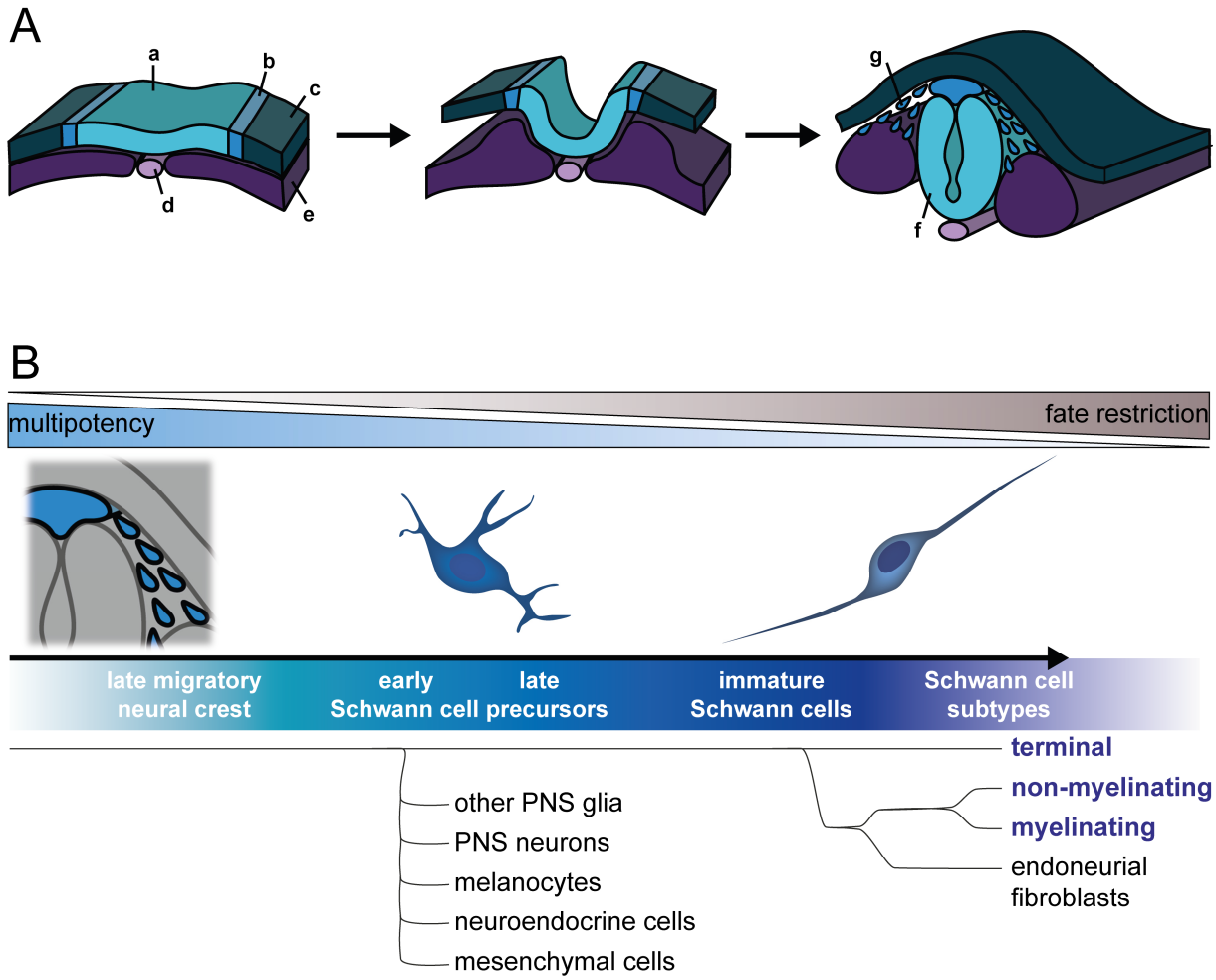


Figure 1-3: Development of Schwann cells. (**A**) Among the structures which form during neurulation are the neural plate (a), adjacent to it the neural plate border (b), located between neural plate and non-neural ectoderm (c), as well as surrounding structures including the notochord (d) and paraxial mesoderm (e). Upon closure of the neural tube (f), neural crest cells (g) derived from the neural plate border territory delaminate and start to migrate. (**B**) Schwann cells develop from the neural crest through the intermediate stages of Schwann cell precursors and immature Schwann cells, which retain multipotent potential through the precursor stage and then become gradually fate restricted towards Schwann cell subtypes. Figure obtained from Hörner et al. 2022 under CC BY 4.0 license.

At this stage, a commitment to the Schwann cell fate happens, marked by upregulation of typical marker proteins (e.g., Krox20, P0, S100b, Oct6), while earlier markers are downregulated (e.g., Ap2α, Pax3, Sox2) [Buchstaller et al., 2004; Jessen and Mirsky, 2005; D'Antonio et al., 2006; Kastriti and Adameyko, 2017; Gerber et al., 2021]. A further characteristic of immature Schwann cells is that they start to secrete basal lamina proteins, and also growth factors, which can act both as autocrine survival factors and as signals for developing neurons [Meier et al., 1999; Wanner et al., 2006; Monk et al., 2015; Jessen and Mirsky, 2019]. Immature Schwann cells orchestrate the process of radial sorting, which starts perinatally and continues until about postnatal day 10 in rodents [Taveggia et al., 2005; Feltri et al., 2016]. Groups of immature Schwann cells organize axons into bundles, and selectively sort axons with larger diameters to the periphery. Upon sorting of an axon, one of the

associated immature Schwann cells in the bundle divides and one of its daughter cells then exclusively associates with this axon, segregating it from the others; this process is termed “defasciculation”. The associated immature Schwann cell then starts to activate gene expression programs associated with myelination, it is then called a “pro-myelinating Schwann cell” and will develop further into the mature myelinating phenotype. When all large-caliber axons have been segregated from the bundle in this manner, the remaining associated immature Schwann cells continue to differentiate into Remak Schwann cells, embracing the remaining non-myelinated axons with trough structures in their cytoplasm, so that the small-caliber axons are surrounded by the Schwann cells’ basal lamina. In the beginning of this process, immature Schwann cells are highly proliferative, and then gradually exit the cell cycle while maturing into the different subtypes. This specification of mature phenotypes occurs relatively late in development: for rodents, it is known to happen mainly postnatally [Brown, 1981; Stewart et al., 1993; Gerber et al., 2021]. So far, two more mature cell types are known to develop through the defined stage of immature Schwann cells; namely terminal Schwann cells of the NMJs (described above) and endoneurial fibroblasts (Figure 1-3B). However, for both of these cell types, it is not known which mechanisms or molecular factors induce their specification. A recent study analyzing differentiation fate choices in the Schwann cell lineage demonstrated that both these cell types diverge from myelinating and Remak fates after the immature Schwann cell stage, whereby the path of terminal Schwann cells seems to be the first one to split from the others, even before endoneurial fibroblasts [Kastriti et al., 2022]. The latter produce a range of ECM molecules, so together with Schwann cells which form their characteristic basal lamina, these cells build up the endoneurial connective tissue of the peripheral nerves.

Throughout the developmental pathway of Schwann cells, a noteworthy characteristic is the remarkable multipotency retained by the intermediate differentiation stages. Neural crest cells are often also referred to as neural crest stem cells, since they give rise to an extraordinary variety of neural and mesenchymal cell types. Importantly, the neural crest generates most cells of the PNS, like the Schwann cells and other glial cells (for example ganglionic satellite glia and enteric glia), and neuronal cells, including postganglionic sympathetic and parasympathetic neurons, sensory neurons, and enteric neurons. However, also other diverse cell types are generated from neural crest, including endocrine cells, melanocytes, and cells of the cranial bone and connective tissue [Abzhanov et al., 2003; Dupin et al., 2018; Rothstein et al., 2018]. Many of these can even be derived from neural crest either with or without progressing through the Schwann cell precursor stage first – this has been shown for melanocytes [Adameyko et al., 2009; Kalcheim and Kumar, 2017] and might also be the case for enteric glia [Muppirala et al., 2021]. To date, quite a range of cells besides Schwann cells and endoneurial fibroblasts [Joseph et al., 2004] have been shown to differentiate from

Schwann cell precursors, including neural cell types (postganglionic parasympathetic neurons [Dyachuk et al., 2014; Espinosa-Medina et al., 2014], a subpopulation of sympathetic neurons in paraganglia [Kastriti et al., 2019], enteric neurons [Uesaka et al., 2015], neuroendocrine chromaffin cells of the adrenal medulla [Furlan et al., 2017] and Zuckerkandl organ [Kastriti et al., 2019]) as well as mesenchymal cell types (dental pulp mesenchymal stromal cells [Kaukua et al., 2014], chondrocytes and osteocytes [Xie et al., 2019]). Based on this striking multipotency overlap between Schwann cell precursors and neural crest, recent work has suggested the existence of Schwann cell precursor substages, with early Schwann cell precursors still largely sharing developmental potential of neural crest cells, and a gradual restriction towards the Schwann cell fate in late precursor stages (Figure 1-3B) [Furlan and Adameyko, 2018; Kastriti et al., 2022].

1.2.4 Sources and culture of Schwann cells in vitro

Schwann cells derived for culture *in vitro* are usually either of rodent or human origin, and can be isolated primary Schwann cells, or derived *in vitro* from various stem cell sources. Primary rodent Schwann cells have been the main source, since they can be maintained without complex requirements and continue proliferating in culture, allowing expansion to high numbers. Furthermore, they can be used efficiently for *in vitro* myelination studies when cocultured with neurons. Primary Schwann cells derived from humans, in comparison, have poor myelination capacity, exhibit a more immature phenotype, and cease proliferation after some passages [Morrissey et al., 1995; Monje et al., 2018; Monje, 2020a, 2020b]. Additionally, primary human tissue material to establish Schwann cell cultures is scarce, especially when compared to rodent tissue; and required culture techniques are more laborious [Monje et al., 2018; Monje, 2020b]. While these differences make the work with rodent Schwann cells easier, they also suggest a molecular difference between Schwann cells of different species, therefore contesting the translatability of data obtained from non-human Schwann cells. Therefore, stem cells pose a valuable alternative source to generate Schwann cells of human origin, to develop better model platforms for researching Schwann cell development, function in health and disease, and to explore their therapeutic potential regarding tissue engineering [Ma et al., 2015; Lehmann and Höke, 2016; Huang et al., 2020]. Again, multipotent mesenchymal stem cells (MSCs) of rodent origin are widely used due to their availability and efficiency. Differentiation mechanisms used for rodent MSCs seem to translate to stem cells of human sources, at least in part, and Schwann cells have been generated from human MSCs of various tissue origins, as well as human embryonic stem cells (hESC) and human induced pluripotent stem cells (hiPSC) [Hörner et al., 2022]. Historically, the first generation of mammalian Schwann cells *in vitro* from a different cell type was demonstrated from primary rodent neural

crest cells, after their isolation from explant cultures by cell sorting [Stemple and Anderson, 1992]. Later, the first directed *in vitro* differentiation protocol towards Schwann cells, which laid the foundation for many protocols to follow, was presented for rat MSCs [Dezawa et al., 2001]. MSCs, both of rodent and human origin, are still preferred over (h)iPSCs and (h)ESCs as cell source in many studies. While especially for hESCs availability and ethical concerns pose hindrances, both MSCs and iPSCs can be generated from diverse adult tissues, including easily accessible ones, like skin or fat tissue; and each of them can be derived as autologous cell source, which is relevant in the context of personalized medical applications. However, derivation of MSCs is usually easier and more efficient than the generation of iPSCs, as MSC culture requires less specialized culture techniques than iPSC, and the latter first need to be reprogrammed to a pluripotency state. In addition, available differentiation protocols for hiPSCs/hESCs are generally more time-consuming than those for MSCs. Therefore, overall, less protocols and studies are available for hiPSC-/hESC-derived Schwann cells than for MSC-derived Schwann cells. On the other hand, established hiPSC/hESC lines can be maintained indefinitely, while MSCs have a limited capacity for proliferation in culture. Furthermore, the increased complexity and resource consumption when working with hiPSCs/hESCs is arguably outweighed by their relevance and potential for developmental and disease modeling. To date, Schwann cells have been differentiated *in vitro* from hiPSCs and hESCs [Ziegler et al., 2011; Liu et al., 2012; Huang et al., 2017; Kim et al., 2017; Muller et al., 2018; Carrió et al., 2019; Mukherjee-Clavin et al., 2019], human MSCs from different sources including skin [Saulite et al., 2018], bone marrow [Shimizu et al., 2007; Cai et al., 2017], tonsils [Jung et al., 2016], dental pulp [Martens et al., 2014], adipose tissue [Razavi et al., 2012; Tomita et al., 2013], and umbilical cord [Zhang et al., 2009; Matsuse et al., 2010]; human skin-derived precursors [McKenzie et al., 2006]; as well as human fibroblasts [Thoma et al., 2014; Mazzara et al., 2017; Kim et al., 2020] and keratinocytes [Bajpai et al., 2017] using transdifferentiation protocols. Regarding non-human cells, besides rat MSCs [Dezawa et al., 2001; Kingham et al., 2007; Xu et al., 2008; Shea et al., 2010; Xie et al., 2017], Schwann cell differentiation has been shown using mouse embryonic fibroblasts [Pan et al., 2021], mouse MSCs [La Bierlein De Rosa et al., 2017], cynomolgous monkey MSCs [Wakao et al., 2010], mouse ESCs [Roth et al., 2007], and rodent skin-derived precursors [Biernaskie et al., 2006; McKenzie et al., 2006].

1.3 Human induced pluripotent stem cells

1.3.1 Introduction to hiPSC properties and applications

Stem cells, by definition, have the following characteristics: (i) they maintain an undifferentiated, non-specified state, (ii) they can self-renew indefinitely by symmetric cell division, and (iii) they can give rise to further differentiated and functionally specialized daughter cells through asymmetric divisions. In embryonic and adult organisms, different types of stem cells can be found. Adult tissues contain tissue-specific somatic (or adult) stem cells in specific locations, which can still differentiate into other cell types, but they are usually lineage-restricted, and therefore called multipotent. Conversely, embryonic stem cells (ESC), which are present at the blastocyst stage, are pluripotent, as they have the ability to differentiate into cell types of all three germ layers. Therefore, ESCs can potentially generate every cell type of a body. The use of hESCs, however, was and is limited through ethical controversy regarding the approval of human embryos or embryonic material for research.

Therefore, the discovery that pluripotent cells highly similar to ESCs can be derived from differentiated somatic cells, like skin fibroblasts, was groundbreaking for the field of stem cell research. The creation of these induced pluripotent stem cells, iPSCs, through genetic reprogramming, was demonstrated by Kazutoshi Takahashi and Shinya Yamanaka first from mouse fibroblasts [Takahashi and Yamanaka, 2006] and, shortly after, from human fibroblasts [Takahashi et al., 2007; Park et al., 2008], and was awarded with the Nobel Prize in Physiology or Medicine in 2012. The reprogramming of differentiated somatic cells to hiPSC (Figure 1-4) was achieved through transgene expression of the four transcription factors Oct4, Sox2, Klf4, and c-Myc, which are also called pluripotency factors, or Yamanaka factors. This in turn induces cascades of downregulation of differentiation-associated genes and upregulation of pluripotency-associated genes. The obtained hiPSCs have highly similar expression profiles to hESCs and, likewise, the capacity to differentiate into cell types of all three germ layers (Figure 1-4). Besides technical and ethical accessibility, hiPSCs have more advantages over hESCs: since hiPSCs can be generated from patient biopsies, derived cells could be used for autologous cell transplantation, and also, *in vitro* models reflecting the genetic background (including pathological mutations) of the patient can be established (Figure 1-4).

To maintain the pluripotent, undifferentiated state in culture, molecular factors have to be constantly present in the medium which block differentiation pathways and stimulate self-renewal of stem cells [Pease et al., 1990; Ogawa et al., 2006]. Upon withdrawal of such factors, stem cells start to spontaneously differentiate [Takahashi and Yamanaka, 2006]. To achieve directed differentiation towards specific lineages and target cell types, the differentiation signals and pathways occurring *in vivo* need to be mimicked. During embryonic development,

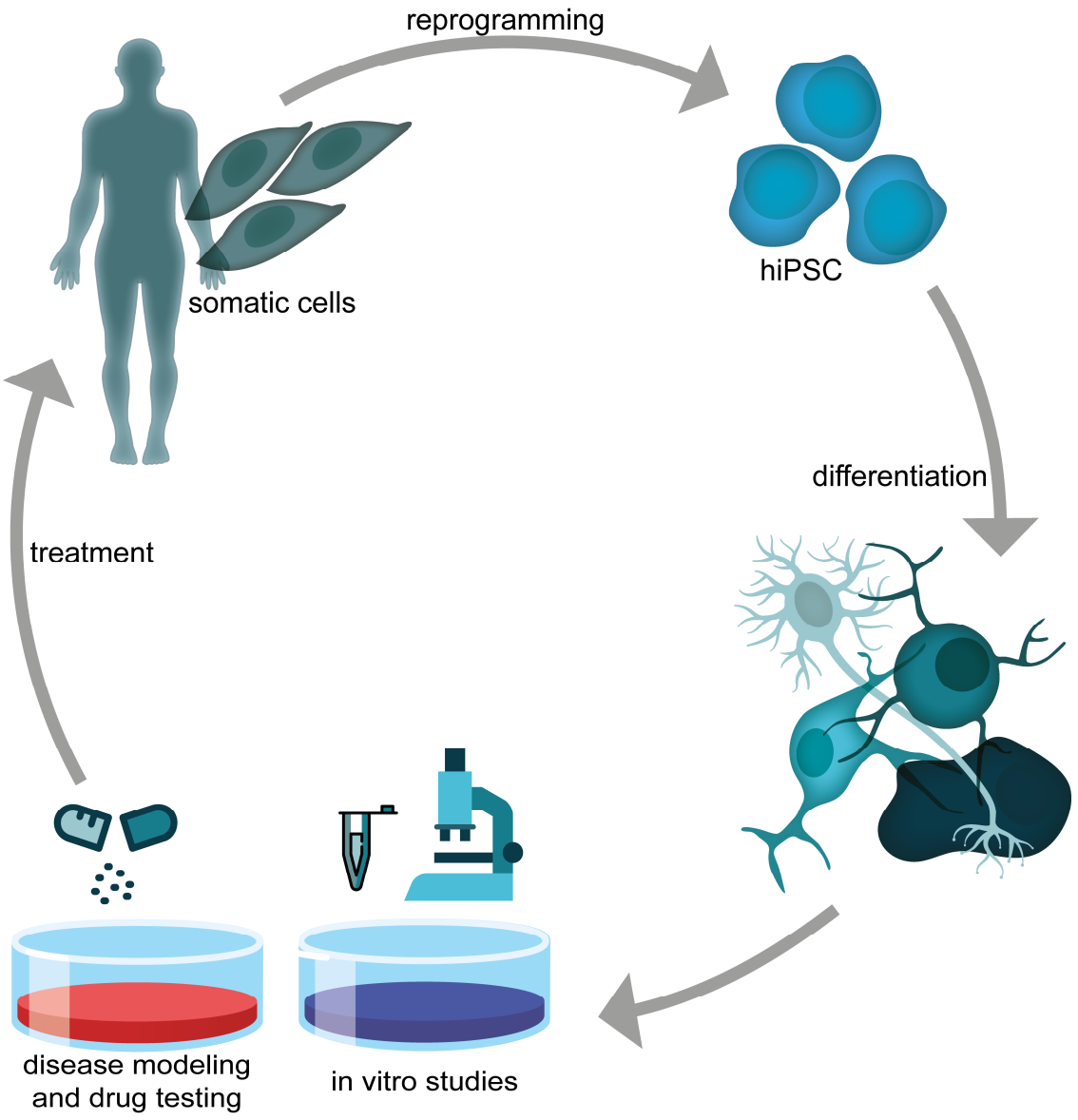


Figure 1-4: Derivation and applications of hiPSC. hiPSC are obtained through genetic reprogramming from somatic cells to assume a pluripotent state. From there, they can be differentiated again into specified cells using appropriate protocols. Such hiPSC-derived cells are useful for *in vitro* studies of cell biology and interactions, particularly in the context of disease modeling and drug testing, and hold potential in clinical applications to treat diseases through transplantation.

different types of tissues are induced and organized through signals which are precisely regulated spatially and temporally. Hereby, developing cells produce signaling molecules, which then diffuse and act on surrounding structures. Such molecules are termed “morphogens”, as suggested by Alan Turing, who predicted correctly that tissue patterning can be installed by opposing concentration gradients of diffusing morphogens [Turing, 1952], long before such mechanisms were actually observed *in situ*. Decades later, bicoid was the first protein to be identified as a morphogen as part of Christiane Nüsslein-Volhard’s groundbreaking work on *Drosophila melanogaster* embryonic development [Driever and Nüsslein-Volhard, 1988]. By exogenous addition of such morphogen combinations to the

culture medium at precise concentrations and time sequences, it is possible to control and direct the differentiation of both hESCs and hiPSCs *in vitro* towards specific fates.

1.3.2 Differentiation of hiPSC into motoneurons

Developmentally, lower spinal motoneurons are part of the CNS, as they develop from the neural tube. Indeed, their somata remain in the ventral horn of the spinal cord as part of the CNS, while their axons project outwards through the spinal nerves to innervate muscle fibers. The developmental steps towards motoneuron fate and the signaling mechanisms governing them are comparably well known, and therefore, a number of differentiation protocols are available [Wichterle et al., 2002; Hu and Zhang, 2009; Amoroso et al., 2013; Davis-Dusenbery et al., 2014; Faravelli et al., 2014; Gouti et al., 2014; Qu et al., 2014; Du et al., 2015; Maury et al., 2015; Patani, 2016; Sances et al., 2016; Yi et al., 2018]. To generate motoneurons from hiPSC *in vitro*, the first step is an induction towards neural precursor cells, which are subsequently driven towards the motoneuron fate by patterning factors. Figure 1-5 shows a schematic depiction of differentiation stages and associated signaling which is targeted in many differentiation protocols for motoneurons, along with examples for typical small molecules used in this context.

To induce neuralization, early differentiation protocols for all kinds of neural cells mostly relied either on embryoid body formation and the subsequent auto- and/or paracrine signaling happening in these dense cell aggregates, and coculture with stromal cells which release neuralizing signals. However, since the discovery that neural fate can be induced robustly in pluripotent cultures by blocking mesodermal and endodermal differentiation fates, and that this can be achieved by small molecules which inhibit TGF-β/activin/nodal and BMP signaling [Chambers et al., 2009], this is the method of choice for protocols aiming to generate neural cells. As both, TGF-β and BMP signaling, act through Smad proteins (Smad2/3 and Smad1/5/8, respectively), this method is also known as dual Smad inhibition [Chambers et al., 2009]. The most widely used TGF-β signaling inhibitor is the small molecule SB431542, which is then usually combined with a BMP inhibitor, like noggin, dorsomorphin, LDN193189, or DMH1 (Figure 1-5). Dual Smad inhibition efficiently induces hiPSC cultures to differentiate into structures called neural rosettes, which mainly consist of neural precursors positive for Sox1, Sox2, and Pax6. To drive these precursors towards a spinal cord fate, Wnt activating molecules like CHIR99021 are typically added at the same time (Figure 1-5), as brain regionalization is driven by a rostrocaudal Wnt gradient which increases in caudal direction, meaning that high Wnt activity induces spinal cord fate, while rostral forebrain fates develop in the absence of Wnt signals [Nordström et al., 2002]. Regions of the spinal cord are further patterned by retinoic acid signaling, wherefore retinoic acid is added for further caudal

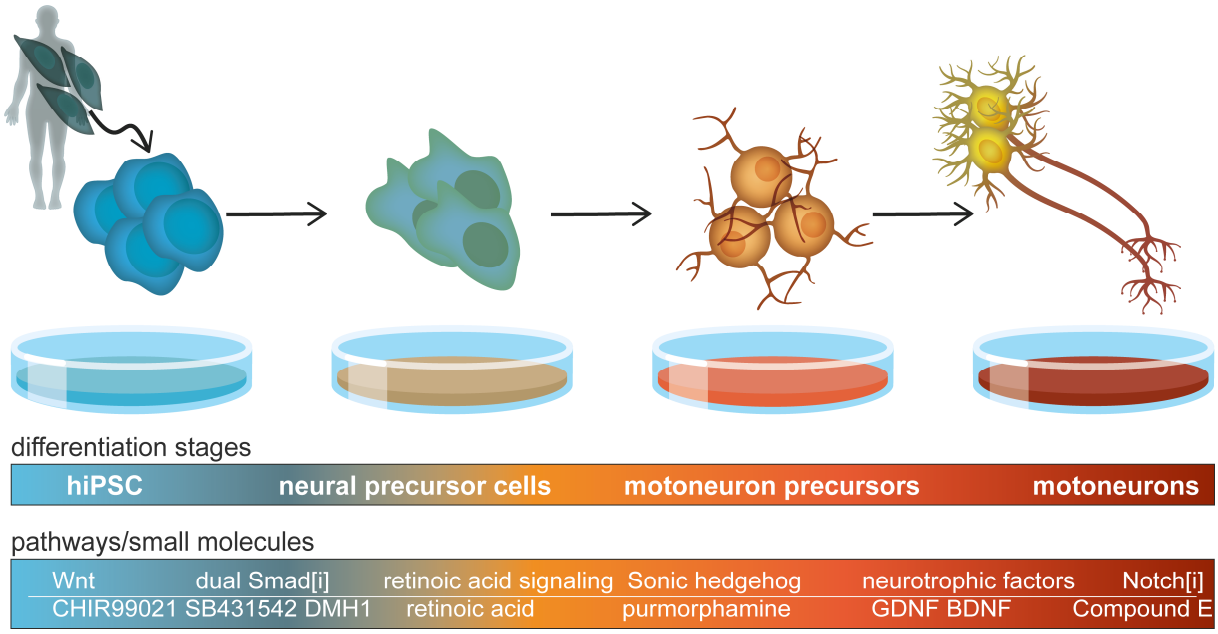


Figure 1-5: Differentiation of motoneurons from hiPSC. Schematic depiction of the differentiation stages from stem cells to motoneurons and examples for corresponding small molecules typically used to engage the signaling pathways involved. [i] = inhibition.

patterning of precursor cells [Liu et al., 2001; Maden, 2007]. In addition to rostrocaudal patterning, specific domains are established along the dorsoventral axis of the neural tube by opposing gradients of dorsally expressed BMP and ventral Sonic hedgehog (Shh) secreted from the floor plate and notochord [Chiang et al., 1996]. Motoneuron precursors are specified in the pMN domain which is located in the ventral part close to the floor plate, and therefore require Shh signals [Ericson et al., 1996], which is provided *in vitro* by adding Shh agonists such as smoothened agonist or purmorphamine (Figure 1-5). Regarding *in vitro* differentiation protocols, it seems beneficial to provide Wnt activators (and maybe also BMP inhibitors) used in the first phase of neuralization also during this second phase of motoneuron precursor patterning, improving differentiation speed and efficiency [Du et al., 2015; Maury et al., 2015] in comparison to other protocols [Hu and Zhang, 2009; Hester et al., 2011]. Subsequently, motoneuron precursors are further matured into post-mitotic neurons, sometimes in the continued presence of retinoic acid and Shh activators, and with addition of maturation and/or survival signals like neurotrophins or inhibition of Notch signaling [Du et al., 2015; Yi et al., 2018] (Figure 1-5).

1.3.3 Differentiation of hiPSC into Schwann cells

Schwann cells are part of the PNS and derived from the neural crest. As described in section 1.2.3 and schematically depicted in Figure 1-6, they develop through the intermediate stages

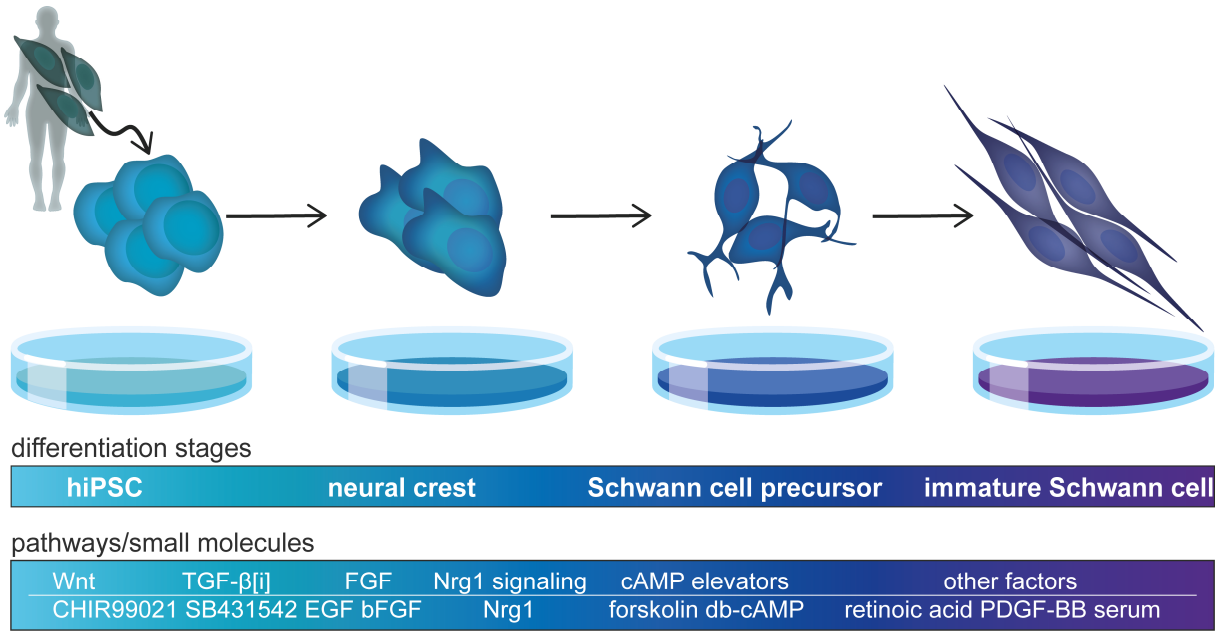


Figure 1-6: Differentiation of Schwann cells from hiPSC. Schematic depiction of the differentiation stages from stem cells to Schwann cells and examples for corresponding small molecules typically used to engage the signaling pathways involved. [i] = inhibition.

of Schwann cell precursors and immature Schwann cells. In comparison to the mechanisms determining motoneuron fate described in the previous section, the signals and their coordination involved in the developmental pathway of Schwann cells are much less clear, consequently translating into a lower number of available differentiation protocols [Ziegler et al., 2011; Liu et al., 2012; Huang et al., 2017; Kim et al., 2017; Carrió et al., 2019; Mukherjee-Clavin et al., 2019], which moreover are less efficient. Usually, these protocols can be divided into a first phase, dedicated to neuralization and neural crest induction, and a second phase to specify Schwann cells [Hörner et al., 2022].

The differentiation of neural crest from hiPSC, for a long time, has been very inefficient: in cultures neuralized by methods described in the previous section, i.e., mainly embryoid body formation or dual Smad inhibition, a major part of cells usually develops towards Pax6+ neuroectodermal fates related to CNS cell types; but often a small number of cells negative for Pax6 but positive for neural crest markers, e.g., Sox10 and p75NTR, can be found. To differentiate these cells further, they first have to be purified from these mixed neural cultures, which is usually done by FACS [Lee et al., 2007; Pomp et al., 2008; Ziegler et al., 2011; Liu et al., 2012; Kreitzer et al., 2013; Huang et al., 2017; Shi et al., 2018]. Good results regarding more homogenous and efficient neural crest cultures were achieved in defined approaches including Wnt activation, especially if a TGF-β signaling inhibitor was used without inhibition of BMP [Menendez et al., 2011; Leung et al., 2016; Hackland et al., 2017]. This also led to

improved Schwann cell differentiation protocols which do not require sorting [Kim et al., 2017; Carrió et al., 2019].

Subsequently, hiPSC-derived neural crest cells should be driven towards a Schwann cell precursor and then, Schwann cell identity. Axon-derived Nrg1 type III is the most important factor known so far for the development of Schwann cells (see section 1.2.3) and was shown to be important in all major steps of this process [Jessen et al., 1994; Garratt et al., 2000; Birchmeier and Nave, 2008] as well as for Schwann cell differentiation and survival *in vitro* [Lemke and Brockes, 1984; Shah et al., 1994; Leimeroth et al., 2002]. Consequently, it is added in almost all Schwann cell culture and differentiation protocols (Figure 1-6) in the form of recombinant soluble Nrg1 EGF-like domain peptides [Monje, 2020a]. The two other most common elements are supplementation with serum as well as agents elevating intracellular cAMP. Further factors frequently used include various combinations of PDGF-BB, bFGF, ascorbic acid, retinoic acid, β-mercaptoethanol, bovine serum albumin (BSA), CNTF, and Y-27632 [Hörner et al., 2022].

1.4 Neuromuscular cell culture models

1.4.1 Purpose and categories of in vitro neuromuscular models

The NMJ is a comparably well-known biological structure, thanks to decades of research in animal models. While such *in vivo* research models are still very important for research on the neuromuscular circuit in health and disease, they come with certain limitations and ethical issues, and the complexity of an organism as research model poses both advantages as well as disadvantages, depending on the research question. Maybe most importantly, non-human models cannot always be used to faithfully mimic human biology and pathology, resulting in limited translatability of animal-research derived results in many cases. Therefore, *in vitro* models of the neuromuscular junction have increasingly come to the fore, even more so since the advent of hiPSC technology (see section 1.3.1) allows generation of human-based and even personalized disease models. Neuromuscular cocultures to model NMJs can be grouped into different types of setups, schematically depicted in Figure 1-7. The simplest version is the direct coculture of motoneurons and myotubes in 2D adherent cultures (Figure 1-7A). Usually, motoneurons are seeded on top of pre-differentiated myotubes to form a cell bilayer. Such cultures have been done for a long time, including rodent, chick, and human cells [Shimada et al., 1969; Li et al., 2005; Das et al., 2010; Guo et al., 2011; Demestre et al., 2015; Steinbeck et al., 2016; Vilmont et al., 2016], and are therefore well characterized [Castellanos-Montiel et al., 2020]. While those cultures stay relatively immature, they have the capability to form functional synaptic contacts between motor neurons and myotubes, sometimes called "*in vitro*

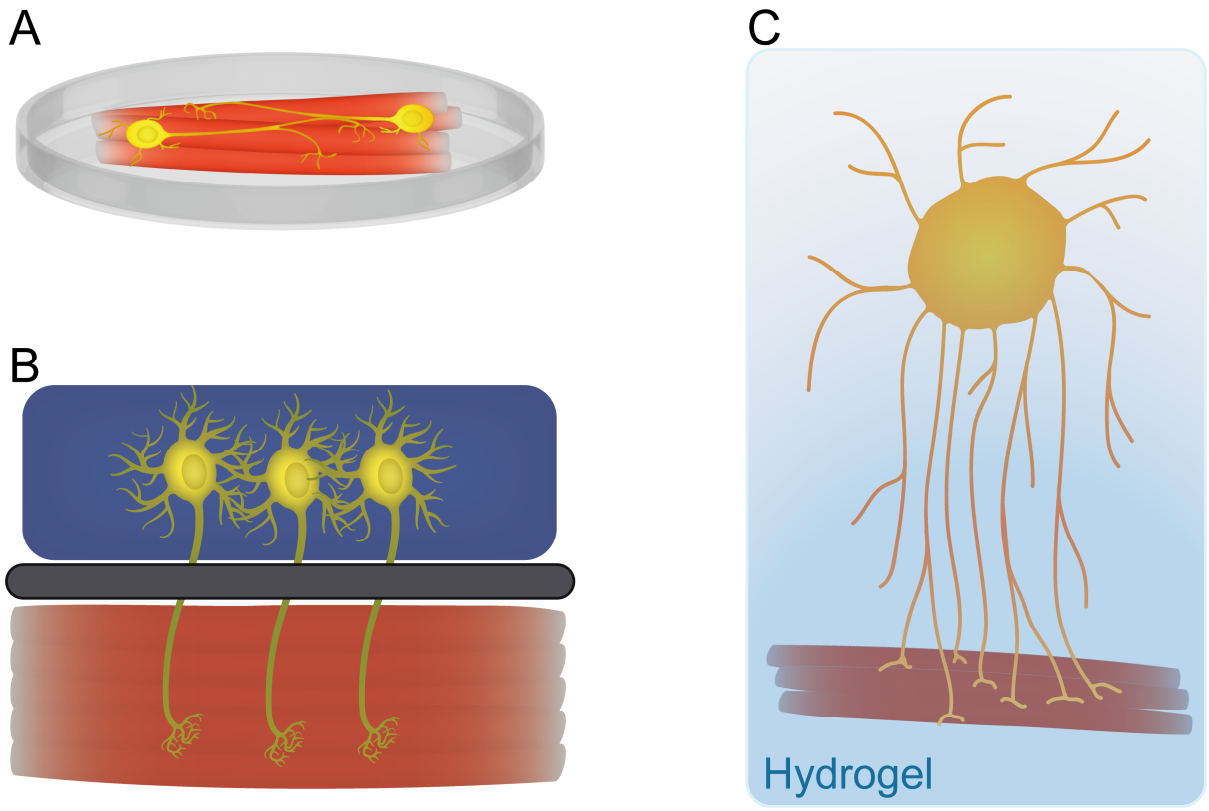


Figure 1-7: Categories of NMJ cultures. Most NMJ *in vitro* studies used 2D bilayer cocultures of motoneurons and muscle cells (**A**). Such cocultures can be compartmented (**B**) to separate motoneuron somata from muscle cells. Advanced 3D cultures are mainly done by culturing cells in hydrogels (**C**).

NMJs" to distinguish them from fully developed NMJs *in vivo*. However, 2D adherent layer cultures can typically not be maintained long-term for maturation, as myotubes detach from rigid surfaces with differentiation [Thomson et al., 2012; Wang et al., 2012a]. To introduce spatial organization in such cocultures, compartmentalized culture vessels can be used (Figure 1-7B), which is often done in the form of microfluidic devices [Park et al., 2013; Southam et al., 2013; Ionescu et al., 2016; Santhanam et al., 2018]. Such setups allow for spatial separation of neuronal cell bodies from the muscle compartment, connected by growth channels permissive for axons, which provides separate microenvironments and targeted stimulation of the individual cell types. Currently, the most complex *in vitro* models have been achieved through 3D cell culture methods (Figure 1-7C). 3D cultures are better suited to model cell environment and tissue architecture, and therefore have the potential for increased physiological relevance and with this, increased translatability to *in vivo* mechanisms. On the other hand, their increased complexity comes at the cost of being more resource intensive and low throughput [Edmondson et al., 2014; Centeno et al., 2018; Fralish et al., 2021]. Several 3D engineered neuromuscular *in vitro* models have been published to date, using rodent and/or human cells, and, in some cases, also compartmentation of neural and muscle components [Morimoto et al., 2013; Smith et al., 2016; Uzel et al., 2016; Cvetkovic et al., 2017;

Afshar Bakooshli et al., 2019; Osaki et al., 2020; Rimington et al., 2021; Vila et al., 2021]. Another 3D modeling approach specifically enabled by use of PSCs are organoids, which are self-organizing cell clusters containing diverse cell types developed from the same stem cell source, which partly recapitulate self-patterning processes known from development [Lancaster and Knoblich, 2014]. Recently, the very first approaches of NMJ organoids [Faustino Martins et al., 2020] and cortico-motor assembloids [Andersen et al., 2020] have been presented by the groups of Mina Gouti and Sergiu Pașca, respectively.

1.4.2 Short overview of the historic development of neuromuscular cocultures

Based on the observations that functional neuromuscular synaptic contacts seemed to form *in vitro* in frog embryonic tissue explant cultures [Harrison, 1959], further studies followed using frog, chick, rodent, and human cells, which cocultured embryonic spinal cord explants with muscle cells. In the first cultures, nerve explants were dissected with muscle tissue still attached, or cocultured with separate muscle tissue explants [Peterson et al., 1965; Bornstein et al., 1968; James and Tresman, 1968; Crain et al., 1970]. Following cultures plated neural explants on myotube monolayers [Anderson et al., 1977; Kidokoro et al., 1980; Askanas et al., 1987] which were dissociated from explants, or also used dissociated embryonic neurons as well [Fischbach, 1970; Kengaku et al., 1991; Das et al., 2010], which allowed better definition of cultures through isolation of cell types. Subsequently, primary embryonic cells were increasingly replaced by cell lines and *in vitro* stem cell-derived cells [Li et al., 2005; Guo et al., 2010; Chipman et al., 2014]. Particularly, the murine myoblast cell line C2C12 [Yaffe and Saxel, 1977; Blau et al., 1983] gained a lot of popularity to provide the muscle component in many coculture setups, and it was and is still used in many studies [Li et al., 2005; Umbach et al., 2012; Morimoto et al., 2013; Park et al., 2013; Du et al., 2015; Yoshida et al., 2015; Uzel et al., 2016]. The first coculture which used human cells for both cell components combined hESC-derived motoneurons with primary skeletal myoblasts [Guo et al., 2011]. A few years later, the first report of a coculture including both cell types derived from hiPSC was published [Demestre et al., 2015]. Regarding culture formats, the first compartmentalized microfluidic NMJ models used rodent cells [Park et al., 2013; Southam et al., 2013], followed later by human cells [Santhanam et al., 2018]. Furthermore, techniques for 3D culture of muscle cells were developed and combined with motoneurospheres [Morimoto et al., 2013; Smith et al., 2013a; Smith et al., 2016] which led to more advanced culture systems reporting improvements on maturation [Uzel et al., 2016; Osaki et al., 2018; Afshar Bakooshli et al., 2019; Rimington et al., 2021]. Finally, the most recent developments lead towards organoid cultures containing *in vitro* NMJs [Andersen et al., 2020; Faustino Martins et al., 2020]. Due to these developments and the need for neuromuscular models with the aim of disease modeling, the field of *in vitro*

NMJ models received a lot of attention and has been topic of several recent literature reviews [Natarajan et al., 2019; Barbeau et al., 2020; Castellanos-Montiel et al., 2020; Vila et al., 2020; Luttrell et al., 2021; Lynch et al., 2021; Raffa et al., 2022; Strickland et al., 2022]. In broad consensus, the introduction of human stem cell culture and 3D culture techniques were identified as the two biggest advancements for improvement of neuromuscular *in vitro* cultures. At the same time, they pointed out the lack of integration of other cell types, in particular, Schwann cells. The appearance of cells with Schwann cell identity was reported for self-organizing NMJ organoids [Faustino Martins et al., 2020], and putative myelin+/S00b+ Schwann cells also appeared in 2D mixed multilineage neuromuscular differentiation protocols in two studies [Lin et al., 2019; Mazaleyrat et al., 2020]; however, so far, no human stem-cell based *in vitro* model had integrated Schwann cells in a selective manner.

1.4.3 hiPSC-derived cells in neuromuscular in vitro models

To date, a few models have been published which combine both hiPSC-derived motoneurons and hiPSC-derived muscle. Of course, these include the organoid approaches presented by Faustino Martins et al. [2020] and Andersen et al. [2020]. In another approach, hiPSC-derived muscle cells were differentiated in 3D hydrogels, and hiPSC-derived neural precursors were added to further differentiate towards motoneurons in coculture [Maffioletti et al., 2018]. This method was further advanced by combining compartmentalized microfluidics with 3D-culture containing both hiPSC-derived cell types in 3D structures [Osaki et al., 2018], and an hiPSC-derived system combined with 2D microfluidics was demonstrated as well [Bellmann et al., 2019]. In direct 2D cocultures, both cell types have either been pre-differentiated separately and then combined [Demestre et al., 2015; Picchiarelli et al., 2019; Guo et al., 2020], or were allowed to differentiate in parallel in mixed cultures [Puttonen et al., 2015; Lin et al., 2019; Mazaleyrat et al., 2020]. As the differentiation of motoneurons from hiPSC is better established than the differentiation of skeletal muscle, some studies (both 2D and 3D) combined primary human muscle with hiPSC-derived motoneurons to create human-based cocultures [Maury et al., 2015; Santhanam et al., 2018; Afshar Bakooshli et al., 2019; Vila et al., 2019; Lamotte et al., 2020; Duc et al., 2021; Rimington et al., 2021; Yamamoto et al., 2021]. Furthermore, hiPSC-derived motoneurons have been combined with non-human muscle, like the murine cell line C2C12 [Yoshida et al., 2015; Kong et al., 2021; Shimizu et al., 2022].

1.5 Aims of this thesis

As described in the preceding sections, neuromuscular *in vitro* models are valuable tools for research, and their development towards increased complexity and relevance is advancing at a fast pace. It is acknowledged that the critical parameters for their improvement are, next to more sophisticated culture methods to achieve spatial organization of cultures, the use of hiPSC-derived cells to adequately model human biology, and the integration of multicellular structures recapitulating *in vivo* architecture. Still, to date there has been no success in selectively integrating hiPSC-derived Schwann cells, the third principal component of NMJs, into culture systems – despite their critical role in NMJ development and maintenance. Among the likely reasons for this deficiency are the facts that not many differentiation protocols for hiPSC-derived Schwann cells are available, and most of them are complex, lengthy, and inefficient. Furthermore, multicellular models which adequately support all integrated cell types, while being robustly reproducible and reasonably accessible for analysis, are challenging to achieve.

As a contribution to more relevant NMJ *in vitro* models, the aim of this study was to demonstrate integration of hiPSC-derived Schwann cells into neuromuscular cocultures, including the establishment of robust protocols for Schwann cell differentiation and their coculture with motoneurons and muscle cells.

To this end, I optimized a protocol for the robust differentiation of Schwann cells from hiPSC, reproduced it in several cell lines, and characterized differentiated Schwann cells by marker protein expression. Furthermore, I have set up medium conditions supportive for all three cell types while evaluating the influence on Schwann cell maturation. Subsequently, I have established a reproducible and reasonably short protocol to establish 2D tricultures comprised of hiPSC-derived Schwann cells, hiPSC-derived motoneurons, and murine C2C12 myotubes. Using these tricultures, I have analyzed the effect of Schwann cell and/or motoneuron coculture on the formation of nAChR clusters on myotubes. Finally, I have tested different approaches to constitute advanced 3D neuromuscular cultures and demonstrated the possibility to integrate Schwann cells in different culture formats.

2 MATERIAL AND METHODS

2.1 Cell culture

2.1.1 Cell lines

In this study, six cell lines were used, comprising five human iPSC lines (three of those generated from healthy donors, one line with a disease-causing mutation, and one genetically engineered isogenic control line to the latter) as well as the murine cell line C2C12. The hiPSC lines 028#1, 028#4-GCaMP6f#2, and 009#3 were kindly provided by Philipp Koch (Hector Institute for Translational Brain Research at the Central Institute of Mental Health, Medical Faculty Mannheim of Heidelberg University, Mannheim, Germany). These lines were generated from healthy donors. The hiPSC lines WC035i-SOD1-D90D and WC034i-SOD1-D90A were purchased from WiCell Research Institute (Madison, WI, USA). Those cell lines were deposited with WiCell by Su-Chun Zhang, University of Wisconsin [Chen et al., 2014] and are derived from cell line ND29149 from the NINDS Human Genetics Resource Center at the Coriell Institute for Medical Research. The murine myoblast cell line C2C12 was kindly provided by Tomasz Prószyński (Nencki Institute of Experimental Biology, Polish Academy of Sciences, Warsaw, Poland).

2.1.2 General cell culture methods, reagents, and materials

All cells were cultured under standard conditions at 37 °C with 5 % CO2 in humidified atmosphere in a cell culture incubator and handled using aseptic technique in biosafety class II cabinets. Penicillin-streptomycin was added at 1X concentration routinely with regularly performed antibiotic-antimycotic free subcultures to check for masked contaminations. All cell lines were tested for mycoplasma contaminations and confirmed to be mycoplasma free before expansion. Standard media compositions are listed in Table 1, and differing compositions or additions to standard formulations for specific experiments are further specified in the respective methods or results sections. Formulations reported for Schwann cell media are reported as used in the final modified differentiation protocol, and previously tested compositions are described in the respective sections. N2 supplement (Table 2) was either bought from Stemcell Technologies (Vancouver, Canada), Thermo Fisher Scientific (Waltham, MA, USA), or prepared in the laboratory by supplementing DMEM/F12 media with insulin (500 µg/ml), transferrin (10 mg/ml), sodium selenite (520 ng/ml), putrescine (1.611 mg/ml), and progesterone (630 ng/ml). All supplier specifications for standard media components are listed in Table 2, and separately in Table 3 for small molecules used for differentiation media. All other reagents used for cell culture procedures are listed in Table 4. Small molecules were prepared in ultrapure water, DMSO, or 100 % ethanol according to the datasheets at stock

concentrations indicated in Table 3, and prepared in small working aliquots to avoid freeze thaw cycles. Solutions and media containing light sensitive molecules were prepared with direct light inside the biosafety cabinet switched off. Consumable plasticware for cell culture including serological pipettes (50 mL, 25 mL, 10 mL, 5 mL), sterile low retention filter tips (1000 µL, 200 µL, 20 µL, 10 µL), conical polypropylene tubes with screw caps (15 mL, 50 mL), micro reaction tubes with snap caps (1.5 mL, 2 mL), cryovials (2 mL), culture dishes (Ø 100 mm, height 20 mm), culture flasks (75 cm²) and multiwell plates (24 well, 6 well, 6 well suspension) were purchased from Greiner Bio-One (Frickenhausen, Germany). Chamber slides (8 well, 4 well) and glass bottom dishes (Ø 35 mm) suited for immersion microscopy were purchased from ibidi (Gräfelfing, Germany). Sterile Luer-lock syringes, 0.2 µm PES-membrane syringe filters, microcentrifuge tubes (0.2 mL), glass pasteur pipettes, and round Ø12 mm cover glasses were purchased from VWR International (Darmstadt, Germany). Vacuum filtration units with 0.2 µm PES-membrane were purchased from Thermo Fisher Scientific (Waltham, MA, USA).

Table 1: Culture media compositions

Medium / *cell type*	**Components**	**Concentrations**
E8 complete /	DMEM/F12 with L-glutamine and HEPES	1 X
hiPSC	L-ascorbic acid 2-phosphate	64 µg/mL
(maintenance)	Sodium selenite	14 ng/mL
	transferrin	11 µg/mL
	insulin	20 µg/mL
	bFGF	100 ng/mL
	TGF-β	2 ng/mL
TeSR-E8 / *hiPSC*	TeSR-E8 Basal Medium	1 X
(maintenance)	TeSR-E8 Supplement	1 X
mTeSR / *hiPSC*	mTeSR Basal Medium	1 X
(maintenance)	mTeSR Supplement	1 X
MNBM / *hiPSC*	DMEM/F12 without HEPES	0.5 X
(MN differentiation)	Neurobasal	0.5 X
	GlutaMAX	1 X
	N2 Supplement	0.5 X
	B27 or SM1 Supplement	0.5 X
MNDM1 / *hiPSC*	MNBM	1 X
(MN differentiation)	ascorbic acid	0.1 mM
	CHIR99021	3 µM

Table 1 *cont.* **Medium */ cell type***	**Components**	**Concentrations**
	DMH1	2 µM
	SB431542	2 µM
MNDM2 */ hiPSC* *(MN differentiation)*	MNBM	1 X
	ascorbic acid	0.1 mM
	CHIR99021	1 µM
	DMH1	2 µM
	SB431542	2 µM
	purmorphamine	0.5 µM
	all-trans retinoic acid	0.1 µM
MNDM3 */ hiPSC* *(MN differentiation)*	MNBM	1 X
	ascorbic acid	0.1 mM
	purmorphamine	0.1 µM
	all-trans retinoic acid	0.5 µM
	BDNF	10 ng/mL
	GDNF	10 ng/mL
	IGF-1	10 ng/mL
MNDM4 */ hiPSC* *(MN differentiation)*	MNBM	1 X
	ascorbic acid	0.1 mM
	purmorphamine	0.1 µM
	all-trans retinoic acid	0.5 µM
	Compound E	0.1 µM
	BDNF	10 ng/mL
	GDNF	10 ng/mL
	IGF-1	10 ng/mL
SCBM */ hiPSC* *(SC differentiation)*	Advanced DMEM/F12	0.5 X
	Neurobasal	0.5 X
	GlutaMAX	1 X
	N2 Supplement	1 X
	B27 or SM1 Supplement	1 X
SCPM1 */ hiPSC* *(SC differentiation)*	SCBM	1 X
	SB431542	2 µM
	CHIR99021	3 µM
SCPM2 */ hiPSC* *(SC differentiation)*	SCBM	1 X
	SB431542	2 µM
	CHIR99021	3 µM

Table 1 *cont.* **Medium */ cell type***	**Components**	**Concentrations**
	Nrg1	50 ng/mL
	BMP4	15 ng/mL
	DMH1	1 µM
SCPM3 */ hiPSC* *(SC differentiation)*	SCBM	1 X
	SB431542	2 µM
	CHIR99021	3 µM
	Nrg1	50 ng/mL
SCM */ hiPSC* *(SC differentiation)*	DMEM low glucose	1 X
	GlutaMAX	1 X
	FBS	1 %
	Nrg1	200 ng/mL
SCM+ */ hiPSC* *(SC differentiation)*	SCM	1 X
	PDGF-BB	10 ng/mL
SCM+++ */ hiPSC* *(SC differentiation)*	SCM+	1 X
	all-trans retinoic acid	0.1 µM
	PDGF-BB	10 ng/mL
triM */ hiPSC* *(cocultures)*	MNBM	1 X
	ascorbic acid	0.1 mM
	purmorphamine	0.1 µM
	all-trans retinoic acid	0.5 µM
	Nrg1	200 ng/mL
	BDNF	10 ng/mL
	GDNF	10 ng/mL
	IGF-1	10 ng/mL
GM */ C2C12*	DMEM/F12 high glucose, with l-glutamine, without sodium pyruvate	1 X
	FBS	20 %
DM */ C2C12*	DMEM/F12 high glucose, with l-glutamine, without sodium pyruvate	1 X
	horse serum	2 %

Table 2: Components for media preparations

Reagent	Cat. No.	Supplier
Advanced DMEM/F12	12634010	Thermo Fisher Scientific, Waltham, MA, USA
ascorbic acid	3525.1	Carl Roth, Karlsruhe, Germany
B-27 Supplement	17504044 Lot: 2389177	Thermo Fisher Scientific, Waltham, MA, USA
bFGF	GFH146	Cell Guidance Systems, Cambridge, UK
DMEM with GlutaMAX, low glucose	21885025	Thermo Fisher Scientific, Waltham, MA, USA
DMEM/F12 with GlutaMAX, without HEPES	10565018	Thermo Fisher Scientific, Waltham, MA, USA
DMEM/F12 with HEPES	31330038	Thermo Fisher Scientific, Waltham, MA, USA
DMEM/F12 with L-glutamine, without sodium pyruvate, high glucose	D5796	Sigma Aldrich (Merck), Darmstadt, Germany
FBS	S1810-500 Lot: S17448S1810	Biowest, Nuaillé, France
GlutaMAX	35050-038	Thermo Fisher Scientific, Waltham, MA, USA
horse serum	26050088 Lot: 172504	Thermo Fisher Scientific, Waltham, MA, USA
insulin	91077C	Sigma Aldrich (Merck), Darmstadt, Germany
L-ascorbic acid 2-phosphate	A8960	Sigma Aldrich (Merck), Darmstadt, Germany
mTeSR1 Complete Kit	85850	Stemcell Technologies, Vancouver, Canada
N2 Supplement-A	07152 Lot: 1000024021	Stemcell Technologies, Vancouver, Canada
N2 Supplement	17502-048 Lot: 2389235	Thermo Fisher Scientific, Waltham, MA, USA
Neurobasal	21103-049	Thermo Fisher Scientific, Waltham, MA, USA
NeuroCult SM1	05711 Lots: 18L96935, 1000003847, 1000019113, 1000047986	Stemcell Technologies, Vancouver, Canada
Penicillin-Streptomycin	P4333	Sigma Aldrich (Merck), Darmstadt, Germany
progesterone	P8783	Sigma Aldrich (Merck), Darmstadt, Germany
putrescine	51799	Sigma Aldrich (Merck), Darmstadt, Germany
sodium selenite	S5261	Sigma Aldrich (Merck), Darmstadt, Germany
TeSR-E8 Kit	05990	Stemcell Technologies, Vancouver, Canada
TGF-β	GFH39	Cell Guidance Systems, Cambridge, UK

Table 2 *cont.*		
Reagent	**Cat. No.**	**Supplier**
transferrin	T3705	Sigma Aldrich (Merck), Darmstadt, Germany

Table 3: Small molecules for differentiation media

Reagent	Cat. No.	Supplier	Stock conc. prepared
all-trans retinoic acid	72264	Stemcell Technologies, Vancouver, Canada	5 mM
ascorbic acid	A4403	Sigma Aldrich (Merck), Darmstadt, Germany	0.5 M
BDNF	GFH1AF	Cell Guidance Systems, Cambridge, UK	50 µg/mL
BMP4	120-05	Peprotech, Hamburg, Germany	0.1 mg/mL
CHIR99021	4423 SML1046	Tocris (Bio-Techne), Wiesbaden, Germany Sigma Aldrich (Merck), Darmstadt, Germany	10 mM
DMH1	S7146	Selleck Chemicals, Planegg, Germany	20 mM
Forskolin	SM18-2	Cell Guidance Systems, Cambridge, UK	4 mM
GDNF	GFH2AF	Cell Guidance Systems, Cambridge, UK	50 µg/mL
Heregulinβ-1 (Nrg1)	100-03	Peprotech, Hamburg, Germany	1 mg/mL
IGF-1	AF-100-11	Peprotech, Hamburg, Germany	50 µg/mL
PDGF-BB	AF-100-14B	Peprotech, Hamburg, Germany	0.1 mg/mL
purmorphamine	SM30-5 72204	Cell Guidance Systems, Cambridge, UK Stemcell Technologies, Vancouver, Canada	5 mM
SB431542	SM33-10	Cell Guidance Systems, Cambridge, UK	20 mM
Valproic acid	P4543	Sigma Aldrich (Merck), Darmstadt, Germany	250 mM
γ-Secretase Inhibitor XXI, Compound E	565790	Merck Millipore, Darmstadt, Germany	1 mM

Table 4: Other cell culture reagents

Reagent	Cat. No.	Supplier
Accumax solution	A7089 00-4666-56	Sigma Aldrich (Merck), Darmstadt, Germany Thermo Fisher Scientific, Waltham, MA, USA
DMSO	A994.1	Carl Roth, Karlsruhe, Germany
Dulbecco's Phosphate Buffered Saline (PBS)	D8537	Sigma Aldrich (Merck), Darmstadt, Germany
EDTA ultrapure 0.5 M	15575020	Thermo Fisher Scientific, Waltham, MA, USA
EZ-LiFT Stem Cell Passaging Reagent	SCM139	Sigma Aldrich (Merck), Darmstadt, Germany
Geltrex LDEV-free hESC-qualified	A14133-02	Thermo Fisher Scientific, Waltham, MA, USA

Table 4 ***cont.***

Reagent	Cat. No.	Supplier
Laminin 521 (rh)	LN521-05	BioLamina, Sundbyberg, Sweden
Matrigel hESC-qualified	354277	Corning, Corning, NY, USA
NT-3	450-03	Peprotech, Hamburg, Germany
PluriSTEM Dispase-II	SCM133	Sigma Aldrich (Merck), Darmstadt, Germany
Poly-L-Lysine hydrobromide	P2636	Sigma Aldrich (Merck), Darmstadt, Germany
Resveratrol	72862	Stemcell Technologies, Vancouver, Canada
Stempro accutase	A1110501	Thermo Fisher Scientific, Waltham, MA, USA
TrypLE Express Enzym	12605028	Thermo Fisher Scientific, Waltham, MA, USA
Trypsin 0.5 % - 0.2 % EDTA	59418C	Sigma Aldrich (Merck), Darmstadt, Germany
Y-27632	SM02	Cell Guidance Systems, Cambridge, UK

2.1.3 hiPSC culture and expansion

Cultures of hiPSC lines were kept in feeder-independent conditions in suited media formulations, namely mTeSR, TeSR-E8 or self-made E8 medium (see Table 1 and Figure 2-1). Cell lines WC035i-SOD1-D90D and WC034i-SOD1-D90A were kept in mTeSR medium, all other lines were cultured in TeSR-E8 or E8 medium. Culture media were never warmed in a water bath, but only prewarmed at RT before medium changes, and aliquots of complete medium were not used for longer than 14 days after preparation. At least one day before seeding cells, sterile multiwell tissue culture plates with 6 wells (Greiner Bio-One Cellstar cat. no. 657 160) were coated with 1 mL of basement membrane matrix coating solution per well. To prepare coating solution, Geltrex (LDEV-free, hESC-qualified, growth factor reduced) was thawed slowly on ice, and diluted 1:100 in ice-cold DMEM/F12 medium directly before use. Plates were then sealed with parafilm and stored at 4 °C, at least overnight, but at maximum for 14 days. Coating solution was aspirated from wells directly before seeding cells, and coating solution was reused to coat more well plates, but for a maximum of 3 uses or 14 days in total. For routine maintenance culture of hiPSC, medium was changed daily, and cultures were microscopically inspected daily to monitor confluence, stem cell morphology, and spontaneous differentiation.

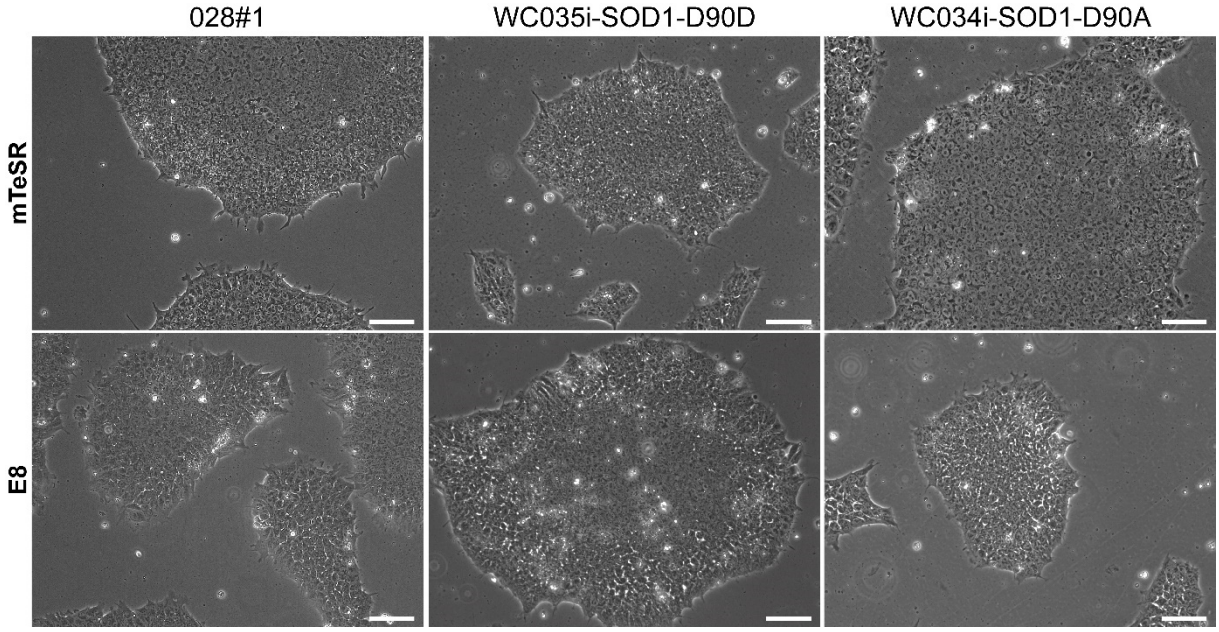


Figure 2-1: hiPSC culture. Representative phase contrast images of undifferentiated hiPSC colonies in maintenance culture for three of the hiPSC lines used in this study, as indicated above image panels, in mTeSR or E8 medium, as indicated right of the panels. Scale bars: 100 µm.

For subcultivation, cultures were routinely split upon reaching 80 – 90 % of confluence. To maintain cultures without expanding them or to purify them from low levels of differentiation, non-enzymatic EDTA splitting technique was used. To this end, wells were initially washed 1 – 2 times with 3 mL PBS per well at RT to remove dead cells and cell debris. After aspiration of PBS, 0.5 mL of 0.05 mM EDTA solution was added to each well and incubated for 4 min at RT, leaving the plate undisturbed in the cell culture cabinet. Subsequently, EDTA solution was aspirated, and a portion of cell colonies were dissociated from the well by manually washing them down using a P1000 micropipette and culture medium. Colonies were dissociated to small cell aggregates by manually triturating 1 – 2 times, but care was taken to not dissociate colonies into single cells. The cell suspension was then transferred to a fresh well which had been incubated at 37 °C with seeding medium to warm up, and cells were passaged like this at an approximate splitting ratio of 1:5 to 1:8. HiPSC lines cultured in E8 were supplemented with 5 µM of the ROCK inhibitor Y-27632 to prevent dissociation-induced and therefore improve viability of dissociated stem cells, while Y-27632 was not used for cell lines split in mTeSR medium. If Y-27632 was used, it was removed with the next medium change, and was never used longer than 24 h. If cultures should be expanded, EDTA splitting was done as described above but incubation of EDTA solution was prolonged to 6 min. After aspiration, all cells were washed down from the well and replated at a 1:6 ratio. If cultures showed differentiation levels above 5 – 10 % which were not recovered after 2 – 3 maintenance EDTA splits, cultures were either discarded and started with a fresh cryovial, or alternatively they were split using EZ-LiFT reagent instead of EDTA to remove differentiated cells. In that case,

wells were split at 70 – 80 % confluence. EZ-LiFT reagent as well as seeding medium was prewarmed to 37 °C before splitting. Then, culture medium was aspirated, and cells were washed twice with 1.5 mL of EZ-LiFT reagent, aspirating after each washing step. After washing, 1 mL EZ-LiFT reagent was added per well and incubated at 37 °C. After 4 min, the plate was removed from the incubator, and the bottom of the plate was tapped rapidly to loosen cell aggregates, before putting the plate back at 37 °C. After additional 4 min of incubation, plates were again tapped, and then inspected using a phase contrast microscope. Usually, floating cell clumps were observed at this step, but if not, the incubation step was repeated until detached clumps became visible. The split reagent containing floating cell clumps was collected into a 15 mL conical polypropylene tube with a P1000 micropipette very gently to not disturb still attached cells, and pelleted by centrifuging at 150 ×g for 3 min. After centrifugation, the supernatant was carefully taken off manually and discarded, cells were resuspended in culture medium, and distributed to prepared wells at a 1:3 to 1:6 ratio. When cultures recovered and reverted to differentiation-free cultures, routine splits were done with the EDTA method again.

To freeze cell vials, the EDTA method was used as for expanding cultures, and all cells were collected in a 15 mL conical polypropylene tube. Cells were then centrifuged at 300 ×g for 4 min, and the supernatant was aspirated. The pellet was resuspended in chilled culture medium supplemented with 10 % DMSO and 10 µM Y-27632. Cell suspension was then distributed into cryovials at a ratio of 1 well per 1 cryovial, and vials were frozen at a controlled cooling rate using cell-freeze containers at -80 °C. For long-term storage, cryovials were transferred to liquid nitrogen. To thaw cells, cryovials were recovered from liquid nitrogen and thawed rapidly by gently swirling in a waterbath at 37 °C until only a small lump of ice was left in the vial. Pre-warmed culture medium was then added dropwise into the vial, before gently transferring the cell suspension into a 15 mL conical polypropylene tube with 10 mL of culture medium or DMEM/F12 medium at 37 °C. The cell suspension was then centrifuged at 300 ×g for 4 min to pellet and the supernatant was discarded. Cells were resuspended in culture medium and seeded at a ratio of 1 cryovial per well into coated wells of a 6-well plate. After thawing, culture medium was supplemented for 24 h with Y-27632 at 5 µM or 10 µM depending on the cell line. For cell lines WC035i-SOD1-D90D and WC034i-SOD1-D90A, no Y-27632 was used for plating in mTeSR. Only hiPSC cultures exhibiting well-defined, compact colonies with typical stem cell morphology and less than 5 % of differentiation were used for cryopreservation and experiments. Before inducing directed differentiation, hiPSC cultures were split at least 2 times after thawing to recover.

2.1.4 Differentiation of hiPSC-derived motoneurons

Motoneurons were differentiated from hiPSCs based on published protocols [Du et al., 2015; Yi et al., 2018] with slight modifications [Hörner et al., 2021]. The base medium for all motoneuron differentiation media, MNBM, consisted of an equal parts mixture of DMEM/F12 and Neurobasal media, which was supplemented with GlutaMAX as well as B27 and N2 supplements as described in Table 1. Two days before induction of differentiation, hiPSC were split into Geltrex-coated 6-well plates as described in section 2.1.3. When cultures reached 30 – 40 % confluence, which was usually about 48 h later, hiPSC culture medium was changed to MNDM1 medium containing ascorbic acid, CHIR99021, SB431542, and DMH1 as described in Table 1, to start neural induction of cells, therefore defining day 0 of differentiation. For differentiations starting from cell monolayers described in section 3.1, 80 – 90 % confluent hiPSC cultures were singularized with TrypLE Express enzyme and seeded at a 3:2 well ratio in hiPSC medium containing 10 µM ROCK inhibitor Y-27632 to create homogenous, confluent cell layers. Culture medium was switched to MNDM1 the next day. Culture medium was changed daily with fresh MNDM1, and the volume of medium used was gradually increased from 2 mL on the first day to 4 – 5 mL on the fifth day, to prevent acidification of medium as cultures became increasingly dense up to day 6. On day 6 of differentiation, cultures were detached and singularized using accutase, which was prewarmed to RT before. The culture medium was aspirated, 1 mL of accutase enzyme solution was added per well and incubated for 5 – 10 minutes at room temperature, until the cell layers started to break up and cells detached upon gently tapping the plate. Then, 1 mL of MNBM (Table 1) was added to each well, and cells were detached from the plate by washing with a P1000 micropipette. The cell suspension was collected in a 15 mL polypropylene tube and centrifuged at 300 ×g for 4 min. Cells were then resuspended in MNDM2 containing ascorbic acid, CHIR99021, DMH1, SB431542, purmorphamine, and retinoic acid, as described in Table 1. Additionally, the medium was supplemented with 10 µM Y-27632 for plating. Cells were distributed into Geltrex-coated 6-well plates at a 1:6 split ratio and with 2 mL medium volume per well. The next day, culture medium was changed to MNDM2 without Y-27632, and subsequently, medium was changed daily with 2 mL MNDM2 per well. If needed, medium volume was increased to 3 – 4 mL per well approaching day 12. On day 12 of differentiation, cells were split into floating culture. To this end, the culture medium was aspirated, and wells were washed with 2 mL of PBS per well. After aspirating the PBS, 1 mL of dispase-II solution, prewarmed to room temperature, was added to each well. Plates were then incubated at 37 °C. After 5 min of incubation, plates were checked under the microscope with a 5× magnification objective. If cells were starting to round and small holes started to appear in the cell layer, plates were taken back to the biosafety cabinet to proceed, otherwise, the plate was put back at 37 °C for

3 more min. Then, dispase solution was aspirated, and wells were washed carefully two times with 2 mL PBS per well each time, before washing down cells using a P1000 micropipette in medium. At this step, cells were not singularized, but detached from the plate with as little pipetting steps as possible to leave cells in small aggregates. As medium, MNDM3 containing ascorbic acid, purmorphamine, retinoic acid, BDNF, GDNF, and IGF-1 as described in Table 1 was used with additional supplementation of 5 µM Y-27632. The cell suspension was then transferred into 6-well suspension culture plates, which have a hydrophobic, not tissue culture treated surface (Greiner Bio-One Cellstar cat. no. 657 185), at a split ratio of 1:2 wells, and in a medium volume of 4 mL per well. The next day, medium with cell aggregates was collected from the plates into a 15 mL polypropylene tube. If cell aggregates had settled and adhered to the bottom of the plate, they were gently washed off by pipetting. The cell aggregates were allowed to settle in the conical tube, and after 2 – 3 minutes, the medium was carefully removed. Cell aggregates were then resuspended without breaking them apart in MNDM3 without Y-27632, and then transferred back into the suspension plate in a volume of 5 mL medium per well. Subsequently, a 50 % partial medium change was done every other day, by carefully removing and adding medium directly from the wells manually without removing cell aggregates. If cell aggregates adhered to the bottom or clumped together, they were gently detached or broken up by pipetting. On day 18 of differentiation, cell aggregates were dissociated and seeded for terminal differentiation. One day prior, laminin-coated 6-well plates were prepared for the terminal differentiation seeding. To this end, a sterile poly-l-lysine (PLL) solution was prepared in ultrapure water at a concentration of 0.1 mg/mL. For each well to be coated, 2 mL of the PLL solution were added, and plates were incubated for 1 – 2 h at RT inside the biosafety cabinet. Then, PLL solution was aspirated, and wells were washed two times with 2 mL of cold ultrapure water each. Wells were then allowed to dry completely by leaving well lids open under sterile airflow inside the biosafety cabinet. Then, laminin coating solution was added at 1 mL per well. If cover glasses were placed inside the wells, 1.5 mL of coating solution were added. The coating solution was prepared in DMEM/F12 medium with human recombinant laminin isoform 521 at a concentration of 5 µg/mL. Plates were sealed with parafilm and incubated at 4 °C overnight. The next day, before seeding cells, plates were placed in the incubator at 37 °C for 15 min – 1 h. Then, coating solution was aspirated before adding culture medium or cell suspension to the well. Coated wells were not allowed to dry before adding media or cells. To prepare cells for terminal differentiation seeding, all cell aggregates were collected on day 18 and 1 – 4 wells were pooled in a 15 mL conical polypropylene tube. Again, aggregates were allowed to settle to the bottom of the tube, and medium was removed with a pipette. Then, 10 mL PBS were added, and the tube was mixed by gently inverting 2 – 3 times. After aggregates had settled again, the PBS was removed and 1 – 3 mL of accumax solution was added (depending on how many aggregates were pooled).

accumax solution had been prewarmed to RT. Cell aggregates were incubated in the accumax solution at RT and every 3 – 5 minutes, the suspension was triturated using a P1000 micropipette. This process was repeated until the solution appeared as a turbid single cell suspension and no cell aggregates were visible by eye anymore. Then, cells were pelleted by centrifugation at 300 ×g for 4 min, and the supernatant was removed. Cells were gently resuspended in MNDM4, containing ascorbic acid, purmorphamine, retinoic acid, BDNF, GDNF, IGF-1, and Compound E, as described in Table 1. Additionally, MNDM4 was supplemented with 10 µm Y-27632 for plating. Then, cells were seeded into laminin-coated plates prepared as described above at a split ratio of 1:1 – 1:3, and in a medium volume of 2 mL MNDM4 per well. On the following day, medium was changed to MNDM4 without Y-27632. After that, a partial medium change of 75 % was done every other day. A schematic depiction of this differentiation protocol timeline including differentiation stages and culture conditions is shown in Figure 2-2.

If motoneurons were differentiated for 3D cultures, they were not dissociated into single cells on day 18 but were cultured as neurospheres in MNDM3 up to day 30 at maximum. Between day 20 and day 30 of differentiation, neurospheres could be collected to 3D cultures as described in sections 2.1.8 and 2.1.9. As for general hiPSC culture, all culture media were never warmed in a water bath, but only prewarmed at RT before medium changes, and aliquots of complete medium were not used for longer than 14 days. Aliquots of retinoic acid as well as media containing retinoic acid, i.e., MNDM3 and MNDM4, were protected from light at all times. Therefore, aliquots were kept in lightproof tubes, and direct light was switched off when changing culture medium.

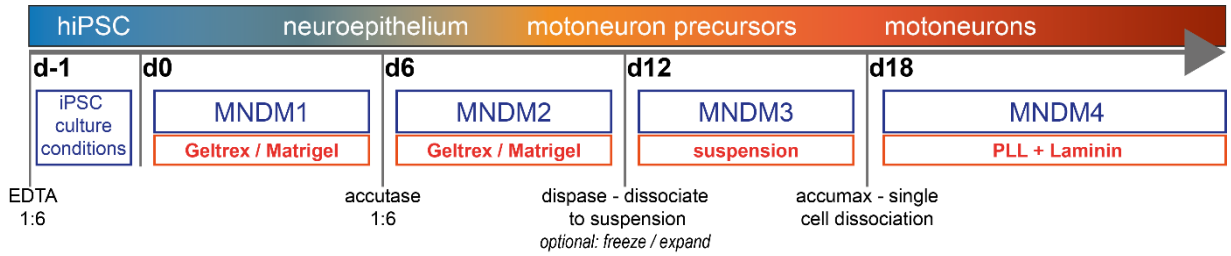


Figure 2-2: Motoneuron differentiation protocol. Schematic depiction of hiPSC-motoneuron differentiation protocol stages, timeline, and culture conditions. Differentiation stages of cells and time points are indicated in the timeline on top. Starting with hiPSC cultures on day 0 of differentiation (d0), cells developed towards neuroepithelial identity first, which was present after around 6 days of differentiation culture. After around 12 days, cells had differentiated into motoneuron precursors which could be expanded and frozen. After a subsequent suspension culture phase of 6 days, immature motoneurons were obtained, which were further matured in adherent culture under terminal differentiation conditions. Boxes show differentiation media (in blue) and plate coating (in red) conditions as described in the main text. Passage timepoints and techniques are indicated below. MNDM = motoneuron differentiation medium, PLL = poly-L-lysine.

For some experiments, cells were not split into floating culture on day 12 but expanded in the motoneuron precursor stage and/or cryopreserved, as described in section 3.1. To expand precursor cells, day 12 cultures were split with accutase as described for day 6 and plated in MNDM2 medium additionally containing 0.5 mM valproic acid. Cultures were maintained for another six days in this medium, and were then either expanded for one more passage, or split into suspension as described above. If precursor cells were cryopreserved, they were detached on day 12 with accutase as described above but resuspended in chilled MNBM (Table 1) containing 10 µM Y-27632 and 10 % DMSO. Per cryovial, 1 mL of cell suspension containing cells harvested from 1 – 2 wells were frozen at a controlled cooling rate using cell-freeze containers at -80 °C. For long-term storage, cryovials were transferred to liquid nitrogen. To recover frozen cells, vials were thawed rapidly by gently swirling in a waterbath at 37 °C until only a small lump of ice was left in the vial. Pre-warmed MNBM was then added dropwise into the vial, before gently transferring the cell suspension into a 15 mL conical polypropylene tube with 10 mL of MNBM medium at 37 °C. Cells were pelleted by centrifugation at 300 ×g for 4 min and resuspended in MNDM2 additionally containing 10 µM Y-27632 and 0.5 mM valproic acid. Cells of one cryovial were plated into one well of a Geltrex-coated 6-well plate in 2 mL of medium. The next day, medium was changed to MNDM2 containing valproic acid, but without Y-27632. Subsequently, medium was changed daily, and cultures were maintained for 2 – 5 days until cells had formed a dense, confluent cell layer. Then, cells were either expanded or split into suspension as described above.

2.1.5 Differentiation of hiPSC-derived Schwann cells

Schwann cells were differentiated from hiPSCs based on the protocol published by Kim et al. [2017] with modifications as described in this work and published in Hörner et al. [2021; 2022]. Before induction of differentiation, hiPSC were split into Geltrex-coated 6-well plates as described in section 2.1.3. When cultures reached 40 – 60 % confluence, which was usually about two or three days later, hiPSC culture medium was changed to the first medium of the Schwann cell differentiation protocol, defining day 0 of differentiation. The base medium for Schwann cell differentiation media used in the first protocol phase up to the Schwann cell precursor stage at day 24 was SCBM, consisting of an equal parts mixture of Advanced DMEM/F12 and Neurobasal media, which was supplemented with GlutaMAX as well as B27 and N2 supplements as described in Table 1. The first differentiation medium, SCPM1, was SCBM supplemented with differentiation factors SB431542 and CHIR99021 as described in Table 1. Cultures were kept in SCPM1 from day 0 to day 6 of differentiation with daily medium changes, using 2 mL of medium per well of a 6-well plate on day 0 of differentiation, and increasing the medium volume to 4 mL per well as cultures increased in cell density. On day 6

of differentiation, cultures were split using accutase as described for motoneuron differentiation in section 2.1.4 but using SCBM to detach cells after incubation. The collected cell suspension was centrifuged at 300 ×g for 4 min and the cell pellet was then resuspended in SCPM2, consisting of SCBM supplemented with SB431542, CHIR99021, Nrg1, BMP4, and DMH1, at concentrations specified in Table 1. Additionally, the medium was supplemented with 10 µM Y-27632 for 24 h. The cell suspension was distributed into Geltrex-coated 6-well plates prepared as described in section 2.1.3 at a split ratio of 1:10. Culture medium was changed daily with 2 mL of SCPM2 per well for the following six days. On day 12 of differentiation, cells were split again with accutase as described before, but at a 1:6 plating ratio using SCPM3, consisting of SCBM supplemented with SB431542, CHIR99021, and Nrg1, as described in Table 1, and additionally supplemented with 10 µM Y-27632 for 24 h after plating. Cultures were then maintained in SCPM3 with medium changes every other day until day 24, with another 1:6 accutase split on day 18. From day 24 on, SCM was used as base medium, which consisted of DMEM medium with low glucose concentration (1 g/L) supplemented with GlutaMAX, fetal bovine serum (FBS) and Nrg1 (Table 1). Cultures were split on day 24 with accutase at a ratio of 1:3 – 1:6, depending on culture density, and seeded in SCM+++, which consisted of SCM additionally supplemented with forskolin, retinoic acid, and PDGF-BB as described in Table 1, and additionally 10 µM Y-27632 for 24 h after plating. Cultures were kept in SCM+++ for 4 days with medium changes on days 25 and 27, using 2 mL of medium per well. On day 28, culture medium was switched to SCM+, which consisted of SCM supplemented with PDGF-BB, but without forskolin and retinoic acid (Table 1). Two days later, on day 30 of differentiation, cultures were switched to SCM only supplemented with FBS and Nrg1. Cells were kept in SCM for expansion and were passaged using accutase at a 1:3 ratio upon reaching confluency. If possible, culture confluency was kept above 40 %, as increased cell death was observed in low density cultures. Like this, cells could be maintained until at least day 100 of differentiation. A schematic depiction of the differentiation protocol timeline including differentiation stages and medium conditions is shown in Figure 2-3. Cryopreservation was done at any passage after day 40 as described for motoneuron precursors (2.1.4), using SCM without Nrg1, but supplemented with 20 % FBS and 10 % DMSO as freezing medium. Frozen cells were recovered in SCM supplemented with 10 µM Y-27632 for 24 h after thawing. The first Schwann cell differentiation experiments were done without addition of BMP4 and DMH1 from day 6 to day 12 as described in the Results section 3.1.3. All other modifications of the protocol for individual experiments, such as addition of further factors or differing split timepoints, are described in section 3.1.4. Medium composition and culture conditions for maturation experiments are described in the results section 3.1.5.

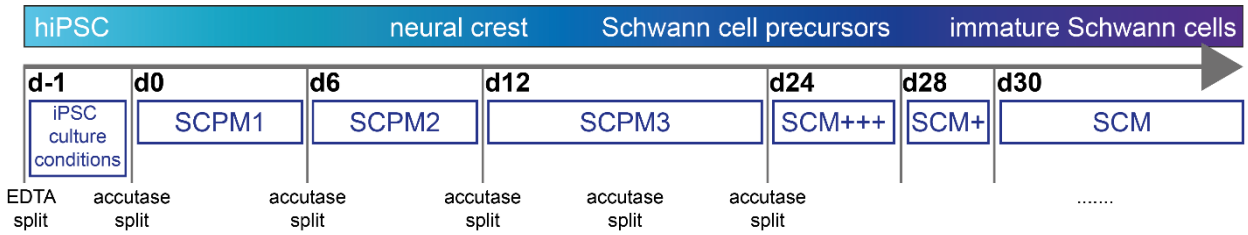


Figure 2-3: Schwann differentiation protocol. Schematic depiction of hiPSC-Schwann cell differentiation protocol stages, timeline, and medium conditions. Differentiation stages of cells and time points are indicated in the timeline on top. Starting with hiPSC cultures on day 0 of differentiation (d0), cells developed through a neural crest identity stage present after around 12 days of differentiation. From day 24 onwards, Schwann cell precursors could be detected, which differentiated further into immature Schwann cells, present after around 30 – 40 days in total. Further culture time was needed for maturation of cells. Boxes in blue show differentiation media for the sequential phases and defined passaging timepoints for the first 24 days are indicated below. After that, cells were passaged depending on culture confluency as described in the main text. SCPM = Schwann cell precursor medium, SCM = Schwann cell medium.

2.1.6 C2C12 culture

C2C12 murine myoblasts were routinely cultured in 100 mm diameter tissue culture dishes (cat. no. 664 160, Greiner bio-one, Frickenhausen, Germany) using C2C12 growth medium (GM) consisting of DMEM/F12 (high glucose, with L-glutamine, with sodium bicarbonate, without sodium pyruvate) supplemented with 20 % FBS. Cultures were never allowed to grow beyond 60 % of confluence and were usually passaged every other day. Medium and split reagents were warmed to 37 °C before medium change or passaging. To split cultures, the culture medium was aspirated, and dishes were washed 2 times with 5 mL of PBS per wash. Then, 2 mL of 0.25 % trypsin solution was added, and dishes were incubated at 37 °C for approximately 3 min, until cells were dissociated. The cell suspension was collected into a 15 mL conical polypropylene tube with 6 mL warmed GM and centrifuged at 400 ×g for 4 min. Subsequently, the supernatant was aspirated, and cells were resuspended in fresh GM. The cell suspension was transferred into fresh dishes and seeded at a split ratio of 1:10 or a cell density of 10,000 cells/cm². The cell number was determined by manual counting using a Neubauer cell counting chamber slide or by automated cell counting (Vi-CELL XR, Beckman Coulter, Brea, CA, USA). For cryopreservation, cells were routinely split and resuspended in chilled GM supplemented with 10 % DMSO. A number of 0.6×10^6 cells was frozen per cryovial. To thaw, vials were thawed rapidly in a waterbath at 37 °C, resuspended in 10 mL GM per vial, and centrifuged at 400 ×g for 4 min. Pellets were resuspended in fresh GM and plated at 0.6×10^6 cells (1 cryovial) per dish. To differentiate C2C12 myoblasts into myotubes, cells were split with trypsin as described but seeded into either 6-well tissue culture plates or chamber slides (µ-Slide 4 well, cat. no. 80426, or µ-Slide 8 well, cat. no. 80826; ibidi, Gräfelfing, Germany) at a density of 0.8×10^5 – 1×10^5 cells/cm² in GM. The day after, it was checked if cultures reached 100 % confluence, and then medium was changed to differentiation medium

(DM), which was supplemented with 2 % horse serum instead of 20 % FBS, to induce differentiation. Subsequently, cells were not split anymore, culture medium was changed every other day, and cultures were monitored daily to check myotube differentiation. In Figure 2-4, fusion of C2C12 cells increasing with time cultured in DM can be observed. Appearance of myotubes was usually seen 3 days after induction, and spontaneous contractions were observed in many cultures starting 4 – 5 days after induction. For all experiments, only cells with a passage number lower than 20 were used, and similar passage numbers were used for experiment replicates. As passage number seemed to have a noticeable effect on nAChR cluster formation, data from experiments with identical passage numbers of C2C12 at time point of differentiation induction were used for quantitative analysis of nAChR clusters.

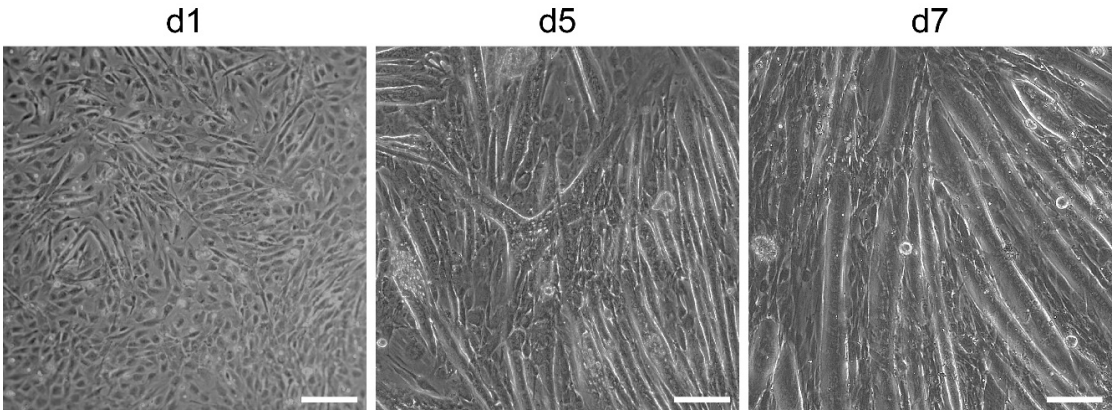


Figure 2-4: Differentiation of C2C12 myoblasts to myotubes. Representative phase contrast images of C2C12 cultures differentiated as described, at 1 day (d), 5 days, and 7 days after switching cultures to DM (differentiation medium). Time points are indicated above images. Scale bars: 100 µm.

2.1.7 2D cocultures

To generate cocultures, C2C12 were seeded at 0.8×10^5 – 1×10^5 cells/cm² into 6-well tissue culture plates coated with Geltrex, prepared beforehand as described in section 2.1.3, and differentiation was induced the next day by switching to DM as described in section 2.1.6. Next, 24 h later, hiPSC-derived motoneurons and/or Schwann cells prepared as described in sections 2.1.4 and 2.1.5 were seeded onto C2C12 cultures. For motoneurons, predifferentiated neurospheres cultured in MNDM3 were dissociated and seeded as described for motoneuron differentiation. Differentiated Schwann cells were cultured in SCM as described and dissociated with accutase. Schwann cells between days of differentiation 50 – 80 were used for cocultures. If tricultures containing both cell types were seeded, motoneurons and Schwann cells were dissociated in parallel and mixed in the plating medium. For motoneuron / Schwann

cell cocultures without C2C12, dissociated cells were plated together into wells coated with laminin as described for terminal motoneuron differentiation. All cocultures were plated in triculture medium (triM) supplemented with 10 µM Y-27632. 24 h after plating, medium was replaced with fresh triM without Y-27632. Thereafter, medium was changed partially every other day by carefully replacing 75 % of medium volume with fresh medium to not disturb the cell layer.

2.1.8 3D cultures in gelatin mesh

For 3D culture experiments which used manually seeded gelatin scaffolds, sterile Scaffolene (cat. no. CL100, Freudenberg, Weinheim, Germany) was used, which is a nonwoven fiber material manufactured by rotatory spinning of collagen polymers. Thin strips of this material were cut with sterilized scissors and placed in 6-well tissue culture plates. To immobilize Scaffolene strips in wells and prevent free floating in culture medium, different approaches using magnets or Velcro strips were tried[1]. Data shown in the results section (3.2.3) were obtained using self-adhesive Velcro strips (cat. no. AC-2002, Klettshop24.de, Heidesee, Germany) to fix Scaffolene strips to the bottom of culture wells. Two pieces of adhesive Velcro were glued to the bottom of the plate at a distance of the width of the Scaffolene strip to be placed. Wells including Velcro strips were incubated in 70 % ethanol for 1 – 2 h at RT to sterilize. Subsequently, wells were washed with sterile ultrapure water for at least 3 × 10 min and allowed to dry under sterile airflow inside the biosafety cabinet. To store plates for later use, lids were sealed with parafilm. To fix Scaffolene inside wells, each end of a Scaffolene strip was pushed into the Velcro hooks using sterilized forceps, using the Velcro as anchor points at both sides of the Scaffolene strip. Immediately before cells were added, culture medium was added drop-wise directly onto the Scaffolene until no dry spots were visible anymore on the fiber material. C2C12 were harvested upon passaging as described in section 2.1.6, whereby cells collected from one dish were resuspended in 300 µL of prewarmed GM after pelleting and then pipetted directly onto the Scaffolene. Another 500 µL of GM were added to the bottom of the well, so that the Scaffolene strip was not covered, but was prevented from drying out. Plates were then incubated at 37 °C for 1 h to allow cells to settle into the scaffold. Then, another 2.5 mL of GM prewarmed at 37 °C was added per well, to submerge cell-laden scaffolds. To induce differentiation of C2C12, culture medium was changed to DM the next day. Another 48 h later, neurospheres were added for coculture. To this end, neurospheres prepared as described in section 2.1.4 were collected from suspension culture,

[1] Contribution from Madleine Grob, see Table 12: Contributions from other persons, p.157

transferred to a 15 mL conical polypropylene tube, and were allowed to settle to the bottom of the tube. Medium supernatant was removed carefully, and neurospheres were resuspended gently in triM containing 10 µM Y-27632, using a medium volume of 600 µL per neurosphere well collected. Then, culture medium was carefully aspirated from wells containing C2C12 cells in Scaffolene strips. For each strip, 200 µL of neurosphere suspension were pipetted onto the strips, placing the neurospheres on top of the scaffolds. Again, 500 µL of culture medium were added to the bottom of each well, and plates were incubated at 37 °C for 1 – 2 h, before submerging all scaffolds in culture medium, adding another 2.5 – 3 mL of triM per well. After 24 h, medium was removed and replaced with fresh triM without Y-27632. Subsequently, medium was changed partially every other day by renewing 50 % of the culture medium per well. Scaffolds were fixed with 4 % PFA after 10 days of coculture.

2.1.9 3D-bioprinting

Suppliers and catalogue numbers of materials used for 3D-(bio)printing specifically are listed in Table 5. For 3D cultures created by bioprinting of hydrogels, three different print models were designed (Figure 2-5). The exact dimensions of the printed design were as follows. The design shown in Figure 2-5A measured 7 mm in length, 2.5 mm in width, and 3.75 mm in height. Each of the two pocket structures measured 6 mm in length, 0.5 mm in width, and were 3.5 mm deep. The spacing between the two pocket structures as well as between each pocket and the outer wall was 0.5 mm. The design shown in Figure 2-5B measured 11 mm in length, 8.7 mm in width, and 0.5 mm in height; with spacings of 0.5 mm between print strands. Regarding the design shown in Figure 2-5C, the outer diameter of the silicone support structure measured 34.2 mm. The two pillar structures which served as anchor points for the hydrogel print were 3 mm high, 2 mm wide, and spaced 5 mm apart from each other. The hydrogel structure itself, which was printed onto the silicone support structure, measured 10 mm in length, 4 mm in width, and 1.5 mm in height regarding the outer dimensions. The pocket structure in the middle measured 4 mm in length, 3 mm in width, and was 1 mm deep. To produce CAD designs, corresponding stl files, and graphic depictions as shown in the upper panel of Figure 2-5, the programs Fusion 360 (version 2.0.14793, Autodesk, San Francisco, CA, USA), 3D Builder (version 18.0.1931.0, Microsoft Corporation, Redmond, WA, USA), and Creo (version 6.0, PTC, Boston, MA, USA) were used.[2] The silicone support structures for the print design shown in Figure 2-5C were 3D-printed using a 3D-Bioplotter (Manufacturer series, cat. no. BIO-01-1002, EnvisionTEC, Gladbeck, Germany) equipped with a low temperature print head (cat. no. BIO-00-2021, EnvisionTEC, Gladbeck, Germany). The software PerfactoryRP (version 3.2.3594.1909 EnvisionTEC, Gladbeck, Germany) and VisualMachines (version 2.10.130r13 Infotech AG, Solothurn, Switzerland) were used to prepare the sliced stl

file for printing and execution of the printing process at the 3D-Bioplotter, respectively. As material, medical grade UV-curable silicone was used, which was prepared by mixing silicone and catalyst in a 50:1 ratio either the same day or the day before. The silicone mixture was loaded into 30 mL cartridges and stored at RT protected from light until printing. The material was extruded through a 22G conical nozzle (inner diameter 410 µm) with a pressure of 180 kPa at a printing speed of 3 mm/s. After the printing process, silicone prints were photocured under 365 nm UV light for 30 min.[2] Before use as support structures for hydrogel prints, silicone parts were sterilized by autoclaving, dried, and transferred into 6-well plates under sterile conditions. All hydrogel prints were done on a BIO X bioprinter (cat. no. D16110020717, Cellink, Gothenburg, Sweden) equipped with pneumatic printheads (cat. no. 000000020340, Cellink, Gothenburg, Sweden) using DNA Studio software (version 2.0, Cellink, Gothenburg, Sweden). Structures as shown in Figure 2-5A were printed into 4-well ibidi chamber slides, structures as shown in Figure 2-5B were printed into 12-well culture plates, and structures as shown in Figure 2-5C were printed into 6-well culture plates. Prints

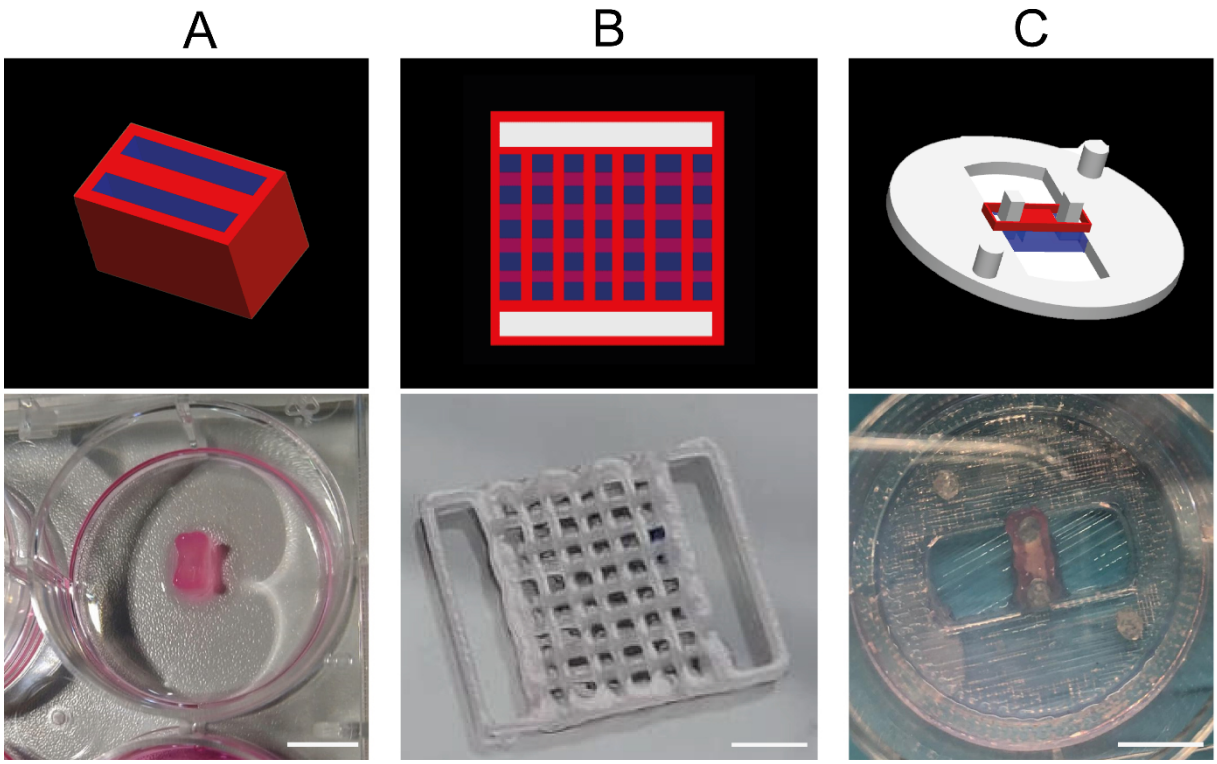


Figure 2-5: 3D-bioprinting designs. Upper panels show three different CAD-modeled designs used in this work. Structures shown in red depict parts printed with hydrogel, either without (**A**) or with (**B**, **C**) cells mixed into the gel. Structures shown in blue were printed using non-crosslinkable support gel, which was washed out subsequently, to create pocket structures. White represents support structures made from non-biological material. Lower panels show photographs of printed hydrogel structures. The lower panel of (**A**) shows a print without cells added yet but incubated in culture medium. (**B**) shows a print made with test gel beforehand without addition of cells or medium. (**C**) shows a printed structure with integrated C2C12 cells in the hydrogel (reddish color) suspended on a support structure made of transparent silicone, and neurospheres (whitish structure in the middle) added into a pocket structure after printing; after several days of culture. Scale bars: 10 mm (**A**, **C**), 2.5 mm (**B**).

were produced either directly from the stl files, or by generating G-codes from stl files using the BIO X software which were then manually adapted using Text Build (version 3.2.2, Sublime HQ Pty Ltd, Sydney, Australia) or Visual Studio Code (version 1.63.2, Microsoft Corporation, Redmond, WA, USA).[2] Before experiments, execution of G-codes and resulted printing paths were simulated in 3D using CAMotics (version 1.2.0, Joseph Coffland).[2] Printing designs were tested first without cells and in non-sterile conditions using colored XPLORE bioink to adapt printing parameters and design properties.[2] For experiments, GelXA bioink was used as hydrogel, which is based on gelatin methacryloyl with a methacrylation degree of 45 – 55 %. It furthermore includes xanthan gum and alginate as well as the photoinitiator LAP, which serves to assist crosslinking of the gel post-printing via UV light. Alternatively, GelXA can be ionically crosslinked with a calcium chloride solution, however, in all experiments described in this work, photocuring was used as crosslinking method. Before an experiment, the printing chamber of the BIO X was sterilized by wiping with 70 % ethanol and UV-C light. The printing process was carried out under sterile conditions employing the BIO X' clean chamber mode with HEPA filtered airflow. Materials were prepared under sterile conditions in a separate biosafety cabinet and then transported to the bioprinter inside a sterile, closed container. Single-use amber UV-shielding cartridges were sterilized by autoclaving and loaded with the desired amount of hydrogel, which was taken out of the fridge 1 h before to acclimatize at RT.

If cells were mixed into the hydrogel before printing, the desired amount of hydrogel was first taken up into a sterile 2.5 mL Luer lock syringe and warmed to 37 °C for 15 min in a waterbath. Air bubbles were removed by tapping the syringe or short centrifugation if required. In parallel, C2C12 cells were detached from culture plates and pelleted as described in section 2.1.6.[3] Cells were prepared to yield a final concentration of approximately 3×10^6 cells per mL of hydrogel. After centrifugation, the supernatant was removed, and the pellet was gently resuspended in a minimum amount of culture medium, corresponding to 10 % of the volume of hydrogel which was used for mixing. Using the same micropipette as for resuspension, the cell suspension was injected into a sterile 2.5 mL Luer lock syringe by pipetting. Afterwards, air was carefully removed from the syringe by tapping and slowly pushing up the plunger, until only cell suspension remained in the syringe. The prepared hydrogel syringe was connected to a female/female Luer lock adaptor, which was then carefully filled with hydrogel before connecting the cell suspension syringe to the other side of the adaptor, to avoid an air gap. The hydrogel was then mixed with the cell suspension by gently moving the mixture back and forth through the two syringes. When the mixture appeared homogenous, it was moved into

[2] Contribution from Daniele Gueiber, see Table 12: Contributions from other persons, p.157
[3] Contribution from Nathalie Couturier, see Table 12: Contributions from other persons, p.157

one of the syringes entirely, and the other syringe was disconnected. Again, air bubbles were removed by tapping, before connecting the UV-shielding printing cartridge to the Luer lock adaptor and transferring the hydrogel/cell mixture into the cartridge. The cartridge was then connected to a sterile nozzle for extrusion, placed inside a printhead of the BIO X, and connected to the pneumatic tubing. The cartridge was allowed to come to RT before the printing process was started.[4] For all three designs shown in Figure 2-5, structures depicted in red were printed using GelXA bioink either without cells (Figure 2-5A) or with (Figure 2-5B-C) cells, and structures depicted in blue were printed using START bioink. The latter is a non-crosslinkable hydrogel which was acting as support structure during the printing process and was washed out after stabilizing the GelXA structures by crosslinking. For all prints, 25G conical nozzles (inner diameter 250 µm) were used with GelXA, and 25G blunt needles with 12.7 mm needle length were used for START bioink. If GelXA was printed without cells (Figure 2-5A), it was extruded at 65 - 70 kPa at a printing speed of 7 mm/s. For prints which included cells in the bioink (Figure 2-5B-C), GelXA was extruded at the same speed, but extrusion pressure was initially set to 13 kPa and then increased in steps of +1 kPa until the printing result looked satisfactory. The value used varied between experiments and sometimes needed to be adjusted during the printing process, being in a range of 15 – 20 kPa. For START bioink, 180 kPa extrusion pressure and 7 mm/s printing speed were used. All prints were crosslinked with UV light at 405 nm using a photocuring toolhead (cat. no. D16110020850, Cellink, Gothenburg, Sweden) at a distance of 1.7 cm. Prints without cells (Figure 2-5A) were crosslinked for 5 s after each layer printed, while prints with cells (Figure 2-5B-C) were crosslinked for 5 s in total only after printing of the last layer.

Afterwards, plates were transferred into the biosafety cabinet, and prints were washed with PBS to remove START bioink. Then, prints were submerged in culture medium (GM) and placed in the incubator. For cell-free prints (Figure 2-5A), C2C12 spheroids were placed into one of the two pocket structure after washing out the START bioink. These spheroids had been prepared beforehand by seeding 2×10^5 C2C12 cells per well into a U-bottom 96-well microplate (cat. no. 650970, Greiner bio-one, Frickenhausen, Germany) and subsequent centrifugation at 200 ×g for 5 min. Spheroids were cultured in GM for 4 days before transferring them into print structures. Then, spheroids were harvested and collected into a conical tube, allowed to settle to the tube bottom, and the medium was removed.[5] A few spheroids were taken up at once into a 200 µL pipette tip and manually transferred into the printed pocket structure. Prints were then submerged in DM to induce differentiation of C2C12 and incubated

[4] Contribution from Daniele Gueiber, see Table 12: Contributions from other persons, p.157
[5] Contribution from Nathalie Couturier, see Table 12: Contributions from other persons, p.157

at standard culture conditions. The next day, medium was removed and hiPSC-derived neurospheres and/or Schwann cells harvested as described in the previous sections were added into still empty pocket structures. Culture medium was then switched to triM and cultures were kept for 8 – 10 more days until fixation with partial medium changes every other day. Structures which were printed containing C2C12 in the hydrogel (Figure 2-5B-C) were cultured in GM for 7 days before switching medium to DM to induce C2C12 differentiation. Another 48 h later, neurospheres prepared as described in previous sections were harvested and added to the printed structures, either directly on top of the print (Figure 2-5B), or inside a pocket structure (Figure 2-5C), depending on the design. Culture medium was switched to triM and cultures were kept for additional 4 days (Figure 2-5B) or 10 days (Figure 2-5C) with partial medium changes every other day.

Table 5: Materials for 3D-printing and bioprinting

Material	Cat. No.	Supplier
2.5 mL Luer-lock syringes	613-1591	VWR International, Darmstadt, Germany
3 mL cartridges	CSC011011102	Cellink, Gothenburg, Sweden
3 mL UV-shielding cartridges	CSO010311502	Cellink, Gothenburg, Sweden
30 mL cartridges	7012134	Nordson EFD, Westlake, OH, USA
Catalyst compound for UV silicone 60A MG	BIO-83-6001	EnvisionTEC, Gladbeck, Germany
Conical nozzles, sterile 25G 22G	 NZ4250005001 NZ4220005001	Cellink, Gothenburg, Sweden
Female/female Luer lock adapter	OH000000010	Cellink, Gothenburg, Sweden
GelXA bioink	IK3X21020301	Cellink, Gothenburg, Sweden
Standard blunt needles, sterile 25G, needle length 12.7 mm	 NZ5250505001	Cellink, Gothenburg, Sweden
START bioink sterile	IK190001	Cellink, Gothenburg, Sweden
UV silicone 60A MG	RES-83-6001	EnvisionTEC, Gladbeck, Germany
XPLORE bioink	IK1021400309	Cellink, Gothenburg, Sweden

2.2 Immunofluorescence stainings

2.2.1 Immunofluorescence stainings of 2D cultures

For immunofluorescence stainings, cells were cultured either in ibidi chamber slides suited for microscopy, or on Ø12 mm glass coverslips which were placed in 6-well or 24-well culture plates. Detailed information on staining reagents are listed Table 6 and Table 7 in subsection 2.2.3.

2D cell cultures were fixed using cold 4 % PFA solution for 15 min at RT. For cultures which were prone to detachment from glass coverslips, like C2C12 and motoneuron cocultures, the PFA solution was warmed to RT before incubation. All following steps were carried out at RT if not indicated otherwise. After fixation, the PFA solution was removed, and samples were washed 3 × 5 min with PBS. Optionally, plates were sealed with parafilm at this point and stored at 4 °C until the protocol was proceeded. If samples were stored, then fixation and washing steps were carried out under sterile conditions.

For 2D cell cultures, two different immunofluorescence protocols were used either with Triton X-100 or saponin-mediated permeabilization depending on the target proteins to be labeled. For stainings of Schwann cell monocultures, Triton X-100 permeabilization was used, except for labelling of proteins p75NTR and P0. For stainings of motoneuron monocultures, saponin permeabilization was used if vAChT or synaptophysin were labeled, and Triton X-100 was used if Olig2, Sox2, Pax6, Hb9, Isl1, or Ki67 were labeled. For labelling of proteins Tubb3, tau, Map2, peripherin, ChAT, and GAP-43; saponin was used for permeabilization if they were combined with vAChT and/or synaptophysin stainings, otherwise, Triton X-100 was used. For immunofluorescence stainings of cocultures including C2C12 combined with motoneurons and/or Schwann cells, the saponin permeabilization protocol was used in all cases.

For the Triton X-100 permeabilization protocol, samples were incubated with 0.1 % Triton X-100 in PBS for 3 min. Permeabilization solution was removed and samples were washed with PBS for 3 × 5 min. Then, samples were incubated in blocking solution, consisting of 2 % BSA in PBS for 1 h at RT. Blocking solution was then replaced by primary antibody solution, which consisted of blocking solution containing primary antibodies at dilutions as listed in Table 7. The primary antibody solution was incubated either for 1 h at RT or overnight at 4 °C. After removing the primary antibody solution, samples were washed for 3 × 5 min with blocking solution and then incubated with secondary antibody solution for 45 min in the dark. Secondary antibody solution consisted of blocking solution containing secondary antibodies, DAPI, and optional additional dyes at dilutions as listed in Table 7. From this step onwards, samples were protected from light to avoid fluorophore bleaching. After removal of the secondary antibody solution, samples were washed with blocking solution for 2 × 5 min, followed by washes using ultrapure water for 2 × 5 min. Then, samples were prepared for imaging, by carefully blotting

liquid off the cover glasses using a paper towel, and subsequent mounting in Mowiol solution onto a microcopy glass slide. Slides were allowed to dry overnight in the dark. If chamber slides were used instead of cover glasses, the last two washing steps were done with PBS, and chamber slide wells were subsequently filled with either PBS or 88 % glycerol.

If the saponin permeabilization protocol was used, samples were incubated in a combined blocking and permeabilization solution consisting of 0.2 % gelatin and 0.1 % saponin in PBS for 10 min. Then, primary antibody solution was added, which consisted of 0.2 % gelatin, 0.01 % saponin, and primary antibodies diluted as listed in Table 7, in PBS. The primary antibody solution was incubated either for 1 h at RT or overnight at 4 °C. Subsequently, samples were washed using blocking-permeabilization solution for 3 × 5 min. Secondary antibodies and dyes were diluted in PBS containing 0.2 % gelatin and 0.01 % saponin, as used for the primary antibody solution, and were incubated for 45 min in the dark. Samples were then washed with blocking-permeabilization solution containing 0.2 % gelatin and 0.1 % saponin for 2 × 5 min, followed by washes using ultrapure water for 2 × 5 min. Cover glasses were then blotted on paper towel to remove excess liquid and mounted onto microscope slides using Mowiol.

For labelling of nAChR only on myotubes as shown in Figure 3-20A, no permeabilization was used. Instead, cultures were fixed and washed as described, and subsequently incubated with fluorescently labeled α-bungarotoxin diluted in PBS according to Table 7 for 20 min at RT. Afterwards, samples were washed with PBS for 2 × 5 min, followed by one washing step with ultrapure water for 5 min and mounting of samples.

2.2.2 Immunofluorescence stainings of 3D cultures

Cell-laden scaffolds described in section 2.1.8 were fixed with 4 % PFA for 30 min. All steps were carried out at RT if not indicated otherwise. After fixation, samples were washed with PBS for 3 × 15 min. For permeabilization and blocking, samples were then incubated in PBS containing 0.2 % gelatin and 0.1 % saponin for 3 h. Primary antibodies were diluted according to Table 7 in PBS containing 0.2 % gelatin and 0.01 % saponin and were incubated for 18 – 20 h. Then, samples were washed with blocking-permeabilization solution for 3 × 20 min with gentle agitation using a horizontal shaker. Secondary antibodies were diluted according to Table 7 in PBS containing 0.2 % gelatin and 0.01 % saponin and incubated for 3 – 4 h in the dark. Again, samples were washed with blocking-permeabilization solution for 3 × 20 min with gentle agitation, and additionally 1 × 20 min using ultrapure water. Afterwards, water was removed, and samples were submerged in 88 % glycerol. Samples were left at RT in glycerol for at least 24 h before imaging.

For immunofluorescence stainings of bioprinted hydrogel cultures described in section 2.1.9, samples were fixed with 4 % PFA at RT for 1 h. Then, samples were washed with PBS for 3 × 15 min with very gentle agitation using a horizontal shaker. All following steps were performed with gentle agitation as well, but at 37 °C. Permeabilization and blocking was done by incubating samples overnight in PBS containing 0.2 % gelatin, 0.1 % saponin, and 0.2 % Tween-20 (for data shown in Figure 3 26A-B, 0.5 % saponin were used). Primary antibodies were diluted according to Table 7 in PBS containing 0.2 % gelatin, 0.1 % saponin, and 0.2 % Tween-20 (for data shown in Figure 3 26A-B, 0.5 % saponin were used) and were incubated for 24 h. Samples were washed in blocking solution for 5 × 10 min and subsequently incubated overnight with secondary antibodies and dyes, diluted in the same buffer as primary antibodies. Again, samples were washed 5 × 10 min, using ultrapure water for the final washing step. 3D samples which had been cultured in multiwell plates were transferred into Ø35 mm glass bottom dishes (cat. no. 81158, ibidi, Gräfelfing, Germany) for microscopy.

2.2.3 Materials for immunofluorescence stainings

For staining of 3D cultures, customized staining chambers were 3D-printed using silicone (PCI Silcoferm S transparent, cat. no. 2209, PCI Augsburg, Augsburg, Germany) to be able to perform staining procedures of 3D cultures directly in well plates while limiting the volume of staining solutions required. These silicone staining chambers were placed inside the well, around the sample, and were sealed using addition-curing duplicating silicone picodent twinsil (cat. no. 1300 1000, Picodent, Wipperfürth, Germany). Supplier information for all reagents used for immunofluorescent staining protocols including antibodies are listed in Table 6. Detailed information on antibodies and dyes including host species and dilutions used are listed in Table 7. Three antibodies were obtained from the Developmental Studies Hybridoma Bank (DSHB) which were deposited there by other researchers. DSHB hybridoma products 81.5C10 (recognizing Hb9) and 40.2D6 (recognizing Isl1) were deposited to the DSHB by Jessell, T.M., and Brenner-Morton, S. [Ericson et al., 1992; Tanabe et al., 1998]; MF 20 (recognizing MHC) was deposited by Fischman, D.A. [Bader et al., 1982].

Table 6: Antibodies, reagents, and materials for immunostainings. 1° Ab = primary antibody, 2° Ab = secondary antibody.

Reagent	Cat. No.	Supplier
1° Ab α ChAT	AB144P Lot: 3029486	Sigma Aldrich Chemicon (Merck), Darmstadt, Germany
1° Ab α Desmin	ab32362 Lot: GR152193-43	Abcam, Cambridge, UK

Table 6 ***cont.***

Reagent	Cat. No.	Supplier
1° Ab α GAP-43 (5E8)	NBP-50052 Lot: 091414	Novus Biologicals (Bio-Techne), Wiesbaden, Germany
1° Ab α Hb9	81.5C10-c Lot: 1ea 10/26/17	Developmental Studies Hybridoma Bank, Iowa City, IA, USA
1° Ab α Isl1	40.2D6-c Lot: 1ea 10/26/17	Developmental Studies Hybridoma Bank, Iowa City, IA, USA
1° Ab α Ki-67	AB9260 Lot: 3047666	Sigma Aldrich Chemicon (Merck), Darmstadt, Germany
1° Ab α Map 2 antibody	188 011 Lot: 1-9	Synaptic Systems, Göttingen, Germany
1° Ab α MF 20 (MHC)	MF 20-c Lot: 1ea 6/25/20	Developmental Studies Hybridoma Bank, Iowa City, IA, USA
1° Ab α Myelin Basic Protein (MBP) (aa 82-87)	MAB386 Lot: 3390056	Sigma Aldrich Chemicon (Merck), Darmstadt, Germany
1° Ab α Myelin Protein Zero (P0)	57518S Lot: 1	Cell Signaling Technology, Danvers, MA, USA
1° Ab α Olig2	MABN50 clone 211F1.1 Lot: 3043565	Sigma Aldrich (Merck), Darmstadt, Germany
1° Ab α p75NTR (D4B3)	8238S Lot: 2	Cell Signaling Technology, Danvers, MA, USA
1° Ab α Pax6	901301 Lot: PRB-278P	BioLegend, San Diego, CA, USA
1° Ab α Peripherin	AB1530 Lot: 3188604	Sigma Aldrich Chemicon (Merck), Darmstadt, Germany
1° Ab α Rapsyn (H-205)	sc-28933 Lot: E1506	Santa Cruz Biotechnology, Dallas, TX, USA
1° Ab α S100b	HPA015768 Lot: 000006247	Sigma Aldrich (Merck), Darmstadt, Germany
1° Ab α SOX10 (D5V9L)	89356S Lot: 1	Cell Signaling Technology, Danvers, MA, USA
1° Ab α SOX2	347 003 Lot: 347003/1-2	Synaptic Systems, Göttingen, Germany
1° Ab α Synapsin1	106 011 Lot: 1-14	Synaptic Systems, Göttingen, Germany

Table 6 ***cont.***

Reagent	Cat. No.	Supplier
1° Ab α Synaptophysin	101 011 Lot: 3-35	Synaptic Systems, Göttingen, Germany
1° Ab α Tau	314 004 Lot: 1-17	Synaptic Systems, Göttingen, Germany
1° Ab α vAChT	139 103 Lot: 4-54	Synaptic Systems, Göttingen, Germany
1° Ab α Vimentin	MA5-11883	Thermo Fisher Scientific, Waltham, MA, USA
1° Ab α β-III-tubulin (Tuj1)	302 304 Lot: 1-10	Synaptic Systems, Göttingen, Germany
2° Ab α goat-AF647	A21477 Lot: 1010075	Thermo Fisher Scientific, Waltham, MA, USA
2° Ab α guinea pig-AF488	A-11073 Lot: 1990462	Thermo Fisher Scientific, Waltham, MA, USA
2° Ab α guinea pig-AF555	A-21435 Lot: 2015338	Thermo Fisher Scientific, Waltham, MA, USA
2° Ab α mouse-AF488	A11001 Lot: 1834337	Thermo Fisher Scientific, Waltham, MA, USA
2° Ab α mouse-AF555	A21424 Lot: 2123594	Thermo Fisher Scientific, Waltham, MA, USA
2° Ab α mouse-AF647	A31571 Lot: 2045337	Thermo Fisher Scientific, Waltham, MA, USA
2° Ab α rabbit-AF488	A32794 Lot: UI284002	Thermo Fisher Scientific, Waltham, MA, USA
2° Ab α rabbit-AF555	A32794 Lot: UI284002	Thermo Fisher Scientific, Waltham, MA, USA
2° Ab α rabbit-AF647	A21246 Lot: 55002A	Thermo Fisher Scientific, Waltham, MA, USA
Albumin Fraktion V (BSA)	8076.3	Carl Roth, Karlsruhe, Germany
cover glasses Ø12 mm	631-1577	VWR International, Darmstadt, Germany
DAPI	D9542 Lot: 28114320	Sigma Aldrich (Merck), Darmstadt, Germany
Gelatin (from cold water fish skin)	G7041	Sigma Aldrich (Merck), Darmstadt, Germany
Glycerol	G7893	Sigma Aldrich (Merck), Darmstadt, Germany
Mowiol 4-88	713.2	Sigma Aldrich (Merck), Darmstadt, Germany
PFA	0335.3	Carl Roth, Karlsruhe, Germany

Table 6 *cont.*

Reagent	Cat. No.	Supplier
Phalloidin-AF555	A34055 Lot: 1780358	Thermo Fisher Scientific, Waltham, MA, USA
Saponin	84510	Sigma Aldrich (Merck), Darmstadt, Germany
Triton X-100	T9284	Sigma Aldrich (Merck), Darmstadt, Germany
Tween-20	9127.2	Carl Roth, Karlsruhe, Germany
α-Bungarotoxin-AF488	B13422 Lot: 1750294	Thermo Fisher Scientific, Waltham, MA, USA
α-Bungarotoxin-AF647	B35450 Lot: 1795417	Thermo Fisher Scientific, Waltham, MA, USA

Table 7: Host species and dilutions for antibodies and dyes used for stainings. Ab = antibodies, m = monoclonal, p = polyclonal, AF = Alexa Fluor.

	Ab target / dye	Host (clonality)	dilution (2D cultures)	dilution (3D cultures)
1° Ab	ChAT	goat (pAb)	1:200	-
	Desmin	rabbit (mAb)	1:500	1:400
	GAP-43	mouse (mAb)	1:400	-
	Hb9	mouse (mAb)	1:100	-
	Isl1	mouse (mAb)	1:100	-
	Ki-67	rabbit (pAb)	1:500	-
	Map2	mouse (mAb)	1:300	-
	MF20 (MHC)	mouse (mAb)	1:600	1:600
	myelin basic protein (MBP) (aa 82-87)	rat (mAb)	1:200	-
	Myelin Protein Zero (P0)	rabbit (pAb)	1:200	-
	Olig2	mouse (mAb)	1:800	-
	p75NTR (D4B3)	rabbit (mAb)	1:1000	-
	Pax6	rabbit (pAb)	1:200	-
	Peripherin	rabbit (pAb)	1:250	-
	Rapsyn (H-205)	rabbit (pAb)	1:200	-
	S100b	rabbit (pAb)	1:400	1:400
	SOX10 (D5V9L)	rabbit (mAb)	1:500	-
	SOX2	rabbit (pAb)	1:500	-
	Synaptophysin	guinea pig (mAb)	1:500	1:300
	Tau	guinea pig (pAb)	1:500	-
	vAChT	rabbit (mAb)	1:400	1:200

	Table 7 *cont.* Ab target / dye	Host (clonality)	dilution (2D cultures)	dilution (3D cultures)
1° Ab	Vimentin	mouse (mAb)	1:400	-
	β-III-tubulin (Tuj1)	guinea pig (pAb)	1:750	1:500
2° Ab	α guinea pig-AF488	goat	1:1000	1:600
	α guinea pig-AF555	goat	1:1000	1:600
	α goat-AF647	donkey	1:1000	-
	α mouse-AF488	donkey	1:1000	1:600
	α mouse-AF555	goat	1:1000	-
	α mouse-AF647	donkey	1:1000	-
	α rabbit-AF488	donkey	1:1000	1:600
	α rabbit-AF555	donkey	1:1000	1:600
	α rabbit-AF647	donkey	1:1000	1:600
dyes	DAPI	-	1:1000	1:1000
	Phalloidin-AF555	(Amanita phalloides)	1:1000	-
	α-Bungarotoxin-AF488	(Bungarus multicinctus)	1:1000	-
	α-Bungarotoxin-AF647	(Bungarus multicinctus)	1:1000	1:500

2.3 Microscopy

Phase contrast images were acquired using an Axiovert 200M inverted microscope equipped with an EC Plan-Neofluar 10x/0,3 Ph1 air objective and AxioVision Rel.4.8 software (Carl Zeiss Microscopy, Oberkochen, Germany). Fluorescence image data presented in Figure 3-1D were acquired using the imaging platform Celldiscoverer 7 (Carl Zeiss Microscopy, Oberkochen, Germany). Fluorescence image data presented in Figure 3-14B and Figure 3-17B were acquired using a Leica Aperio VERSA slide scanner equipped with an HC PL FLUOTAR 20×/0.55 DRY objective and DAPI (excitation 350 nm, emission 460 nm), Spectrum Green (excitation 485 nm, emission 525 nm), and Cy5 (excitation 640 nm, emission 690 nm) filters, with Aperio VERSA software version 1.0.4 (Leica Biosystems, Wetzlar, Germany). All other fluorescence microscopy images presented were acquired using an inverted Leica TCS SP8 confocal microscope equipped with an HC PL APO 20×/0.75 IMM CORR CS2 objective and 405 nm, 488 nm, 552 nm, and 638 nm lasers, in Leica Application Suite X software version 3.5 (Leica Microsystems, Wetzlar, Germany). Cover glass samples mounted in Mowiol were imaged using Type F immersion oil (11513859, Leica Microsystems, Wetzlar, Germany), while Type G immersion oil (11513910, Leica Microsystems, Wetzlar, Germany) was used for samples mounted in 88 % glycerol, and

the objective correction collar was adjusted accordingly. If not stated otherwise in the following sections, scan settings used were: 2048 × 2048 or 1024 × 1024 px² resolution for 2D and 3D culture images, respectively; a line average of 3, pinhole diameter set to 1 Airy Unit (corresponding to 56.7 µm), bi-directional scanning, scan frequency of 400-600 Hz, PMT gain set between 400 – 750 V, and laser power set between 0.5 % - 4 % for 2D cultures, or up to 6 % in 3D cultures. Confocal images of 2D cultures which are shown in figures were acquired as z-stacks of 5 – 20 focal planes with a z-spacing of 1.04 µm to include the whole cell layer, and maximum z-projections were generated for figures. In case of 3D cultures, projections were generated from larger image stacks, and stack sizes are given in corresponding figure legends. Image data which was used for quantitative analysis of nAChR clusters which is shown in Figure 3-23 and Figure 3-24 was done with 0.75× zoom at 1024 × 1024 px² resolution, using 4 % laser power for excitation of AF647-tagged α-bungarotoxin at 633 nm, with the spectral detection window for emission set to 650 – 775 nm. These image data were collected as single optical planes which were determined by autofocus in the 647 channel, and automated tile scan imaging with 0 % tile overlap was used to collect large regions at random places on the coverslip. For other quantitative analyses, including motoneuron and Schwann cell marker expression analysis, Schwann cell elongation analysis, and colocalization analysis in 2D cocultures, image data either taken with the VERSA slide scanner or the SP8 confocal microscope were used as detailed in the following sections.

2.4 Data analysis

2.4.1 Differentiation marker protein expression of motoneurons and Schwann cells

For quantification of motoneuron precursor cells positive for Olig2 as well as motoneurons positive for vAChT, shown in Figure 3-1C; as well as Schwann cell culture quantifications shown in Figure 3-7D, image data acquired with the Leica SP8 confocal microscope was used. For quantification of cells positive for Sox10 in Schwann cell differentiation cultures shown in Figure 3-8, Figure 3-9, Figure 3-10, Figure 3-11, and Figure 3-18; image data acquired with the Leica Aperio VERSA slide scanner microscope was used. Except for the data shown in Figure 3-7, those quantifications were done using the Bead-Net software[6] [Scherr et al., 2020]. To train and test the algorithm for this application, a dataset of 31 images with a size of 128 × 128 px² each was created from VERSA slide scanner microscopy data of Schwann cell cultures and labeled manually. Using a DAPI signal channel, nuclei were segmented, and their center points determined in Bead-Net. These nuclei center points were then used to create 3 × 3 px² regions centered at those locations in a second image channel, containing the staining signal to be analyzed, smoothed by a Gaussian filter ($\sigma = 0.5$). Maximum intensity

values inside these 3 × 3 px² regions were calculated[6]. For each staining signal, a threshold value was determined manually beforehand, and measured values exceeding this threshold value were counted as positive. The percentage of positive cells was then determined using the total number of segmented nuclei. For quantifications shown in Figure 3-7, a self-made ImageJ macro script was used for batch analysis of confocal microscopy images. Images were prepared as two-channel tif files with DAPI staining signal in the first image channel and the signal to be quantified (Sox2 or Sox10) in the second channel. The macro script then executed the following operations in ImageJ sequentially: Image channels were split and cell nuclei were segmented as ROIs using the DAPI signal channel. This was done by manually setting a threshold value and then converting the image to binary masks (white background). Overlapping nuclei were segmented using the watershed function. Next, the "Analyze Particles" tool was used to locate and analyze nuclei as objects. Particles smaller than 20 µm² and objects on image edges were excluded from analysis, and "Show Outlines" as well as "Add to Manager" functions were used to create measurable ROIs as well as a control picture showing ROI outlines. Next, those ROIs were retrieved from the ROI manager and projected onto the second channel image to measure mean intensities, and results were saved as csv files. The percentage of total ROIs which were positive for the signal in the second image channel was calculated, whereby ROIs with a mean intensity higher than the background mean intensity plus two times its SD were counted as positive.

2.4.2 Schwann cell maturation analysis

For Schwann cell maturation analysis in different media formulations regarding cell marker expression shown in Figure 3-16 and cell elongation shown in Figure 3-17, image data acquired with the Leica Aperio VERSA slide scanner microscope was used. For nuclear markers Ki67 and Pax3, the percentage of positive cells was determined using the Bead-Net software [Scherr et al., 2020] as described in the previous section 2.4.1. To determine the percentage of cells positive for cytoplasmic markers, including p75NTR, GAP-43, S100b, and P0, the same principle was applied; i.e., segmenting nuclei using the DAPI signal, measuring signal intensities in a second staining channel at these nuclei locations, and determining positive cells by a user-defined threshold. However, nuclei segmentation was not done with Bead-Net, but using the TWANG algorithm [Stegmaier et al., 2014] implemented in XPIWIT [Bartschat et al., 2016] to segment the whole nuclei areas instead of center point determination. In a second channel which contained the marker staining signal, mean intensity

[6] Contribution from Roman Bruch, see Table 12: Contributions from other persons, p.157

values were then obtained from these segmented nuclear areas.[7] For the analysis of bipolar Schwann cell elongation which is shown in Figure 3-17, VERSA slide scanner microscopy images of cell cultures stained for DAPI and S100b were used. The number of cells positive for S100b was determined as described above. Using the S100b staining signal channels, several image processing steps were carried out to ultimately determine the summed major axis lengths of narrow structures present corresponding to elongated cell processes. This summed length was divided by the number of cells positive for S100b to obtain a numerical value, which was termed “elongation index”. This image analysis process was designed and executed by Roman Bruch[7] and details of processing steps are described in Hörner et al., 2021. The workflow steps are also depicted schematically in Figure 3-17 along calculation results.

2.4.3 2D coculture analysis

Image data for quantitative analysis shown in Figure 3-24 was acquired with the SP8 confocal microscope as described in section 2.3. For segmentation and analysis of nAChR clusters, single optical plane images were used, with a single image channel showing nAChR labeled with α-bungarotoxin. Acquired images were reviewed to exclude images which showed obvious detachment of C2C12 cells over a major part of the imaging area. Remaining images were then used for nAChR cluster segmentation using a self-made ImageJ macro script which sequentially applied the following operations: Images were duplicated, and a median filter (radius = 1) was applied on the duplicate image for smoothing. Using manual thresholding and the “Wand Tool”, nAChR clusters were manually segmented from the smoothened image and segmented outlines were added as ROIs into the ROI manager. ROI masks were then used to measure signal mean intensity, ROI area, and total number of ROIs from the raw data image. Then, using the smoothened duplicate image, brightness and contrast values were changed until the outlines of whole myotubes became visible. These areas were again segmented using the wand tool to measure the total area of myotubes, which was used to calculate the number of nAChR clusters per myotube area. Like this, an area of at least 25 mm² was analyzed for each condition. To measure the percentage of nAChR clusters positive for rapsyn, image sets with co-stainings of nAChR and rapsyn in separate channels were used. nAChR clusters were segmented as described before, and ROI masks were then transferred to the image channel containing rapsyn staining signal to measure mean signal intensities inside ROI masks. Using these measurements, the percentage of nAChR ROIs double-positive for rapsyn was

[7] Contribution from Roman Bruch, see Table 12: Contributions from other persons, p.157

calculated, whereby ROIs were counted as positive if the mean intensity in the rapsyn channel was higher than the background mean intensity plus two times its SD. Finally, analysis of Schwann cell / neurite alignment as well as quantification of Schwann cell / neurite colocalizations with nAChR clusters was performed manually by going through confocal image stacks of tricultures including entire cell layers, and counting the total number of Schwann cells, the number of Schwann cells aligned with neurites, the total number of nAChR clusters, and the numbers of nAChR clusters which colocalized with Schwann cells and/or motoneurons.

2.4.4 Statistical analysis

Quantitative and statistical analysis was performed with Microsoft Excel 2019 (Microsoft, Redmond, WA, USA) and GraphPad Prism 8 (GraphPad Software, San Diego, CA, USA). Results are presented as mean ± SD. Numbers n of experimental replicates used for analysis are indicated in corresponding figure legends; statistical analysis was performed only on data obtained from at least three independent experiments. Normal distribution of data was tested by Kolmogorov–Smirnov or Shapiro-Wilk tests. Results were analyzed statistically using t-tests (Figure 3-11 and Figure 3-18) or one-way ANOVA with Tukey's multiple comparisons test (Figure 3-9, Figure 3-16, Figure 3-17, and Figure 3-24). *p*-values less than 0.05 were considered significant and significance levels were reported as * $p < 0.05$, ** $p < 0.01$, *** $p < 0.001$.

2.4.5 Other software

Figures were created in Adobe Illustrator CC 2018 (Adobe, San José, CA, USA). For some schemes, also Microsoft PowerPoint 2019 (Microsoft, Redmond, WA, USA) was used. Graphs were prepared in GraphPad Prism 8 (GraphPad Software, San Diego, CA, USA). The Fiji distribution version 2.1.0 [Schindelin et al., 2012] of ImageJ version 1.53c (Rasband, W.S., National Institutes of Health, Bethesda, MD, USA) was used for image analysis and preparation of microscopy images for figures.

3 RESULTS

3.1 Differentiation of motoneurons and Schwann cells from hiPSC

3.1.1 Motoneurons can be derived from hiPSC robustly using a published protocol with small modifications

As the first step towards developing hiPSC-based neuromuscular cell culture models, hiPSC culture technique was established as described in chapter 2.1.3. Several hiPSC lines were acquired, expanded and cryobanked. Next, a small molecule protocol to differentiate motoneurons from hiPSCs described in literature [Du et al., 2015; Yi et al., 2018] was tested with five different hiPSC lines. To date, several protocols are available in literature for differentiation of hiPSCs and/or hESCs into motoneurons [Wichterle et al., 2002; Hu and Zhang, 2009; Amoroso et al., 2013; Davis-Dusenbery et al., 2014; Gouti et al., 2014; Qu et al., 2014; Du et al., 2015; Maury et al., 2015; Sances et al., 2016; Yi et al., 2018]. After an initial literature research and comparison, the small molecule protocol first published by Du and colleagues was chosen, as they reported higher yields of functionally mature motoneurons (> 90 % of cells) in a shorter differentiation time (28 days) than other protocols without the need for cell sorting steps or virus-mediated gene delivery [Du et al., 2015]. Moreover, this protocol was reported to generate an expandable population of motoneuron progenitors after 12 days which could be frozen and thawed with high recovery rates. Indeed, this was accomplished via patterning by a sequential combination of small molecules in chemically defined media, as outlined in Figure 3-1A. Firstly, neural induction was achieved through dual Smad inhibition by combining SB431542, an inhibitor of TGF-β/activin/nodal signaling, and DMH1, an inhibitor of BMP signaling. At the same time, CHIR99021 was used for activation of Wnt (via inhibition of GSK-3β to stabilize β-catenin), to promote neural induction and drive anteroposterior patterning towards spinal cord identity. Resulting neuroepithelial progenitor cells of caudal identity were then further patterned towards motoneuron precursors with retinoic acid and Shh agonist purmorphamine for caudalization and ventralization, respectively. For maturation of neurons, the Notch inhibitor Compound E was added in the final differentiation medium.

In this work, the differentiation protocol presented by Du et al. [2015] was used with some slight modifications as described in a later study, which characterized several hiPSC lines. These modifications included the use of accutase instead of dispase to passage neuroepithelial progenitors, as well as addition of neurotrophic factors GDNF, BDNF, and IGF1 to the differentiation media from day 12 onwards [Yi et al., 2018]. Additionally, the final plating of neuronal cells on day 18 was done in plates coated with laminin instead of Matrigel, as described in the published protocols, to promote adhesion and maturation of neurons. The scheme in Figure 3-1A depicts the differentiation protocol with modifications as it was used in

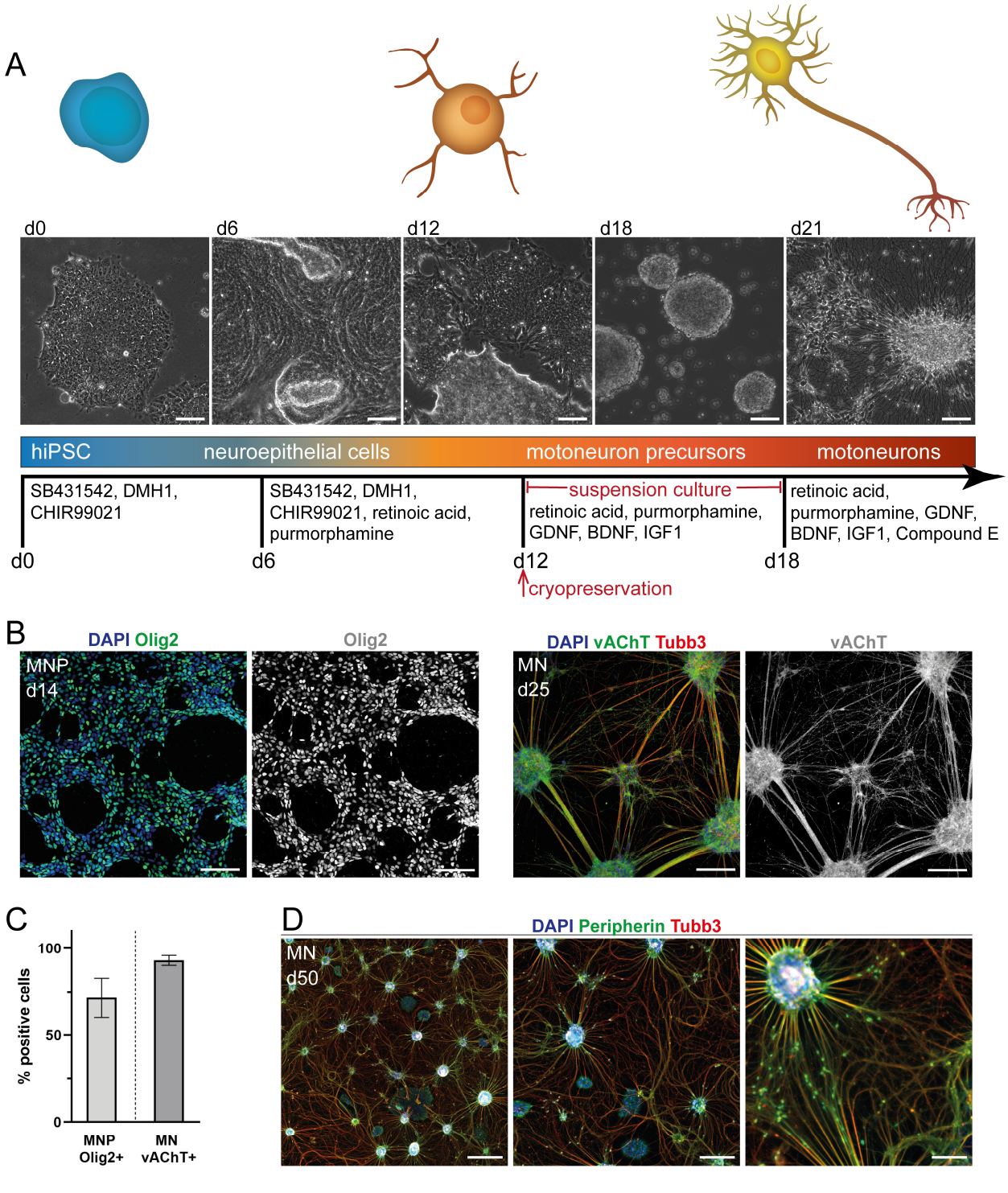


Figure 3-1: Motoneurons can be differentiated from hiPSC via precursor cells. (**A**) Scheme of differentiation protocol timeline listing small molecules used in differentiation media alongside representative brightfield images of successive differentiation stages at time points indicated. Scale bars: 100 µm. (**B**) Representative micrographs showing immunofluorescence signals for Olig2 in motoneuron precursors (MNP) at day 14 (left) as well as vAChT and Tubb3 in motoneurons (MN) at day 25 (right). Nuclei were labeled with DAPI. Color codes in merge images as indicated. Scale bars: 100 µm. (**C**) Quantification of Olig2+ cells at day 14 (n = 5) and vAChT+ cells at day 25 (n = 4) normalized to total cell count. Graphs depict mean ± SD. (**D**) Long-term culture of hiPSC-derived motoneurons at day 50 stained for DAPI (blue), peripherin (green), and Tubb3 (red). Scale bars: 400 µm (left), 200 µm (middle), 100 µm (right). d = day. Parts of figure adapted from Hörner et al. [2021] under CC BY 4.0 license.

this work, and includes representative brightfield images of successive differentiation stages, including hiPSCs on day 0 of differentiation, neuroepithelial progenitor cells on day 6, motoneuron precursors on day 12, neurospheres in suspension culture on day 18, and motoneurons on day 21. Throughout the differentiation, cultures were immunostained for characteristic marker proteins to monitor differentiation progress and cell identity. To assess differentiation efficiency, the proportion of cells expressing a motoneuron precursor marker, Olig2, on day 14 (Figure 3-1B) was quantified from image data, revealing that 71.5 ± 11.4 % (mean ± SD, n = 5 experiments) of cells were positive for Olig2 (Figure 3-1C). Likewise, the number of cells expressing a cholinergic motoneuron marker, vAChT, on day 25 (Figure 3-1B) was 93.0 ± 2.9 % (mean ± SD, n = 4 experiments). Motoneurons were also positive for Tubb3 (Figure 3-1B+D) and peripherin (Figure 3-1D). It was then tested if motoneurons could be kept in culture beyond day 28 and if this would result in further maturation of cells. As neuronal cultures could not be split anymore after the final plating on day 18 and neurites became prone to detachment with longer incubation times, long-term cultures of adherently plated motoneurons were very delicate, and often detached from plates. However, in some cases, motoneuron cultures were kept in final differentiation medium up to day 50. These cultures showed clustering of neuronal cell bodies into adherent spheres which were up to around 150 µm in diameter, and showed ample outgrowth of neurites. The latter organized in thick bundles around the cell body clusters and then branched to form fine neurite networks (Figure 3-1D).

To increase robustness and reproducibility of differentiations, different culture conditions were compared, including cell density at induction of differentiation (Figure 3-2A) and plate coating for maturation and long-term culture (Figure 3-2B). In the first case, hiPSC cultures were split either with EDTA as described in chapter 2.1.3 to produce cell colonies by avoiding singularization of hiPSC. Alternatively, hiPSCs were split with TrypLE Express to singularize cells and then seeded as a dense monolayer the day before induction of differentiation. In the monolayer condition, differentiation was only induced if cells had formed a dense cell layer with 100 % confluency. Subsequent differentiation steps as well as splits were done the same in both conditions according to the protocol described and cell survival as well as differentiation were assessed. Representative brightfield images of successive differentiation stages for both conditions are depicted in Figure 3-2A. The first column shows hiPSC cultures in colonies or as monolayer on day 0, i.e., right before the switch to differentiation. After four days, cells in the colonies condition had proliferated to a confluent culture, which appeared structured, while monolayer cultures seemed to grow more homogenously. Two days after the first split (day 8), both conditions appeared structured, but more cell aggregation as well as detachment were seen in the monolayer condition. In the final differentiation stage (day 30), neurons were

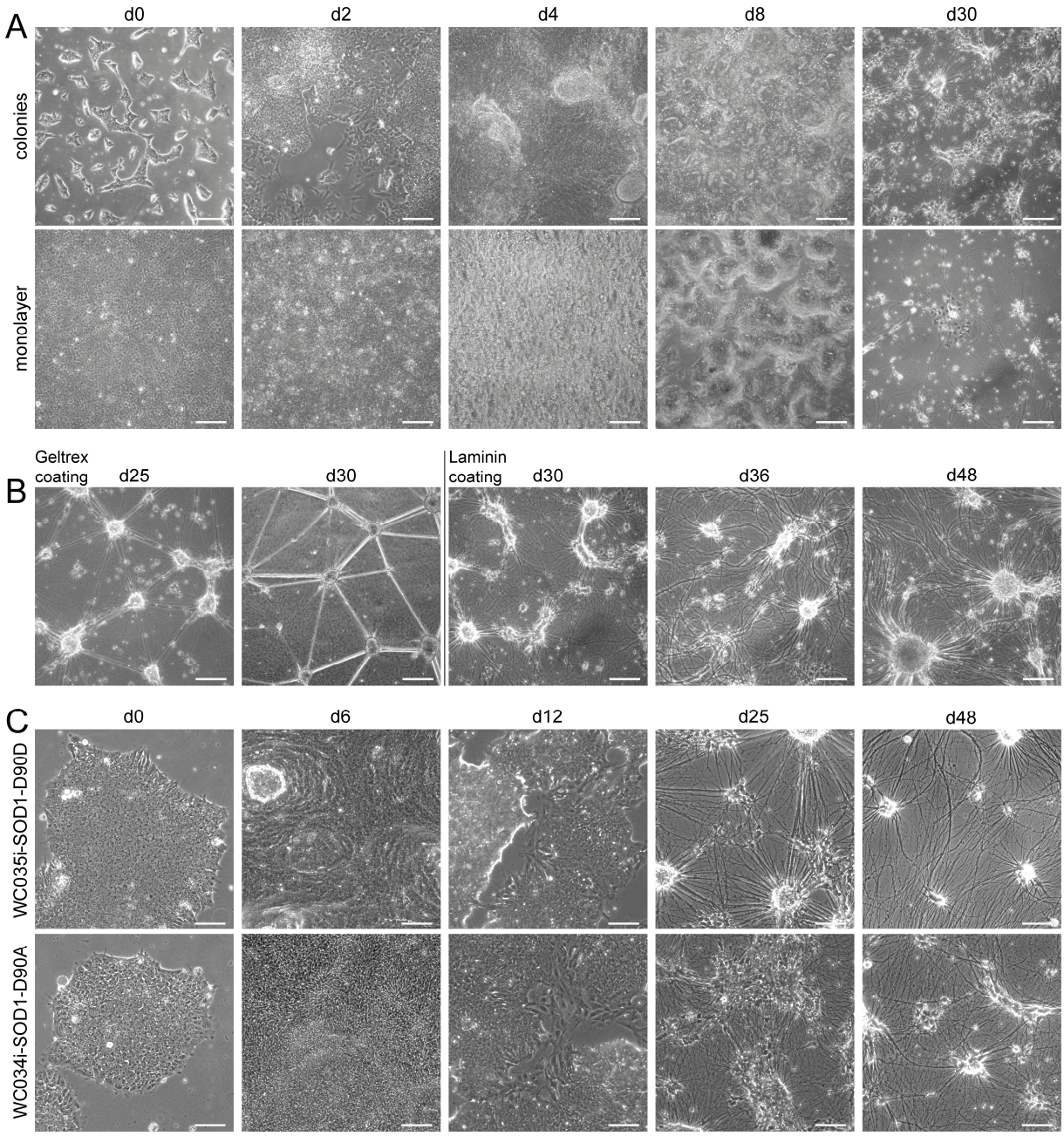


Figure 3-2: Cell density at induction and plate coatings influence differentiation of motoneurons. (**A**) hiPSC were split into either cell colonies without singularization of cells or singularized and seeded as dense monolayers before induction of differentiation. Figure shows representative brightfield images for time points indicated. Scale bars: 100 µm. (**B**) Final maturation of hiPSC-derived motoneurons was performed in tissue culture plates coated with Geltrex (left) or laminin (right). Scale bars: 100 µm. (**C**) Representative brightfield images of successive differentiation stages using optimized culture conditions of one control hiPSC line (upper row) as well as one patient-derived disease-specific hiPSC line (lower row). Scale bars: 100 µm. d = day.

present in both conditions, but cultures derived from the colonies condition showed more neuronal cells. This experiment was repeated five times, and in four of those, differentiations from the colonies condition could be kept beyond d30, fixed, and immunostained. In contrast, cells from the monolayer condition could be successfully differentiated and stained in only one out of the five experiments. In two of the remaining runs, monolayer cells detached before

day 30. In the last two trials, monolayer cells could be kept beyond day 30 and apparently contained neuronal cells but detached upon fixation and could not be stained. This demonstrated a superior robustness of differentiations started from colony cultures, and accordingly, all following motoneuron differentiations were started from those.

Additionally, the coating of tissue culture plates used for plating the cells on day 18 and following final maturation influenced attachment and survival of cells (Figure 3-2B). Three coating substrates were compared: Geltrex and Matrigel, which are both basement membrane extracts prepared from murine Engelbreth-Holm-Swarm tumors, as well as laminin. Representative images in Figure 3-2B show cultures grown on either Geltrex or laminin at time points indicated, as Geltrex and Matrigel cultures were comparable. Overall, neuronal cultures showed improved adhesion and less detachment in long-term culture when plated on laminin as compared to the other substrates. Moreover, growth of non-neuronal cells was observed more often on Geltrex/Matrigel-coated plates (Figure 3-2B, second image), and attachment as well as outgrowth of neurites and fine neurite networks seemed improved on laminin coating. Accordingly, laminin coating was used in all following motoneuron differentiations from day 18 on as described in chapter 1.3.2. Figure 3-2C shows representative brightfield images of successive differentiation stages of control hiPSCs (WC035i-SOD1-D90D line) as well as disease-specific hiPSCs (WC034i-SOD1D90A line) differentiated under these conditions. For characterization, cells were immunostained for established marker proteins at different time points throughout the differentiation. After two weeks, cells expressed the marker proteins Sox2, Pax6, Nestin, and Olig2. In the third and fourth week of differentiation, cells gradually became positive for the motoneuron markers Hb9, Islet-1, ChAT, and vAChT, as well as the more general neuronal markers Tubb3, Map2, synaptophysin, GAP-43, tau, and peripherin. Figure 3-3A shows exemplary immunofluorescence images of motoneuron cultures at time points indicated. These results were reproducible across five hiPSC lines, including three lines derived from healthy donors (028#1, 028#4-GCaMP6f#2, 009#3), one cell line derived from an ALS patient exhibiting a mutation in the SOD1 gene (WC034i-SOD1D90A), and one control cell line modified from the latter which was genetically engineered to correct the mutation (WC035i-SOD1-D90D). Representative images of motoneurons differentiated from those five cell lines and labeled for Tubb3 and vAChT are shown in Figure 3-3B.

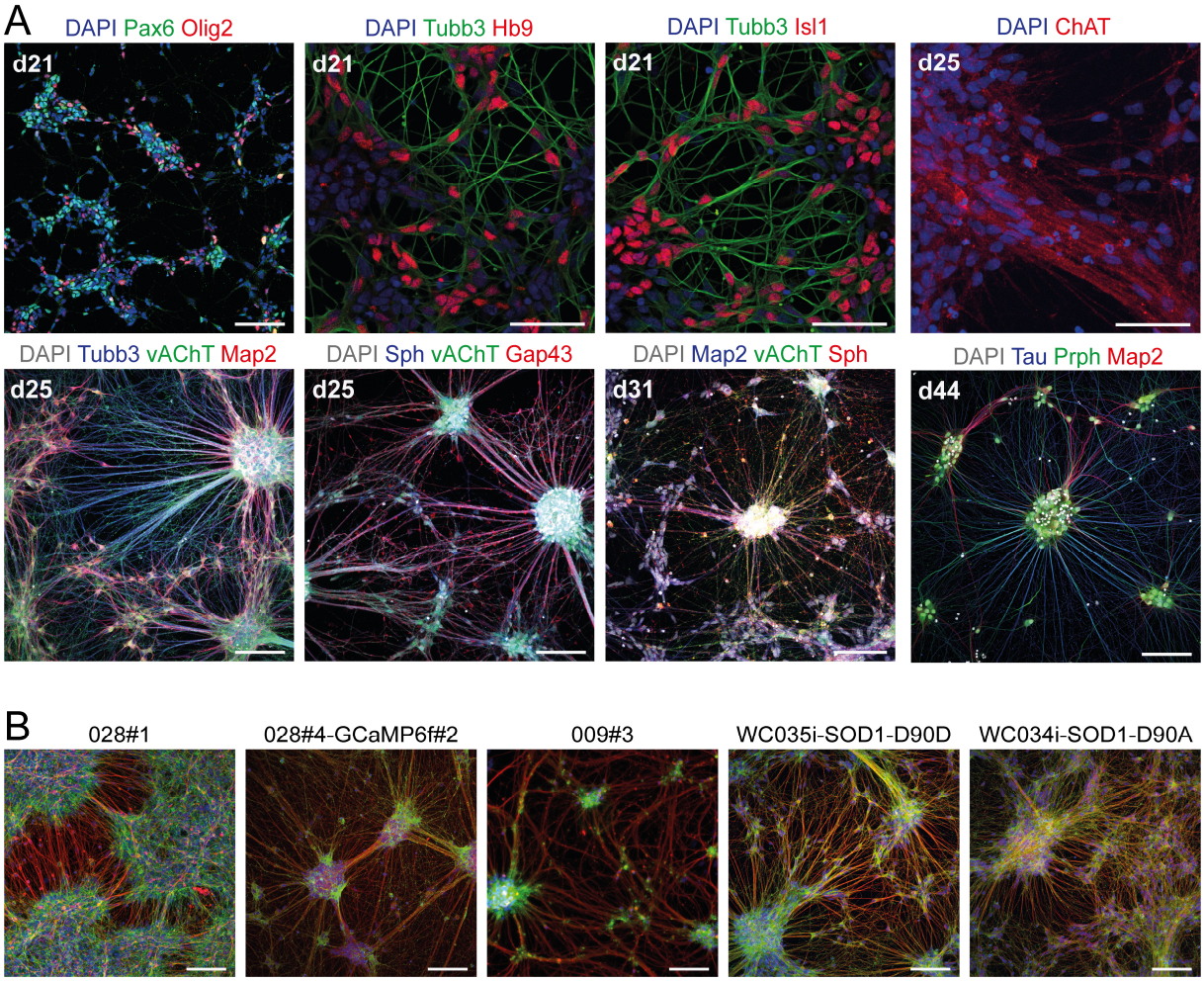


Figure 3-3: hiPSC-derived motoneurons express typical marker proteins. (**A**) Cells express precursor markers Pax6 and Olig2, motoneuron markers Hb9, Islet-1 (Isl1), ChAT, and vAChT, and neuronal markers Tubb3, Map2, synaptophysin (Sph), GAP-43, tau, and peripherin (Prph). Nuclei were labeled with DAPI. Color codes and time points of fixation indicated. Scale bars: upper row first image 100 µm, others 50 µm; lower row 100 µm. Parts of figure adapted with modifications from Hörner et al. [2021] under CC BY 4.0 license. (**B**) Differentiated motoneurons from five different hiPSC lines stained for Tubb3 (red) and vAChT (green). Nuclei were labeled with DAPI. Scale bars: 100 µm. d = day.

3.1.2 Motoneuron precursors can be expanded but exhibit variability with increasing passage number

Next, it was tested if Olig2+ motoneuron precursors obtained after two weeks could be expanded and cryopreserved as described in the original protocol publication. To this end, cells on day 12 of differentiation were kept in expansion medium as described in chapter 2.1.4. Every six days, cells were split, whereby one part of the culture was kept in expansion medium for another six days, one part was frozen, and one part was fixed and immunostained for Sox2, Olig2, and Ki67. After the first, second, and third expansion passage, motoneuron precursors retained expression of Sox2 and Olig2, as well as proliferation marked by Ki67 (Figure 3-4A).

Frozen cells could also successfully be cryopreserved with high recovery rate and sustained expression of those markers (Figure 3-4A), and such expanded and thawed precursor cells could also successfully be differentiated further into vAChT+ motoneurons (Figure 3-4B). However, following a fourth expansion passage, the proportion of cells positive for Sox2, Olig2, and Ki67 seemed to decrease, and some cells stained positive for Tubb3 (Figure 3-4C). Outgrowth of neurites was also observed in brightfield images (Figure 3-4D), while precursor cells which were expanded only for one passage showed larger cell bodies and no elongated cell processes. Still, cultures which were passaged four times in expansion medium could further be differentiated into motoneuron cultures, but with decreased cell yield. Therefore, expansion and cryopreservation were used in subsequent differentiations, but cells were only expanded for a maximum of three passages. These expansion passages were done either before or after freezing, and precursor cells expanded for longer times were not used for experiments, to keep cell yield as well as the degree of maturation consistent among motoneuron cultures.

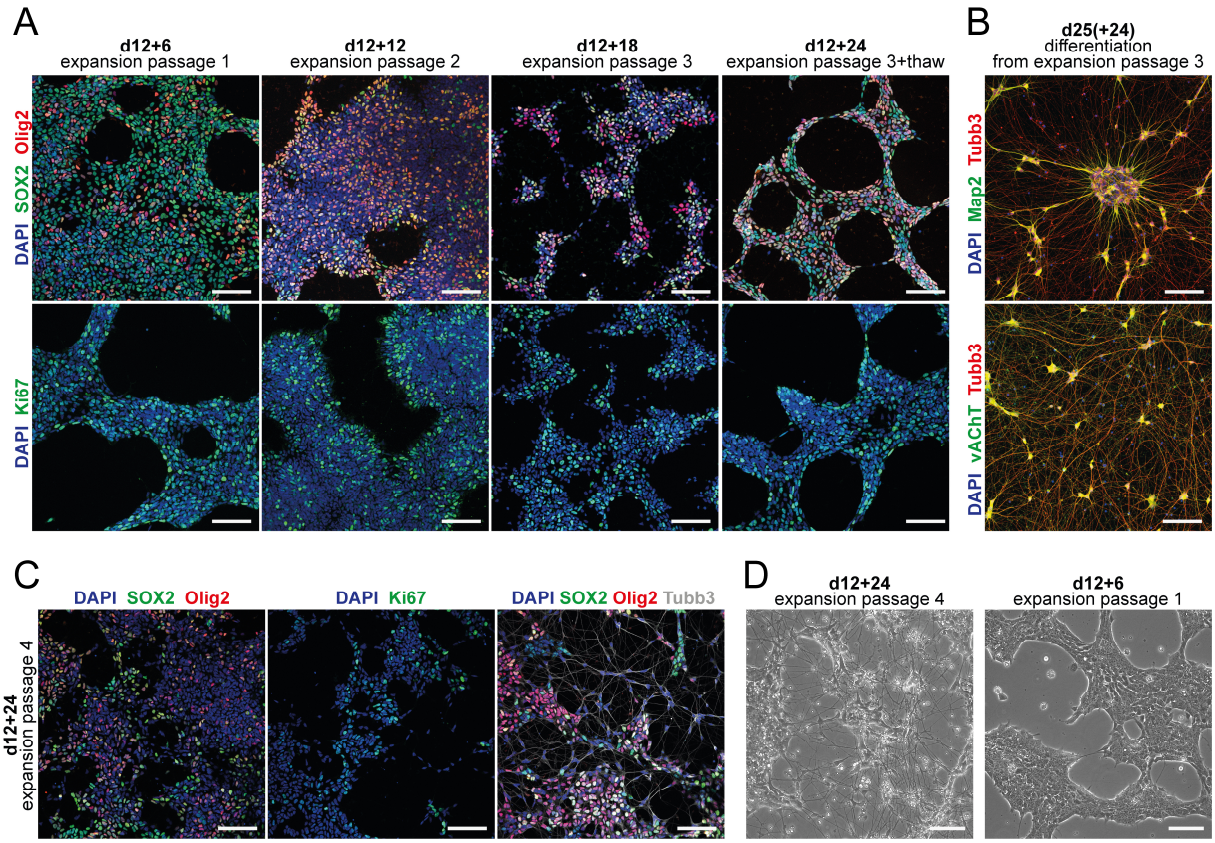


Figure 3-4: Motoneuron precursors can be expanded and cryopreserved. (**A**) Precursor cells obtained on day 12 were expanded and passaged every 6 days. Cells were stained for Sox2, Olig2, and Ki67 upon passaging and after thawing. Nuclei were labeled with DAPI. Color codes indicated in panels. Scale bars: 100 µm. (**B**) Motoneurons were differentiated from expanded and cryopreserved precursor cells and labeled for Tubb3, Map2, and vAChT. Nuclei were labeled with DAPI. Color codes indicated in panels. Scale bars: 100 µm. (**C**) Precursor cells were expanded for four passages and labeled for Sox2, Olig2, Ki67, and Tubb3. Nuclei were labeled with DAPI. Color codes indicated in panels. Scale bars: 100 µm. (**D**) Brightfield images of precursor cells which were expanded for four passages (left) compared to precursor cells expanded for one passage (right). Scale bars: 100 µm. d = day.

3.1.3 *Schwann cells can be differentiated from hiPSC using a published protocol, but with low efficiency and robustness*

For the differentiation of Schwann cells from hiPSC, a small molecule protocol as published by Kim et al. was tested [Kim et al., 2017]. This used TGF-β/activin/nodal inhibitor SB431542 and Wnt activator CHIR99021 for the initial neuralization phase, and additionally Nrg1, β-mercaptoethanol (β-ME), and BSA. This combination was supposed to drive differentiation of Schwann cell precursors within 24 days, which was followed by a maturation phase into Schwann cells, where a factor cocktail including FBS, Nrg1, PDGF-BB, retinoic acid, and forskolin was used. The timeline and differentiation factors of this protocol are shown schematically in Figure 3-5A. Cells were characterized by immunostainings for characteristic marker proteins at different time points during the differentiation. As early markers of neuralization and neural crest development, respectively, Sox2 and Sox10 were labeled. To check for differentiation of Schwann cells, S100b and GAP-43 were used. In first differentiation experiments, cells positive for Sox10 could successfully be induced, albeit at comparably low yields. The first Sox10+ cells appeared around day 8, and their proportion increased during the second week of differentiation (Figure 3-5B). However, a second cell population remained in cultures which was negative for Sox10 and positive for Sox2. Around day 30, Sox10+ cells started to express S100b and GAP-43, which increased with continued culture time (Figure 3-

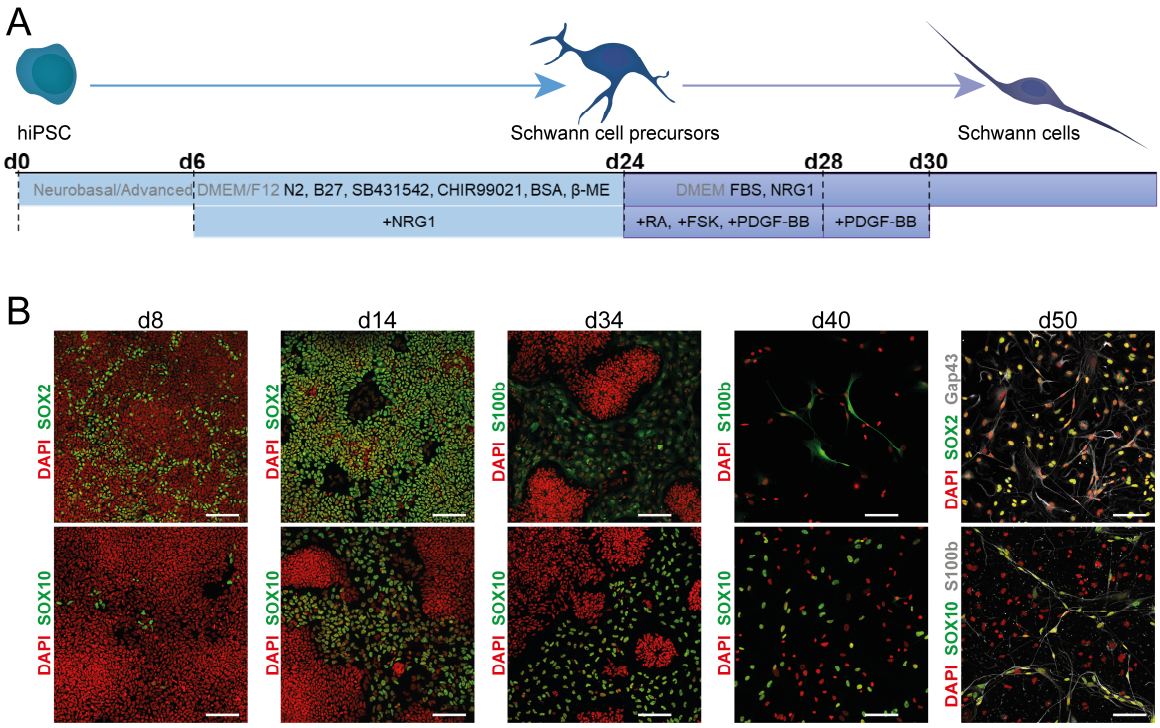


Figure 3-5: Initial Schwann cell differentiation experiments showed low differentiation yields. (**A**) Timeline of differentiation and molecular factors used as presented by Kim et al. [2017]. (**B**) Representative micrographs of immunostainings for Sox2, Sox10, S100b, and GAP-43, at time points indicated. Nuclei were labeled with DAPI. Color codes indicated in panels. Scale bars: 100 µm. d = day.

5B). Still, the Sox10-/Sox2+ cell population remained present also in long-term culture. Moreover, this cell population remained more proliferative than the cells expressing Schwann cell markers. Therefore, cultures containing Sox10-/Sox2+ cells could not be kept long-term without decreasing the yield of Sox10+/S100b+ cells. In addition, success and efficiency of Schwann cell differentiation was highly variable between differentiation batches, even if the same cell line was used. Cryopreservation of cells was tested in two different stages of differentiation, either as Schwann cell precursors (day 24) or as Schwann cells (after day 35). When cells were frozen in the precursor stage, recovery after thawing was poor in most cases, and cultures which could be propagated showed only low levels of Schwann cell markers after further differentiation. In comparison, cells frozen at later time points showed better recovery. Still, the ability of cell cultures to be propagated after thawing, as well as cell morphology and Schwann cell marker expression, were rather variable between batches. This is illustrated in Figure 3-6, which shows brightfield images shortly after thawing and after some time in culture (Figure 3-6A), as well as immunostainings for Schwann cell markers after 16 days in culture post thaw (Figure 3-6B). Culture variability was seen between differentiation batches, labeled (i) – (iii) in Figure 3-6, but also between cells cryopreserved at different time points from the same differentiation batch (labeled (iii-a) – (iii-c)).

3.1.4 Tuning of BMP signaling activity to an intermediate level increases robustness and yield of Sox10+ cell differentiation

To increase robustness and reproducibility of the differentiation protocol, several modifications were tested. These included addition of small molecules BMP4, DMH1, resveratrol, or ROCK inhibitor Y-27632; omission of compounds β-ME, BSA, or FBS; as well as different split ratios and therefore culture densities of differentiating cells.

Since initial experiments indicated an insufficient induction of Sox10+ cells of neural crest identity, and literature suggested an important role of BMP signaling here, it was tried if activation of BMP signaling in the second week of differentiation would increase the proportion of Sox10+ cells. In human stem cell cultures, an increase in Sox10+ neural crest cells was demonstrated before upon treatment with 100 ng/mL BMP4 to activate BMP signaling [Cimadamore et al., 2011], or treatment with 15 ng/mL BMP4 combined with 1 µM DMH1 [Hackland et al., 2017]. In the latter case, the BMP antagonist DMH1 was used for top-down titration of BMP signaling activity level. This method allowed a precise tuning of BMP signaling activity level independent of culture-inherent differences in endogenous BMP signaling levels. Therefore, in a first experiment, different BMP4 treatments combined with DMH1, according to Hackland et al. [2017], or without DMH1, according to Cimadamore et al. [2011], were tested starting from day 6 of differentiation. For better overview, Table 8 lists BMP4 concentrations,

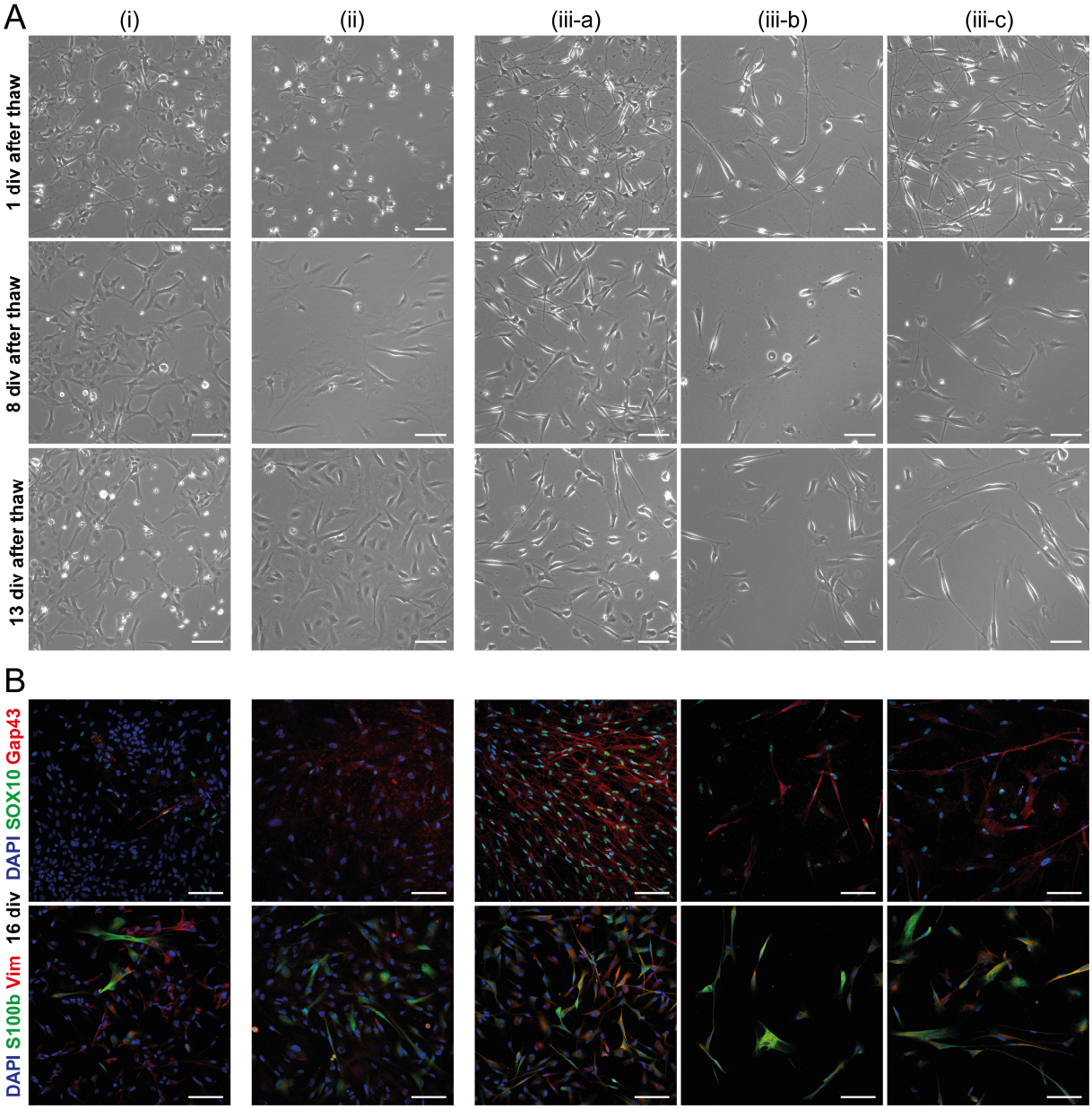


Figure 3-6: Heterogeneity between hiPSC-derived Schwann cell differentiation and cryopreservation batches. (**A**) Brightfield images of Schwann cell differentiation cultures 1 day, 8 days, and 13 days in vitro (div) after thawing. (i) – (iii) represent three individual batches of differentiation. (iii-a) – (iii-c) represent three different time points of cryopreservation of the same batch of differentiation. (**B**) Representative micrographs of immunostainings for Sox10, GAP-43, S100b, and vimentin (Vim) 16 days after thawing. Nuclei were labeled with DAPI. Color codes indicated in panels. Scale bars: 100 µm.

DMH1 concentrations, and duration in days for the treatment conditions labeled 1 – 6 in Figure 3-7. In the control condition, cells were differentiated according to the initial protocol without addition of BMP4 or DMH1. After a total differentiation time of 21 days (Figure 3-7A-B) or 41 days (Figure 3-7C), cells were fixed and stained for Sox2 and Sox10. The total number of cells as well as the proportions of Sox2+ and Sox10+ cells were quantified (Figure 3-7D). On day 21 of differentiation, almost all cells were positive for Sox2, except for conditions 1 and 2, which had been treated with BMP4 only (control: 99.3 % Sox2+ cells, 1: 21.3 %, 2: 20.7 %, 3: 99.9 %,

Table 8: Different BMP activation treatment conditions in Figure 3-7.

condition	1	2	3	4	5	6
BMP4	100 ng/mL	100 ng/mL	15 ng/mL	15 ng/mL	100 ng/mL	100 ng/mL
DMH1	-	-	1 µM	1 µM	1 µM	1 µM
days	4	6	4	6	4	6

4: 99.8 %, 5: 96.2 %, 6: 99.2 %; n = 1 experiment, mean values of 3 technical replicates). Similarly, the percentage of cells expressing Sox10 on day 21 was low in conditions 1 and 2 (1: 14.6 %, 2: 34.9 %), and it was high in the other conditions (control: 93.2 %, 3: 96.4 %, 4: 89.3 %, 5: 97.7 %), with the exception of condition 6. There, cultures had the highest total cell numbers in comparison to the other conditions, and while almost all of them were positive for Sox2, only 29.9 % were positive for Sox10. Also, while the proportion of both Sox2+ and Sox10+ cells was high in the control condition, there was a lot of cell detachment and control cultures were much sparser than BMP4/DMH1 treated conditions. On day 41 of differentiation, condition 1 could not be evaluated, as all cells had detached. Similarly, almost all cells in the control condition had detached as well. Although the few remaining cells in the control condition were largely positive for Sox10 (86.8 %), these cultures could not be expanded or differentiated further. In condition 2, no obvious cell detachment was observed, but cultures were sparser and of a different morphology than all other conditions, and only a small proportion of cells was positive for Sox10 (9.2 %). In condition 3, no cell detachment was observed as well, and 60.3 % of cells were positive for Sox10. In conditions 4, 5, and 6, the proportions of Sox10+ cells were the highest, with all cells present in these conditions staining positive for Sox10 (100.0 %). However, in conditions 5 and 6, considerable cell detachment occurred, which was not the case for condition 4, where cells kept attached robustly and could be expanded. Based on these preliminary data, the combination of 15 ng/mL BMP4 and 1 µM DMH1 for 6 days as used in condition 4 was replicated in further experiments.

Additionally, it was tested if passaging the differentiating cultures at different time points and ratios would influence survival and development of cells. To this end, five different passaging conditions were tested, including fixed passaging days or passaging upon 80 % culture confluency. These tested conditions are schematically depicted in Figure 3-8A (labeled (i) to (v)), two of those additionally included suspension culture phases. Each condition was done both with and without addition of BMP4 and DMH1 as described above, resulting in ten culture conditions in total ((i) – (v), ± BMP4/DMH1). Cultures were immunostained at different time points to assess differentiation efficiency, and Figure 3-8B shows proportions of Sox10+ cells for all conditions. In panels C and D of Figure 3-8, representative images of culture conditions (i) – (iii) are shown, each condition either with or without BMP4 and DMH1, and additionally

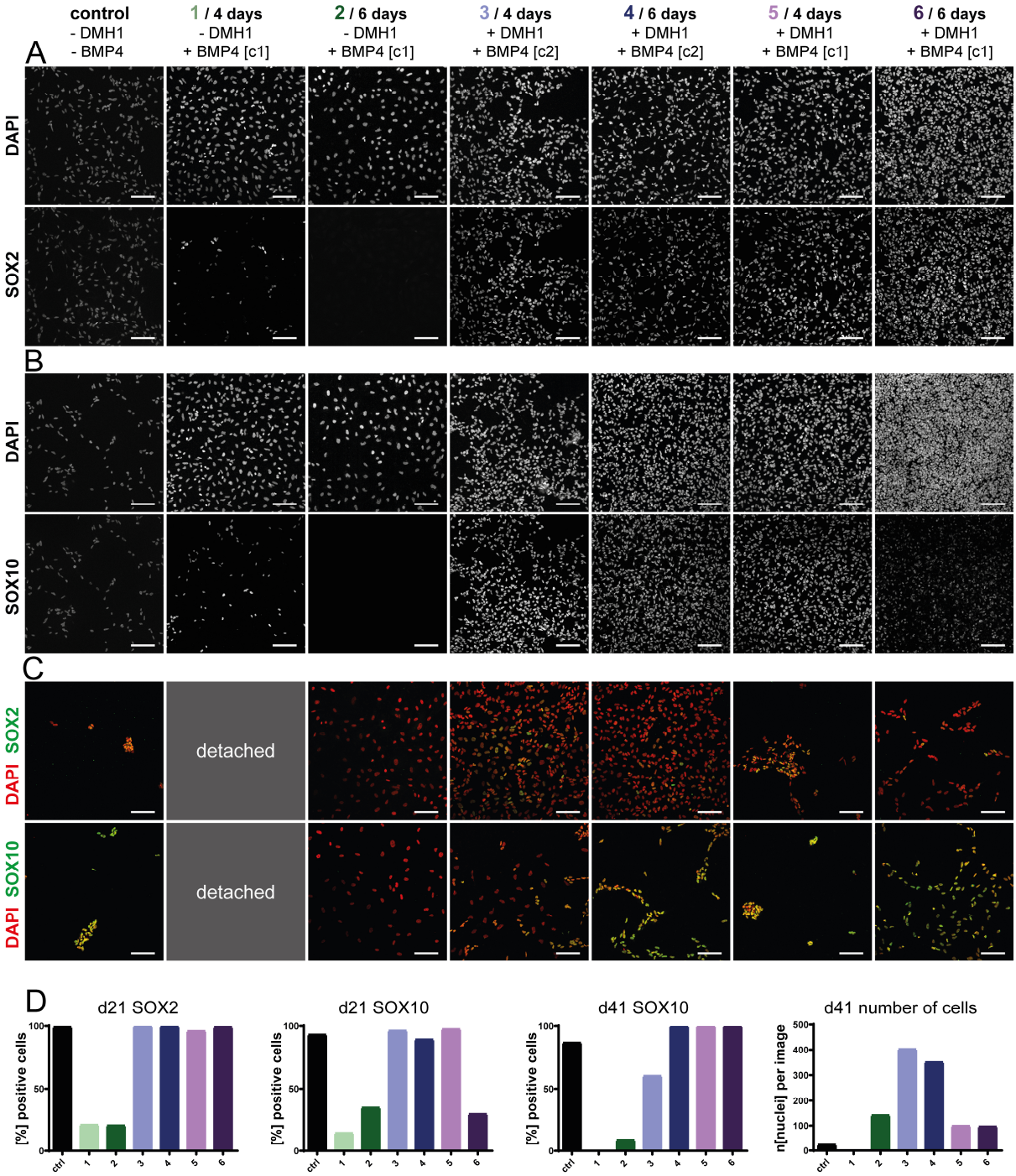


Figure 3-7: Different treatments with BMP4 and DMH1 influence cell differentiation and survival. (**A**) Cultures were immunostained for Sox2 on day 21 of differentiation. Nuclei were labeled with DAPI. Culture conditions are indicated above panels; c1 = 100 ng/mL, c2 = 15 ng/mL. Scale bars: 100 µm. (**B**) Cultures were immunostained for Sox10 on day 21 of differentiation. Nuclei were labeled with DAPI. Scale bars: 100 µm. (**C**) Cultures were immunostained for Sox2 and Sox10 on day 41 of differentiation. Nuclei were labeled with DAPI. Color codes indicated in panels. Scale bars: 100 µm. (**D**) Quantifications for the proportions of Sox2+ and Sox10+ cells on day 21, Sox10+ cells on day 41, and total numbers of cells present on day 41 for all conditions (n = 1 experiment, mean values of 3 technical replicates). d = day.

stained for S100b on day 32 (D). The percentages of cells positive for Sox10 and Sox2 were quantified at several time points (days 12, 26, and 32). On day 12, cultures which had been passaged only on day 6 (conditions (i) – (iii)) contained 1.0 % Sox10+ and 96.0 % Sox2+ cells,

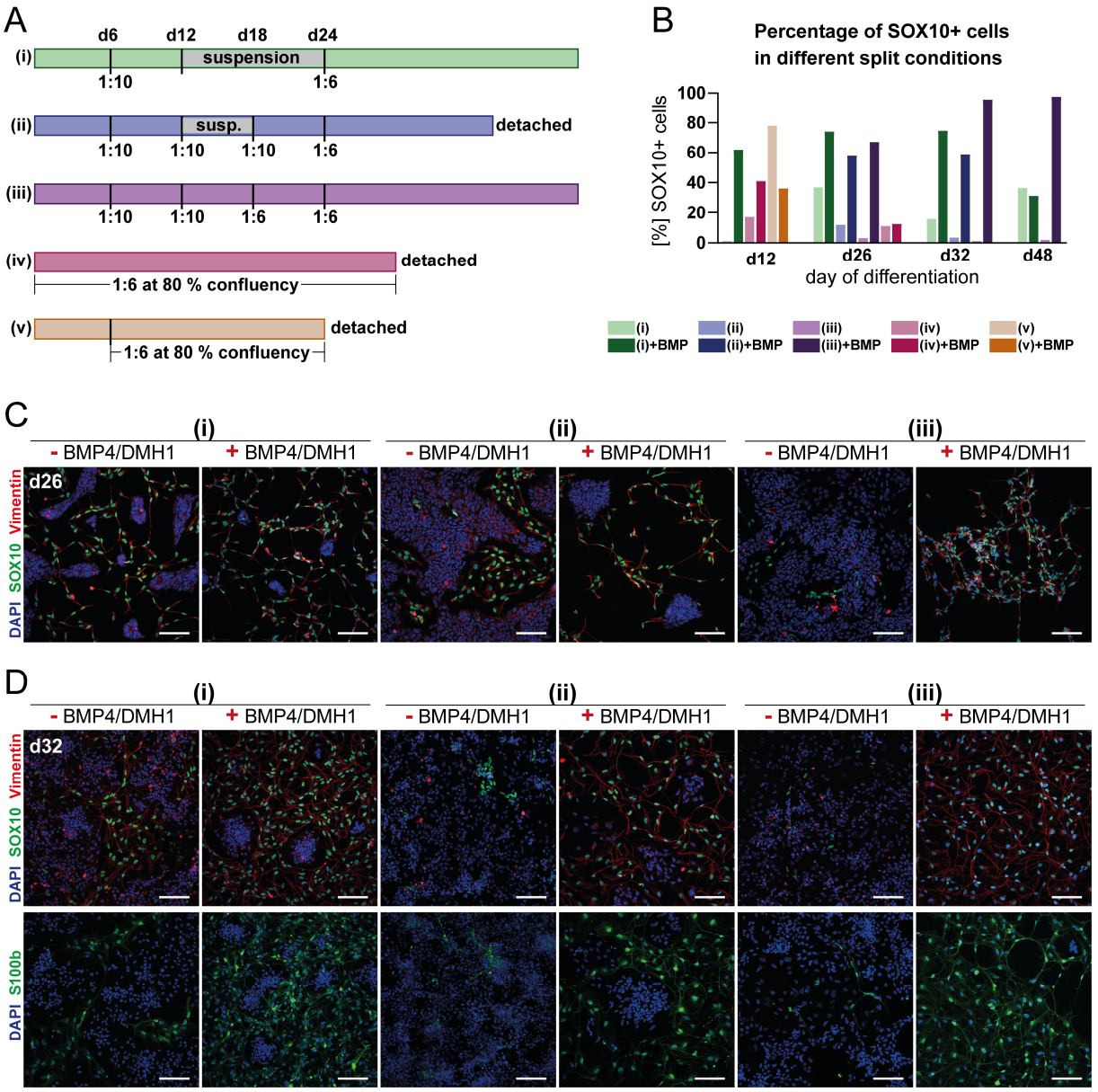


Figure 3-8: Both BMP4/DMH1 treatment and cell density during differentiation influence Sox10+ cell yield. (**A**) Schematic depiction of the different passaging conditions including time points and split ratios. For culture conditions in which cells detached, a time window is indicated. (**B**) Quantification of the proportions of Sox10+ cells on days 12, 26, 32, and 48 for all culture conditions tested (n = 1 experiment, mean values of 3 technical replicates). Colors indicate conditions as shown in legend, lighter colors represent conditions without BMP4/DMH1, darker colors represent conditions with BMP4/DMH1. (**C** – **D**) Cultures were immunostained for Sox10 (green) and vimentin (red) on day 26 (**C**) and day 32 (**D**). Lowest panel additionally shows S100b on day 32 (**D**). Nuclei were labeled with DAPI and are shown in blue. Representative images for three different passaging conditions labeled (i) – (iii), each differentiated either with or without BMP4/DMH1. Conditions (i) and (ii) included suspension culture phases of different lengths, while condition (iii) only included adherent culture. All three conditions were split every six days except during suspension phases at ratios indicated in panel A. Scale bars: 100 µm. d = day.

which increased to 61.5 % Sox10+ and 98.5 % Sox2+ cells if BMP4/DMH1 were added (n = 1 experiment, mean values of 3 technical replicates). In condition (iv), without BMP4/DMH1, 16.7 % of cells were Sox10+ and 87.9 % Sox2+, while 40.5 % were Sox10+ and 82.2 % Sox2+ with BMP4/DMH1 included. Finally, in condition (v), 77.6 % of cells were Sox10+ and 98.5 % Sox2+, which decreased to 35.8 % Sox10+ and 97.1 % Sox2+ if BMP4/DMH1 was

added. Cells cultured according to condition (v) detached before day 26 and were therefore not considered further. For most other conditions, the proportion of Sox10+ cells increased from day 12 to day 26, and addition of BMP4/DMH1 increased the percentage of Sox10+ cells in all cases ((i): 36.5 %, (i)+BMP4/DMH1: 73.7 %, (ii): 11.5 %, (ii)+BMP4/DMH1: 57.8 %, (iii): 2.8 %, (iii)+BMP4/DMH1: 66.7 %, (iv): 10.7 %, (iv)+BMP4/DMH1: 12.0 %; n = 1 experiment, mean values of 3 technical replicates). Conversely, the percentage of Sox2+ cells was decreased from day 12 to day 26 in all conditions ((i): 68.8 %, (i)+BMP4/DMH1: 29.9 %, (ii): 89.0 %, (ii)+BMP4/DMH1: 38.9 %, (iii): 93.2 %, (iii)+BMP4/DMH1: 8.3 %, (iv): 80.7 %, (iv)+BMP4/DMH1: 1.3 %). Cells cultured according to condition (iv) detached before day 32 and were therefore not considered further. On day 32, the percentages of Sox10+ cells were constant or increased for conditions cultured with BMP4/DMH1, but decreased in conditions without BMP4/DMH1 when compared to day 24 ((i): 15.4 %, (i)+BMP4/DMH1: 74.2 %, (ii): 3.1 %, (ii)+BMP4/DMH1: 58.5 %, (iii): 0.9 %, (iii)+BMP4/DMH1: 95.4 %; n = 1 experiment, mean values of 3 technical replicates). Again, addition of BMP4/DMH1 increased the percentage of Sox10+ cells in all conditions. Conversely, the percentage of Sox2+ cells was decreased in conditions with BMP4/DMH1 ((i): 78.1 %, (i)+BMP4/DMH1: 31.7 %, (ii): 92.4 %, (ii)+BMP4/DMH1: 42.9 %, (iii): 97.9 %, (iii)+BMP4/DMH1: 1.5 %). Cells cultured according to condition (ii) detached before day 48, therefore, only conditions (i) and (iii) were then evaluated for expression of Schwann cell markers, Sox10 and S100b, as well as the proliferation marker Ki67. For all three of those, condition (iii)+BMP4/DMH1 showed the highest percentages of positive cells. In condition (i) without BMP4/DMH1, no cells were detected which stained positive for S100b, while 23.6 % of cells were S100b+ if BMP4/DMH1 was included. Percentages of Sox10 and Ki67 were similar for both conditions ((i): 36.0 % Sox10+, 59.6 % Ki76+; (i)+BMP4/DMH1: 30.9 % Sox10+, 67.9 Ki67+; n = 1 experiment, mean values of 3 technical replicates). In condition (iii), the percentage of Ki67+ cells was similar between both conditions as well ((iii): 82.9 % Ki67+, (iii)+BMP4/DMH1: 87.5 % Ki67+). However, Schwann cell markers Sox10 and S100b dramatically increased when BMP4/DMH1 were added ((iii): 1.6 % Sox10+, 2.4 % S100b+; (iii)+BMP4/DMH1: 97.2 % Sox10+, 94.8 % S100b+). Since condition (iii) with addition of BMP4/DMH1 yielded the most robust cultures with the highest proportion of cells positive for Sox10 and S100b, cells of all following experiments were passaged as described for this condition.

Since the addition of BMP4 and DMH1 was found to increase differentiation of Sox10+ cells regardless of passaging methods, additional experimental replicates were done to confirm this finding. On top, further changes to the differentiation cocktail were tested as indicated in the top panel of Figure 3-9A. This included the omission of BSA and β-ME and an increased Nrg1

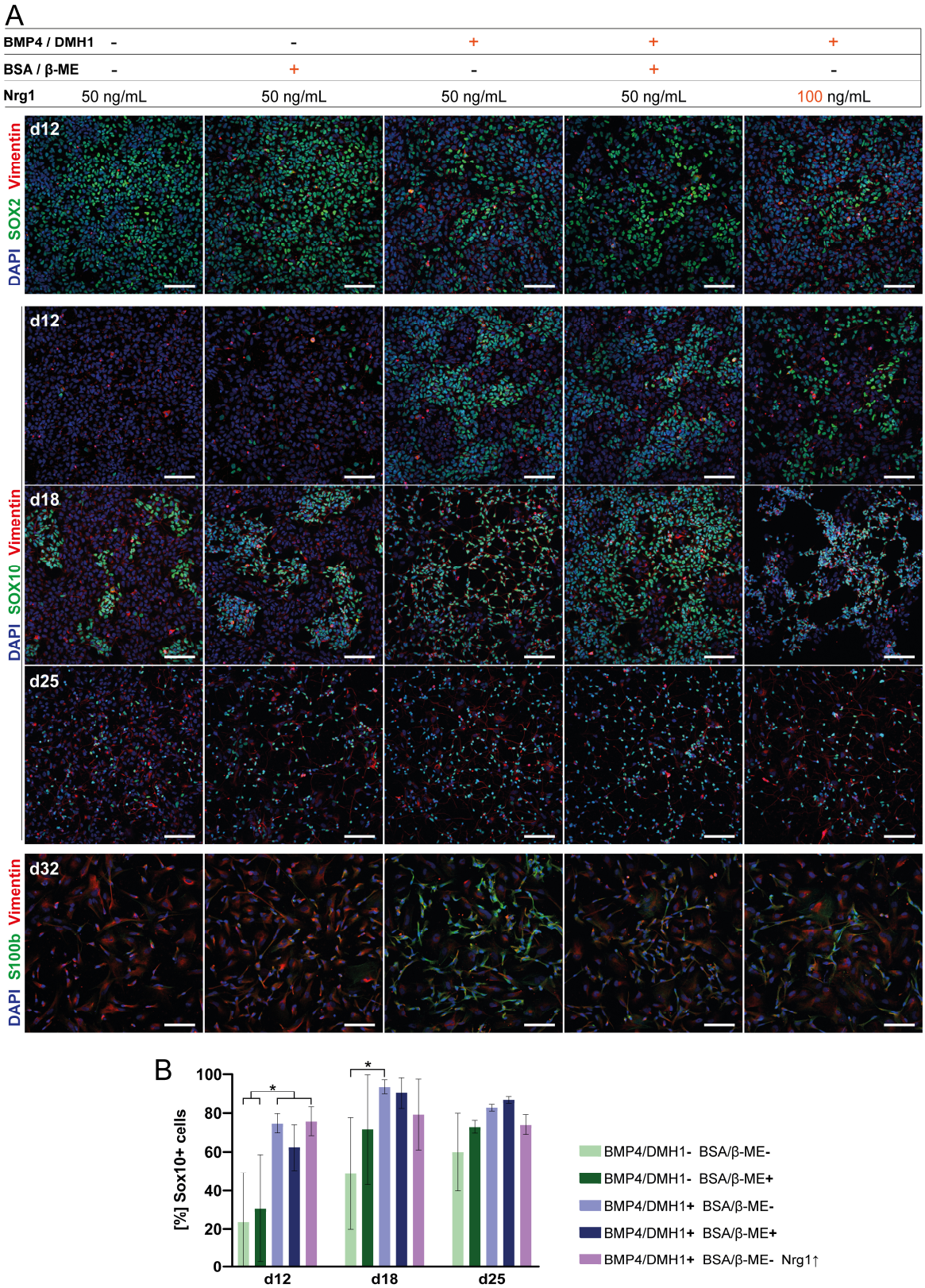


Figure 3-9: Addition of BMP4/DMH1 increases Sox10+ cells but addition of BSA/β-ME does not. (**A**) Representative images of cultures differentiated with or without BMP4/DMH1 in combination with or without BSA/β-ME (β-ME), or with a higher concentration of Nrg1, as indicated above panels. Color codes and time points of fixation indicated in panels. Scale bars: 100 µm. Parts of figure adapted from Hörner et al. [2021] under CC BY 4.0 license. (**B**) Quantification of the proportions of Sox10+ cells on days 12, 18, and 25 for all culture conditions tested. Graph depicts mean ± SD (n = 3 experiments). * $p < 0.05$ (multiple t-tests). Colors indicate conditions as shown in legend. d = day.

concentration as indicated (Figure 3-9A). Cells were fixed on days 12, 18, and 25, and immunostained for Sox10 and vimentin. On day 12, additionally Sox2 was labeled. After 32 days of differentiation, cells were labeled for vimentin and S100b, to assess whether they had differentiated into Schwann cells. This showed that neither BSA and β-ME nor a higher concentration of Nrg1 increased the amount of Sox10+ cells, but addition of BMP4 and DMH1 did (Figure 3-9A). In cultures without BMP4 and DMH1, 23.5 ± 25.9 % of cells were positive for Sox10 without BSA/β-ME, and 30.7 ± 27.9 % with BSA/β-ME on day 12 (mean ± SD, n = 3 experiments). The proportion of Sox10+ cells on day 12 increased in cultures differentiated with BMP4 and DMH1 (74.7 ± 5.1 % without BSA/β-ME, 62.3 ± 11.8 % with BSA/β-ME, 75.7 ± 7.5 without BSA/β-ME and with 100 ng/mL of Nrg1). This increase was significant in the two conditions without BSA/β-ME. On day 18, the proportion of Sox10+ cells was higher in conditions with BMP4/DMH1 (93.5 ± 3.7 % without BSA/β-ME, 90.3 ± 8.0 % with BSA/β-ME, 79.2 ± 18.3 % without BSA/β-ME and with 100 ng/mL of Nrg1) than in conditions without BMP4/DMH1 (48.8 ± 29.0 % without BSA/β-ME, 71.8 ± 28.7 % with BSA/β-ME) as well. Again, the difference was only significant in cultures without BSA/β-ME (Figure 3-9B). On day 25, no significant differences were determined, but still the measured proportions of Sox10+ cells were higher in conditions with BMP4/DMH1 (82.7 ± 1.7 % without BSA/β-ME, 86.7 ± 1.7 % with BSA/β-ME, 74.0 ± 5.2 % without BSA/β-ME and with 100 ng/mL of Nrg1) than without BMP4/DMH1 (59.9 ± 20.0 % without BSA/β-ME, 72.9 ± 3.4 % with BSA/β-ME). However, on day 32 (Figure 3-9A lowest panel), almost no cells positive for S100b were observed in cultures differentiated without BMP4/DMH1, and the highest amount of S100b+ cells was present in cultures differentiated with BMP4/DMH1, without BSA/β-ME, and with a concentration of 50 ng/mL for Nrg1 (Figure 3-9 middle column). Thus, all following differentiations were done according to this protocol.

Subsequently, it was tested if additional treatment with either 1 µM resveratrol [Pinchot et al., 2010] or 10 µM ROCK inhibitor Y-27632 [Kim et al., 2015] from day 6 to day 12 could further enhance differentiation of Sox10+ neural crest cells. Cultures were fixed on days 19, 25, and 33, and immunostained for vimentin and Sox10 (Figure 3-10). On day 19, cultures were additionally labeled for Sox2, and also compared to cells cultured in parallel without BMP4 and DMH1. Again, cells cultured without BMP4/DMH1 showed higher proportions of Sox2+ cells and lower proportions of Sox10+ cells than all other conditions (Figure 3-10A). Cultures treated with resveratrol looked similar to those treated only with BMP4/DMH1 on day 19, while treatment with Y-27632 led to denser cultures, suggesting increased cell proliferation (Figure 3-10B). Also, Y-27632-treated cultures had the highest proportion of Sox10+ cells on day 19 (89.6 % Sox10+ cells, compared to 72.6 % in resveratrol treated cultures and 73.8 % in control cultures only treated with BMP4/DMH1; mean values, n = 2 experiments) (Figure 3-10C). However, at later time points, both resveratrol and Y-27632-treated cultures exhibited lower

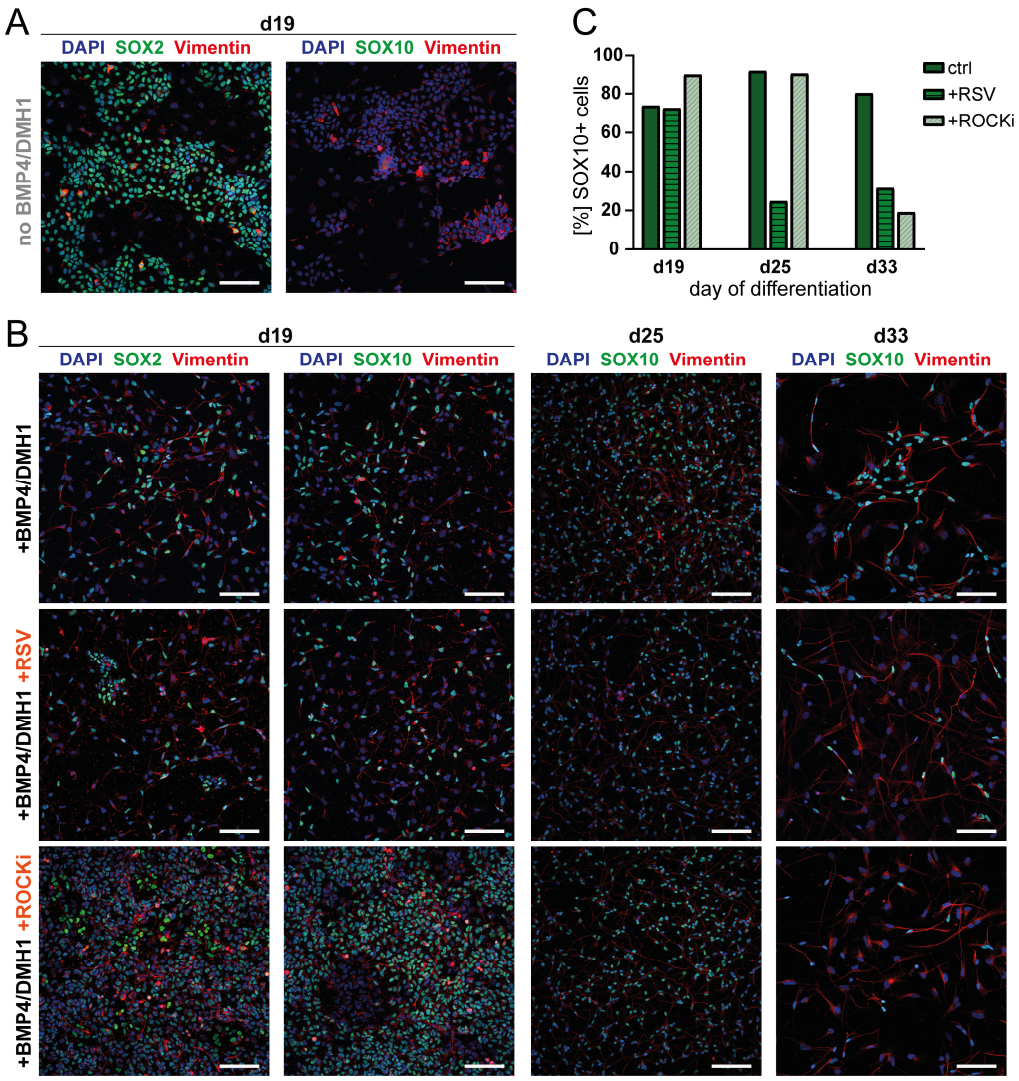


Figure 3-10: Addition of resveratrol or ROCK inhibitor has no beneficial effects on Sox10+ cell yield. (**A**) Cultures were differentiated without BMP4/DMH1 and evaluated on day 19. Color codes for immunostained proteins are indicated above panels. Nuclei were labeled with DAPI. Scale bars: 100 µm. (**B**) Cultures were differentiated with BMP4/DMH1, either without additional molecules (first row), with addition of resveratrol (RSV, middle row), or addition of ROCK inhibitor Y-27632, and evaluated at different time points for Sox2 (day 19 only), Sox10 and vimentin. Nuclei were labeled with DAPI. Color codes and time points of fixation indicated above panels. Scale bars: 100 µm. (**C**). Quantification of the proportions of Sox10+ cells on days 19, 25, and 33 for cultures differentiated with BMP4/DMH1, either without additional molecules (ctrl), with addition of resveratrol (+RSV), or addition of Y-27632 (+ROCKi) (n = 1 experiment, mean values of 3 technical replicates). d = day.

levels of Sox10+ cells (day 25 control: 91.5 %, resveratrol: 24.7 %, Y-27632: 90.21 %; day 33 control: 80.2 %, resveratrol: 31.47 %, Y-27632: 19.0 %). Therefore, both of these molecules were not further investigated.

Since in all experiments described above, the addition of BMP4 and DMH1 improved differentiation of Sox10+ cells, this was reproduced in several independent experiments with three different hiPSC lines, to confirm this effect (Figure 3-11). Cells cultured either in the presence of BMP4 and DMH1 or without both molecules were analyzed for the percentage of Sox10+ cells after 12, 19, and 26 days of differentiation. Addition of BMP4/DMH1 significantly

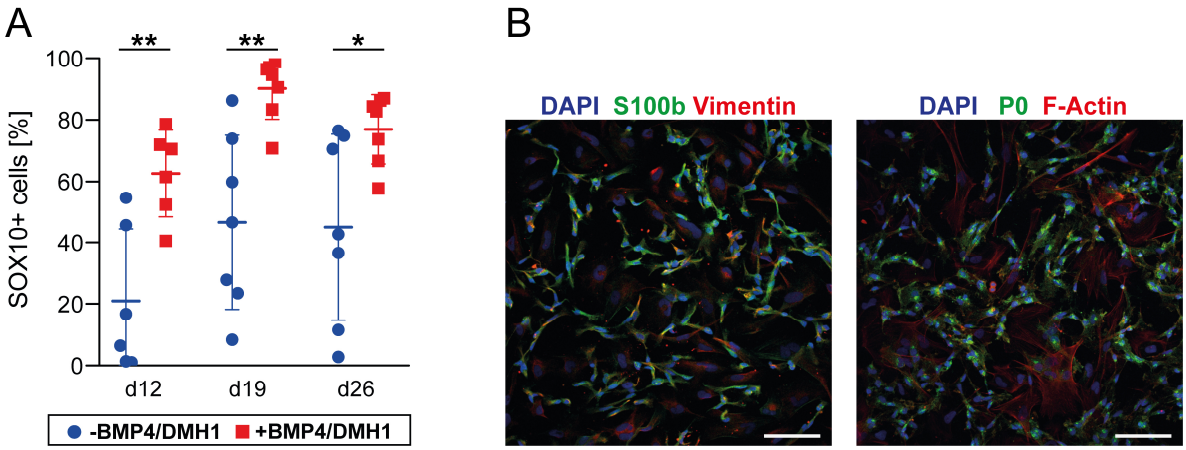


Figure 3-11: Addition of BMP4/DMH1 robustly improves yield of Sox10+ cells which are competent for Schwann cell differentiation. (**A**) Cells were differentiated either without (blue) or with (red) addition of BMP4 and DMH1 as described. Cultures were fixed at time points indicated and the proportion of Sox10+ cells was quantified. Graph depicts mean ± SD (n = 6 experiments for day 12; n = 7 experiments for days 19 and 26). * $p < 0.05$, ** $p < 0.01$ (t-tests). d = day. (**B**) Representative images of cultures differentiated in the presence of BMP4 and DMH1 on day 32, showing fluorescence signals for Schwann cell markers S100b and P0. Nuclei were labeled with DAPI. Color codes indicated above panels. Scale bars: 100 µm. Adapted from Hörner et al. [2021] under CC BY 4.0 license.

increased the proportion of Sox10+ cells at all time points evaluated. On day 12, 62.6 ± 14.1 % of cells were Sox10+ after differentiation with BMP4/DMH1, compared to 21.0 ± 23.5 % of cells without BMP4/DMH1 (mean ± SD, n = 6 experiments). At the following time points, the proportion of Sox10+ cells increased in the presence of BMP4/DMH1 from 46.6 ± 28.4 % to 90.2 ± 10.0 % on day 19 and from 45.1 ± 30.3 % to 77.0 ± 11.3 % on day 26 (mean ± SD, n = 7 experiments) (Figure 3-11A). As evident from the values and graph, BMP4/DMH1 not only enhanced the mean yield of Sox10+ cells, but also the robustness and consistency of differentiation success. Furthermore, Sox10+ cells which were differentiated in the presence of BMP4/DMH1 were successfully differentiated into Schwann cells expressing S100b and P0 (Figure 3-11B). Therefore, BMP4 and DMH1 were included in the Schwann cell differentiation protocol for all subsequent experiments.

The final protocol timeline and differentiation factors are depicted schematically in Figure 3-12 alongside representative brightfield images of cultures at various time points throughout the differentiation. This modified protocol included tuning of BMP signaling activity using BMP4/DMH1, omitted the use of BSA or β-ME, and passaging was done as described in the previous paragraph. Furthermore, the small molecule SB431542 was applied at a tenfold lower concentration as compared to the original protocol [Kim et al., 2017], as this was sufficient to induce neuralization. With this protocol, Schwann cells positive for S100b and P0 could be obtained after about 40 days of differentiation. Schwann cells could be expanded for several passages until at least day 100, and cells could be cryopreserved at every passage after

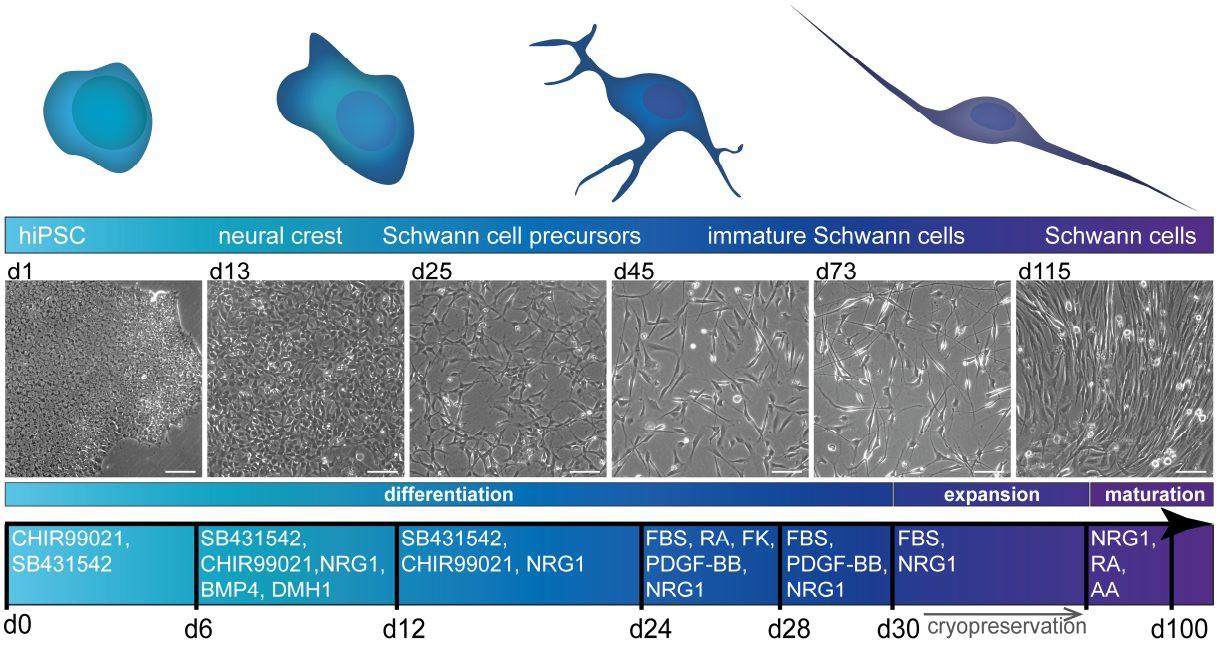


Figure 3-12: Modified Schwann cell differentiation protocol including tuning of BMP activity. Schematic representation of cell differentiation stages, differentiation protocol timeline, and molecules used. Micrographs show representative brightfield images of cell cultures at time points indicated above images. Scale bars: 100 µm. d = day. Adapted with modifications from Hörner et al. [2021; 2022] under CC BY 4.0 license.

day 40. Furthermore, this protocol worked robustly to derive Schwann cells from several hiPSC lines, as shown in Figure 3-13. Between cell lines, there was a llimited variation regarding the efficiency of differentiation, the time needed for cell maturation, as well as cell morphologies in the differentiated stage. This variation in cell morphology or appearance is also visible in the image panels of Figure 3-13. Furthermore, some cell lines consistently resulted in higher Schwann cell yields as others, e.g., Schwann cell cultures using the cell line WC035i-SOD1-D90D yielded a higher proportion of cells positive for marker proteins S100b and P0, as compared to the cell line WC034i-SOD1-D90A after 60 – 80 days of differentiation. While the difference regarding S100b expression was negligible (95.7 ± 2.9 % S100b+ cells for WC035i-SOD1-D90D, 86.6 ± 12.2 % S100b+ cells for WC034i-SOD1-D90A; mean ± SD, n = 3 experiments), the proportion of cells positive for P0 was significantly lower ($p < 0.05$) for WC034i-SOD1-D90A (63.7 ± 14.4 %) compared to WC035i-SOD1-D90D (89.5 ± 9.2 %). However, all hiPSC lines evaluated could be differentiated into Schwann cells positive for marker proteins S100b, Sox10, P0, and p75NTR at sufficient quantities (Figure 3-13). Besides these four marker proteins, Schwann cells were also positive for GAP-43, vimentin, and GFAP. However, while S100b, Sox10, P0, p75NTR, GAP-43, and vimentin were expressed consistently, GFAP was seen only in some cultures and at low levels. Expression of mature myelination marker MBP was not detected in immunofluorescence stainings, which was expected, as Schwann cells were not cocultured long-term with neurons to induce myelination.

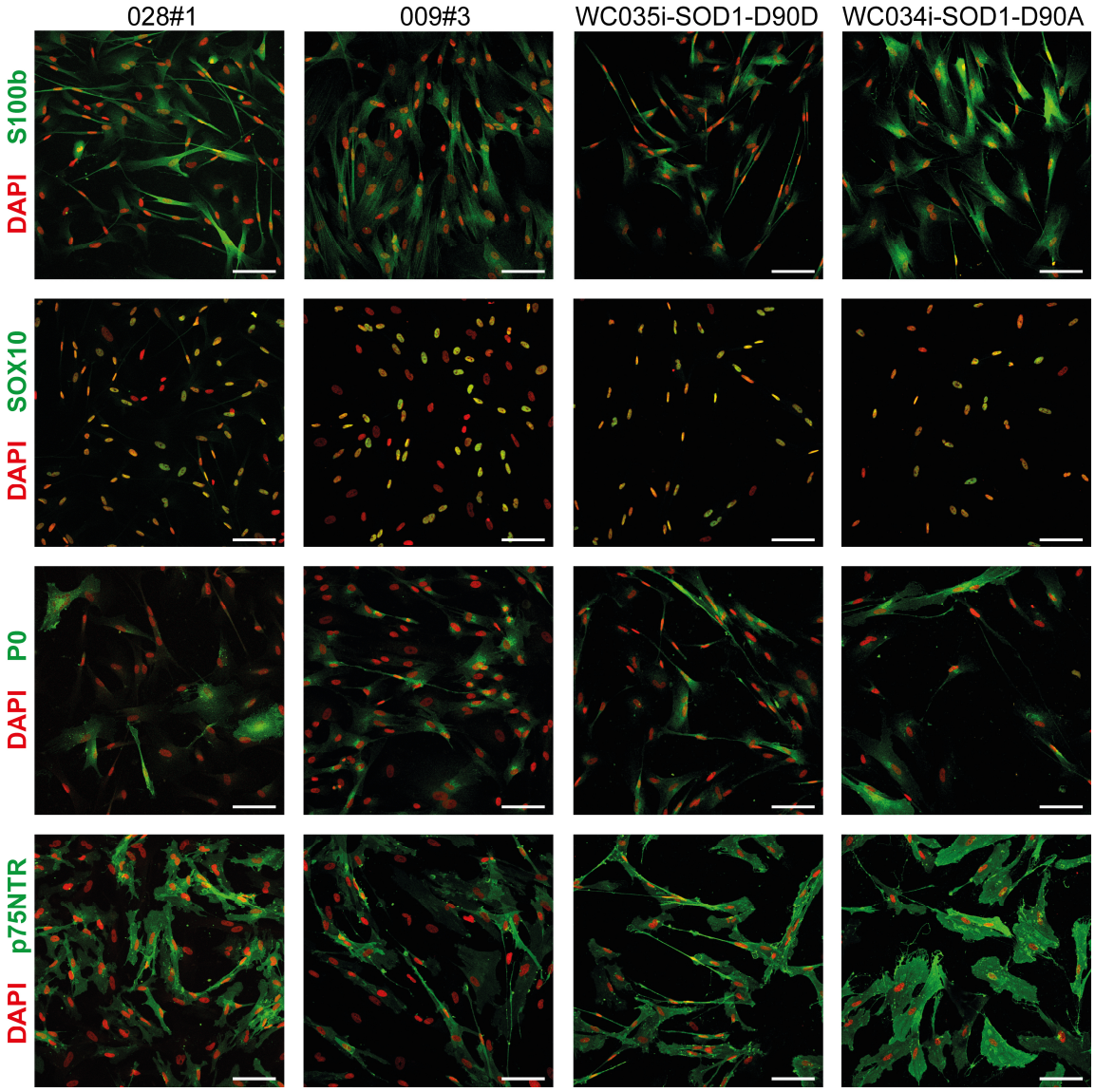


Figure 3-13: The modified protocol allows robust differentiation of Schwann cells from different hiPSC lines. Names of cell lines are indicated above panels. Cells were differentiated for at least 50 days and immunostained for S100b, Sox10, P0, and p75NTR. Color codes indicated on the left. Nuclei were labeled with DAPI. Scale bars: 100 µm.

3.1.5 Maturation of hiPSC-derived Schwann cells is improved in serum-free media designed for neuromuscular cocultures

To prepare triculture experiments, a medium formulation which could support neuronal, muscle, and Schwann cells was developed. This was based on MNDM4, the final medium of the motoneuron differentiation protocol (see section 2.1.4), as this formulation seemed to support maturation of both, motoneurons as well as C2C12 myotubes (section 3.2.1). To adjust MNDM4 for Schwann cell culture, compound E was replaced by Nrg1. Differentiated Schwann cells were then incubated in this medium, termed triculture medium (triM), and compared to cells of the same differentiation batch cultured in the standard Schwann cell medium (SCM). SCM was prepared from DMEM with low glucose concentration (1 g/L) supplemented with

FBS and Nrg1 [Kim et al., 2017]. TriM was composed of an equal parts mixture of DMEM/F12 and Neurobasal media, supplemented with ascorbic acid, purmorphamine, retinoic acid, BDNF, GDNF, IGF-1, and Nrg1. To assess whether Schwann cells were supported by triM, they were stained for markers of the neural crest and Schwann cell lineage including p75NTR, S100b, Pax3, GAP-43, and P0, as well as proliferation marker Ki67, after three days of incubation in either SCM or triM (Figure 3-14). This combination of marker proteins was chosen to give an impression of the differentiation stage of cultures, as these markers are expressed differentially with maturation along the Schwann cell lineage (Figure 3-14A). Cells in both media, SCM and triM, expressed all tested markers, but in different distributions. As shown in Figure 3-14B, signals associated with Schwann cell differentiation were increased in triM (p75NTR, S100b, GAP-43, P0), while early markers were decreased (Ki67, Pax3). Moreover, morphology and overall appearance of cell cultures changed with triM incubation, which is particularly evident from the immunofluorescence panels for p75NTR and S100b in Figure 3-14B. Confocal microscopy images of Ki67, GAP-43, S100b, and P0 stainings combined with those for vimentin and f-actin to visualize cell morphology confirmed these findings and suggested a shift towards a more elongated, often spindle-shaped cell morphology in triM (Figure 3-15A). To evaluate which components of triM might be responsible for these effects, cells were incubated in six different medium formulations: (i) SCM, (ii) fully supplemented triM, (iii) basal triM without any supplemented differentiation factors (BM), and (iv) – (vi) BM supplemented with different molecule combinations as shown in Table 9.

Table 9: Overview of media compositions for Schwann cell maturation experiments.

	(i) SCM	(ii) triM	(iii) BM	(iv)	(v)	(vi)
DMEM low glucose base	x					
DMEM/F12-Neurobasal base		x	x	x	x	x
FBS	x					
N2 + B27 supplements		x	x	x	x	x
Nrg1	x	x		x	x	x
retinoic acid (RA)		x			x	x
purmorphamine (Pur)		x			x	
ascorbic acid (AA)		x				x
GDNF		x				
BDNF		x				
IGF-1		x				

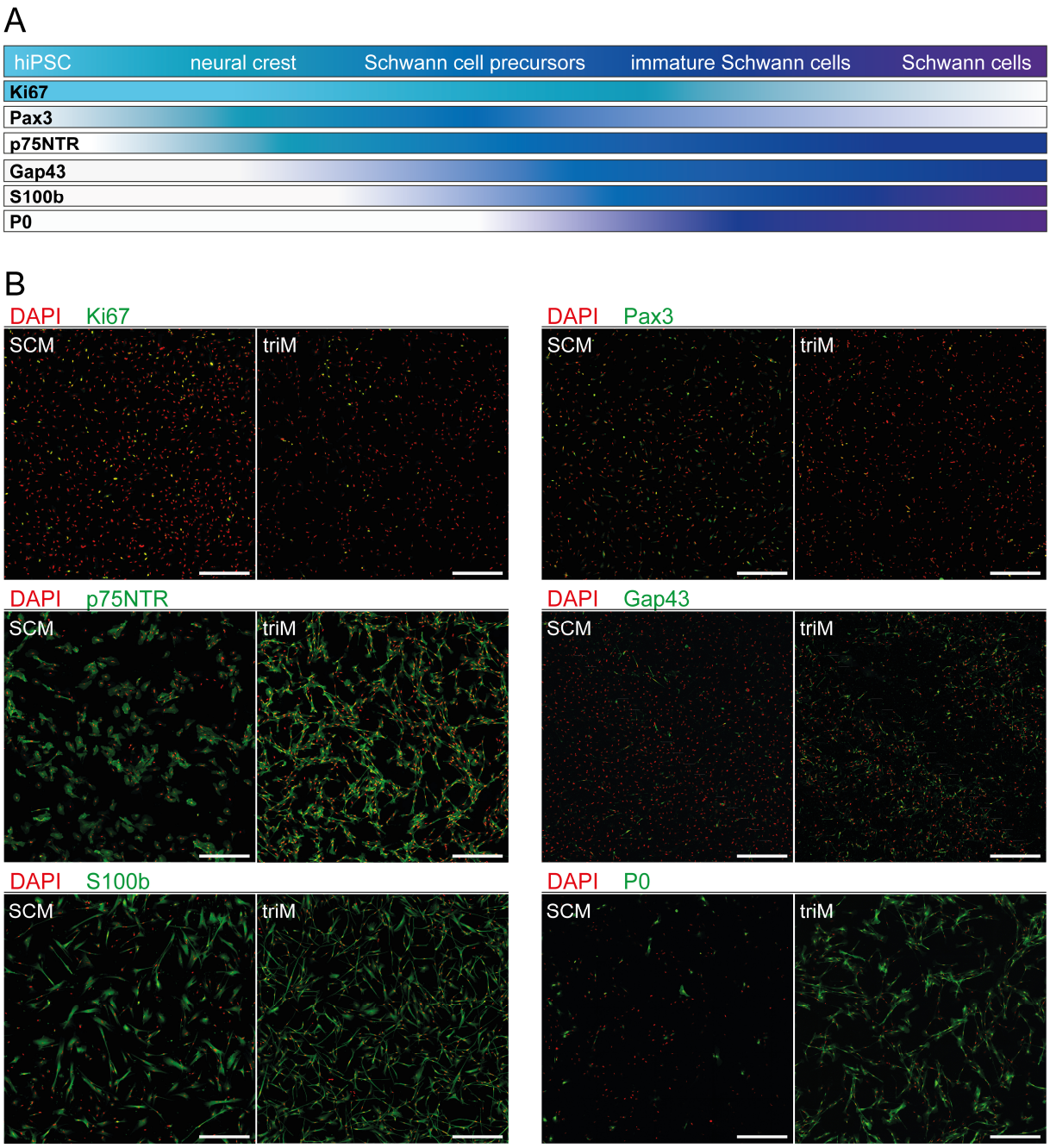


Figure 3-14: Distribution of marker stainings in differentiated Schwann cell cultures changes upon culture in different media. (**A**) Schematic representation of expression timelines of evaluated marker proteins throughout Schwann cell differentiation. (**B**) Representative images of differentiated Schwann cell cultures which were incubated either in SCM or triM for three days as indicated in panels. Immunostained proteins and color codes indicated above panels. Nuclei were labeled with DAPI. Scale bars: 500 µm.

After three days of incubation in these media, Schwann cells were immunostained for several marker proteins (Figure 3-15B), and the proportions of cells positive for Ki67, Pax3, p75NTR, GAP-43, S100b, and P0 were quantified (Figure 3-16A). The quantitative results are summarized in Table 10 for better overview. As evident from the graph and table, the percentage of cells positive for Ki67 was significantly decreased in triM (ii), as well as in media (v) and (vi) when compared to the control condition, SCM (i). No significant differences to SCM

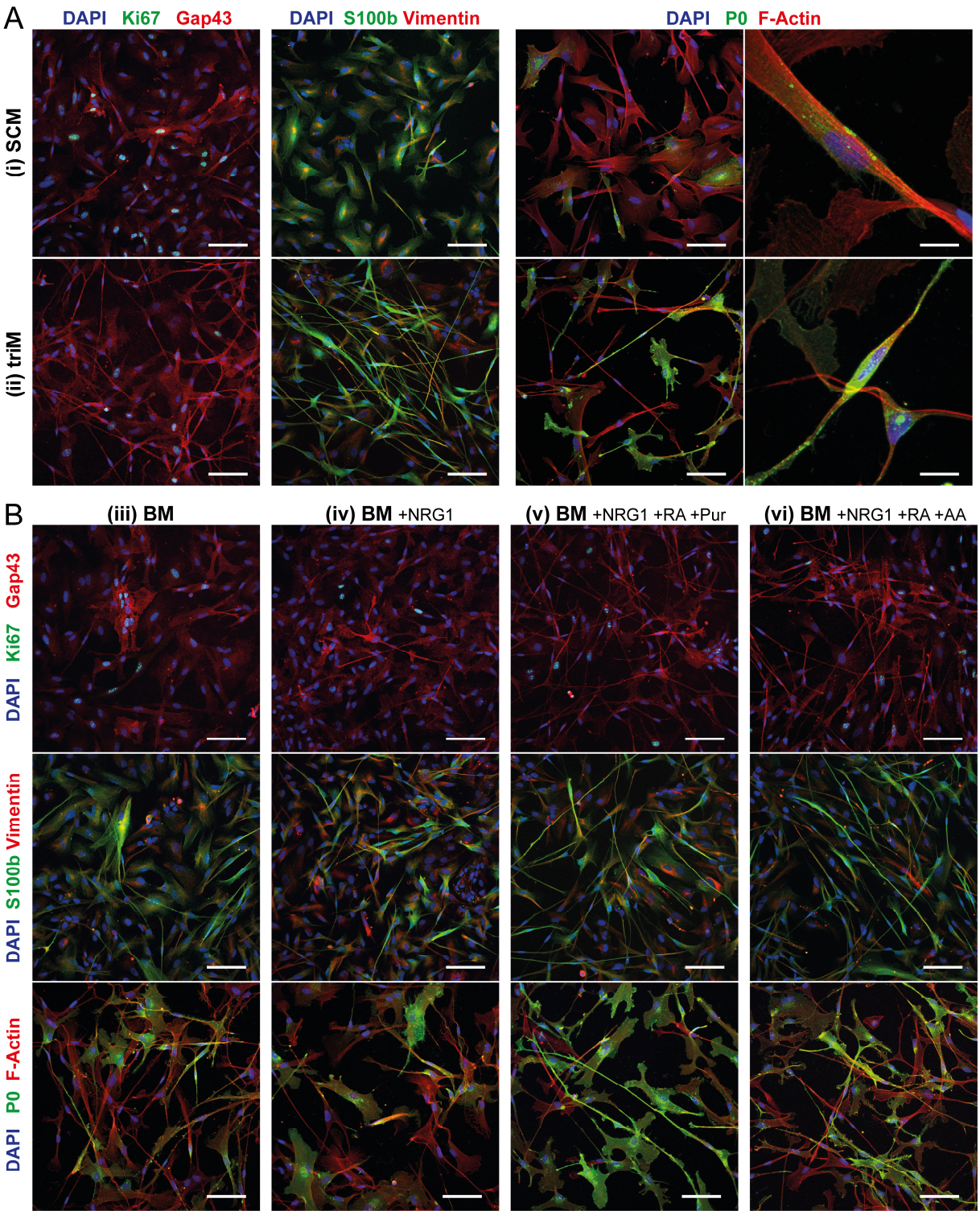


Figure 3-15: Marker protein distribution and cell morphology depend on medium conditions. (**A**) Representative immunofluorescence images of Schwann cells incubated either in SCM (standard Schwann cell medium) or triM (triculture medium) for three days. Immunostained proteins and color codes indicated above panels. Nuclei were labeled with DAPI. Scale bars: 100 µm, zoom images on the right: 20 µm. (**B**) Representative images of cells incubated in additional medium conditions as described. Immunostained proteins and color codes indicated on the left. Nuclei were labeled with DAPI. Scale bars: 100 µm. Adapted from Hörner et al. [2021] under CC BY 4.0 license.

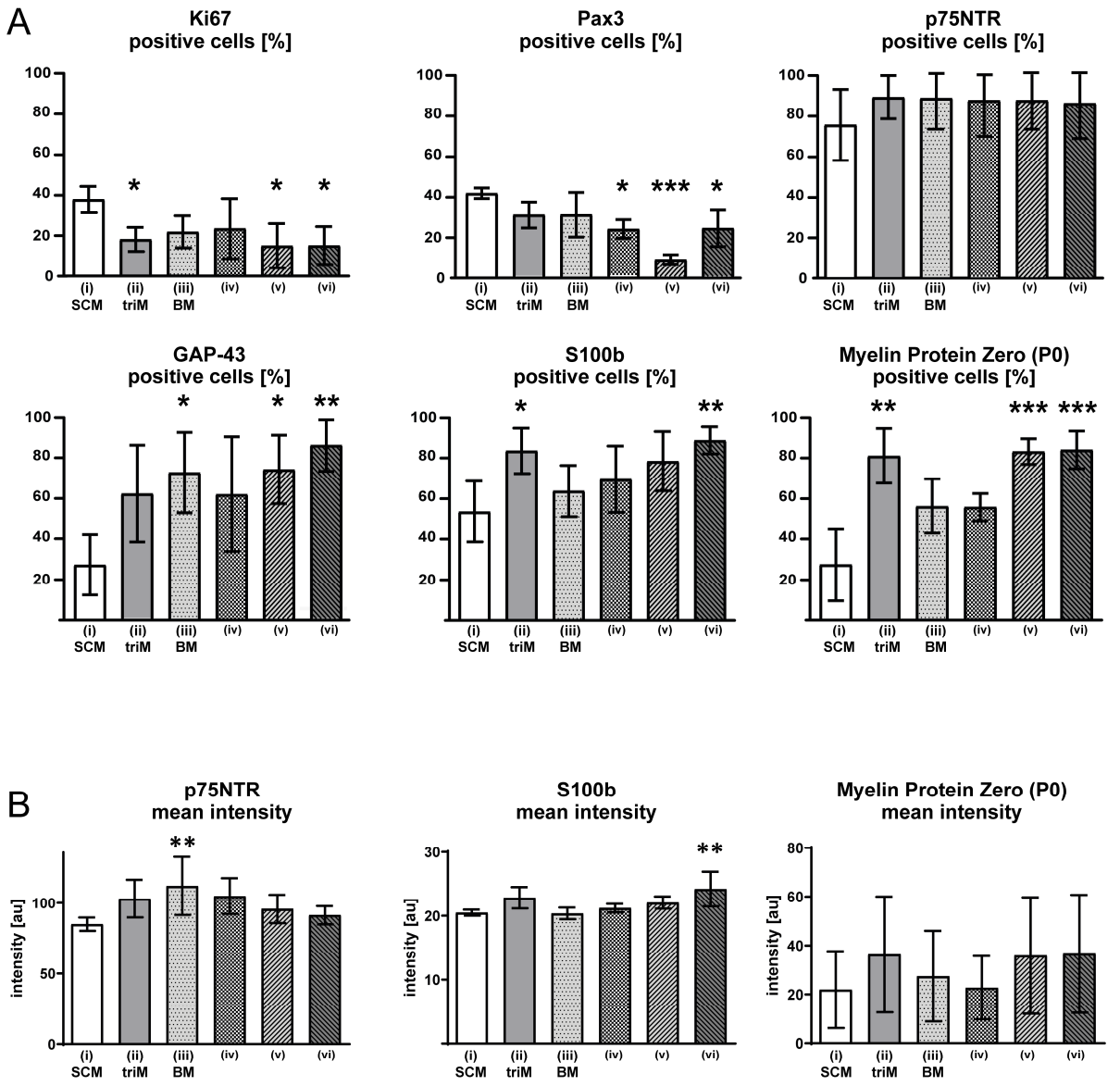


Figure 3-16: Cell differentiation measured by marker protein expression is increased in several medium conditions. (**A**) Cells were incubated in medium conditions as described for three days and the percentages of cells positive for Ki67, Pax3, p75NTR, GAP-43, S100b, and P0 were quantified for each condition. Graphs depict mean ± SD (n = 5 experiments for Ki67, p75NTR, and S100b; n = 4 for GAP-43; n = 3 for Pax3 and P0). * $p < 0.05$, ** $p < 0.01$, *** $p < 0.001$ (one-way ANOVA). Partly adapted from Hörner et al. [2021] under CC BY 4.0 license. (**B**) Quantifications of relative intensities for p75NTR, S100b, and P0. Graphs depict mean ± SD (n = 5 experiments for p75NTR and S100b; n = 3 for P0). ** $p < 0.01$ (one-way ANOVA).

were observed in media (iii) and (iv) (n = 5 experiments). Regarding Pax3, there was no significant difference between (i) SCM, (ii) triM, and (iii) BM, but it was decreased in (iv), (v), and (vi), when compared to SCM (n = 3 experiments). For p75NTR, higher mean values were measured for all triM/BM conditions when compared to SCM, but there were no significant differences (n = 5 experiments). GAP-43 was increased in all conditions when compared to SCM, which was significant for (iii), (v), and (vi); but not for (ii) triM and (iv) (n = 4 experiments). Likewise, the proportion of S100b+ cells was also lowest in (i) SCM. In (ii) triM and (vi), the

percentage of S100b+ cells was increased significantly, while the difference was not significant in the other media (n = 5 experiments). Finally, also the percentages of cells positive for P0 were elevated in all conditions when compared to (i) SCM, which was significant for (ii) triM, (v), and (vi) (n = 3 experiments). Next, the mean signal intensities of positive cells were compared for p75NTR, S100b, and P0 (Figure 3-16B). Results are summarized in Table 11. The mean relative intensity of p75NTR was increased in (iii) BM when compared to (i) SCM, while no differences were observed for the other medium conditions (n = 3 experiments). Similarly, there were no differences of S100b mean relative intensity in most medium conditions when compared to (i) SCM, except for an increase in (vi) (n = 4 experiments). Regarding P0 mean relative intensity, no significant differences were observed in any medium condition (n = 3 experiments). Taken together, these results suggested an improved maturation of Schwann cells particularly in the media (ii) triM, (v) containing Nrg1, retinoic acid,

Table 10: Percentages of cells positive for marker proteins listed in first column, quantified for different media as indicated in header. Values given as mean ± SD. Color code indicates decreased and increased values compared to (i) SCM as shown below. Data produced jointly with Roman Bruch, see Table 12, p. 157.

	(i) SCM	(ii) triM	(iii) BM	(iv)	(v)	(vi)
Ki67	38.0 ± 6.3	18.1 ± 5.9	21.8 ± 7.9	23.5 ± 14.8	15.0 ± 10.9	15.1 ± 9.2
Pax3	40.3 ± 2.6	29.7 ± 6.4	29.8 ± 10.9	22.8 ± 4.5	8.1 ± 2.3	23.3 ± 9.1
p75NTR	74.6 ± 17.4	88.2 ± 10.6	87.8 ± 15.2	86.7 ± 17.7	86.7 ± 14.2	85.3 ± 17.4
GAP-43	26.1 ± 14.8	61.1 ± 23.8	71.5 ± 19.7	60.8 ± 28.2	73.0 ± 16.8	85.0 ± 12.7
S100b	53.6 ± 15.1	83.4 ± 11.1	63.7 ± 12.6	69.5 ± 16.3	78.4 ± 14.6	88.6 ± 6.6
P0	27.3 ± 17.8	80.8 ± 13.4	56.1 ± 13.4	55.6 ± 6.7	83.0 ± 6.3	83.8 ± 9.2

Table 11: Mean signal intensity values for marker proteins listed in first column, quantified for different media as indicated in header. Values given as mean ± SD. Color code indicates decreased and increased values compared to (i) SCM as shown below. Data produced jointly with Roman Bruch, see Table 12, p.157.

	(i) SCM	(ii) triM	(iii) BM	(iv)	(v)	(vi)
p75NTR	84.9 ± 4.8	103.0 ± 13.3	112.0 ± 20.6	104.8 ± 12.7	95.7 ± 10.1	91.3 ± 6.5
S100b	20.5 ± 0.5	22.8 ± 1.7	20.4 ± 0.9	21.2 ± 0.7	22.1 ± 1.0	24.2 ± 2.7
P0	22.0 ± 15.7	36.3 ± 23.7	27.5 ± 18.6	22.7 ± 13.0	35.9 ± 23.9	36.6 ± 24.1

unchanged (± 1 SD)	decrease	significant decrease	increase	significant increase

and purmorphamine; and (vi) containing Nrg1, retinoic acid, and ascorbic acid. To confirm this, an image analysis pipeline was set up to calculate a numerical value representing bipolar cell elongation, to obtain a comparable quantification of the observed changes in cell morphology (Figure 3-17). To this end, fluorescence images of Schwann cell cultures in different media were segmented and processed as described in section 2.4.2 and schematically depicted in Figure 3-17A. For this analysis, images of cultures stained for S100b were used, as these clearly and consistently visualized cell morphology across different conditions (Figure 3-17B). Through several processing steps, narrow structures representing thin cell processes were segmented[8]. Subsequently, the major axis lengths of these segments were summed up and divided by the number of S100b+ cells present in the image. The resulting numerical value was termed “elongation index” and represented cell elongation, i.e., the higher the elongation index value was, the more and/or longer cell processes were present. This value was determined for all medium conditions tested (Figure 3-17C), revealing that cell elongation was increased significantly in the following media: (ii) triM (23.9 ± 9.3), (v) BM containing Nrg1, retinoic acid, and purmorphamine (19.3 ± 7.0), and (vi) BM containing Nrg1, retinoic acid, and ascorbic acid (31.2 ± 9.7), when compared to (i) SCM (5.3 ± 5.0). For (iii) BM and (iv) BM supplemented with only Nrg1, no significant difference was found (8.6 ± 6.0 and 6.7 ± 4.5, respectively; mean ± SD, n = 5 experiments), supporting the marker analysis results shown in Figure 3-16.

Besides these conditions, it was also tested if additional supplementation with the neurotrophic factor NT-3 would promote Schwann cell maturation. Cells were incubated in SCM with and without NT-3 as well as in triM with and without NT-3 for three days. However, while cells looked different depending on whether they were kept in SCM or triM, NT-3 did not seem to have an additional effect in this experiment (Figure 3-18A). Furthermore, completely serum-free culture was tested, by replacing FBS in differentiation media used from day 24 onwards with serum-free culture supplements B27 and N2. Cells were cultured like this for 14 additional days after day 24 and fixed for evaluation on day 38. For the last three days before fixation, cultures were either switched to triM or left in serum-free modified SCM. Then, cultures were stained for Ki67, GAP-43, S100b, vimentin, and Sox10 (Figure 3-18B). While cells expressing Schwann cell markers were observed in serum-free conditions, the majority of cells was negative for those markers (Figure 3-18B). Moreover, this contaminating cell population was

[8] Contribution from Roman Bruch, see Table 12: Contributions from other persons, p. 157

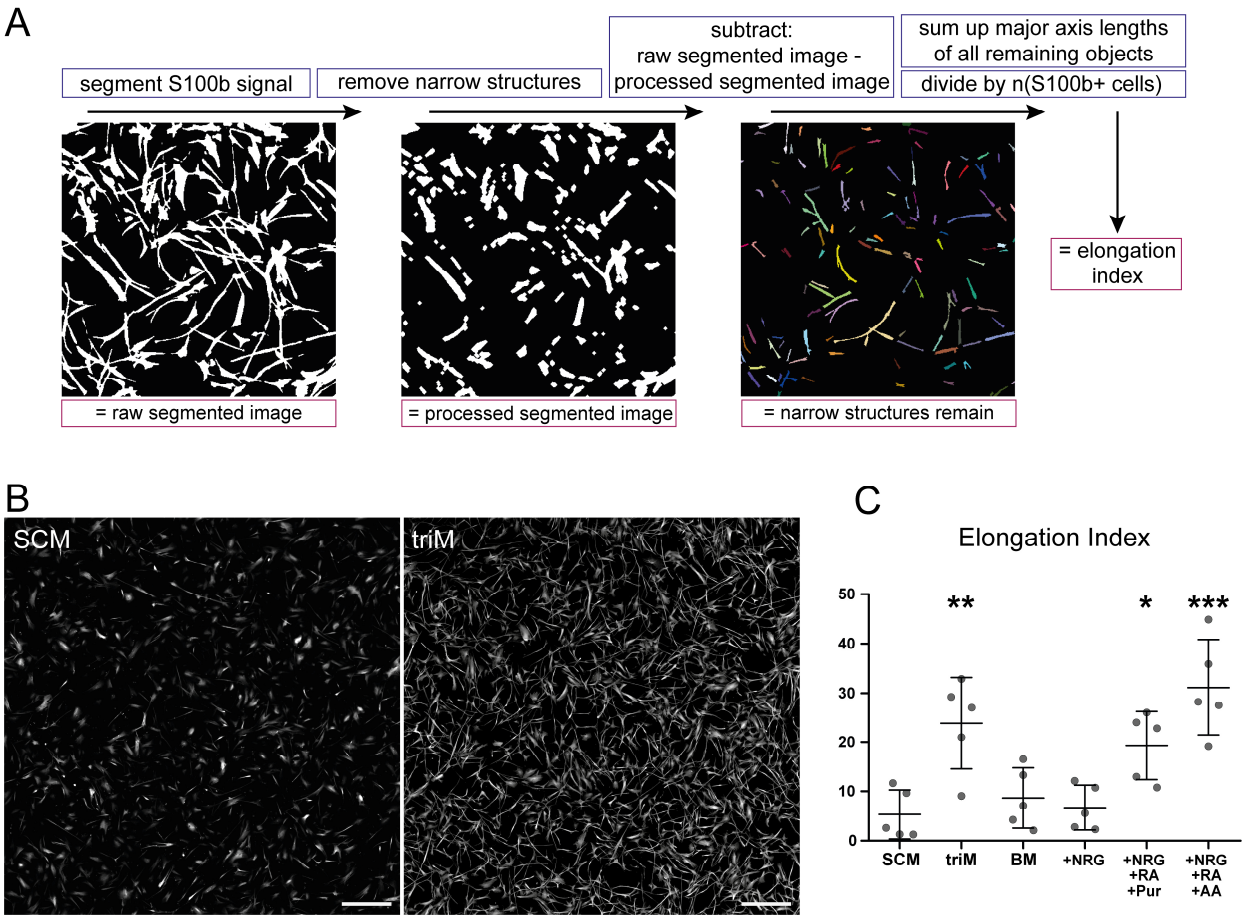


Figure 3-17: Cell elongation is increased in several medium conditions. (**A**) Schematic representation of the image analysis workflow to determine the cell elongation index value (data produced jointly with Roman Bruch, see **Table 12,** p. 157). (**B**) Representative images of cells incubated in either SCM or triM and stained for S100b as used for segmentation to determine the elongation index. Scale bars: 500 µm. (**C**) Cells were incubated in medium conditions as described for three days and the elongation index was quantified for each condition. Graphs depict mean ± SD (n = 5 experiments). * $p < 0.05$, ** $p < 0.01$, *** $p < 0.001$ (one-way ANOVA). Parts of figure adapted with modifications from Hörner et al. [2021] under CC BY 4.0 license

proliferative, labeling positive for Ki67, and therefore gradually overgrowing present Schwann cells. In serum-free modified SCM cultures, the percentages of cells positive for Sox10 and S100b were clearly decreased to 18.7 ± 5.7 % and 20.6 ± 6.3 % (mean ± SD, n = 3 experiments), respectively, when compared to control cultures containing FBS (Sox10: 77.0 ± 11.3 %, n = 4 experiments; S100b: 53.6 ± 15.1 %, n = 5 experiments) (Figure 3-18B, right side). Therefore, in all following experiments, Schwann cells were differentiated in medium containing FBS from day 24 on according to the protocol until at least day 36 before switching to serum-free triM.

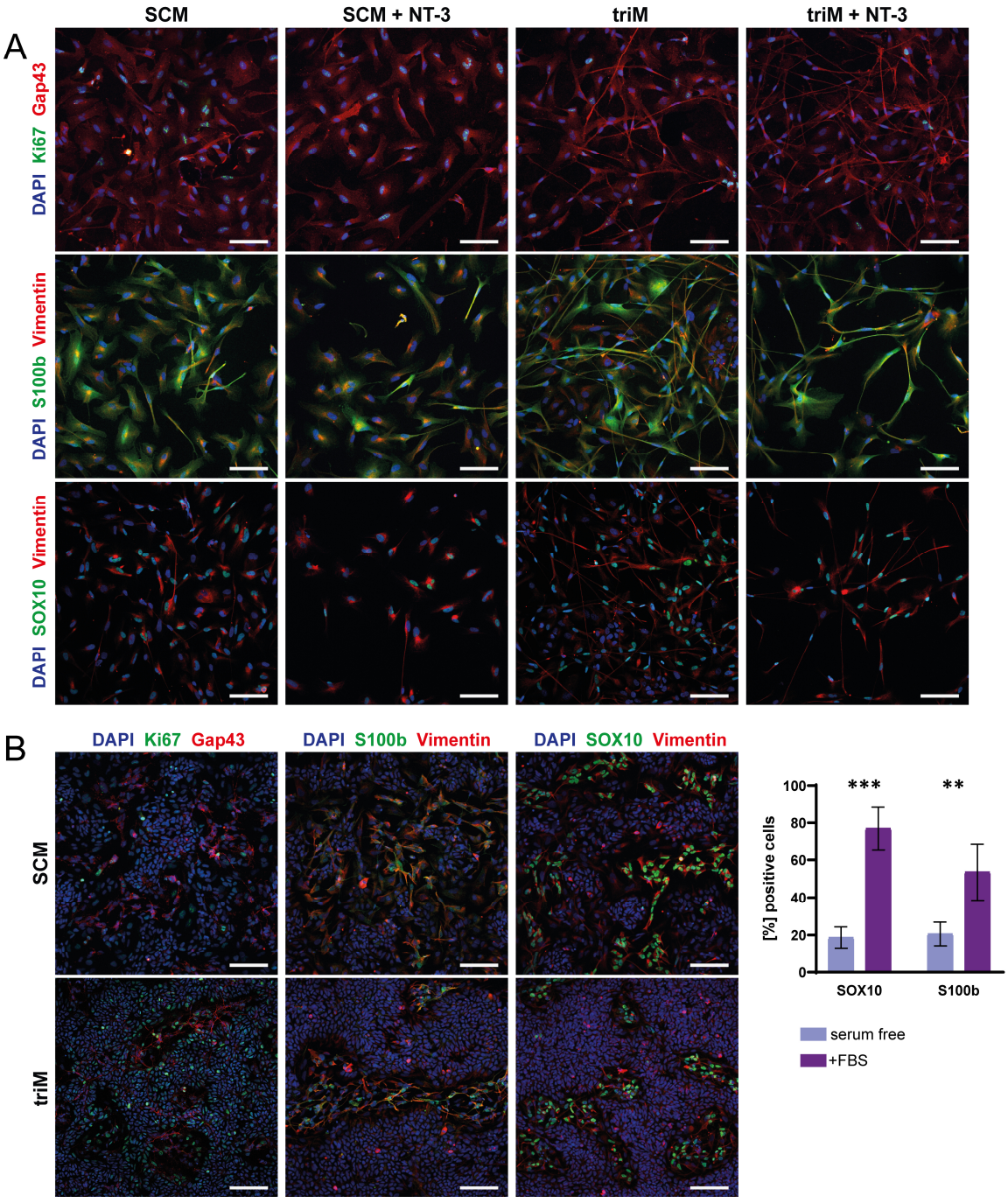
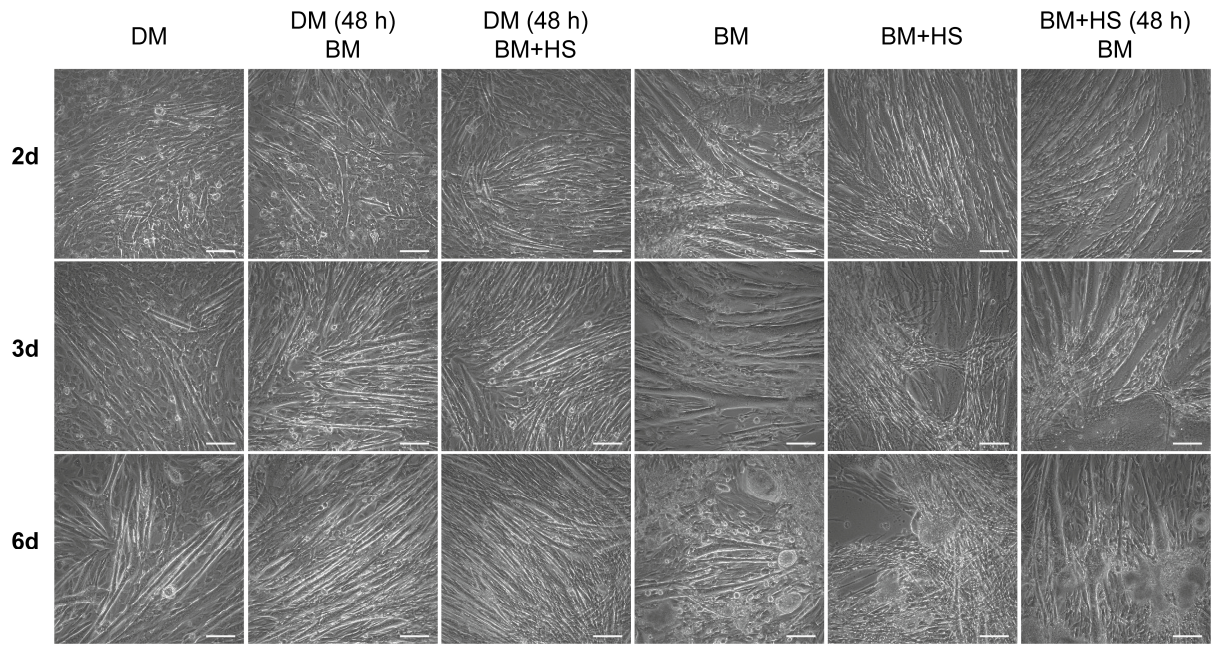


Figure 3-18: NT-3 does not seem beneficial for cell maturation, but serum supplementation is necessary. (**A**) Representative images of cells incubated in either SCM or triM with and without NT-3 as indicated above panels for three days. Cultures were stained for Ki67, GAP-43, vimentin, S100b, and Sox10. Nuclei were labeled with DAPI. Color codes indicated on the left. Scale bars: 100 µm. (**B**) Representative images of cells cultured in modified serum-free medium from day 24 on. Cultures were either switched to triM (lower panels) for the last three days before fixation or left in modified serum-free SCM (upper panels). Cells were fixed on day 38 and labeled for Ki67, GAP-43, vimentin, S100b, and Sox10. Nuclei were labeled with DAPI. Color codes indicated on top of panels. Scale bars: 100 µm. The proportion of Sox10+ and S100b+ cells was determined for cells cultured in modified serum-free SCM and compared to cells cultured in standard SCM containing FBS (right side). Graphs depict mean ± SD (n = 3 experiments for serum-free conditions; n = 4 experiments for Sox10 in medium containing FBS, n = 5 experiments for S100b in medium containing FBS). ** $p < 0.01$, *** $p < 0.001$ (t-tests). Partly adapted with modifications from Hörner et al. [2021] under CC BY 4.0 license.

3.2 Neuromuscular cocultures

3.2.1 2D neuromuscular cocultures can be established in nine days from predifferentiated cells

After optimization of the Schwann cell differentiation protocol as described in the previous sections, hiPSC-derived motoneurons and Schwann cells were combined into neuromuscular tricultures together with a murine myoblast cell line, C2C12. To this end, it was first tested if C2C12 myoblasts could be differentiated into fused myotubes according to standard protocols as described in section 2.1.6. Contractile myotubes could be obtained after few days of incubation in C2C12 differentiation medium (DM) consisting of DMEM/F12 containing L-glutamine and a high concentration of glucose (4.5 g/L), supplemented with 2 % horse serum. To find a medium formulation for neuromuscular tricultures, which was supposed to promote survival and differentiation of all three cell types, ideally without the need for serum, myotube differentiation was assessed in the serum-free base medium for neuronal differentiation and designated triculture medium (BM). BM consisted of an equal parts mixture of DMEM/F12 and Neurobasal media, supplemented with GlutaMAX (l-alanyl-l-glutamine), B27, and N2. Six different medium conditions were tested for differentiation of myotubes (Figure 3-19). As control condition, cells were differentiated in DM according to the standard protocol. In the second condition, cultures were normally switched to DM for induction of differentiation, and 48 h later switched again to BM. The third condition was cultured like the second condition, but horse serum was additionally supplemented to BM. Cultures in the fourth condition were directly switched to serum-free BM for induction of differentiation, and the fifth condition used BM supplemented with horse serum. Finally, cells were switched to BM supplemented with horse serum for 48 h, and then changed to serum-free BM. Cell survival, myotube formation and occurrence of spontaneous contractions were assessed using brightfield microscopy after two, three, and six days of differentiation (Figure 3-19). In the control condition, cells did not show noticeable detachment from cell culture plates. Myotube formation was seen starting on day 2 after induction of differentiation and increased until day 6. Spontaneous contractions were observed starting on day 3 of differentiation. In comparison, cultures which were induced to differentiate in DM for 48 h and subsequently switched to BM showed some cell detachment after the second medium switch, however, the cultures still largely stayed attached and showed sufficient cell viability. After the switch to BM, myotubes continued to grow and even seemed denser than in the control conditions. Similarly, spontaneous contractions were also detected starting on day 3, but they seemed to occur more frequently than in the control condition. When cultures were switched to BM supplemented with horse serum after 48 h in DM, cultures looked similar on day 6, with spontaneous contractions occurring comparable to the control condition.



viability	++	+	+	--	-	--
myotubes	+	++	++	+	+	-
contractions	+	++	+	+	-	-

Figure 3-19: C2C12 myotube differentiation can be done serum-free after an induction phase in standard medium. Representative brightfield images of C2C12 cells 2 days (d), 3 days, and 6 days after induction of myotube differentiation, cultured in medium conditions as indicated above panels (DM = standard differentiation medium including HS, BM = serum-free basal medium, HS = horse serum 2 %). Cell viability/attachment, formation of myotubes, and occurrence of spontaneous contractions were assessed (panel below images) in comparison to the control condition in DM only (first column). Scale bars: 100 µm.

When DM was not used at all but differentiation of myotubes was induced directly in BM with or without serum supplementation, cultures showed high degrees of cell detachment. When only serum-free BM was used for culture, spontaneous contractions were visible already on day 2 of differentiation, however, no contractions were observed in day 6 cultures anymore. In cultures which were induced in BM supplemented with horse serum, no spontaneous contractions were seen at any time point, regardless of whether cultures were switched to serum-free BM after 48 h or not. On day 6, vast cell detachment was observable in all three BM-induced conditions, but conditions with only BM or only serum-supplemented BM still showed presence of myotubes comparable to the control condition. If cells were induced in BM containing serum and subsequently switched to serum-free BM, most of the myotubes which had formed were detached by day 6. As this experiment suggested highest differentiation success in the second condition, where myotube differentiation was induced with DM and cultures were changed to BM after 48 h, it was tested if the full triM formulation with all supplements could be used instead of BM, and if the induction period in DM could be shortened to 24 h instead of 48 h. Both changes did not seem to affect myotube differentiation

in comparison to the previous condition. Therefore, a 24 h DM induction phase followed by a medium change to triM was used for the following coculture experiments.

To establish cocultures, it was first assessed if C2C12 myotubes could form nAChR clusters in the new medium formulation. C2C12 were induced to myotube differentiation in DM, and after 24 h, the medium was changed either to the basal BM, the fully supplemented triM, or cells were left in DM as control condition. Additionally, each condition was also repeated in coculture with hiPSC-derived motoneurons, which were added with switching culture media 24 h after myotube induction. Cultures were kept for three more days and subsequently fixed for staining of nAChR using fluorescently tagged α-bungarotoxin (Figure 3-20A). In the control

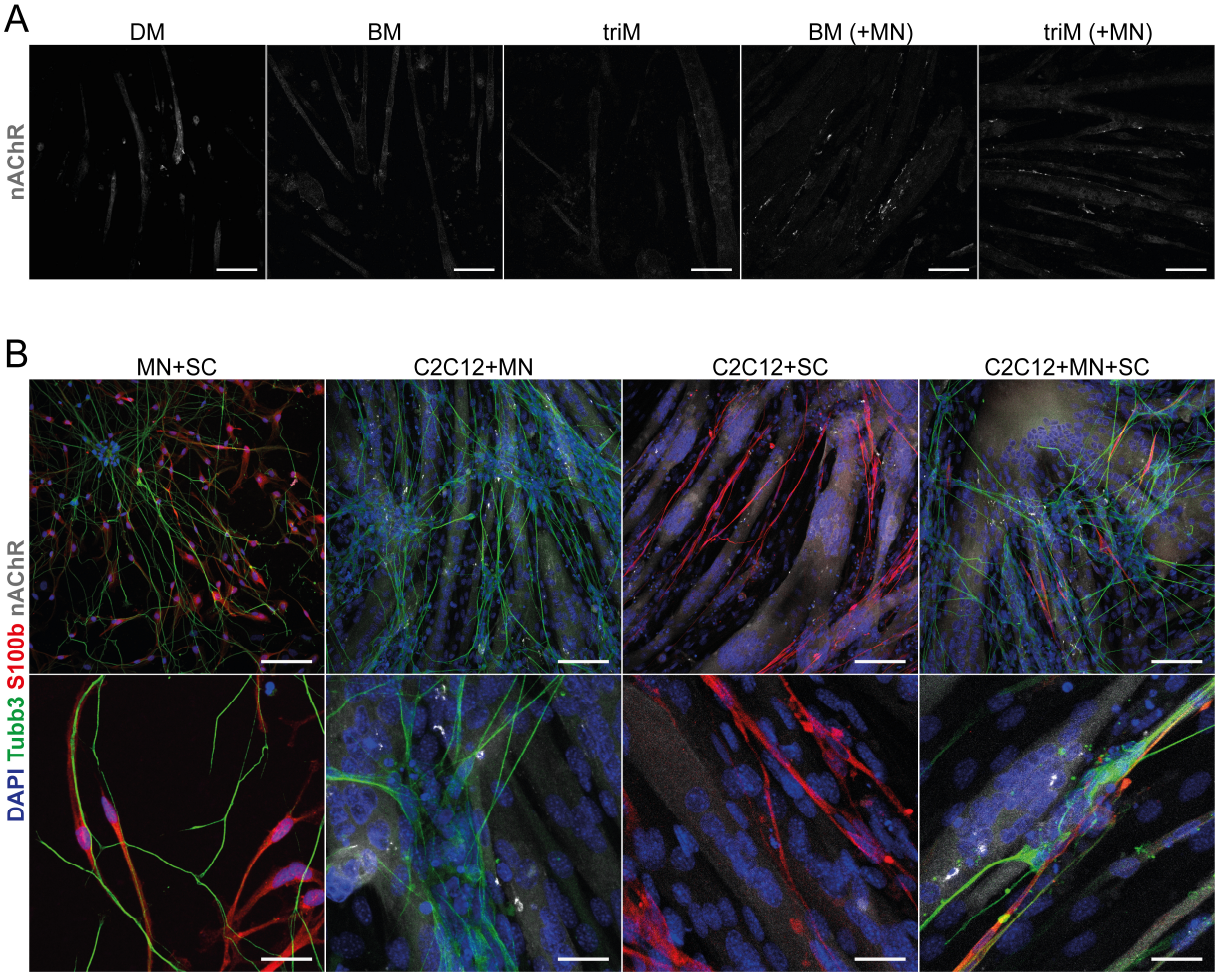


Figure 3-20: C2C12 myotubes, hiPSC-derived motoneurons, and hiPSC-derived Schwann cells can be cocultured in a compatible medium formulation. (**A**) Representative fluorescence images of C2C12 myotubes labeled for nAChR with α-bungarotoxin after three days of monoculture in either DM, BM, or triM; as well as coculture with motoneurons (+MN) in BM or triM as indicated above panels. Scale bars: 100 µm. (**B**) Representative immunofluorescence images of cocultures consisting of hiPSC-derived motoneurons (MN), hiPSC-derived Schwann cells (SC), and C2C12 myotubes (C2C12). Motoneurons were differentiated for at least 30 days and Schwann cells were differentiated for at least 40 days before combining different cell types. C2C12 were induced to differentiate into myotubes 24 h before addition of other cell types. Cocultures were fixed 8 days (MN+SC) or 3 days (conditions with C2C12) after combining cell types, and labeled for Tubb3 to visualize motoneurons (green), S100b to visualize Schwann cells (red), and α-bungarotoxin to visualize nAChR on myotubes (grey). Nuclei were labeled with DAPI and are shown in blue. Scale bars: 100 µm (upper row), 20 µm (lower row).

condition, where C2C12 were differentiated in standard DM without neurons, myotubes showed some fluorescence signal including few small receptor clusters. In BM and triM, this nAChR clustering of monocultured C2C12 was reduced, but still a few fluorescent clusters were observed. However, upon addition of motoneurons, nAChR expression and clustering were apparently induced in both, BM and triM, and numerous brighter fluorescent clusters were present (Figure 3-20A). In DM, motoneurons did not survive, and therefore no cocultures could be obtained for this condition. Subsequently, all three cell types were combined into cocultures using triM and stained for cell-specific marker proteins (Figure 3-20B). In cocultures containing C2C12, myoblasts were seeded and induced to differentiate towards myotubes in DM as described. After 24 h, either hiPSC-derived motoneurons, hiPSC-derived Schwann cells, or both together were seeded onto C2C12 in triM. Motoneurons had been differentiated before for at least 21 days, and Schwann cells for at least 50 days. Cocultures were kept for three days if C2C12 were present, to prevent myotube detachment upon long-term culture, and for eight days in motoneuron / Schwann cell cocultures without C2C12. Then, cultures were fixed and immunostained for a neuronal marker, Tubb3, and a Schwann cell marker, S100b. To visualize myotubes, fluorescent α-bungarotoxin was used to label nAChR. As demonstrated in Figure 3-20B, all cell types were present in the respective coculture conditions and could be well distinguished from each other. Additionally, Schwann cells frequently aligned with neurites in conditions which contained both, Schwann cells and motoneurons (see zoom image in the first column (MN+SC) of Figure 3-20B).Based on these preparatory experiments, a protocol was developed to establish tricultures consisting of hiPSC-derived motoneurons, hiPSC-derived Schwann cells, and C2C12 myotubes, in a robust and time-efficient way, which is schematically depicted in Figure 3-21. Tricultures for all subsequent 2D culture experiments were prepared according to this protocol as follows. For both hiPSC-derived cell types, pre-differentiated, cryopreserved cells were used. For motoneurons, cells were frozen on day 12 of differentiation in the motoneuron precursor stage as described in sections 2.1.4 and 3.1.2. Schwann cells were differentiated as described in sections 2.1.5 and 3.1.4 for at least 40 days and at most 70 days before cryopreservation. To prepare tricultures, motoneuron precursors, Schwann cells, and C2C12 were thawed separately on the same day. Three days later, motoneurons were split to suspension culture as described in section 2.1.4. Schwann cells were split once as well, depending on culture density, about four days after thawing. C2C12 myoblasts were split three days after thawing and then two more times every other day, as described in section 2.1.6. At the last split, C2C12 were seeded at high density for differentiation, and the medium was changed to DM 24 h later. Another 24 h later, i.e., nine days in total after thawing cells, neurospheres were dissociated to a single cell suspension and Schwann cells were detached according to standard protocols, and both were added to the

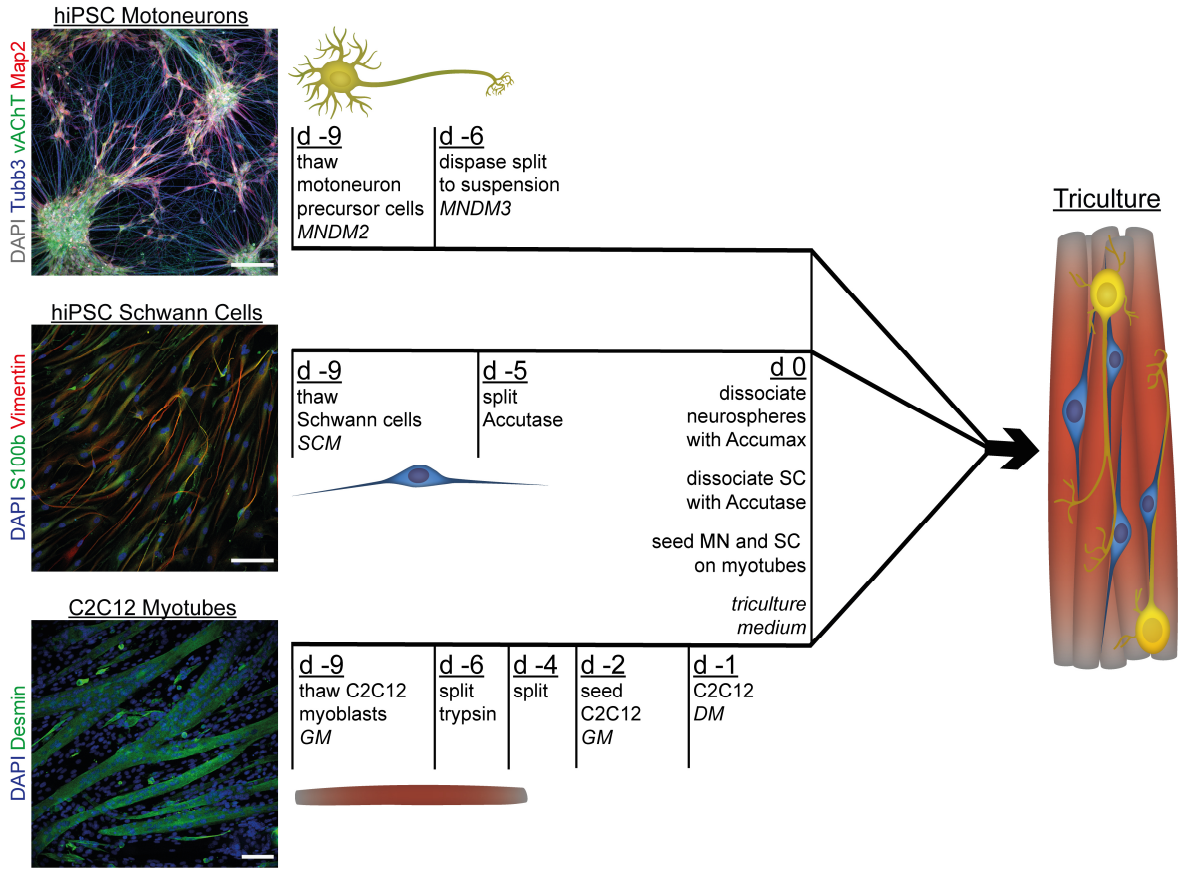


Figure 3-21: Tricultures can be established from frozen precursor cells within nine days. Schematic timeline and protocol for establishing tricultures of hiPSC-derived motoneurons, hiPSC-derived Schwann cells, and C2C12 myotubes, from frozen cell stocks in nine days. Micrograph inserts on the left show representative individual cultures stained for typical marker proteins, immunostained proteins and color codes are indicated on the left. Scale bars: 100 µm. Timeline shows cell culture steps to obtain tricultures from individual cultures. MNDM: motoneuron differentiation medium, SCM: Schwann cell medium, GM: myoblast growth medium, DM: myotube differentiation medium, d: day. Adapted with modifications from Hörner et al. [2021] under CC BY 4.0 license.

prepared C2C12 cultures, switching to triM at the same time. Tricultures which were prepared like this could be kept in culture for up to ten days at maximum, however, cell detachment started to occur beginning after four days of coculture, probably due to contraction of myotubes. Therefore, cultures prepared for all subsequent experiments were fixed for analysis after three days of coculture, to avoid cell detachment.

3.2.2 hiPSC-derived motoneurons and Schwann cells align, colocalize with nAChR clusters on myotubes, and influence cluster formation

In such tricultures, formation of nAChR clusters and frequent colocalization of neurites with these clusters were observed. In many cases, even colocalization of motoneurons and Schwann cells with nAChR clusters were seen at the same time. Representative fluorescence images of different marker staining combinations showing such colocalizations in tricultures which were collected from three independent experiments are shown in Figure 3-22. To quantitatively evaluate if coculture with the two different hiPSC-derived cell types had an effect

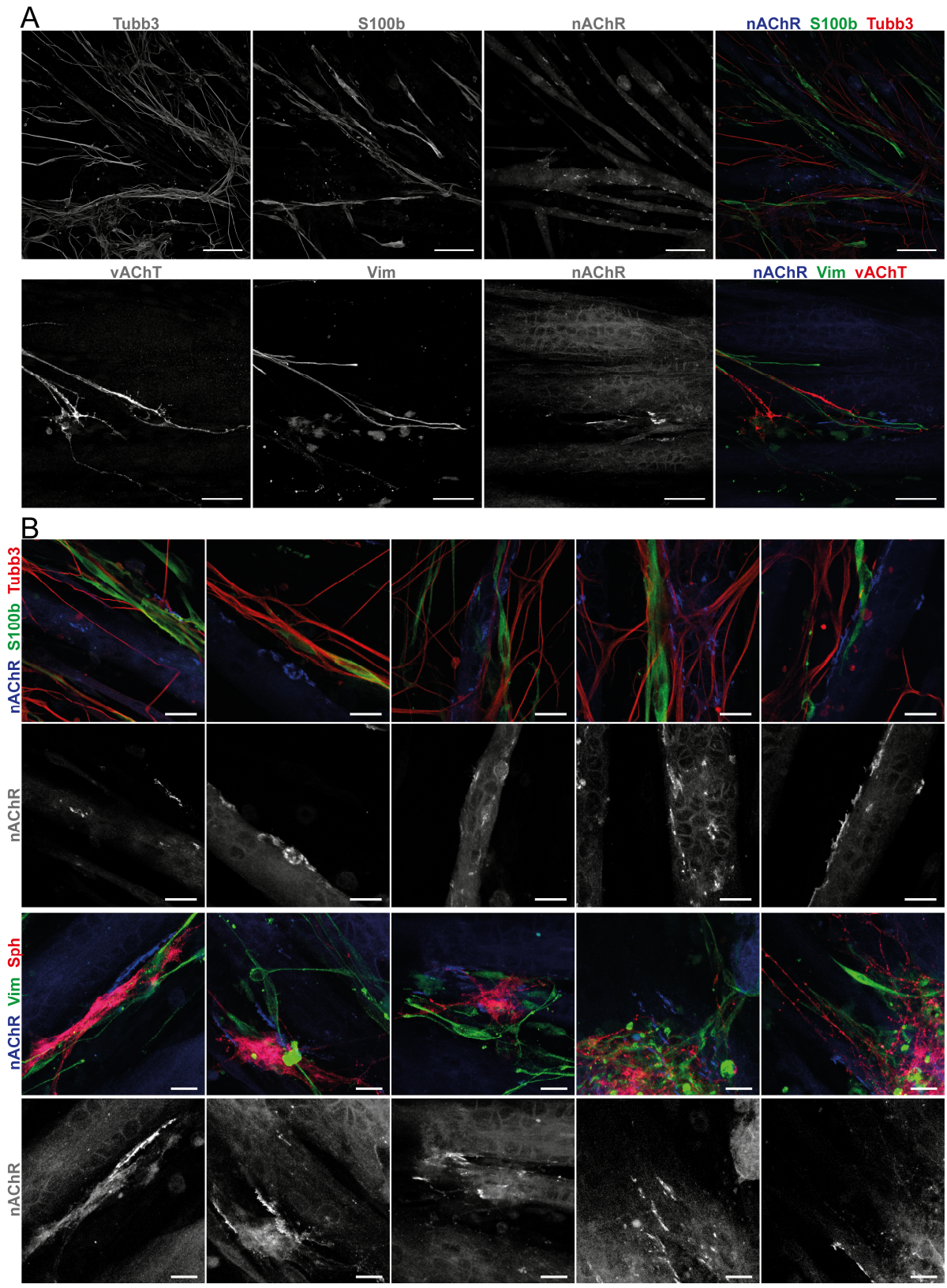


Figure 3-22: Motoneurons and Schwann cells colocalize with nAChR on myotubes in tricultures. (**A**) Representative fluorescence images of different marker staining combinations showing nAChR in blue, Schwann cells in green, and motoneurons in red. Immunostained proteins and color codes indicated above images. Scale bars: 100 µm (first row), 50 µm (second row). (**B**) Zoom images collected from three independent experiments showing colocalizations of motoneurons and Schwann cells with nAChR clusters. Immunostained proteins and color codes indicated on the left. Scale bars: 20 µm. Parts of the figure adapted with modifications from Hörner et al. [2021] under CC BY 4.0 license.

on C2C12 myotubes, the fluorescently labeled nAChR clusters were analyzed for morphological parameters via image analysis and compared between coculture conditions. Therefore, C2C12 were differentiated in DM and triM as described before, either in monoculture, in coculture with Schwann cells only, in coculture with motoneurons only, or in coculture with both, Schwann cells and motoneurons (Figure 3-23). Cells were fixed after three days of coculture and nAChR were labeled with fluorescent α-bungarotoxin. Fluorescent nAChR clusters were then segmented from confocal microscopy images (Figure 3-23A) and analyzed as described in section 2.4.3. Additionally, cultures were immunostained for the protein rapsyn, to evaluate the percentage of rapsyn+ nAChR clusters (Figure 3-23B). Further, the mean nAChR cluster area, mean fluorescence intensity, as well as mean number per myotube area were determined for all conditions (Figure 3-24A), and values determined in cocultures were compared to the C2C12 monoculture condition. In conditions which contained neurons, the mean area of nAChR clusters was significantly reduced to 19.6 ± 1.7 µm² and 22.4 ± 5.0 µm² in cocultures with motoneurons only and tricultures, respectively, when compared to C2C12 monocultures (142.7 ± 48.6 µm²; mean ± SD, n = 3 experiments)[9]. In cocultures with Schwann cells only, a reduced mean area of 90.5 ± 31.3 µm² was measured as well, but this decrease was not significant. The mean fluorescence intensity of nAChR clusters showed a trend towards increasing values in cocultures when compared to C2C12 monoculture, but no significant differences were detected (C2C12 only: 36.1 ± 2.4 a. u., C2C12 + Schwann cells: 41.2 ± 8.0 a. u., C2C12 + motoneurons: 42.9 ± 2.6 a. u., triculture: 45.6 ± 5.3 a. u.). The mean number of nAChR clusters normalized to myotube area increased significantly to 112.8 ± 19.0 and 82.0 ± 14.3 clusters per mm² in cocultures with motoneurons only and tricultures, respectively, when compared to C2C12 monocultures, which had 16.2 ± 15.0 clusters per mm² C2C12 myotube area. No significant difference was detected in cocultures with Schwann cells only, which had 23.1 ± 14.9 clusters per mm² myotube area. A similar pattern was seen for the percentage of rapsyn+ nAChR clusters. While 36.3 ± 3.1 % of clusters were positive for rapsyn in C2C12 monocultures, this increased to 48.6 ± 12.6 % in cocultures with Schwann cells, to 58.0 ± 5.5 % in cocultures with motoneurons, and to 60.2 ± 1.9 % in tricultures. This increase was significant again in the last two conditions (Figure 3-24A). Next, colocalization with motoneurons was found for 70.0 ± 6.6 % and 63.0 ± 8.8 % of nAChR clusters in tricultures and bicultures, respectively (mean ± SD, n = 4 experiments). For Schwann cells, 20.2 ± 12.2 % of nAChR clusters colocalized in tricultures, and 15.9 ± 2.2 % in bicultures (Figure 3-24B). Furthermore, in tricultures, 17.6 ± 10.1 % of all nAChR clusters

[9] Contributions from Nathalie Couturier and Madleine Grob, see Table 12: Contributions from other persons, p. 157

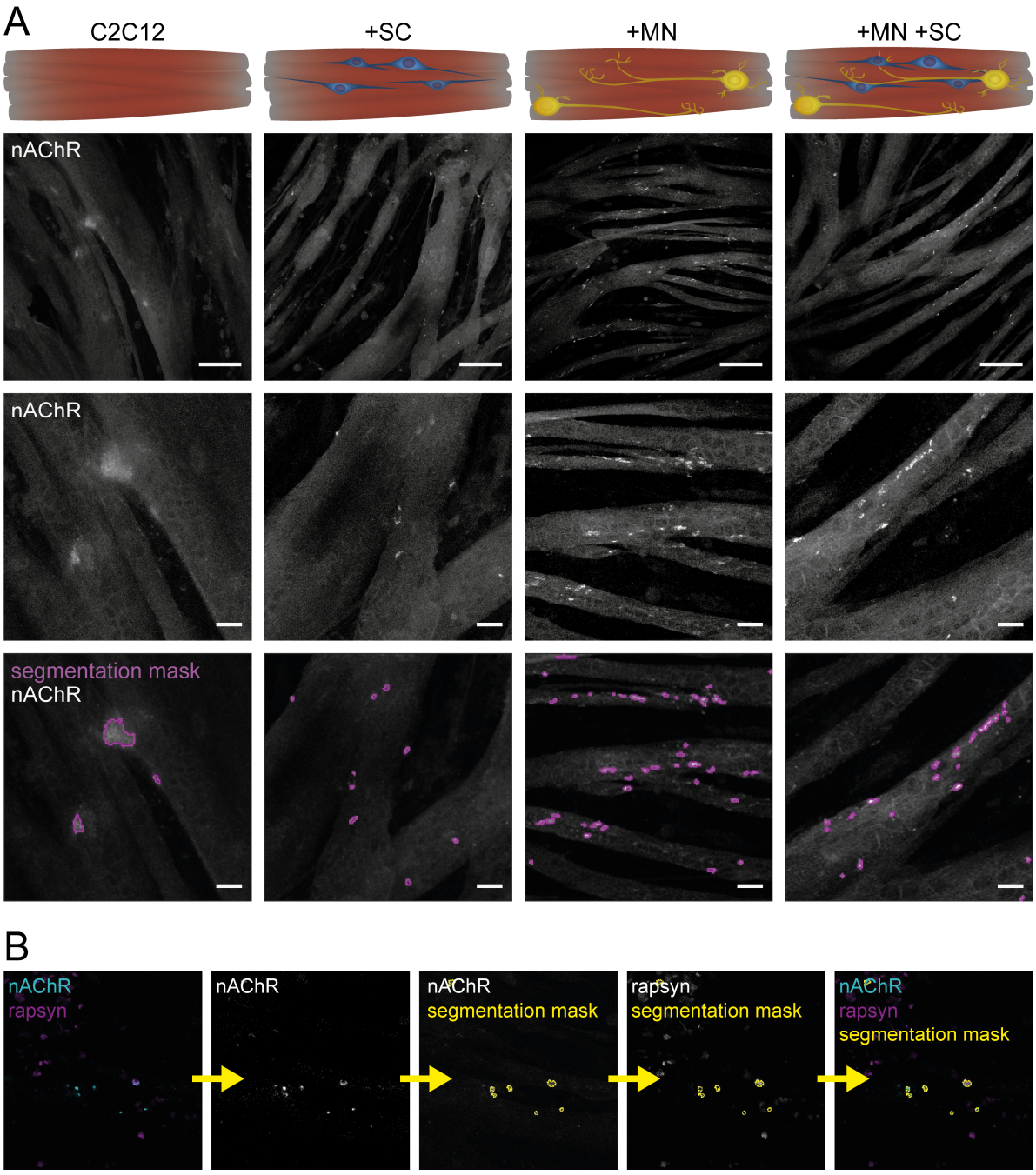


Figure 3-23: Segmentation of nAChR clusters from image data of different coculture conditions. (**A**) Representative micrographs showing nAChR labeled with fluorescent α-bungarotoxin in C2C12 monocultures, cocultures with Schwann cells only (+SC), cocultures with motoneurons only (+MN), or both cell types (+SC +MN). Second row shows zoom images of representative nAChR clusters for each condition, and fourth row shows an overlay including segmentation masks as used for image analysis. Scale bars: 100 µm (first row), 20 µm (second and third row). (**B**) Image analysis workflow to measure the percentage of nAChR clusters positive for rapsyn. nAChR segmentation masks were used to measure fluorescence intensity in a second channel with rapsyn immunostaining to detect rapsyn+ nAChR clusters. Figure adapted with modifications from Hörner et al. [2021] under CC BY 4.0 license.

colocalized with both, motoneurons and Schwann cells, at the same time (Figure 3-24C). 52.4 ± 16.2 % of clusters in tricultures colocalized with motoneurons only, and 2.6 ± 2.7 % colocalized with Schwann cells only; while 27.5 ± 4.0 % did not colocalize with either (Figure

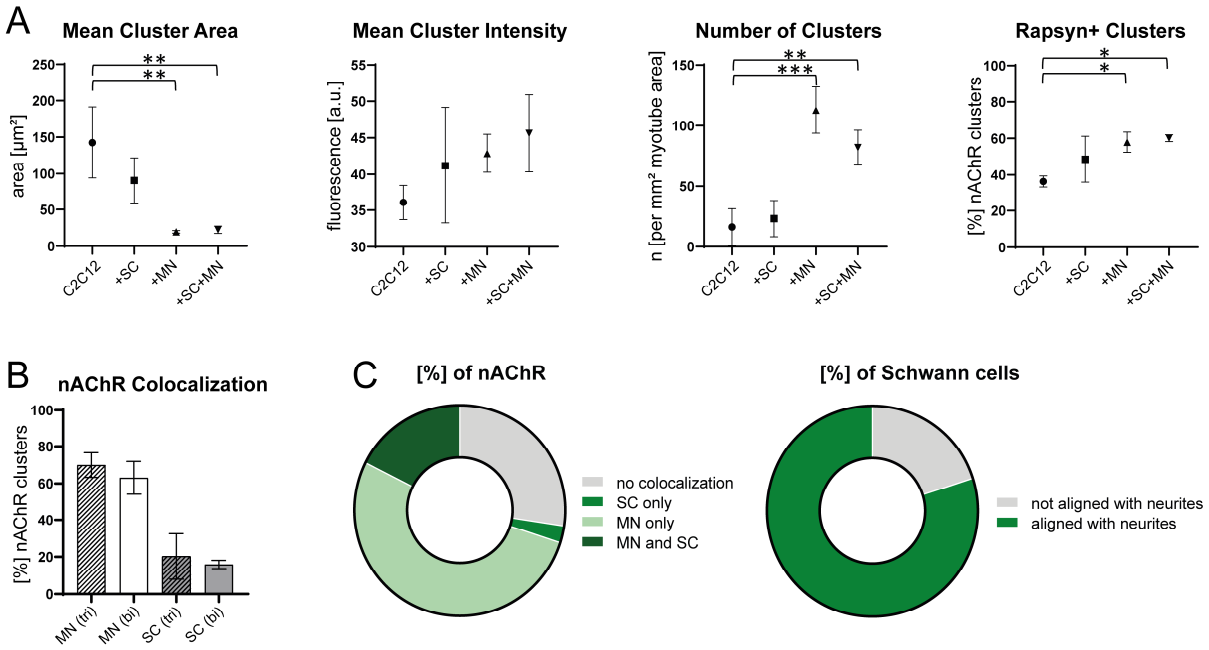


Figure 3-24: Cocultures influence morphological parameters of nAChR clusters. (**A**) C2C12 myotubes were cultured in monoculture, in coculture with Schwann cells only (+SC), in coculture with motoneurons only (+MN), or in coculture with both cell types (+SC+MN) as described. nAChR clusters were labeled with fluorescent α-bungarotoxin and segmented from confocal microscopy images. For all coculture conditions, the mean area, mean fluorescence intensity, and mean number of nAChR clusters were determined, as well as the percentage of rapsyn+ nAChR clusters. Graphs depict mean ± SD (n = 3 experiments). * $p < 0.05$, ** $p < 0.01$, *** $p < 0.001$ (one-way ANOVA). (**B**) Quantification of the percentage of nAChR clusters colocalizing with motoneurons (MN) or Schwann cells (SC) in tricultures including all cell types (tri) and bicultures (bi) with the cell type indicated. Graph depicts mean ± SD (n = 4 experiments). (**C**) Left: percentages of nAChR clusters in tricultures colocalizing with Schwann cells (SC) only, motoneurons (MN) only, both of them at the same time, or none of them (n = 4 experiments). Right: percentages of Schwann cells in tricultures either aligned or not aligned with neurites (n = 4 experiments). Color codes indicated in legends. Parts of figure adapted with modifications from Hörner et al. [2021] under CC BY 4.0 license.

3-24C). As mentioned before, also a frequent alignment of Schwann cells with neurites was observed. In tricultures, 79.9 ± 8.3 % of all Schwann cells present either fully or partially aligned with neurites (mean ± SD, n = 4 experiments).

3.2.3 3D neuromuscular cocultures in hydrogels can achieve spatial organization

To combine the different cell types in 3D, several hydrogel culture approaches were explored. Initially, cell types were combined on top of a gelatin fiber mesh acting as scaffold as described in section 2.1.8. C2C12 myoblasts were seeded on top of the scaffold and switched to DM to induce myotube differentiation 24 h later. Another 24 h later, the culture medium was switched to triM and neurospheres of a day 18 hiPSC motoneuron differentiation culture were added on top of the scaffolds. When inspected with brightfield microscopy, morphology of individual cells could not be assessed, as cell structures could not be distinguished well enough from scaffold structures. However, cell-laden scaffolds did appear different in brightfield compared to control

scaffolds which were incubated in culture medium without cells (Figure 3-25A), confirming the presence of cells in scaffold cultures. After ten days of coculture, the cell-laden scaffolds were fixed and immunostained for Tubb3 to visualize neurons, and nAChR were labeled with α-bungarotoxin (Figure 3-25B). As illustrated by fluorescence images in Figure 3-25B, myoblasts differentiated into myotubes inside the scaffold, and expressed nAChR, which appeared in well-defined clusters. Neuronal cell bodies stayed organized in sphere-like clusters, and these showed outgrowth of long and ramified neurites into the scaffold, which colocalized with nAChR clusters on myotubes (Figure 3-25B, right image). Moreover, myotubes did not seem to detach visibly after 12 days of culture in the scaffolds. Next, to enable spatial arrangement of cells, 3D-bioprinting was explored to create hydrogel structures for cell culture. Using a bioink formulation based on gelatin methacryloyl, different structures were 3D-printed as described in section 2.1.9.[10] With bioprinting, it is possible to create 3D structures from hydrogel materials by pneumatic extrusion, and cells can be mixed into the hydrogel before the printing process or added to the structures afterwards. Both of these cell integration approaches were tried in different designs. To test cell behavior in the printed hydrogel and combine cell types in a structured way, a cuboid shape with two separate pocket structures was designed and printed into cell culture plates as depicted in Figure 3-25C. For printing, hydrogel without any cells mixed in was used for the parts depicted in red, and a second gel was used for the pocket structures depicted in blue, which could be washed out after the printing process, thereby creating empty pocket structures as described in section 2.1.9. C2C12 cells, motoneurons, and Schwann cells were then placed inside the separate pocket structures in different combinations and cultured for eight to ten days before fixation, immunostaining, and microscopy. Figure 3-25D shows exemplary fluorescence images of 3D culture constructs, where neurospheres were placed in one pocket, and C2C12 spheroids were placed in the second pocket with or without singularized Schwann cells. After eight days of coculture, constructs were fixed and stained for Tubb3 to label motoneurons, S100b to label Schwann cells, and myosin heavy chain (MHC) to label myotubes. nAChR clusters were marked with α-bungarotoxin. Microscopy showed cell types which were seeded in separate gel pockets, i.e., neurons and myotubes, in contact with each other. Since the 3D gel construct was rather delicate, its precise structure could not be preserved through the staining and imaging process, and therefore, it was not possible to determine if both cell types migrated through the gel, or if only one of them migrated or grew towards the other. However, some C2C12 cells seemed to migrate through the gel and settle on the plate bottom outside of the

[10] Contribution from Daniele Gueiber, see Table 12: Contributions from other persons, p. 157

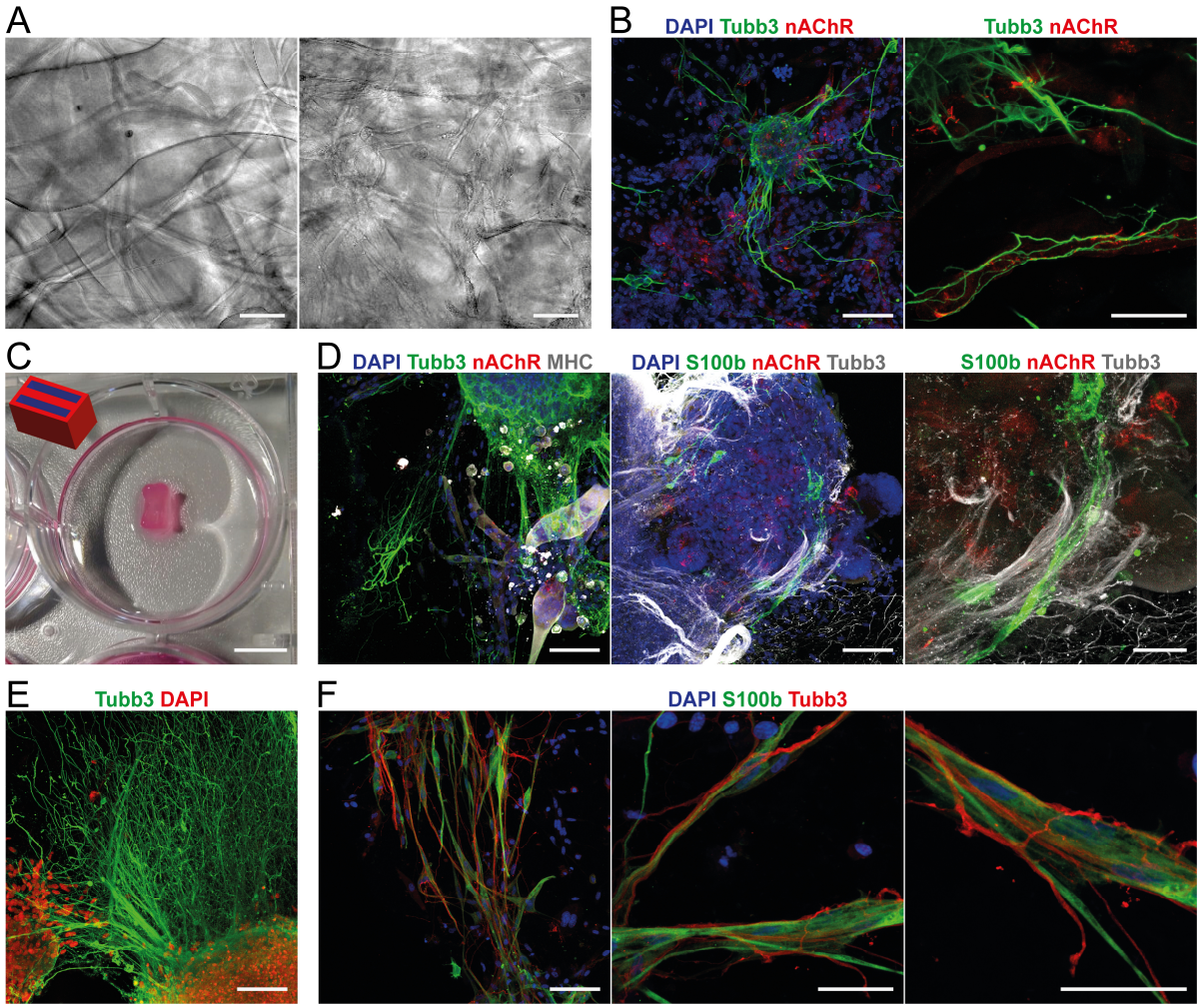


Figure 3-25: Cell types can be combined in 3D using hydrogel scaffolds or printed hydrogel chambers. (**A**) Brightfield images of gelatin scaffolds used for cell culture without cells (left) and with cells (right). Scale bars: 100 µm. (**B**) Exemplary fluorescence images of C2C12 myotubes and hiPSC-derived motoneurons after ten days of coculture in scaffolds. Neurons were visualized with a Tubb3 immunostaining (green) and nAChR on myotubes were labeled with α-bungarotoxin (red). Nuclei were labeled with DAPI and are shown in blue (left image). Images are maximum z-projections of 163 (left image) and 41 (right image) focal planes with 1.04 µm spacing. Scale bars: 100 µm (left), 50 µm (right). (**C**) 3D-printed hydrogel construct with chambers for placement of cells. Photograph of one printed structure in a well plate after incubation in medium. Image in the upper left corner depicts the printed design with hydrogel shown in red and cell pockets shown in blue. Scale bar: 10 mm. Data produced jointly with Daniele Gueiber, see **Table 12**, p. 157. (**D**) Exemplary fluorescence images of C2C12 / motoneuron cocultures in 3D-printed pocket structure without (left) or with (middle and right images) Schwann cells after eight days of coculture. Right image shows a zoom image of the middle image containing all three cell types. Immunostained proteins and color codes indicated above panels. Images are maximum z-projections of 128 (left image) and 230 (middle and right images) focal planes with 1.04 µm spacing. Scale bars: 50 µm (right image), others 100 µm. (**E**) Neurospheres cultured in printed hydrogel structure for ten days immunostained for Tubb3 (green) showing outgrowth of neurites into the hydrogel. Nuclei were labeled with DAPI and are shown in red. Maximum z-projection of 119 focal planes with 1.04 µm spacing. Scale bar: 100 µm. (**F**) Schwann cells cocultured with neurospheres in printed hydrogel structures for ten days immunostained for S100b (green) to visualize Schwann cells and Tubb3 (red) to visualize neurons. Nuclei were labeled with DAPI and are shown in blue. Images are maximum z-projections of 29 (left image), 16 (middle image), and 15 (right image) focal planes with 1.04 µm spacing. Scale bars: 100 µm (left image), others 50 µm.

3D structure. Also, neurites were clearly able to grow through the gel and form ample neurite networks inside the constructs (Figure 3-25E). The C2C12 cells, which were integrated into

the pockets as spheroids, did not seem to spread or elongate along the gel structure, but were found mainly in clump-like structures as shown in Figure 3-25D. Still, they seemed to have differentiated to some degree, as multinucleated structures and nAChR clusters were detected. These C2C12 structures were often contacted by neurites, which sometimes seemed to wrap the C2C12 or grew inside those structures. Some S100b+ Schwann cells could also be detected in association with the other cell types, although they were not found frequently. In other constructs, where Schwann cells were placed directly in the neurosphere pocket together with the neurons, instead of the C2C12 pocket, many S100b+ Schwann cells were found in association with motoneurons, often closely aligned with neurites (Figure 3-25F). Next, it was tested to 3D-bioprint hydrogel structures with singularized C2C12 myoblasts integrated into the hydrogel before the printing process as described in section 2.1.9. Initially, a sheet-like design with just two layers printed from parallel strands with a 90° shift between layers, as shown in the insert on the left of Figure 3-26A, was produced. These hydrogel sheets containing C2C12 were cultured free floating for two days before addition of neurons. In these free-floating cultures, the hydrogel sheets did not maintain their flat, rectangular shape, but the edges of the sheets seemed to curl into a bowl-like structure. This feature was exploited for seeding of neurospheres, which were placed in the middle of those bowl-like shapes (yellow arrow in Figure 3-26A(i)) and allowed to adhere before submerging the whole structure in culture medium. Similar to previous 3D cultures in the gelatin fiber scaffolds, cells could not be assessed using brightfield microscopy, but the structure of gels which did not contain any cells (Figure 3-26A(ii)) appeared different compared to gel structures containing cells (Figure 3-26A(iii)). Furthermore, some C2C12 myoblasts seemed to migrate out of the gel structures to settle on the well bottom. Among those cells, multinucleated myotubes were observed (Figure 3-26A(iv)), which indicated that C2C12 were viable after the printing process and retained differentiation capacity. After four days of coculture, the 3D structures were fixed and immunostained for Tubb3 in combination with synaptophysin (Sph) to label motoneurons, desmin for myotubes, and nAChR were labeled with α-bungarotoxin. As can be seen in Figure 3-26B, myotubes in some of those constructs were differentiated and seemed to align along the structure of printed gel strands. However, in many constructs, no or only very few differentiated myotubes were detected. Neurospheres adhered on top of the printed gels and projected neurites into the structures, which in many cases aligned with the myotubes (Figure 3-26B, upper row). While the neurites were seen to grow into the gel structures, the cell bodies mostly seemed to stay organized in sphere structures as they were seeded. In some cases, those remained as compact spheres sitting on top of the gel. In other cases, the spheres were flattened and spread a bit along the gel surface, but the neuronal cell bodies still remained in a large cluster (Figure 3-26B, lower row). In some places, also nAChR clusters could be observed on the myotubes (Figure 3-26B, lower row, zoom image on the right).

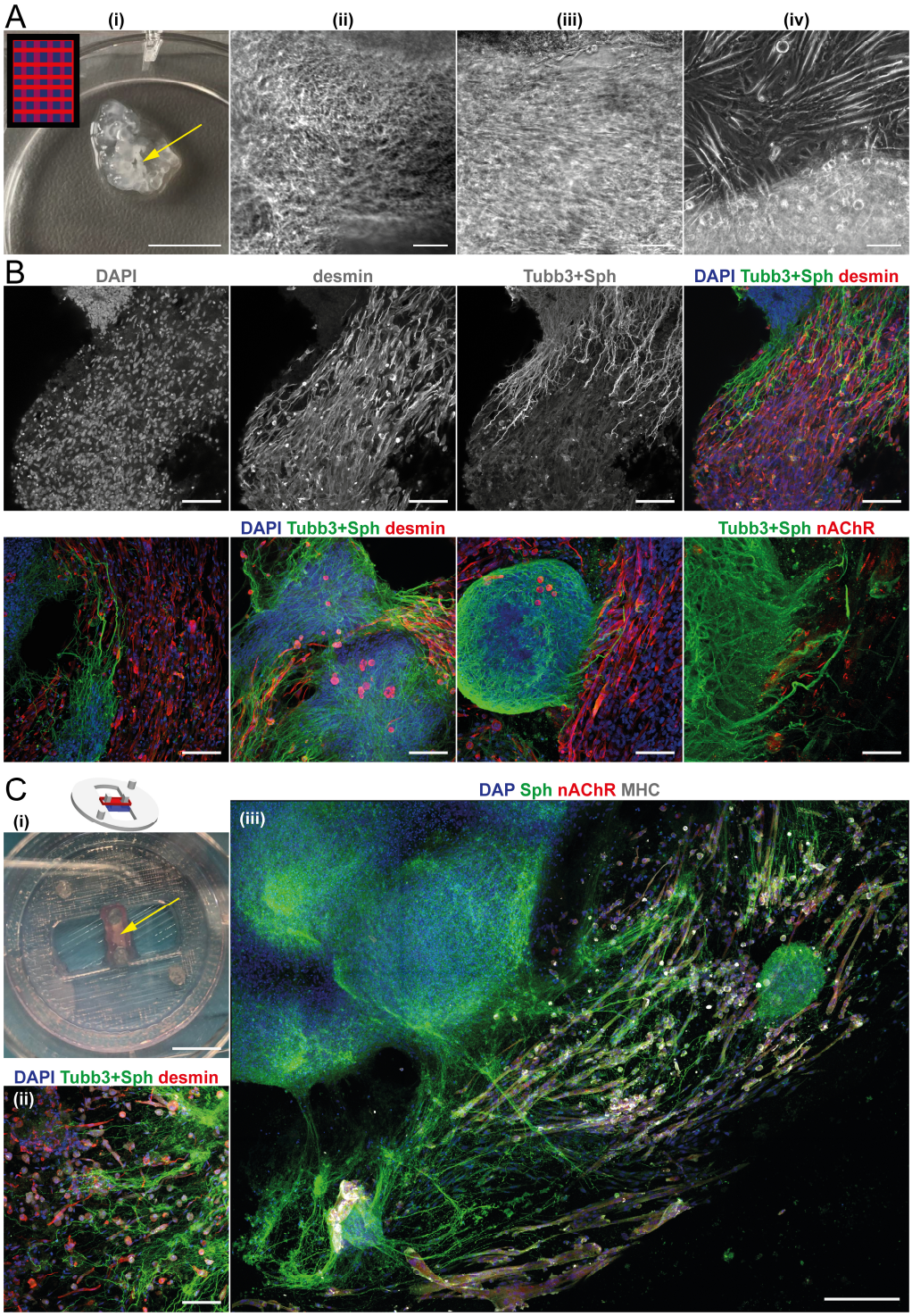


Figure 3-26: C2C12 can be bioprinted and cocultured with neurospheres to achieve spatial separation of cell bodies in 3D. (**A**) Photograph of a printed sheet structure including C2C12 with neurospheres added on top (yellow arrow). Image in upper left corner depicts print design (i). Scale bar: 10 mm. Brightfield images of an empty gel (ii), a gel printed with cells integrated (iii), and cells growing on the plate bottom after migrating out of the gel (iv). Scale bars: 100 µm. (**B**) Exemplary fluorescence images of bioprinted C2C12 cocultured with neurospheres for four days. Immunostained proteins and color codes indicated above panels. Images are maximum z-projections of 41 (upper row), 24 (lower row, first image), 32 (second image), and 200 (third and fourth image) focal planes with 1.04 µm spacing. Scale bars: 50 µm (lower row, right image), others 100 µm. (**C**) Bioprinted hydrogel in support structure with neurospheres in pocket structure (yellow arrow). Depiction of print design above image. Scale bar: 10 mm (i). Exemplary fluorescence images of constructs after ten days of coculture. Immunostained proteins and color codes indicated above panels. Images are maximum z-projections of 71 (ii) and 66 (iii) focal planes with 1.04 µm spacing. Scale bars: 100 µm (ii), 250 µm (iii). Data produced jointly with Daniele Gueiber and Nathalie Couturier, see **Table 12**, p. 157.

Finally, a more complicated and spatially organized structure was designed, combining the integration of C2C12 myoblasts into the gel before printing with the creation of pocket structures to place the neurospheres (Figure 3-26C). The image on the top of Figure 3-26C(i) shows the print design, with C2C12-laden hydrogel in red, which was printed on a base of washout gel (in blue), to create an elevated gel structure suspended between two pins of a support structure (in white). The support structure was 3D-printed beforehand from silicone and prepared as described in section 2.1.9 before adding hydrogel prints. C2C12 in those hydrogels were cultured for two days before addition of neurospheres into a pocket structure in the middle section of the printed gel. In the photograph shown in Figure 3-26C(i), the neurospheres sitting in the pocket structure appear in a whitish color (yellow arrow), while the printed hydrogel containing C2C12 appears in a reddish color. These constructs were kept in culture for ten more days after addition of neurospheres before fixation and staining for neuronal and myotube marker proteins. Similar to the previous cultures, differentiation of C2C12 myotubes could not be achieved reproducibly across experiments. In some constructs, only very few elongated desmin+ or MHC+ C2C12 cells were found, and many cells were rounded and looked detached (Figure 3-26C(ii)). In other constructs, differentiated and multinucleated myotubes were found, mainly in regions with high cell densities in the gel (Figure 3-26C(iii)). However, the spatial organization of cell types was clearly promoted with this print design, as C2C12 cells were observed solely in the printed gel regions where they were integrated, and neuronal cell bodies again remained in clusters in the pocket structures. From there, the neurons projected long and ramified neurites towards the myotube gel regions, which is visible in Figure 3-26(iii). Even in regions were C2C12 seemed detached, neurites often grew in a parallel manner into the gel, suggesting that C2C12 might have elongated and aligned in those regions as well before detaching, and that neurites had grown along those structures (Figure 3-26(ii)).

4 DISCUSSION

The main goal of this thesis was to integrate hiPSC-derived Schwann cells into neuromuscular *in vitro* cultures, since Schwann cells are critical for development and maturation of NMJs *in vivo* [Sanes and Lichtman, 1999; Reddy et al., 2003; Feng and Ko, 2008; Sugiura and Lin, 2011; Ko and Robitaille, 2015; Barik et al., 2016; Alvarez-Suarez et al., 2020], and since *in vitro* Schwann-cell coculture using primary cells was found to have beneficial effects on motoneurons [Ullian et al., 2004; Gingras et al., 2008; Ragancokova et al., 2009; Hyung et al., 2015]. Despite this, the only hiPSC-derived cultures to date which report the presence of Schwann cells are based on mixed differentiations [Lin et al., 2019; Faustino Martins et al., 2020; Mazaleyrat et al., 2020]. Integration in a selective and therefore controllable way was so far not possible. This was identified as a major deficiency of current models by numerous authors in the field [Badiola-Mateos et al., 2018; Bucchia et al., 2018; Barbeau et al., 2020; Castellanos-Montiel et al., 2020; Vila et al., 2020; Luttrell et al., 2021]. Literature reports that in explant cultures, when whole tissue sections were cultured including mixed cell types reflecting the *in vivo* situation, *in vitro* NMJs achieved higher maturation levels than in conventional motoneuron – muscle cocultures [Vilmont et al., 2016], and a link between co-differentiating glial cells present in such cultures and *in vitro* NMJ maturation was suggested [Mars et al., 2001]. Also, one study reported a rodent cell line-based neuromuscular coculture system, in which myotube differentiation was improved upon addition of a Schwann cell line [Singh and Vazquez, 2019]. A likely reason for the lack of hiPSC-derived Schwann cells in neuromuscular cell models has been the limited methodology available so far to efficiently derive pure Schwann cell cultures from hiPSCs [Hörner et al., 2022]. Therefore, an integral part of this thesis consisted of improving the derivation of Schwann cells from hiPSC and to characterize their maturation status. To this end, I initially tested and established a protocol for differentiation of motoneurons from hiPSC. Subsequently, I optimized a Schwann cell differentiation protocol by testing several modifications, to achieve robust and efficient yields across cell lines. In this context, the precise level of BMP signaling during the neural crest induction phase proved to be critical and this was achieved using a top-down inhibition approach [Hackland et al., 2017]. To prepare integration of Schwann cells into cocultures, I developed a medium formulation termed “triM” (for triculture medium) to support survival and differentiation of hiPSC-derived Schwann cells as well as hiPSC-derived motoneurons and C2C12 myotubes. This medium was found to improve Schwann cell maturation, which I then further investigated using evaluation of differentiation marker proteins under various medium conditions. Based on this, I established a protocol which allowed to generate neuromuscular tricultures including Schwann cells in as short as nine days, by use of cryopreserved precursor cells. In such cultures, the formation of nAChR on myotubes was evaluated under different

coculture conditions, showing that motoneurons – as expected – had a measurable influence on that parameter, while addition of Schwann cells resulted in a significant effect on this readout only in synergy with neurons. Cultures were evaluated morphologically as well, and Schwann cells were found to align with neurons. Both, neurites and Schwann cells, colocalized with nAChR clusters in many cases. To additionally demonstrate Schwann cell integration into more complex culture systems, several approaches for 3D cocultures were successfully explored, including scaffold culture and 3D-bioprinting. Those different aspects of the project and its results are discussed in more detail in the following sections.

4.1 Differentiation of motoneurons from hiPSC

Regarding the development of motoneurons, the developmental pathways and mechanisms to specify this cell type are comparably well known. For this reason, quite some protocols for the differentiation of motoneurons from hESC and/or hiPSC have been published to date, including different methods for induction, namely, small molecules or virus-mediated gene delivery [Wichterle et al., 2002; Li et al., 2005; Hu and Zhang, 2009; Hester et al., 2011; Amoroso et al., 2013; Davis-Dusenbery et al., 2014; Gouti et al., 2014; Qu et al., 2014; Du et al., 2015; Maury et al., 2015; Sances et al., 2016; Schaefers et al., 2022]. Still, many of those protocols are inefficient and require cell sorting to generate sufficiently purified motoneuron cultures. Furthermore, cells oftentimes need long differentiation times to mature, and some studies do not provide proof of marker expression associated with more mature motoneurons such as ChAT or vAChT [Sances et al., 2016], but only use markers for characterization which turn up already earlier in young motoneurons, like Hb9 or Isl-1.

The protocol which was used in this work [Du et al., 2015] reported an efficient derivation of mature motoneurons without the need for cell sorting and demonstrated colocalization of ChAT+ neurites with nAChR clusters on C2C12 myotubes upon coculture. With small modifications, this protocol proved to be reproducible in this study with robust results across five hiPSC lines. However, the initial experiments described in section 3.1.1 demonstrated that seemingly minor parameters, which are not even always reported in published protocols, can have a critical influence on differentiation efficiency and culture survival. Along these lines, different protein coatings for culture plates were evaluated, as well as different culture densities at differentiation induction. In this study, the best differentiation efficiencies were achieved when starting with an hiPSC colony culture at around 40 % confluency plated on Geltrex-coated plates. Geltrex was used for the first 12 days of differentiation. Following this and a suspension culture phase, coating culture plates with recombinant laminin for the terminal differentiation phase seemed to have beneficial effects over ECM protein mixtures like Geltrex.

Besides, the expansion of motoneuron precursors was evaluated. While expansion, cryopreservation, and subsequent terminal differentiation into motoneurons overall worked well, there was an increasing variability with increasing number of expansion passages, associated to lower cell yields in further steps. Therefore, motoneuron precursors were passaged only for a maximum of three passages before further differentiation, to keep resulting motoneuron cultures used in experiments consistent.

In these conditions, on average 71.5 ± 11.4 % Olig2+ motoneuron precursors were obtained after 14 days of differentiation, and cultures contained 93.0 ± 2.9 % of vAChT+ motoneurons after 25 days. When compared to the yields reported in the original study of Du et al. [2015], the yield of motoneuron precursors seemed slightly lower, as they reported 82 ± 9 % Olig2+ cells in precursor cultures. However, the yield of mature motoneurons, determined by ChAT expression in the original study and vAChT expression in the present study, was rather comparable, as 91 ± 6 % ChAT+ cells are reported in the original study. Furthermore, upon prolonged culture, hiPSC-derived motoneurons showed clustered cell bodies and ample neurite outgrowth, indicative of further maturation. Despite ChAT and vAChT, these cultures also expressed other neuronal marker proteins, including GAP-43, a marker for synaptogenesis, axonal outgrowth and pathfinding [Benowitz and Routtenberg, 1997; Denny, 2006]. In some cultures, patch-like structures positive for GAP-43 were seen (Figure 3-3A, second image of second row), which might possibly represent growth cones [Donnelly et al., 2013; Morita and Miyata, 2013]. Further, expression of peripherin was observed in many neurons, in a very heterogenous manner (Figure 3-1C). As the intermediate filament protein peripherin is not specific to motoneurons, but rather expressed in various cell types of the PNS and CNS [Eriksson et al., 2008], it is not often used for characterization of directed *in vitro* differentiation cultures. However, peripherin expression has been associated with the elongation of neurites and axonal outgrowth in development [Portier et al., 1993; Undamatla and Szaro, 2001; Barclay et al., 2007], and can therefore provide additional information on culture maturation. Indeed, the combined expression of peripherin together with synaptic markers and motoneuron-specific markers was suggested as indication of hiPSC-motoneuron maturation *in vitro* [Schaefers et al., 2022]; and in the present study, differentiated motoneurons expressed peripherin, ChAT, vAChT, and synaptophysin. Furthermore, the differential distribution evident in immunostainings of dendritic protein Map2 in combination with tau, a widely used characterization staining for neuronal cultures, indicated neuronal maturation regarding polarization. Also, in combined immunostainings for peripherin and Map2, strongly Map2+ neurites did not show distinct signals for peripherin, and vice versa (lower right image of Figure 3-3A). This supports the interpretation of peripherin as a marker for axonal outgrowth, in contrast to Map2 indicating dendrite specification. These hiPSC-

derived motoneurons were then used in coculture experiments, which are further discussed below in sections 4.3 and 4.4.

4.2 Differentiation of Schwann cells from hiPSC

4.2.1 Evaluation of various parameters for protocol optimization

Few protocols have been published which demonstrate differentiation of Schwann cells from hiPSC, and most have considerable drawbacks, such as low reproducibility and low efficiency, as well as immaturity of derived Schwann cells. The first study to present a directed differentiation protocol to derive Schwann cells from hESC was presented in 2011 [Ziegler et al., 2011], followed by a second protocol which also included hiPSC the following year [Liu et al., 2012]. Both used comparable methods and molecules for induction, and necessitated a cell sorting step to purify neural crest cells after the first phase of differentiation. Additionally, they used non-defined factors to induce neural crest by coculture with stromal cells, and required very long culture times of 85 – 100 days to obtain Schwann cells. Among the few original protocols which have been presented since then, some were still based on a similar method and timeline [Huang et al., 2017; Shi et al., 2018]. While stromal cell cocultures have been replaced by defined media, neural crest cells nevertheless had to be purified by FACS, and protocols were still very lengthy. Recently, four small molecule-based protocols have been presented which reduced the differentiation time needed to obtain Schwann cells to around 30 – 50 days [Kim et al., 2017; Muller et al., 2018; Carrió et al., 2019; Mukherjee-Clavin et al., 2019]. Of those, the protocol by Kim et al. was the only one which reported high cell yields without any purification steps.

Accordingly, this protocol was tested in the present work for the generation of Schwann cells from hiPSC. However, the first differentiation results were rather inconsistent and inefficient (section 3.1.3). Therefore, several modification approaches covering all different phases of Schwann cell differentiation (Figure 4-1A) were tested to optimize the differentiation protocol. In Figure 4-1B, the timeline of small molecules used in the original protocol [Kim et al., 2017] in correspondence to Schwann cell differentiation stages (Figure 4-1A) are shown. Different modifications were tested, some regarding the applied small molecules, and some regarding the culture conditions. These modifications including their timelines of application are depicted and highlighted in Figure 4-1C. Regarding small molecules, the omittance of BSA and β-ME was tested, as well as the addition of BMP4, BMP4 combined with DMH1, resveratrol, or ROCKi. Regarding culture conditions, different split ratios and therefore culture densities were tested, as well as a suspension culture phase. Additionally, serum-free medium alternatives

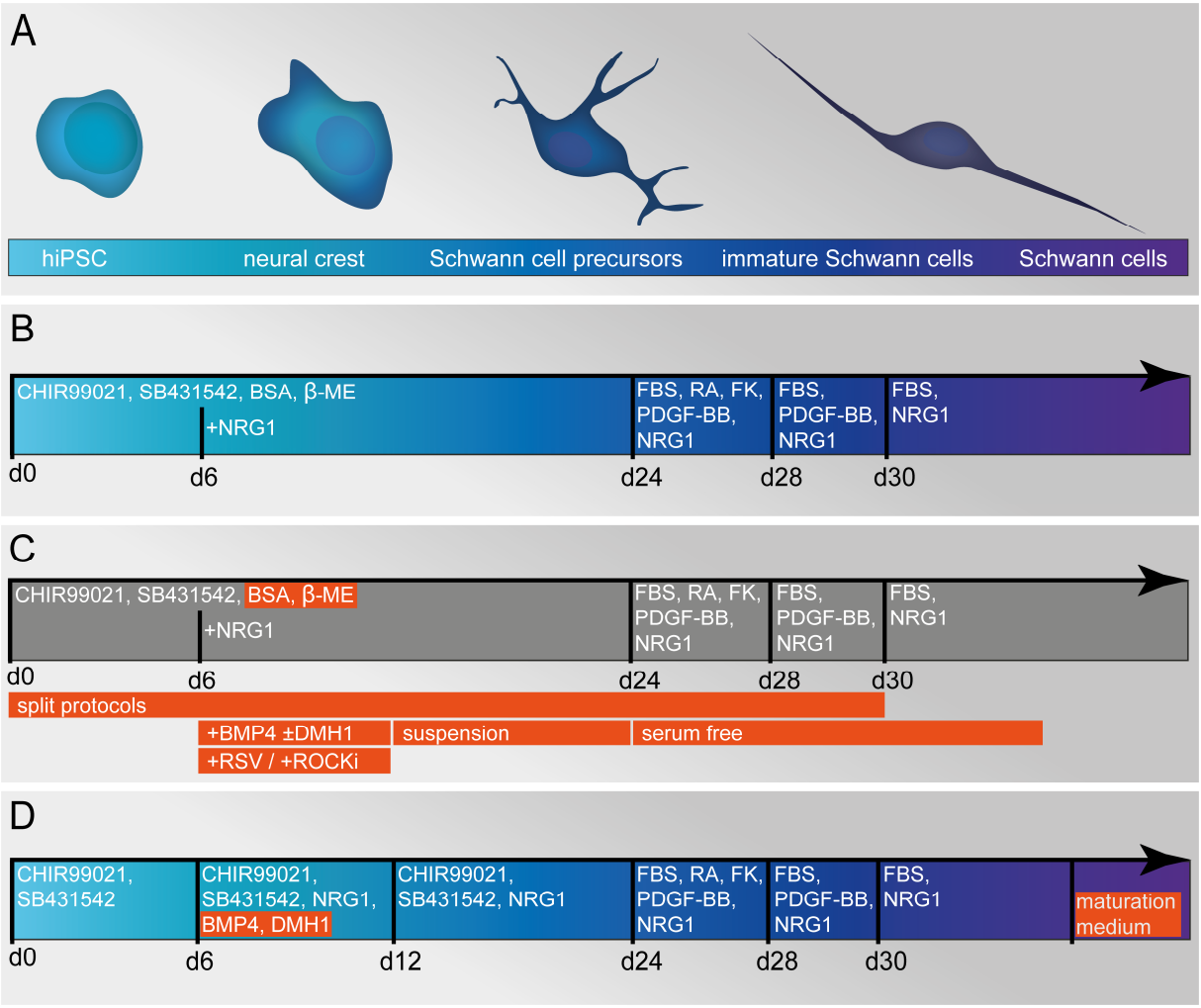


Figure 4-1: Modifications of the Schwann cell differentiation protocol. (**A**) Schematic depiction of the differentiation timeline from hiPSC to Schwann cells alongside differentiation protocols as used in this work initially [Kim et al., 2017] (**B**), with all modifications (orange) tested in this work (**C**), and in the final version as used for subsequent experiments (**D**). d = day, BSA = bovine serum albumin, β-ME = β-mercaptoethanol, FBS = fetal bovine serum, RA = retinoic acid, FK = forskolin, RSV = resveratrol, ROCKi = ROCK inhibitor.

were explored. It should be noted that some of these initial experiments were done without replicates, as indicated in the results section, and results should therefore be interpreted cautiously. This approach was chosen as Schwann cell differentiation experiments were rather lengthy and resource-intensive, and only a limited number of approaches could be tried at the same time. To increase the chances of success, a higher number of modifications was tried initially without replicates, and only those conditions which indicated a potentially positive effect were replicated in further experiments. Adjustments to the protocol were then made based on statistically sound data, as reported in the results section. Finally, two modifications were found to critically improve the protocol: the addition of BMP4 in combination with DMH1 to tune BMP signaling activity, and an additional maturation phase in a serum-free medium formulation. The final differentiation protocol used for subsequent experiments was adjusted accordingly and is depicted in Figure 4-1D. The omittance of BSA and β-ME did not lead to disadvantages in the

differentiation and was therefore also adopted (Figure 4-1D). Furthermore, testing of split ratios revealed one optimum condition which was then used in further experiments. Addition of BMP4 alone, resveratrol, or ROCKi did not lead to any improvements of the protocol. Furthermore, it was not possible to omit serum from the culture medium in the Schwann cell precursor phase beginning on day 24. However, after longer differentiation times, Schwann cells could be transferred and even further matured in serum-free medium.

4.2.2 Tuning of BMP signaling activity critically improves protocol efficiency and robustness

Initial differentiation experiments suggested an insufficient induction towards neural crest fates, indicated by a population of Sox10-/Sox2+ cells, which did not differentiate towards the Schwann cell lineage, but remained proliferative and, therefore, hugely contaminated the derived cultures at later stages. Therefore, a literature search was conducted to find signaling pathways which are known or suggested to be involved in neural crest differentiation but were not targeted in the protocol, and to identify small molecules which could potentially improve the differentiation. As one candidate, the activation of BMP signaling emerged. BMP signaling is a central regulator for developmental tissue patterning processes, including the differentiation fates of stem cells in the CNS as well as the PNS [Bond et al., 2012]. At the same time, BMP signaling is modulated by other signals and regulated precisely both spatially and temporally, allowing for dynamic functions throughout developmental stages and different tissues [Rider and Mulloy, 2010; Bier and Robertis, 2015]. The class of BMP morphogens includes more than 30 different molecules; of those, BMP4 and BMP2 are especially important for vertebrate neural development [Mehler et al., 1997]. Most of the time, a precisely balanced interplay between BMP activating and inhibiting molecules is responsible for the modulation of BMP signaling effects [Rider and Mulloy, 2010; Bond et al., 2012]. BMPs act by binding to tetrameric BMP receptors as molecule dimers, which exert downstream effects by phosphorylation of intracellular molecules upon activation [Massagué, 1998]. The canonical pathway for BMP signaling acts through proteins of the Smad family, which ultimately translocate into the nucleus to regulate gene expression [Wrana, 2000]. Various types of BMP antagonists are at play *in vivo* and can be likewise employed *in vitro*, some of those acting extracellularly in a competitive manner, others intracellularly by blocking receptors or target molecules. In neural differentiation protocols, BMP inhibitors are typically used in combination with blocking TGF-β signaling for dual Smad inhibition. This method was also employed in the motoneuron differentiation protocol which was used in this study, as in most protocols to generate neuroepithelial CNS precursors, since inhibition of BMP signaling is needed to specify neuroectoderm in contrast to epidermal fate. In the differentiation protocols dedicated

to inducing a neural crest fate, different approaches can be found for neuralization. Some protocols used the described dual Smad inhibition to neuralize cultures and subsequently purified putative neural crest cells. While the majority of cells under these conditions differentiated into Pax6+ neural rosettes, corresponding to CNS precursors, a small cell population positive for neural crest markers Sox10 and p75NTR can emerge in the periphery of these rosette structures under the right plating conditions [Chambers et al., 2009; Lee et al., 2010]. However, these neural crest cells can only be used for further differentiation if they are purified, most commonly by FACS [Lee et al., 2010]. Similarly, neural crest cells can also be purified from cultures which have been neuralized through embryoid body culture. Some neural crest differentiation protocols used BMP inhibitors [Chambers et al., 2009; Chambers et al., 2012; Kreitzer et al., 2013; Mica et al., 2013], while others used TGF-β inhibition without any BMP inhibitors [Lee et al., 2007; Menendez et al., 2011; Fukuta et al., 2014; Avery and Dalton, 2016; Huang et al., 2016]. In protocols to derive Schwann cells specifically, the only protocol to date reporting high cell yields without sorting did not use any BMP-interfering molecules [Kim et al., 2017]. As mentioned earlier, most Schwann cell protocols required sorting steps, and most of them either used dual Smad inhibition [Mukherjee-Clavin et al., 2019] or embryoid body culture [Ziegler et al., 2011; Liu et al., 2012; Huang et al., 2017; Shi et al., 2018]. Although there are other protocols which did not include a sorting step, both with BMP inhibition [Muller et al., 2018] or without [Carrió et al., 2019], these protocols did not report cell yields obtained. These two approaches, inhibition of BMP signaling or no interference with BMP signaling at all, seem to contradict the described situation *in vivo*: it is known that, in contrast to neuroectoderm, the formation of neural crest requires BMP signaling activity [Marchant et al., 1998; Simões-Costa and Bronner, 2015]. Still, BMP activators have been used rarely for differentiation of neural crest, and with contradicting results, as some authors reported improvement of neural crest differentiation [Cimadamore et al., 2011; Denham et al., 2015], while others observed an inhibition [Menendez et al., 2011; Fukuta et al., 2014]. Before this work, BMP activators had not been used in protocols to differentiate Schwann cells.

In embryonic development, BMP signaling is required at a distinct intermediate activity level, as the developing neural crest is located in the middle of a mediolateral BMP activity gradient, generated by opposing concentration gradients of BMP inhibitors and activators secreted by surrounding structures (illustrated in Figure 4-2A) [Marchant et al., 1998; Sela-Donenfeld and Kalcheim, 1999; Tribulo et al., 2003; Anderson et al., 2006; Groves and LaBonne, 2014; Simões-Costa and Bronner, 2015; Pla and Monsoro-Burq, 2018]. To achieve such a precise activation of a signaling target *in vitro* poses a greater challenge than a binary signal, i.e., complete inhibition or saturated activation. In accordance with the developmental processes *in vivo*, induction of neural crest from hPSC *in vitro* was achieved by combining TGF-β inhibition with low concentrations of the morphogen BMP4 to activate BMP signaling, while

increasing concentrations of BMP4 induced non-neural ectoderm, and inhibition of both resulted in neuroectoderm [Tchieu et al., 2017]. These results were reproduced in different hESC and hiPSC lines, although with variable efficiencies regarding differentiation capacities for different lineages. [Tchieu et al., 2017]. A likely reason for the latter lies in the particularly high variability between individual hESC and hiPSC lines, which manifests even in differences regarding differentiation bias towards specific cell fates. In a study comparing 17 different hESC lines, this bias was found to result in more than hundredfold differences for expression of some genes related to specific cell lineages [Osafune et al., 2008]. What is more, gene expression in hPSC was also impacted by culture environment – to such a great extent that "lab-specific gene expression signatures" were found upon comparison of hPSC lines cultured in different labs [Newman and Cooper, 2010]. One explanation for this might be the finding that individual hPSC lines can have varying endogenous signaling activities of pathways influencing differentiation [Blauwkamp et al., 2012]. This is also the case for BMP signaling [Hackland et al., 2017], which further complicates the aim of precise and reproducible BMP signaling activation: Individual cell lines express different amounts of BMP ligands, resulting in different levels of endogenous BMP activity levels among cultures, which is illustrated in Figure 4-2B(i). Therefore, depending on endogenously present BMP activity, addition of BMP-modulating molecules would alter BMP signaling to different levels among cell lines (Figure 4-2B(ii). Hence, to achieve the same signaling level through addition of BMP activators, the precise concentration required would need to be titrated for each single cell line and microenvironment, which is practically not feasible. Moreover, depending on endogenous signaling levels, it is even possible that some cell lines and/or culture conditions would require BMP inhibition, while others would require BMP activation. This hypothesis is consistent with results from a recent study [Kim et al., 2021], which reported "fine-tuning of dual Smad inhibition" to differentiate neural crest. By decreasing the concentration of the BMP inhibitor DMH1 used as part of the dual Smad inhibition system, they tuned the level of BMP signaling to increase the yield of neural crest cells. Adjustment of DMH1 concentration as well as most of the experiments reported were based on one cell line, H9, a widely used hESC line. The finding that neural crest cells were more efficiently derived at the determined (lower) optimum concentration of DMH1 than compared to a high DMH1 concentration (and therefore, complete inhibition of BMP) was reproduced in one further hESC line. Since for the second line, no other concentrations were compared, it is possible that the DMH1 concentration reported would be the optimum concentration to tune BMP signaling in the specific H9 cell line, and under the specific culture conditions used. Furthermore, in many experiments there was a considerable amount of Pax6+ neural precursors present as well, and the percentage of cells with neural crest identity was variable even between experiments using the same cell line and condition.

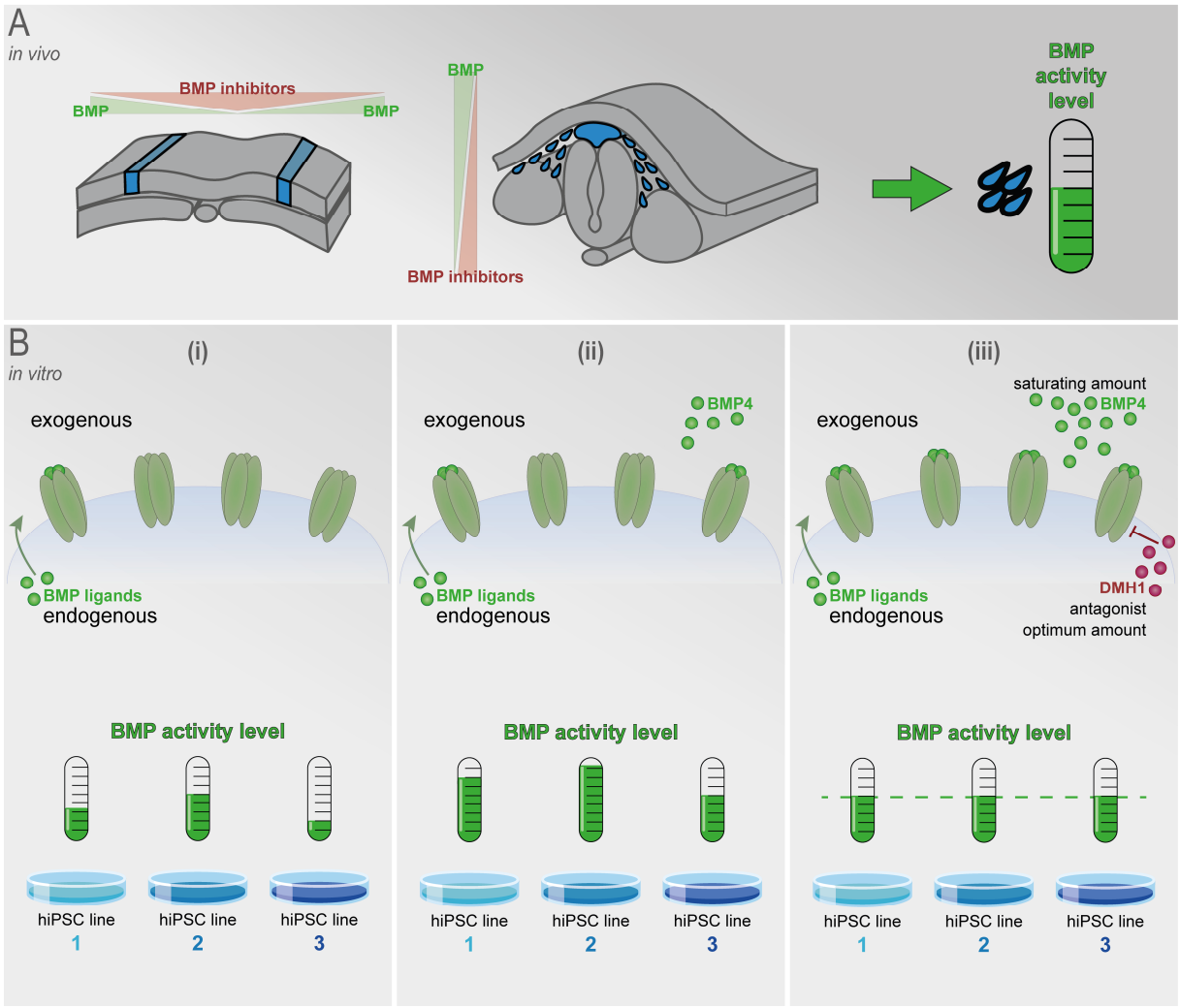


Figure 4-2: Principle of BMP signaling tuning to achieve an intermediate activity level. (**A**) Neural crest cells *in vivo* develop under intermediate BMP signaling levels created by opposing morphogen gradients. Schematic depiction, neural plate border and neural crest cells highlighted in blue. (**B**) Schematic depiction of BMP receptors (green) of cells in culture. Endogenous BMP signaling activity is present in hiPSC cultures and can vary between cell lines and culture systems (i). Addition of exogenous BMP4 in a sub-saturating concentration does therefore not result in controllable, reproducible BMP activity levels (ii). A precise level of signaling activity across several cultures can be achieved by top-down inhibition, i.e., applying a saturating amount of BMP4 together BMP antagonist DMH1 (iii).

To address such inconsistencies and achieve reproducible differentiation of neural crest cells from different hPSC lines, an elegant solution was suggested by Hackland et al. [2017], which they termed “top-down inhibition”. The principle is depicted schematically in Figure 4-2B(iii): here, recombinant BMP4 is applied simultaneously with DMH1, which inhibits BMP type I receptors. BMP4 is applied at a saturating concentration, and therefore, differences in endogenous BMP expression do not result in different BMP activity levels anymore. At the same time, a precisely titrated concentration of DMH1 is used, which acts inhibitory on BMP receptors intracellularly, and therefore attenuates the BMP activity level. The extracellular agonist – intracellular antagonist mechanism is critical, as other BMP antagonists may act differently, i.e., through extracellular competition with BMP ligands or reduction of BMP by

binding to ligands, both of which would not result in the precisely controlled mechanism required. By exploiting this agonist/antagonist combination, the optimum level of BMP signaling activity can be achieved robustly in different cultures with varying initial levels of endogenous activity. In the original study, this approach worked reproducibly to derive Sox10+ neural crest cells from hESC and hiPSC. Therefore, I tested this approach for consistent induction of Sox10+ cells in hiPSC cultures and if these were competent to differentiate into Schwann cells. To this end, in a first preliminary experiment, different conditions were tested: (1) addition of BMP4 alone at a concentration previously reported to induce differentiation of Sox10+ neural crest cells in hESC cultures [Cimadamore et al., 2011], (2) the combination of DMH1 and BMP4 to achieve top-down inhibition as described by Hackland et al. at the same concentrations used in their study, and (3) BMP4 at the concentration of condition (1) combined with DMH1 at the concentration of condition (2). Additionally, each of those three conditions were tested either for a duration of four days or six days. Regarding the timepoint, the second week of differentiation was chosen, to push the desired neural crest fate after an initial neuralization of cultures [Ma et al., 2015]. The evaluation of cell survival and differentiation of Sox10+ cells indicated best results if BMP4 and DMH1 were combined as suggested in the original study (condition 2) [Hackland et al., 2017] for a duration of 6 days. Therefore, this condition was reproduced in several experiments using different hiPSC lines, which confirmed a substantially improved efficiency and reproducibility of induction of Sox10+ neural crest cells, as evident from Figure 3-11. Importantly, cells generated with this method could successfully be differentiated into Schwann cells, that expressed typical marker proteins, including Sox10, p75NTR, GAP-43, S100b, and P0. GFAP, which is also frequently used as a marker for Schwann cells, was only weakly expressed, but this is in accordance with literature which reports poor expression of GFAP in human Schwann cells *in vitro* [Weiss et al., 2016; Monje, 2020]. Furthermore, no expression of MBP was detected, which was also to be expected, since the Schwann cells were not kept in myelination-inducing conditions, i.e., longterm coculture with neurons [Hyung et al., 2015; Monje et al., 2018; Monje, 2020]. All in all, these results confirm the usefulness of tuned BMP activation for efficient generation of neural crest cells from different hiPSC lines and provide evidence for its usefulness for Schwann cell differentiation protocols specifically.

4.2.3 Culture passaging and densities influence differentiation efficiency

As discussed in section 4.1, seemingly minor details concerning general cell culture parameters can have a critical influence on differentiations, such as the cell density at the timepoint of differentiation induction as well as during different stages of the differentiation. During first Schwann cell differentiation experiments reported in this work, I noticed that cell

density throughout differentiation impacted differentiation and survival. Therefore, a systematic experiment was designed to compare differentiation success in differently passaged cultures, as described in section 3.1.4. Additionally, a cell cluster suspension culture phase as opposed to continuously adherent conditions was tried, as suspension culture was used in the past for expansion of neural crest cells [Jiang et al., 2008; Li et al., 2015; Hackland et al., 2017]. In the present study, no beneficial effect of suspension culture was observed, and it was therefore not integrated into the protocol. Cell density, on the other hand, had an impact on differentiating cultures, i.e., the more the cultures were passaged, the more cell detachment occurred. Therefore, passaging was subsequently done in a way that kept cultures at a higher confluency throughout. A correlation between culture density and survival suggests dependance of cells on cell-cell contacts or autocrine factors secreted in the culture. In Schwann cell development, a typical transition of differentiation stages is the transition of Schwann cell precursors, which depend on neuronal signals for survival, towards immature Schwann cells, which develop autocrine survival mechanisms [Jessen et al., 1994; Dong et al., 1995; Jessen and Mirsky, 2019]. Therefore, survival of rodent primary immature Schwann cells placed in culture is density-dependent [Meier et al., 1999; Jessen and Mirsky, 2019]. Interestingly, in this work, detachment of hiPSC-derived cultures was predominantly observed around the time window when this transition from Schwann cell precursors to immature Schwann cells was supposed to happen *in vitro*, according to the protocol and observed cell characteristics [Meier et al., 1999; Kim et al., 2017]. This suggests that during differentiation of Schwann cells from hiPSC *in vitro*, cells develop autocrine survival signals after the precursor stage as well, and that there is one or more factor(s) critical for this mechanism which was not supplied here with the culture medium.

4.2.4 BSA and β-ME are not necessary for differentiation and can be omitted

The original differentiation protocol included the compounds BSA and β-ME in all differentiation media from day 0 to day 24. Neither of these serve a clearly defined function for the differentiation of Schwann cells or neural crest, but they are included in most Schwann cell differentiation protocols, usually without explaining a specific motivation [Ziegler et al., 2011; Kim et al., 2017; Muller et al., 2018; Shi et al., 2018; Carrió et al., 2019]. While it is possible that β-ME acts positively on differentiating Schwann cells by serving as a reducing agent, it can also be hypothesized that these compounds might not be needed for the differentiation of Schwann cells from hiPSCs. As demonstrated by the data presented in Figure 3-9, this work could not find any effect of BSA and β-ME on the derivation of Sox10+ neural crest cells. Moreover, cultures which were differentiated in the absence of those compounds showed better differentiation success towards S100b+ cells. Consequently, both compounds were left

out in further experiments. This improves the protocol regarding compound definition and, potentially, reproducibility, as BSA can be subject to batch-to-batch variation, introducing variability into the protocol. Moreover, BSA can potentially bind small molecules designated to steer cell differentiation and therefore affect control of targeted signaling [Francis, 2010; Hackland et al., 2017]. In this context, it is worth discussing the concentration of the applied TGF-β inhibitor, SB431542: in differentiation protocols which included BSA (including the original protocol of Kim et al. [2017]), a ten-fold higher concentration of SB431542 [Menendez et al., 2011; Leung et al., 2016; Kim et al., 2017] was needed to reliably block TGF-β signaling, when compared to protocols which used SB431542 for neuralization in defined conditions [Li et al., 2011; Hackland et al., 2017]. Indeed, in the present work, SB431542 was used at the lower concentration, which was sufficient for efficient neuralization in the absence of BSA and β-ME. This emphasizes the relevance of defined conditions and knowledge of molecular modes of action in hiPSC differentiations. Perhaps, BSA and β-ME have been present in a major part of Schwann cell differentiation protocols by tradition, as they are often a part of culture media. Along these lines, in 2011, the chemically defined medium E8 for hiPSC maintenance was presented. One major improvement compared to TeSR, the medium it was based on, was the removal of BSA, a factor known to introduce variation into hESC/hiPSC cultures [Chen et al., 2011]. TeSR contained both, BSA and β-ME, and the authors found that both compounds could be omitted at the same time; the omittance of β-ME alone led to cell toxicity, which seemed to be counteracted by the BSA. However, their presence in the medium was not necessary for hESC/hiPSC culture [Chen et al., 2011]. A similar mechanism might have been at play in the evolution of Schwann cell differentiation protocols. Interestingly, the first protocols with the purpose of directed *in vitro* differentiation of Schwann cells used MSC as a cell source. These protocols all employed similar combinations of differentiation factors, which are still used – at least partly – in the majority of Schwann cell differentiation protocols for hESC and hiPSC. Before applying this factor cocktail, which typically included FBS, forskolin, bFGF, PDGF, and Nrg1, MSC differentiation protocols included a short “pre-differentiation” phase in which cells were incubated in medium containing β-ME and retinoic acid. This was supposed to promote a switch from mesenchymal to neural fate in MSC before ensuing differentiation [Dezawa et al., 2001; Kingham et al., 2007; Matsuse et al., 2010; Wakao et al., 2014]. Both of these molecules are also used in a number of hESC/hiPSC differentiation protocols which adopted the general differentiation factor cocktail mentioned earlier, although it can be argued that a step purposed to induce a cell fate switch would not be needed in this case. For all these reasons discussed, the omittance of both components and especially BSA demonstrated in this work improved the protocol towards more defined conditions.

4.2.5 ROCKi or resveratrol treatments do not show beneficial effects on neural crest differentiation

Next to BMP activators, two other molecules identified for evaluation in the initial literature research were resveratrol and Y-27632 (an inhibitor of ROCK and therefore termed “ROCKi” in the following). ROCKi is frequently used for routine culture of hESC and hiPSC to increase cell survival upon passaging and cryopreservation [Watanabe et al., 2007; Li et al., 2008; Chambers et al., 2009]. Human stem cells are particularly vulnerable to apoptosis upon cell detachment and dissociation, which was hypothesized in the past to happen via anoikis, a form of dissociation-induced apoptosis specifically induced by loss of adhesion to ECM [Frisch and Screaton, 2001; Watanabe et al., 2007; Krawetz et al., 2009]. However, Ohgushi et al. [2010] observed that dissociated hESC undergo apoptosis even after they had already attached to the culture substrate. This suggested a different mechanism leading to cell death, mainly caused by loss of cell-cell adhesion instead of cell-substrate adhesion [Ohgushi et al., 2010]. Hereby, apoptosis seemed to be directly caused by a hyperactivation of the actomyosin system, initiated through activation of Rho, explaining the effectiveness of ROCKi to block dissociation-induced Rho/ROCK/myosin II activation, therefore preventing apoptosis [Chen et al., 2010; Walker et al., 2010]. This is a standard practice in both, hiPSC maintenance culture as well as many differentiation protocols, as it can substantially increase cell survival and does not seem to affect pluripotency and proliferation [Kurosawa, 2012; Maldonado et al., 2016; Vernardis et al., 2017]. However, ROCK inhibition alters cytoskeletal organization, visible from characteristic stem cell morphologies while cultured in the presence of ROCKi. Upon prolonged exposure, cytoskeletal disruption was observed [Gao et al., 2019], as well as effects on cell differentiation [Maldonado et al., 2016] and metabolism [Vernardis et al., 2017]. Therefore, it is consensus to remove ROCKi from culture media after a maximum of 24 h. Furthermore, it should be included in differentiation protocols only when necessary, as downstream effects could also influence differentiation mechanisms, and negative effects on targeted differentiation at commonly used concentrations were reported [Jiang et al., 2022]. Yet, some differentiation protocols have used ROCKi also for longer incubation times, including hiPSC-Schwann cell differentiation protocols during the first differentiation phase towards neural crest and Schwann cell precursors [Liu et al., 2012; Muller et al., 2018]. Indeed, Rho pathways are involved in the development of neural crest [Fort and Théveneau, 2014], and inhibition of the ROCK/myosin II pathway was demonstrated to induce neural crest differentiation *in vitro* [Kim et al., 2015] possibly through promotion of EMT [Maldonado et al., 2016]. Therefore, I have tried one week of ROCKi treatment using 10 µM Y-27632 [Kim et al., 2015] during the neural crest specification phase of the protocol, i.e., days 6 – 12, in a preliminary experiment. In comparison to the control condition, where ROCKi was withdrawn

after 24 h of passaging-dependent addition, the percentage of Sox10+ cells as a measure for neural crest differentiation initially seemed to increase slightly (ca. 90 % Sox10+ cells after 19 days compared to 74 %). At the same time, the proliferation rate seemed to increase, as ROCKi-treated cultures appeared evidently denser at this timepoint. However, after 25 days of differentiation, there was no obvious difference between both conditions regarding both parameters, and after 33 days, there was a dramatic drop in Sox10+ cells in the ROCKi-treated condition down to 19 %. As explained above, only those conditions which indicated a beneficial effect in preliminary experiments were subsequently reproduced, so these results have not been replicated and should be interpreted with restraint. Still, it is interesting to note that these data do not contradict the hypothesis of a beneficial effect on neural crest differentiation which was reported elsewhere, since an adverse effect was only observed in a later stage, distinctly after neural crest specification. A tentative but interesting explanation would be the possibility that ROCKi might promote differentiation of neural crest cells already primed towards other cell fates, which might then not be able to proliferate and/or differentiate further once the culture conditions are adjusted for Schwann cell specification.

In a second condition, during the same time window, application of the chemical resveratrol was tested. This compound has been reported to improve PSC culture regarding survival and proliferation, and also differentiation in some protocols [Safaeinejad et al., 2018; Wang et al., 2022]. Evidence suggests this to be mediated by antioxidant activity of resveratrol [Chanvitayapongs et al., 1997; Jang et al., 1997] which prevents cells from oxidative damage *in vivo* and *in vitro*, including neural cell models [Carrizzo et al., 2013; Shen et al., 2016; Means et al., 2020]. Besides, resveratrol was identified as an activator of Notch signaling [Pinchot et al., 2010], and was also explored for this reason, since Notch signaling is important for neural crest specification, gliogenesis, and Schwann cell precursor specification [Morrison et al., 2000; Woodhoo et al., 2009; Noisa et al., 2014; Wiszniak and Schwarz, 2019]. However, it should be noted that the literature is not clear on the effects of resveratrol, which seem to be highly dependent on numerous parameters including cell type, treatment concentration, and duration [Peltz et al., 2012; Safaeinejad et al., 2018], and other studies even suggested downregulation of Notch signaling upon treatment [Zhang et al., 2014b; Zhang et al., 2019]. Preliminary experiments did not indicate any beneficial effects of resveratrol on neural crest differentiation: after 19 days of differentiation, no difference was evident compared to the control condition, and at later timepoints, the percentage of Sox10+ cells dramatically decreased. Therefore, this molecule was not further explored.

4.2.6 Addition of serum is necessary during the Schwann cell precursor stage

The Schwann cell differentiation protocol used as a basis of this work [Kim et al., 2017] used FBS in the culture medium from day 24 forward. FBS was already a component of the factor cocktail employed in the first protocols to differentiate Schwann cells from MSC [Dezawa et al., 2001; Kingham et al., 2007], and although the option to work in defined conditions is particularly desirable for hPSC differentiation protocols, most of the protocols available to date use supplementation with serum or serum derivatives [Ziegler et al., 2011; Liu et al., 2012; Kim et al., 2017; Muller et al., 2018; Carrió et al., 2019; Mukherjee-Clavin et al., 2019]. Serum is a non-defined component and contains a variety of nutrients and growth factors which can act on cells non-specifically, also on their differentiation, and therefore interfere with directed differentiation targets. Moreover, it is subject to variability between batches, which leads to inconsistencies in cell culture. This is a major problem for reproducibility of hiPSC differentiation protocols, as they are obviously susceptible to any changes in culture conditions. In addition, defined and xeno-free culture conditions are particularly relevant for cell types which could be useful in clinical applications, as it is the case for Schwann cells. Therefore, I tested if Schwann cells could be differentiated without FBS supplementation using the protocol presented here. To this end, FBS was removed from differentiation medium as of day 24, and replaced with supplements N2 and B27. Screening of cultures differentiated under these conditions for proliferation (Ki67) and Schwann cell markers (GAP-43, S100b, vimentin, Sox10) revealed that the proportion of differentiating Schwann cells was massively decreased when compared to serum-supplemented cultures. Apparently, serum-free culture did not block differentiation of Schwann cells, as they were still present with expected marker expression after additional 14 days of culture. But their population in culture was markedly reduced and clearly overgrown by a second, proliferating cell population. It might be possible to transfer the protocol presented here to completely serum-free conditions by introducing a sorting step around the Schwann cell precursor stage to purify this population, as survival and differentiation still seemed possible in serum-free conditions, but such option was not explored in this work.

As a second approach to reduce non-defined components, a serum-free medium formulation was evaluated at a later stage of the protocol, after some time of incubation in the original serum-supplemented medium. This would still pose the advantage that differentiated Schwann cells could be transferred into serum-free conditions for specific experiments, where non-defined components could interfere, for example coculture with other cell types, as it was aimed at in this study. For this reason, a serum-free medium formulation based on the culture medium used for hiPSC-derived motoneurons was first evaluated in cocultures of motoneurons and myotubes (see section 4.3), and subsequently tested in hiPSC-Schwann cell cultures.

Notably, this medium did not only support survival of Schwann cells, but it had beneficial effects on their maturation, as discussed in the next section. It was then tried if culturing cells in that specific serum-free medium, termed triM, would be able to rescue cultures derived under serum-free conditions as described before. However, there was no difference between completely serum-free cultures switched to triM and those which were not. Following the protocol reported above including serum supplementation, consistently good results were achieved if cultures were switched to triM only after 35 – 40 days of differentiation, i.e., after around two weeks of serum supplementation. This option still poses an improvement over continued culture in non-defined conditions, paving the way for coculture studies as discussed below. However, it should be noted, that proliferation of Schwann cells decreased after transfer to triM, usually to an extent which did not allow passaging of cultures anymore. For expansion of cells, therefore, the original medium should be used. In this study, cells were expanded in the original medium up to a maximum of 100 days of differentiation in total, and those cultures could be switched to defined triM conditions anywhere between days 40 and 100.

4.2.7 Improvement of Schwann cell maturation in triM is mediated by retinoic and ascorbic acid

Upon transfer of Schwann cell cultures to defined triM conditions, cells underwent rapid morphological changes, often towards an elongated, bi-polar spindle shape, which is characteristic for Schwann cells *in vitro* [Monje, 2020b]. This observation led to the hypothesis that triM would promote Schwann cell maturation, which was tested by evaluating marker protein expression and morphological presentation in six different medium conditions. The original Schwann cell medium served as control condition, and was compared to triM, as well as four additional conditions based on triM but containing only a part of its differentiation factors in different combinations. Cells of all conditions were then immunolabeled for the proteins Ki67, Pax3, vimentin, f-actin, p75NTR, GAP-43, S100b, and P0. Of those, p75NTR, GAP-43, S100b, and P0 are among the markers which are most commonly used to characterize Schwann cells differentiated *in vitro*. Combined expression of those four markers is characteristic for the Schwann cell lineage, but their onset of expression corresponds to different developmental stages [Liu et al., 2015; Monje, 2020b]: p75NTR is expressed already in neural crest cells, GAP-43 turns up in Schwann cell precursors, followed by S100b, and P0 starts to be expressed in immature Schwann cells. Besides those, Pax3 is an early marker which starts to be expressed in neural crest and is still present in Schwann cell precursors [Balakrishnan et al., 2016; Jacob, 2017], but subsequently it is downregulated with further maturation. Sometimes, Pax3 has been also reported as a marker of mature non-myelinating Schwann cells, based on a study were Pax3 expression was observed among non-myelinating Schwann cells in mouse

sciatic nerve [Kioussi et al., 1995]. However, other studies identified a small stem-like cell population in adult nerves which was positive for Pax3 [Blake and Ziman, 2013], while its expression was not confirmed in adult non-myelinating Schwann cells [Blake and Ziman, 2013; Balakrishnan et al., 2016]. An overall inverse correlation of Pax3 expression and Schwann cell maturation – regardless of subtype – is also supported by the finding that terminal differentiation of Schwann cells is suppressed by Pax3, while proliferation is upregulated [Doddrell et al., 2012]. Taken together, this evidence suggests that Pax3 (more precisely, its downregulation) could be a useful marker to identify Schwann cell maturation beyond the precursor stage. Ki67 was chosen as a measure of cell proliferation, and a decrease in proliferation was interpreted as an indication for maturation, since high proliferation rates are characteristic for immature Schwann cells, which then gradually exit the cell cycle with maturation [Jessen et al., 2015; Jessen and Mirsky, 2019]. Finally, vimentin and f-actin were labeled to visualize cytoskeletal morphology. Vimentin is an intermediate filament characteristically expressed in mesenchymal cells, and also found in neural crest progeny following EMT. F-actin was labeled since the characteristic change from a flattened into a spindle shape during differentiation of Schwann cells was attributed to reorganization of the f-actin cytoskeleton [Fernandez-Valle et al., 1997; Li et al., 2003]. Staining of f-actin has been reported to be suited for assessing Schwann cell shape [Procacci et al., 2012], and it can visualize structures like stress fibers or lamellipodia, which are associated with Schwann cell migration and differentiation [Li et al., 2003; Wang et al., 2012b; Lee et al., 2014; Mazzara et al., 2017; Rosso et al., 2017; Velasquez et al., 2018].

Upon analysis of cultures regarding the percentage of cells which expressed markers associated with different stages of the Schwann cell lineage (Pax3, p75NTR, GAP-43, S100b, P0) or proliferation (Ki67), distinct observations emerged. Markers associated with more mature stages following the transition to Schwann cell precursors were expressed in more cells after incubation in triM as compared to the standard medium. This difference was found to be significant for S100b and P0, and a trend was observed for GAP-43. At the same time, the proliferation marker Ki67 was decreased. The proportion of Pax3+ cells was highest in control medium, however, in this case, the difference was not significant for triM, but for three other triM-based conditions. This increase in more mature markers combined with a decrease in early marker/proliferation supports the hypothesis that triM promotes the maturation of Schwann cells. The proportion of cells expressing p75NTR did not differ significantly between conditions, which suggests that triM increased the state of maturation, but not the amount of differentiating Schwann cells. Those differences were reproduced in medium which only contained Nrg1, retinoic acid, and ascorbic acid, and none of the other triM differentiation factors. Similarly, it was also reproduced in most conditions (except for S100b) in medium containing Nrg1, retinoic acid, and purmorphamine.

Next to differences in marker protein expression, changes in cell morphology were observed, with cells appearing more elongated and spindle-shaped in triM and triM-based media compared to the control condition. Furthermore, co-stainings of P0 and f-actin revealed that in triM-based media, cells showed spread lamellipodia, which were not as evident in the control medium (Figure 3-15). Notably, this was only a qualitative observation and was not quantified. Yet, while lamellipodia could be found in all media, more of them (or more pronounced ones) seemed to be present in conditions containing retinoic acid. Lamellipodia are critical not only for migration of Schwann cells, but also for differentiation processes. In particular, their role in axonal sorting and maturation into the promyelinating stage is established [Jin et al., 2011; Wang et al., 2012b; Lee et al., 2014]. Further roles of lamellipodia in Schwann cells remain to be explored, one of them being cell-cell communication between Schwann cells, as well as between Schwann cells and axons already in earlier differentiation stages than myelination [Velasquez et al., 2018].

To add a quantitative measure of morphological changes of the cells, the fusiform elongation of cells was chosen, as this is an accepted characteristic of cultured Schwann cells and has been used before as an evaluation parameter of stem-cell derived Schwann cells [Tomita et al., 2013; La Bierlein De Rosa et al., 2017]. For all medium conditions, a numerical value termed “elongation index” was obtained from S100b immunofluorescence data (the method is explained in sections 2.4.2, 3.1.5 and Figure 3-17). This revealed that incubation in triM increased elongation of Schwann cells (determined by S100b signal) when compared to standard medium, and, again, this was reproduced in the conditions containing Nrg1, retinoic acid, and either purmorphamine or ascorbic acid, whereby the latter combination led to the highest increase.

Taken together, this argues for improved Schwann cell maturation in triM, and identifies retinoic acid as a possible mediator of this effect. Retinoic acid is known to be an important regulator of patterning as well as maturation in the developing nervous system, and it was found to specify a posterior identity in neural crest [Villanueva et al., 2002; Huang et al., 2016]. It is also part of the factor cocktail established in early Schwann cell differentiation protocols based on rodent MSC [Dezawa et al., 2001; Kingham et al., 2007], which is still used entirely or in parts throughout many protocols, also hPSC-based ones [Gao et al., 2015; Kim et al., 2017; Kitada et al., 2019]. Still, the exact effect of retinoic acid on Schwann cells and their differentiation is unclear. Retinoic acid signaling is involved in regulation of myelination, but it was suggested to have different effects on Schwann cell physiology depending on context, and Schwann cells express retinoid receptors in the adult stage as well as during development [Latasa and Cosgaya, 2011]. In rodent explant cultures, retinoic acid inhibited the myelination program, but at the same time, in accordance with the results presented here, P0 expression was increased, and proliferation was decreased [Latasa et al., 2010; Latasa et al., 2016]. Further research on

this topic is needed to elucidate the whole picture of retinoic acid signaling mechanisms in Schwann cell biology, and particularly, development; but the data presented in this work and the publications discussed suggest important functions for retinoic acid which would be interesting for differentiation protocols. To follow up on results of this work, further experiments could be designed to clarify more precisely the roles of the individual molecules involved, as not all possible combinations were tested here. In all three conditions tested, Nrg1 was present at the same time, as it is assumed to be the most critical molecule for Schwann cell culture. Thus, it would be interesting to test if presence of Nrg1 is needed or dispensable for the observed effects mediated by retinoic acid. Furthermore, either ascorbic acid or purmorphamine was supplemented additionally. Considering all maturation markers evaluated, the effect was stronger in the presence of ascorbic acid, suggesting that either purmorphamine attenuates maturation effects, or ascorbic acid provides additional benefits. Ascorbic acid is indeed used in several hiPSC-Schwann cell differentiation protocols as well [Ziegler et al., 2011; Liu et al., 2012; Muller et al., 2018; Carrió et al., 2019; Mukherjee-Clavin et al., 2019], and it is known to induce the onset of the Schwann cell myelination program and basal lamina assembly [Eldridge et al., 1987; Huff et al., 2021]. In this context, upregulation of P0 expression and a decrease of proliferation in ascorbic acid-containing media have also been observed by others [Callizot et al., 2011; Bacallao and Monje, 2015], but the exact underlying mechanisms are not clear yet [Huff et al., 2021].

4.3 2D cocultures

4.3.1 Establishment of a neuromuscular coculture protocol including hiPSC-derived Schwann cells

To integrate hiPSC-derived Schwann cells into a neuromuscular coculture model, first of all, the traditional 2D bilayer coculture was chosen. As pointed out in the introduction and as further discussed in the next section, the developments in new neuromuscular cell models have recently mainly focused on 3D culture platforms, as they offer distinct advantages. However, the lower complexity of 2D bilayer models is also beneficial for certain applications and enables more straightforward readouts especially by microscopy analysis. Before this study, no protocol had been published to selectively integrate hiPSC-derived Schwann cells into neuromuscular cocultures. Therefore, the protocol presented here for integration into 2D bilayer cultures, which have been and are still widely used in the field, poses a base to flexibly adapt it to already established NMJ *in vitro* model platforms and assays. As this bilayer model does not use compartmentation, like e.g. microfluidic devices [Southam et al., 2013; Santhanam et al., 2018], it can be challenging to determine defined medium conditions which

support all cellular components present [Besser et al., 2020]. This work describes a medium which is based on differentiation medium for hiPSC-derived motoneurons, but likewise supports the differentiation of hiPSC-derived Schwann cells and C2C12 myotubes. To come as close as possible to the goal of all human-derived cultures, both motoneurons and Schwann cells were differentiated from hiPSC. For the muscle part, an alternative source had to be used, as protocols to differentiate skeletal muscle from hiPSC are still rather inefficient as well, and the focus of this work was not on the optimization of hiPSC-muscle differentiation. Therefore, the murine C2C12 was chosen, as this line can be differentiated *in vitro* from the myoblast stage into fused, multinucleated myotubes. These are an established source for myotubes in neuromuscular *in vitro* models [Uzel et al., 2016; Charoensook et al., 2017; Cvetkovic et al., 2017; Yoshioka et al., 2020], and they have been shown to form nAChR clusters [Morimoto et al., 2013; Happe et al., 2017; Soliman et al., 2018; Kaufman et al., 2020], which can be induced by hPSC-derived motoneurons [Li et al., 2005; Du et al., 2015; Yoshida et al., 2015]. All of these three cell types need to be differentiated separately before combining them into cocultures, particularly the hiPSC-derived cells. For the C2C12, a 24 h period was found to be sufficient to induce differentiation of myotubes, which then fully formed in the coculture phase. In contrast, for the motoneurons, this pre-differentiation phase was 21 days long, and for Schwann cells, it was 50 days or more. Therefore, the timing of separate differentiations to prepare tricultures is complex, and variations in one of the three differentiations could jeopardize the whole experiment. Thus, to establish a practically feasible protocol, it was necessary to work from frozen cryostocks which were pre-differentiated before. Differentiated Schwann cells could successfully be cryopreserved and recovered, allowing more flexibility in their preparation. Motoneurons cannot be frozen in the differentiated stage, but they could be frozen as precursors, which cuts the time needed from thawing of motoneuron precursors to combining the different cell types down to nine days. A protocol was then adjusted to this time span, in which the three cell types were taken into culture on the same day, prepared and pre-differentiated separately, and combined nine days later. In such cocultures, the presence of all three cell types was confirmed by immunostainings for different combinations of cell-type-specific marker proteins. A frequent colocalization of motor neurites with nAChR clusters was observed (at around 70 % of clusters in tricultures and 63 % in bicultures), which has been used as an indication of *in vitro* NMJ formation in other studies [Singh Roy et al., 2005; Du et al., 2015; Yoshida et al., 2015]. However, further experiments including functional readouts would be necessary to test if actual *in vitro* NMJs are formed, as this is a purely morphological description. Also Schwann cells were found to colocalize with nAChR clusters in some cases (at around 20 % of clusters in tricultures and 16 % in cocultures), and some nAChR in tricultures colocalized with both cell types at the same time (around 18 %). An interesting observation here was that the percentage of nAChR clusters which colocalized with Schwann

cells was about the same in bicultures or tricultures, while the number of nAChR clusters increased between these two conditions. In absolute numbers this would mean, that more Schwann cells colocalized with nAChR clusters in tricultures when compared with bicultures. At the same time, the majority of these colocalizations in tricultures (around 90 %) also colocalized with a neurite, suggesting an interaction between motoneurons and Schwann cells in these cultures. This is supported by the observation that most of the Schwann cells in tricultures (around 80 %) aligned with neurites, which was reported in primary Schwann cell – neuron cocultures as well and was attributed to neuron-glial interactions [Bunge et al., 1986; Seilheimer et al., 1989; Wanner and Wood, 2002; Thompson and Buettner, 2006; Bacallao and Monje, 2013].

4.3.2 Analysis of nAChR clusters in different coculture conditions

The increase in the number of nAChR clusters found in cultures containing motoneurons (biculture and triculture) suggested that the neurons released agrin, the key neuron-derived signal in NMJ development for the clustering of nAChR [Ruegg and Bixby, 1998; Wu et al., 2010]. Agrin-induced nAChR clustering and stabilization is dependent on the scaffolding protein rapsyn [Gautam et al., 1995; Mittaud et al., 2001; Moransard et al., 2003; Bruneau and Akaaboune, 2007]. In the present study, colocalization analysis of nAChR clusters and rapsyn immunostaining demonstrated that also the number and proportion of nAChR clusters positive for rapsyn increased in the presence of motoneurons. This suggests that the hiPSC-derived motoneurons induced clustering of postsynaptic nAChR on C2C12 myotubes, which is the prerequisite for *in vitro* NMJs, and has been reported from other cocultures as well [Li et al., 2005; Du et al., 2015; Yoshida et al., 2015]. Furthermore, nAChR clusters in motoneuron cocultures as well as tricultures presented with a smaller and more defined appearance. At first, the decrease of cluster area seemed counterintuitive, as one might rather expect an increase in cluster area in the presence of motoneurons. However, there are several possible explanations for this observation: partially, segmentation variability could contribute to a difference in area, as clusters in neural cultures appeared more defined and were therefore easier to precisely segment than clusters in C2C12 monocultures, which appeared rather diffuse. Furthermore, it is possible that these smaller clusters were more densely packed with receptors, and therefore the amount of receptors per cluster area would be increased. Consequently, if that would be the case, one would expect an increase in mean fluorescence of denser clusters. Although no significant rise in mean fluorescence intensity was detected, there was a trend of increase from C2C12 monoculture to biculture to triculture. Alternatively, molecular mechanisms leading to the dispersion of nAChR clusters were possibly at play, like release of ACh from motoneurons [Misgeld et al., 2002; Lin et al., 2005; Wu et al., 2010].

Next, when myotubes were cocultured with hiPSC-derived Schwann cells only, no significant differences in the evaluated parameters were found. However, there was a non-significant but consistent trend towards an increased number of clusters, as well as an increased proportion of rapsyn+ clusters, and the same was true for the appearance of clusters and their area, as described above. As this trend towards the nAChR cluster phenotype seen in neural cocultures was consistent across all evaluated parameters, it allows the speculation that Schwann cells might contribute to nAChR cluster formation in cocultures, albeit at a much smaller scale than motoneurons. Interestingly, primary Schwann cells express an isoform of agrin, which is able to induce nAChR clustering, but with a distinctly lower efficiency than neural agrin [Ferns et al., 1993; Yang et al., 2001; Darabid et al., 2014; Castro et al., 2020]. In addition, Schwann cells could also influence the differentiation of myotubes via other mechanisms, as they are known to secrete several factors such as neurotrophins which can also act on muscle cells [Chevrel et al., 2006; Sakuma and Yamaguchi, 2011; Kim et al., 2017]. Along these lines, further experiments with the culture system established in this work showed a synergistic effect of Schwann cells and motoneurons on the differentiation of myotubes with increased cytoplasmic areas [Hörner et al., 2021], and other studies have confirmed a beneficial effect of Schwann cell coculture on myogenesis [Singh and Vazquez, 2019; Cai et al., 2022].

Besides this, an interesting effect was observed when all three cell types were cultured together: In tricultures, the number of nAChR clusters per myotube area was also increased in comparison to myotubes cultured alone, but to a lesser extent than in myotube – motoneuron bicultures. Of note, a similar effect was described in a culture system established from primary rodent cells [Chapron et al., 1997]. There, coculture of dissociated myoblasts with spinal cord cells of rat embryos induced numerous AChE patches on the muscle cells, and those AChE patches colocalized with AChR clusters. Two days after addition of Schwann cells, which were purified from neonatal rat sciatic nerve, the number of AChE patches was reduced by 50 %. Along with the reduction in number, other changes were reported, including a more differentiated morphology of patches, suppression of BChE expression, and the appearance of junctional folds. These findings were interpreted as increased maturation of *in vitro* NMJs upon addition of the Schwann cells [Chapron et al., 1997]. In the experiments presented in this thesis, a decrease in nAChR cluster numbers of around 30 % was observed between tricultures compared to bicultures without Schwann cells. As Schwann cells alone did not decrease the number of clusters, this seemed to be a synergistic effect specific to cocultures containing both, motoneurons and Schwann cells. Thus, the question arises, if Schwann cells exert some kind of destabilizing effect on nAChR clusters which is only relevant in the presence of neurons, or if Schwann cells could reduce the capacity of neurons to induce nAChR clustering in this setting. Primary Schwann cells exerted beneficial effects on motoneuron differentiation in cocultures [Ullian et al., 2004; Gingras et al., 2008; Ragancokova et al., 2009;

Hyung et al., 2015], and this could be the case also for hiPSC-derived Schwann cells, which were demonstrated to express a range of neurotrophic factors [Kim et al., 2017]. Thereby, they could indirectly increase ACh levels released by more mature motoneurons. In development, while agrin acts as inducing and stabilizing factor for nAChR clusters, ACh acts as a negative signal, which disperses nAChR clusters. *In vivo*, this leads to destabilization of aneural clusters, which are not locally stabilized by agrin [Misgeld et al., 2002; Lin et al., 2005; Wu et al., 2010]. It could also be speculated that Schwann cells directly influenced agrin levels: Schwann cells at NMJs were found to secrete matrix metalloproteinase-3 (MMP-3), which in turn cleaved agrin [VanSaun and Werle, 2000; VanSaun et al., 2007; Zelada et al., 2021]. This led to a reduction in the concentration of available agrin, and in MMP-3 null mice, nAChR clusters were increased [VanSaun et al., 2003; Chao et al., 2013]. Another intriguing speculation would be that *in vivo*, during the process of synapse elimination, terminal Schwann cells physically blocked nAChR by occupying the synaptic surface [Smith et al., 2013b], which would lead to destabilization of those receptors upon activation of others in the vicinity [Balice-Gordon and Lichtman, 1994]. However, these interpretations and suggestions remain highly speculative, as those mechanisms have not been shown *in vitro* and are incompletely understood *in vivo*.

4.4 3D cocultures

Over the last decades, the field of *in vitro* cell modeling has been shifting continuously from routine 2D monolayers towards more sophisticated 3D culturing methods. These are able to recreate the cellular microenvironment *in vivo* more accurately and therefore provide more realistic conditions for cells regarding a number of parameters including nutrient and oxygen gradients, cell-cell interactions, or cell-matrix interactions [Duval et al., 2017; Langhans, 2018]. In 3D cell scaffolds or conglomerates (spheroids or organoids), cells can grow and migrate freely in all three dimensions, in contrast to being flattened on a rigid surface. Cells sense the stiffness of their environment and respond, e.g., with cytoskeletal reorganization [Discher et al., 2005]. Also, gene expression often differed between 2D and 3D culture, and the 3D results might come closer to the *in vivo* situation [Smith et al., 2012; Centeno et al., 2018]. The same is true for cell morphology and outgrowth or responses to stimuli [Antoni et al., 2015; Centeno et al., 2018]. Therefore, high hopes are placed in (human) 3D cultures to potentially overcome the translation issues persistent between studies in 2D cultures, animal models, and human trials [Benatar, 2007; Antoni et al., 2015; Langhans, 2018; Grenier et al., 2020]. Specifically for neuromuscular cocultures, advantages of 3D culture were also demonstrated [Raffa et al., 2022]. In 3D scaffolds, cultures could be kept for longer times, mainly because in 2D, myotubes

detached from rigid surfaces like plastic dishes once they started contracting [Thomson et al., 2012; Wang et al., 2012a]. 3D cultures also seem to reach a higher degree of maturation [Urciuolo et al., 2020], indicated inter alia by recent work on a human 3D neuromuscular model where γ-subunit to ε-subunit switches were observed for nAChR, which is a characteristic for the transition from the embryonic to the adult stage of NMJs [Afshar Bakooshli et al., 2019]. Besides the clear advantages on muscle cell culture and differentiation [Urciuolo et al., 2020; Jalal et al., 2021], 3D culture was also beneficial for hiPSC-derived neurons [Zhang et al., 2014a; Tang et al., 2016; Centeno et al., 2018] and for Schwann cells derived from adult MSC of human [Entezari et al., 2022; Podder et al., 2022] or rodent [Chen et al., 2015] origin. Importantly, for both cell types, different responses upon drug treatment of 2D and 3D disease model cultures were demonstrated using human cells [Lee et al., 2016; Kraniak et al., 2018].

The potential of neuromuscular cultures that include Schwann cells, which was the focus of this work, lies in the possibility to research the influence that Schwann cells could have on *in vitro* NMJ maturation and stabilization, the individual contributions of the separate cell types to NMJ formation and disease processes, as well as how the different cell types interact with and influence each other's development. For all of these objectives, stable culture formats are needed which can be observed long-term. For this reason, different approaches based on hydrogel scaffolds and bioprinting as described in section 3.2.3 were explored. Indeed, cocultures of C2C12 myotubes and hiPSC-derived neurons could be kept in culture for much longer times than their 2D counterparts without obvious cell detachment. Myotubes expressed clear and brightly stained nAChR clusters, and neurons projected long and branched neurites through 3D structures, often approaching muscle cells. In one of the four different 3D designs tested, hiPSC-derived Schwann cells were incorporated as well. They seemed to be able to migrate through the gel and were found in proximity to muscle cells as well as to neurons, often very precisely aligned to neurites. This demonstrated the principal applicability of the hiPSC-derived Schwann cells as presented in this work into different kinds of culture formats. Additionally, with different 3D-designs, it was tested if the emerging technique of 3D-bioprinting could be used to create spatial organization in 3D cultures of motoneurons and muscle cells, with promising results. By incorporating muscle cells into a printed structure which was designed to hold subsequently added neurospheres in a defined place, somata of both cell types were spatially separated in the same hydrogel structure, and extensive neurite outgrowth towards nAChR-expressing myotubes was observed (Figure 3-26). However, more optimization work is needed to increase reproducible 3D tricultures at this level of complexity, and to develop refined methods for their analysis.

In principle, there are two major approaches to create 3D neuromuscular cell models: (1) organoids, which are scaffold-free and self-organize from a variety of cell types differentiating in parallel from one initial stem cell source [Pașca, 2018], and (2) engineered scaffold-based

approaches, where individual cell types are separately prepared and combined into a support structure that creates and organizes the 3D microenvironment. To date, there is one study published demonstrating the differentiation of NMJ organoids [Faustino Martins et al., 2020] and a second one which reported cortico-motor assembloids [Andersen et al., 2020], consisting of hiPSC-derived cortical and spinal organoids, which were fused with muscle spheroids derived from primary human skeletal myoblasts. Intriguingly, both myelinating and non-myelinating Schwann cells were reported to develop in the NMJ organoids along with neuronal and muscle tissue [Faustino Martins et al., 2020]. However, while most studies investigating 3D neuromuscular models used the approach of scaffold-based tissue engineering, all work available to date in this area is based on motoneuron-muscle coculture without inclusion of Schwann cells [Maffioletti et al., 2018; Afshar Bakooshli et al., 2019; Osaki et al., 2020; Rimington et al., 2021; Vila et al., 2021]. Along these lines, the results and protocols demonstrated in this work pose a contribution to advancing these cultures.

When comparing these two approaches (self-organized or engineered), both have individual advantages and disadvantages for different applications. On the one hand, self-organized organoids are extremely fascinating and promising, as they can recapitulate the developmental differentiation and organization happening *in vivo* most closely. Furthermore, they can be maintained in culture for very long times, facilitating research on different developmental stages of neuromuscular tissue [Faustino Martins et al., 2020]. On the other hand, selectively engineered cocultures enable investigation of cell type-specific contributions to developmental and, particularly, pathological mechanisms, as the individual cell types can be generated from different genetic backgrounds and combined at different timepoints. Therefore, undoubtedly, both approaches, self-organized organoids and engineered selective cocultures, are required to advance neuromuscular research and need to be employed in a complementary way.

4.5 Conclusion and Outlook

In this thesis, I have demonstrated for the first time the selective integration of hiPSC-derived Schwann cells into neuromuscular cell cultures. The protocols presented are adaptable to a wide range of applications, enabling future *in vitro* studies on human Schwann cells in the neuromuscular context. The optimized protocol presented for the differentiation of Schwann cells from hiPSC allowed for their generation at high robustness and efficiency without any purification steps, which will be interesting not only for neuromuscular cell models, but for the field of Schwann cell biology in general, as efficient protocols for human Schwann cell differentiation have been lacking. Furthermore, the serum-free medium formulation used in this work for neuromuscular tricultures supported the differentiation of all three cell types, and it is potentially interesting for other neuromuscular coculture setups as well as other work focusing on Schwann cells themselves, since it allowed for Schwann cell maturation in defined conditions. The experiments done in 2D tricultures provided a very first insight into the relevance of Schwann cells in neuromuscular cocultures, but further work is needed to explore such cocultures in more stable, long-term setups. To achieve this, 3D culture techniques are necessary, and the experiments presented here indicated that Schwann cells can also be integrated into hydrogel-based cultures. Furthermore, 3D-bioprinting was explored as a promising technique to achieve spatial organization in 3D hydrogel-based cocultures.

Further research is necessary to establish robust protocols for the generation as well as analysis of such 3D cultures including muscle cells, motoneurons, and Schwann cells. To come closer to the goal of realistic cell models for human biology, a main focus should be on generating all cell types of such models from hiPSC. Motoneurons have been differentiated routinely from hiPSC already for a number of different models, and this work contributes the tools to add the hiPSC-derived Schwann cells [Hörner et al., 2021; Hörner et al., 2022]. Likewise, protocols to generate hiPSC-derived skeletal muscle were published in the past [Hosoyama et al., 2014; Chal et al., 2016; van der Wal et al., 2018; Metzler et al., 2022]. While those protocols often suffered from a lack of efficiency and cell maturation, some models combined hiPSC-derived motoneurons and muscle cells [Demestre et al., 2015; Maffioletti et al., 2018; Osaki et al., 2018; Bellmann et al., 2019; Guo et al., 2020]. Based on the 2D triculture protocol presented in this thesis, an all hiPSC-derived triculture including hiPSC-muscle cells was demonstrated, using a similar timing of cell type combination and the same defined medium as for the combination with C2C12 myotubes [Hörner et al., 2021]. Consequently, the next step would be to transfer this into more complex formats suited for long-term culture, and to adjust those also to functional analysis, to ultimately explore the formation and maturation of functional *in vitro* NMJs in tricultures. Such improved models would also be highly relevant for disease modeling, as hiPSCs can be generated from patient material and therefore have

disease-specific genotypes. Multicellular models would be especially valuable to investigate diseases where cell-type specific contributions are not yet understood. For example, in ALS, the course of events underlying degeneration mechanisms at NMJs are unclear [Cappello and Francolini, 2017; Alhindi et al., 2021a; Verma et al., 2022]. While it has been understood primarily as a motoneuron disease, both skeletal muscle [Fischer et al., 2004; Badu-Mensah et al., 2020; Badu-Mensah et al., 2022] and terminal Schwann cells [Carrasco et al., 2016; Arbour et al., 2017; Martineau et al., 2020] might be involved as well in pathogenesis. Cell-type specific disease models of neuromuscular junctions could provide valuable insights into such mechanisms. Along these lines, the differentiation of both, motoneurons and Schwann cells, has been demonstrated in this work from several healthy as well as one disease-specific hiPSC line of an ALS background.

Besides, future work could also move along the lines of further improvement of Schwann cell differentiation protocols. The generation of human Schwann cells is not only interesting for their application in coculture studies but has received perhaps the most attention in the context of tissue engineering with the aim of regenerative cell transplantation. However, a prerequisite for such clinical applications are safe and efficient protocols to differentiate high quantities of human Schwann cells in fully defined, xeno-free conditions. It would be interesting to conduct further experiments with various serum replacement supplements or specific molecules, to see if the protocol used here could be adapted to fully defined conditions. Furthermore, a systematic investigation to define the effects of each individual molecule that was contained in the full maturation medium formulation, as well as various combinations of those, could be helpful to define the optimal composition for Schwann cell maturation. Finally, further work is needed to elucidate the largely unknown mechanisms by which Schwann cell subtypes are specified during development, to consequently also develop targeted differentiation protocols for terminal Schwann cells at the NMJ. As these specification signals are most likely provided by cell-cell interactions in developing tissues, *in vitro* co-cultures could also contribute to decipher these processes.

In conclusion, this study focused on the differentiation of hiPSC-derived Schwann cells and their application in neuromuscular cocultures, and therefore provides contributions to the research fields of Schwann cell differentiation as wells as *in vitro* neuromuscular modeling which can be built upon in future work.

5 REFERENCES

Abzhanov, A., Tzahor, E., Lassar, A.B., and Tabin, C.J. (2003). Dissimilar regulation of cell differentiation in mesencephalic (cranial) and sacral (trunk) neural crest cells in vitro. Development *130*, 4567-4579. https://doi.org/10.1242/dev.00673.

Adameyko, I., Lallemend, F., Aquino, J.B., Pereira, J.A., Topilko, P., Müller, T., Fritz, N., Beljajeva, A., Mochii, M., and Liste, I., et al. (2009). Schwann cell precursors from nerve innervation are a cellular origin of melanocytes in skin. Cell *139*, 366-379. https://doi.org/10.1016/j.cell.2009.07.049.

Afshar Bakooshli, M., Lippmann, E.S., Mulcahy, B., Iyer, N., Nguyen, C.T., Tung, K., Stewart, B.A., van den Dorpel, H., Fuehrmann, T., and Shoichet, M., et al. (2019). A 3D culture model of innervated human skeletal muscle enables studies of the adult neuromuscular junction. eLife *8*. https://doi.org/10.7554/eLife.44530.

Agduhr, E. (1920). Sympathetic innervation of the muscles of the extremities. A histo-experimental study. Verhand. Akad. Wetensch. *20*, 1-34.

Aguayo, A.J., Epps, J., Charron, L., and Bray, G.M. (1976). Multipotentiality of Schwann cells in cross-anastomosed and grafted myelinated and unmyelinated nerves: Quantitative microscopy and radioautography. Brain Research *104*, 1-20. https://doi.org/10.1016/0006-8993(76)90643-0.

Alhindi, A., Boehm, I., and Chaytow, H. (2021a). Small junction, big problems: Neuromuscular junction pathology in mouse models of amyotrophic lateral sclerosis (ALS). Journal of anatomy. https://doi.org/10.1111/joa.13463.

Alhindi, A., Boehm, I., Forsythe, R.O., Miller, J., Skipworth, R.J.E., Simpson, H., Jones, R.A., and Gillingwater, T.H. (2021b). Terminal Schwann cells at the human neuromuscular junction. Brain communications *3*, fcab081. https://doi.org/10.1093/braincomms/fcab081.

Alvarez-Suarez, P., Gawor, M., and Prószyński, T.J. (2020). Perisynaptic schwann cells - The multitasking cells at the developing neuromuscular junctions. Seminars in Cell & Developmental Biology *104*, 31-38. https://doi.org/10.1016/j.semcdb.2020.02.011.

Amoroso, M.W., Croft, G.F., Williams, D.J., O'Keeffe, S., Carrasco, M.A., Davis, A.R., Roybon, L., Oakley, D.H., Maniatis, T., and Henderson, C.E., et al. (2013). Accelerated high-yield generation of limb-innervating motor neurons from human stem cells. The Journal of neuroscience : the official journal of the Society for Neuroscience *33*, 574-586. https://doi.org/10.1523/JNEUROSCI.0906-12.2013.

Andersen, J., Revah, O., Miura, Y., Thom, N., Amin, N.D., Kelley, K.W., Singh, M., Chen, X., Thete, M.V., and Walczak, E.M., et al. (2020). Generation of Functional Human 3D Cortico-Motor Assembloids. Cell *183*, 1913-1929.e26. https://doi.org/10.1016/j.cell.2020.11.017.

Anderson, M.J., Cohen, M.W., and Zorychta, E. (1977). Effects of innervation on the distribution of acetylcholine receptors on cultured muscle cells. The Journal of Physiology *268*, 731-756. https://doi.org/10.1113/jphysiol.1977.sp011879.

Anderson, R.M., Stottmann, R.W., Choi, M., and Klingensmith, J. (2006). Endogenous bone morphogenetic protein antagonists regulate mammalian neural crest generation and survival. Developmental dynamics : an official publication of the American Association of Anatomists *235*, 2507-2520. https://doi.org/10.1002/dvdy.20891.

Antoni, D., Burckel, H., Josset, E., and Noel, G. (2015). Three-dimensional cell culture: a breakthrough in vivo. International Journal of Molecular Sciences *16*, 5517-5527. https://doi.org/10.3390/ijms16035517.

Araque, A., Parpura, V., Sanzgiri, R.P., and Haydon, P.G. (1999). Tripartite synapses: glia, the unacknowledged partner. Trends in Neurosciences *22*, 208-215. https://doi.org/10.1016/s0166-2236(98)01349-6.

Arbour, D., Tremblay, E., Martineau, É., Julien, J.-P., and Robitaille, R. (2015). Early and persistent abnormal decoding by glial cells at the neuromuscular junction in an ALS model. The Journal of Neuroscience: The Official Journal of the Society for Neuroscience *35*, 688-706. https://doi.org/10.1523/JNEUROSCI.1379-14.2015.

Arbour, D., Vande Velde, C., and Robitaille, R. (2017). New perspectives on amyotrophic lateral sclerosis: the role of glial cells at the neuromuscular junction. The Journal of Physiology *595*, 647-661. https://doi.org/10.1113/JP270213.

Askanas, V., Kwan, H., Alvarez, R.B., Engel, W.K., Kobayashi, T., Martinuzzi, A., and Hawkins, E.F. (1987). De novo neuromuscular junction formation on human muscle fibres cultured in monolayer and innervated by foetal rat spinal cord: ultrastructural and ultrastructural—cytochemical studies. Journal of Neurocytology *16*, 523-537. https://doi.org/10.1007/BF01668506.

Avery, J., and Dalton, S. (2016). Methods for Derivation of Multipotent Neural Crest Cells Derived from Human Pluripotent Stem Cells. Methods in Molecular Biology (Clifton, N.J.) *1341*, 197-208. https://doi.org/10.1007/7651_2015_234.

Bacallao, K., and Monje, P.V. (2013). Opposing roles of PKA and EPAC in the cAMP-dependent regulation of schwann cell proliferation and differentiation corrected. PLoS ONE *8*, e82354. https://doi.org/10.1371/journal.pone.0082354.

Bacallao, K., and Monje, P.V. (2015). Requirement of cAMP signaling for Schwann cell differentiation restricts the onset of myelination. PLoS ONE *10*, e0116948. https://doi.org/10.1371/journal.pone.0116948.

Bader, D., Masaki, T., and Fischman, D.A. (1982). Immunochemical analysis of myosin heavy chain during avian myogenesis in vivo and in vitro. J Cell Biol *95*, 763-770. https://doi.org/10.1083/jcb.95.3.763.

Badiola-Mateos, M., Hervera, A., Del Río, J.A., and Samitier, J. (2018). Challenges and Future Prospects on 3D in-vitro Modeling of the Neuromuscular Circuit. Frontiers in Bioengineering and Biotechnology *6*. https://doi.org/10.3389/fbioe.2018.00194.

Badu-Mensah, A., Guo, X., McAleer, C.W., Rumsey, J.W., and Hickman, J.J. (2020). Functional skeletal muscle model derived from SOD1-mutant ALS patient iPSCs recapitulates hallmarks of disease progression. Scientific Reports *10*, 14302. https://doi.org/10.1038/s41598-020-70510-3.

Badu-Mensah, A., Guo, X., Nimbalkar, S., Cai, Y., and Hickman, J.J. (2022). ALS mutations in both human skeletal muscle and motoneurons differentially affects neuromuscular junction integrity and function. Biomaterials *289*, 121752. https://doi.org/10.1016/j.biomaterials.2022.121752.

Bajpai, V.K., Kerosuo, L., Tseropoulos, G., Cummings, K.A., Wang, X., Lei, P., Liu, B., Liu, S., Popescu, G.K., and Bronner, M.E., et al. (2017). Reprogramming Postnatal Human Epidermal Keratinocytes Toward Functional Neural Crest Fates. Stem Cells (Dayton, Ohio) *35*, 1402-1415. https://doi.org/10.1002/stem.2583.

Balakrishnan, A., Stykel, M.G., Touahri, Y., Stratton, J.A., Biernaskie, J., and Schuurmans, C. (2016). Temporal Analysis of Gene Expression in the Murine Schwann Cell Lineage and the Acutely Injured Postnatal Nerve. PLoS ONE *11*, e0153256. https://doi.org/10.1371/journal.pone.0153256.

Balice-Gordon, R.J., and Lichtman, J.W. (1994). Long-term synapse loss induced by focal blockade of postsynaptic receptors. Nature *372*, 519-524. https://doi.org/10.1038/372519a0.

Barbeau, S., Tahraoui-Bories, J., Legay, C., and Martinat, C. (2020). Building neuromuscular junctions in vitro. Development (Cambridge, England) *147*. https://doi.org/10.1242/dev.193920.

Barclay, M., Noakes, P.G., Ryan, A.F., Julien, J.-P., and Housley, G.D. (2007). Neuronal expression of peripherin, a type III intermediate filament protein, in the mouse hindbrain. Histochem Cell Biol *128*, 541-550. https://doi.org/10.1007/s00418-007-0340-4.

Barik, A., Li, L., Sathyamurthy, A., Xiong, W.-C., and Mei, L. (2016). Schwann Cells in Neuromuscular Junction Formation and Maintenance. The Journal of neuroscience : the official journal of the Society for Neuroscience *36*, 9770-9781. https://doi.org/10.1523/JNEUROSCI.0174-16.2016.

Bartschat, A., Hübner, E., Reischl, M., Mikut, R., and Stegmaier, J. (2016). XPIWIT—an XML pipeline wrapper for the Insight Toolkit. Bioinformatics *32*, 315-317. https://doi.org/10.1093/bioinformatics/btv559.

Basch, M.L., Bronner-Fraser, M., and García-Castro, M.I. (2006). Specification of the neural crest occurs during gastrulation and requires Pax7. Nature *441*, 218-222. https://doi.org/10.1038/nature04684.

Bellard, M.E. de, Ching, W., Gossler, A., and Bronner-Fraser, M. (2002). Disruption of segmental neural crest migration and ephrin expression in delta-1 null mice. Developmental Biology *249*, 121-130. https://doi.org/10.1006/dbio.2002.0756.

Belle, M., Godefroy, D., Couly, G., Malone, S.A., Collier, F., Giacobini, P., and Chédotal, A. (2017). Tridimensional Visualization and Analysis of Early Human Development. Cell *169*, 161-173.e12. https://doi.org/10.1016/j.cell.2017.03.008.

Bellmann, J., Goswami, R.Y., Girardo, S., Rein, N., Hosseinzadeh, Z., Hicks, M.R., Busskamp, V., Pyle, A.D., Werner, C., and Sterneckert, J. (2019). A customizable microfluidic platform for medium-throughput modeling of neuromuscular circuits. Biomaterials *225*, 119537. https://doi.org/10.1016/j.biomaterials.2019.119537.

Benatar, M. (2007). Lost in translation: Treatment trials in the SOD1 mouse and in human ALS. Neurobiology of Disease *26*, 1-13. https://doi.org/10.1016/j.nbd.2006.12.015.

Benowitz, L.I., and Routtenberg, A. (1997). GAP-43: an intrinsic determinant of neuronal development and plasticity. Trends in Neurosciences *20*, 84-91. https://doi.org/10.1016/s0166-2236(96)10072-2.

Besser, R.R., Bowles, A.C., Alassaf, A., Carbonero, D., Maciel, R., Saporta, M., and Agarwal, A. (2020). A Chemically Defined Common Medium for Culture of C2C12 Skeletal Muscle and Human Induced Pluripotent Stem Cell Derived Spinal Spheroids. Cellular and Molecular Bioengineering *13*, 605-619. https://doi.org/10.1007/s12195-020-00624-1.

Betters, E., Charney, R.M., and Garcia-Castro, M.I. (2018). Early specification and development of rabbit neural crest cells. Developmental Biology *444 Suppl 1*, S181-S192. https://doi.org/10.1016/j.ydbio.2018.06.012.

Bier, E., and Robertis, E.M. de (2015). EMBRYO DEVELOPMENT. BMP gradients: A paradigm for morphogen-mediated developmental patterning. Science (New York, N.Y.) *348*, aaa5838. https://doi.org/10.1126/science.aaa5838.

Biernaskie, J.A., McKenzie, I.A., Toma, J.G., and Miller, F.D. (2006). Isolation of skin-derived precursors (SKPs) and differentiation and enrichment of their Schwann cell progeny. Nature protocols *1*, 2803-2812. https://doi.org/10.1038/nprot.2006.422.

Birchmeier, C., and Nave, K.-A. (2008). Neuregulin-1, a key axonal signal that drives Schwann cell growth and differentiation. Glia *56*, 1491-1497. https://doi.org/10.1002/glia.20753.

Bishop, D.L., Misgeld, T., Walsh, M.K., Gan, W.-B., and Lichtman, J.W. (2004). Axon branch removal at developing synapses by axosome shedding. Neuron *44*, 651-661. https://doi.org/10.1016/j.neuron.2004.10.026.

Blake, J.A., and Ziman, M.R. (2013). The characterisation of Pax3 expressant cells in adult peripheral nerve. PLoS ONE *8*, e59184. https://doi.org/10.1371/journal.pone.0059184.

Blau, H.M., Chiu, C.P., and Webster, C. (1983). Cytoplasmic activation of human nuclear genes in stable heterocaryons. Cell *32*, 1171-1180. https://doi.org/10.1016/0092-8674(83)90300-8.

Blauwkamp, T.A., Nigam, S., Ardehali, R., Weissman, I.L., and Nusse, R. (2012). Endogenous Wnt signalling in human embryonic stem cells generates an equilibrium of distinct lineage-specified progenitors. Nature Communications *3*, 1070. https://doi.org/10.1038/ncomms2064.

Boeke, J. (1909). Die motorische Endplatte bei den höheren Vertebraten, ihre Entwickelung, Form und Zusammenhang mit der Muskelfaser. Anat. Anz *35*, 240-256.

Boeke, J. (1913). Die doppelte (motorische und sympathische) efferente Innervation der quergestreiften Muskelfasern. Anat. Anz *44*, 343-356.

Boerboom, A., Dion, V., Chariot, A., and Franzen, R. (2017). Molecular Mechanisms Involved in Schwann Cell Plasticity. Frontiers in molecular neuroscience *10*, 38. https://doi.org/10.3389/fnmol.2017.00038.

Bond, A.M., Bhalala, O.G., and Kessler, J.A. (2012). The dynamic role of bone morphogenetic proteins in neural stem cell fate and maturation. Developmental neurobiology *72*, 1068-1084. https://doi.org/10.1002/dneu.22022.

Bornstein, M.B., Iwanami, H., Lehrer, G.M., and Breitbart, L. (1968). Observations on the appearance of neuromuscular relationships in cultured mouse tissues. Zeitschrift fur Zellforschung und mikroskopische Anatomie (Vienna, Austria : 1948) *92*, 197-206. https://doi.org/10.1007/BF00335647.

Bosch-Queralt, M., Fledrich, R., and Stassart, R.M. (2023). Schwann cell functions in peripheral nerve development and repair. Neurobiology of Disease *176*, 105952. https://doi.org/10.1016/j.nbd.2022.105952.

Boullerne, A.I. (2016). The history of myelin. Experimental Neurology *283*, 431-445. https://doi.org/10.1016/j.expneurol.2016.06.005.

Bremer, L. (1882). Ueber die Endigungen der markhaltigen und marklosen Nerven im quergestreiften Muskel. Archiv f. mikrosk. Anatomie. *21*, 165-201. https://doi.org/10.1007/BF02952618.

Brown, M. (1981). Schwann cell proliferation in the postnatal mouse: Timing and topography. Experimental Neurology *74*, 170-186. https://doi.org/10.1016/0014-4886(81)90157-6.

Brown, M.C., Jansen, J.K., and van Essen, D. (1976). Polyneuronal innervation of skeletal muscle in new-born rats and its elimination during maturation. The Journal of Physiology *261*, 387-422. https://doi.org/10.1113/jphysiol.1976.sp011565.

Bruneau, E., and Akaaboune, M. (2007). The dynamics of the rapsyn scaffolding protein at individual acetylcholine receptor clusters. Journal of Biological Chemistry *282*, 9932-9940. https://doi.org/10.1074/jbc.M608714200.

Bruneteau, G., Bauché, S., Gonzalez de Aguilar, J.L., Brochier, G., Mandjee, N., Tanguy, M.-L., Hussain, G., Behin, A., Khiami, F., and Sariali, E., et al. (2015). Endplate denervation correlates with Nogo-A muscle expression in amyotrophic lateral sclerosis patients. Annals of clinical and translational neurology *2*, 362-372. https://doi.org/10.1002/acn3.179.

Bucchia, M., Merwin, S.J., Re, D.B., and Kariya, S. (2018). Limitations and Challenges in Modeling Diseases Involving Spinal Motor Neuron Degeneration in Vitro. Frontiers in Cellular Neuroscience *12*. https://doi.org/10.3389/fncel.2018.00061.

Buchstaller, J., Sommer, L., Bodmer, M., Hoffmann, R., Suter, U., and Mantei, N. (2004). Efficient isolation and gene expression profiling of small numbers of neural crest stem cells and developing Schwann cells. J. Neurosci. *24*, 2357-2365. https://doi.org/10.1523/JNEUROSCI.4083-03.2004.

Bunge, R.P., Bunge, M.B., and Eldridge, C.F. (1986). Linkage between axonal ensheathment and basal lamina production by Schwann cells. Annual Review of Neuroscience *9*, 305-328. https://doi.org/10.1146/annurev.ne.09.030186.001513.

Cai, A., Zheng, Z.-M., Himmler, M., Schubert, D.W., Fuchsluger, T.A., Weisbach, V., Horch, R.E., and Arkudas, A. (2022). Schwann Cells Promote Myogenic Differentiation of Myoblasts and Adipogenic Mesenchymal Stromal Cells on Poly-ε-Caprolactone-Collagen I-Nanofibers. Cells *11*. https://doi.org/10.3390/cells11091436.

Cai, S., Tsui, Y.-P., Tam, K.-W., Shea, G.K.-H., Chang, R.S.-K., Ao, Q., Shum, D.K.-Y., and Chan, Y.-S. (2017). Directed Differentiation of Human Bone Marrow Stromal Cells to Fate-Committed Schwann Cells. Stem Cell Reports *9*, 1097-1108. https://doi.org/10.1016/j.stemcr.2017.08.004.

Callizot, N., Combes, M., Steinschneider, R., and Poindron, P. (2011). A new long term in vitro model of myelination. Experimental Cell Research *317*, 2374-2383. https://doi.org/10.1016/j.yexcr.2011.07.002.

Cappello, V., and Francolini, M. (2017). Neuromuscular Junction Dismantling in Amyotrophic Lateral Sclerosis. International Journal of Molecular Sciences *18*. https://doi.org/10.3390/ijms18102092.

Carrasco, D.I., Seburn, K.L., and Pinter, M.J. (2016). Altered terminal Schwann cell morphology precedes denervation in SOD1 mice. Experimental Neurology *275*, 172-181. https://doi.org/10.1016/j.expneurol.2015.09.014.

Carrió, M., Mazuelas, H., Richaud-Patin, Y., Gel, B., Terribas, E., Rosas, I., Jimenez-Delgado, S., Biayna, J., Vendredy, L., and Blanco, I., et al. (2019). Reprogramming Captures the Genetic and Tumorigenic Properties of Neurofibromatosis Type 1 Plexiform Neurofibromas. Stem Cell Reports *12*, 411-426. https://doi.org/10.1016/j.stemcr.2019.01.001.

Carrizzo, A., Forte, M., Damato, A., Trimarco, V., Salzano, F., Bartolo, M., Maciag, A., Puca, A.A., and Vecchione, C. (2013). Antioxidant effects of resveratrol in cardiovascular, cerebral and metabolic diseases. Food and chemical toxicology : an international journal published for the British Industrial Biological Research Association *61*, 215-226. https://doi.org/10.1016/j.fct.2013.07.021.

Castellanos-Montiel, M.J., Velasco, I., and Escobedo-Avila, I. (2020). Modeling the neuromuscular junction in vitro: an approach to study neuromuscular junction disorders. Annals of the New York Academy of Sciences. https://doi.org/10.1111/nyas.14504.

Castro, R., Taetzsch, T., Vaughan, S.K., Godbe, K., Chappell, J., Settlage, R.E., and Valdez, G. (2020). Specific labeling of synaptic schwann cells reveals unique cellular and molecular features. eLife *9*. https://doi.org/10.7554/eLife.56935.

Centeno, E.G.Z., Cimarosti, H., and Bithell, A. (2018). 2D versus 3D human induced pluripotent stem cell-derived cultures for neurodegenerative disease modelling. Molecular neurodegeneration *13*, 27. https://doi.org/10.1186/s13024-018-0258-4.

Chal, J., Al Tanoury, Z., Hestin, M., Gobert, B., Aivio, S., Hick, A., Cherrier, T., Nesmith, A.P., Parker, K.K., and Pourquié, O. (2016). Generation of human muscle fibers and satellite-like cells from human pluripotent stem cells in vitro. Nature protocols *11*, 1833-1850. https://doi.org/10.1038/nprot.2016.110.

Chambers, S.M., Fasano, C.A., Papapetrou, E.P., Tomishima, M., Sadelain, M., and Studer, L. (2009). Highly efficient neural conversion of human ES and iPS cells by dual inhibition of SMAD signaling. Nature Biotechnology *27*, 275-280. https://doi.org/10.1038/nbt.1529.

Chambers, S.M., Qi, Y., Mica, Y., Lee, G., Zhang, X.-J., Niu, L., Bilsland, J., Cao, L., Stevens, E., and Whiting, P., et al. (2012). Combined small molecule inhibition accelerates developmental timing and converts human pluripotent stem cells into nociceptors. Nature Biotechnology *30*, 715-720. https://doi.org/10.1038/nbt.2249.

Chan-Palay, V., Engel, A.G., Wu, J.Y., and Palay, S.L. (1982). Coexistence in human and primate neuromuscular junctions of enzymes synthesizing acetylcholine, catecholamine, taurine, and gamma-aminobutyric acid. Proceedings of the National Academy of Sciences of the United States of America *79*, 7027-7030. https://doi.org/10.1073/pnas.79.22.7027.

Chanvitayapongs, S., Draczynska-Lusiak, B., and Sun, A.Y. (1997). Amelioration of oxidative stress by antioxidants and resveratrol in PC12 cells. Neuroreport *8*, 1499-1502. https://doi.org/10.1097/00001756-199704140-00035.

Chao, T., Frump, D., Lin, M., Caiozzo, V.J., Mozaffar, T., Steward, O., and Gupta, R. (2013). Matrix metalloproteinase 3 deletion preserves denervated motor endplates after traumatic nerve injury. Annals of neurology *73*, 210-223. https://doi.org/10.1002/ana.23781.

Chapron, J., La Porte, S. de, Delépine, L., and Koenig, J. (1997). Schwann cells modify expression of acetylcholinesterase and butyrylcholinesterase at rat neuromuscular junctions. European Journal of Neuroscience 9, 260-270. https://doi.org/10.1111/j.1460-9568.1997.tb01396.x.

Charoensook, S.N., Williams, D.J., Chakraborty, S., Leong, K.W., and Vunjak-Novakovic, G. (2017). Bioreactor model of neuromuscular junction with electrical stimulation for pharmacological potency testing. Integrative Biology: Quantitative Biosciences from Nano to Macro *9*, 956-967. https://doi.org/10.1039/c7ib00144d.

Chen, G., Gulbranson, D.R., Hou, Z., Bolin, J.M., Ruotti, V., Probasco, M.D., Smuga-Otto, K., Howden, S.E., Diol, N.R., and Propson, N.E., et al. (2011). Chemically defined conditions for human iPSC derivation and culture. Nat Methods *8*, 424-429. https://doi.org/10.1038/nmeth.1593.

Chen, G., Hou, Z., Gulbranson, D.R., and Thomson, J.A. (2010). Actin-myosin contractility is responsible for the reduced viability of dissociated human embryonic stem cells. Cell Stem Cell *7*, 240-248. https://doi.org/10.1016/j.stem.2010.06.017.

Chen, H., Qian, K., Du, Z., Cao, J., Petersen, A., Liu, H., Blackbourn, L.W., Huang, C.-L., Errigo, A., and Yin, Y., et al. (2014). Modeling ALS with iPSCs reveals that mutant SOD1 misregulates neurofilament balance in motor neurons. Cell Stem Cell *14*, 796-809. https://doi.org/10.1016/j.stem.2014.02.004.

Chen, Q., Zhang, Z., Liu, J., He, Q., Zhou, Y., Shao, G., Sun, X., Cao, X., Gong, A., and Jiang, P. (2015). A fibrin matrix promotes the differentiation of EMSCs isolated from nasal respiratory mucosa to myelinating phenotypical Schwann-like cells. Molecules and Cells *38*, 221-228. https://doi.org/10.14348/molcells.2015.2170.

Chevrel, G., Hohlfeld, R., and Sendtner, M. (2006). The role of neurotrophins in muscle under physiological and pathological conditions. Muscle & Nerve *33*, 462-476. https://doi.org/10.1002/mus.20444.

Chiang, C., Litingtung, Y., Lee, E., Young, K.E., Corden, J.L., Westphal, H., and Beachy, P.A. (1996). Cyclopia and defective axial patterning in mice lacking Sonic hedgehog gene function. Nature *383*, 407-413. https://doi.org/10.1038/383407a0.

Chipman, P.H., Zhang, Y., and Rafuse, V.F. (2014). A stem-cell based bioassay to critically assess the pathology of dysfunctional neuromuscular junctions. PLoS ONE *9*, e91643. https://doi.org/10.1371/journal.pone.0091643.

Chvátal, A., and Verkhratsky, A. (2018). An Early History of Neuroglial Research: Personalities. Neuroglia *1*, 245-281. https://doi.org/10.3390/neuroglia1010016.

Cimadamore, F., Fishwick, K., Giusto, E., Gnedeva, K., Cattarossi, G., Miller, A., Pluchino, S., Brill, L.M., Bronner-Fraser, M., and Terskikh, A.V. (2011). Human ESC-derived neural crest model reveals a key role for SOX2 in sensory neurogenesis. Cell Stem Cell *8*, 538-551. https://doi.org/10.1016/j.stem.2011.03.011.

Court, F.A., Gillingwater, T.H., Melrose, S., Sherman, D.L., Greenshields, K.N., Morton, A.J., Harris, J.B., Willison, H.J., and Ribchester, R.R. (2008). Identity, developmental restriction and reactivity of extralaminar cells capping mammalian neuromuscular junctions. Journal of Cell Science *121*, 3901-3911. https://doi.org/10.1242/jcs.031047.

Couteaux, R. (1947). Contribution a l'etude de la synapse myoneurale. Rev Canad Biol *6*, 563-711.

Couteaux, R. (1955). Localization of Cholinesterases at Neuromuscular Junctions. In International review of cytology, G.H. Bourne and J.F. Danielli, eds. (New York: Academic Press), pp. 335–375.

Crain, S.M., Alfei, L., and Peterson, E.R. (1970). Neuromuscular transmission in cultures of adult human and rodent skeletal muscle after innervation in vitro by fetal rodent spinal cord. Journal of neurobiology *1*, 471-489. https://doi.org/10.1002/neu.480010409.

Cvetkovic, C., Rich, M.H., Raman, R., Kong, H., and Bashir, R. (2017). A 3D-printed platform for modular neuromuscular motor units. Microsystems & nanoengineering *3*, 17015. https://doi.org/10.1038/micronano.2017.15.

D'Antonio, M., Michalovich, D., Paterson, M., Droggiti, A., Woodhoo, A., Mirsky, R., and Jessen, K.R. (2006). Gene profiling and bioinformatic analysis of Schwann cell embryonic development and myelination. Glia *53*, 501-515. https://doi.org/10.1002/glia.20309.

Darabid, H., Arbour, D., and Robitaille, R. (2013). Glial cells decipher synaptic competition at the mammalian neuromuscular junction. The Journal of neuroscience : the official journal of the Society for Neuroscience *33*, 1297-1313. https://doi.org/10.1523/JNEUROSCI.2935-12.2013.

Darabid, H., Perez-Gonzalez, A.P., and Robitaille, R. (2014). Neuromuscular synaptogenesis: coordinating partners with multiple functions. Nature Reviews. Neuroscience *15*, 703-718.

Darabid, H., St-Pierre-See, A., and Robitaille, R. (2018). Purinergic-Dependent Glial Regulation of Synaptic Plasticity of Competing Terminals and Synapse Elimination at the Neuromuscular Junction. Cell Reports *25*, 2070-2082.e6. https://doi.org/10.1016/j.celrep.2018.10.075.

Das, M., Rumsey, J.W., Bhargava, N., Stancescu, M., and Hickman, J.J. (2010). A Defined Long-Term In Vitro Tissue Engineered Model of Neuromuscular Junctions. Biomaterials *31*, 4880-4888. https://doi.org/10.1016/j.biomaterials.2010.02.055.

Davis-Dusenbery, B.N., Williams, L.A., Klim, J.R., and Eggan, K. (2014). How to make spinal motor neurons. Development (Cambridge, England) *141*, 491-501. https://doi.org/10.1242/dev.097410.

Demestre, M., Orth, M., Föhr, K.J., Achberger, K., Ludolph, A.C., Liebau, S., and Boeckers, T.M. (2015). Formation and characterisation of neuromuscular junctions between hiPSC derived motoneurons and myotubes. Stem Cell Research *15*, 328-336. https://doi.org/10.1016/j.scr.2015.07.005.

Denham, M., Hasegawa, K., Menheniott, T., Rollo, B., Zhang, D., Hough, S., Alshawaf, A., Febbraro, F., Ighaniyan, S., and Leung, J., et al. (2015). Multipotent caudal neural progenitors derived from human pluripotent stem cells that give rise to lineages of the central and peripheral nervous system. Stem Cells (Dayton, Ohio) *33*, 1759-1770. https://doi.org/10.1002/stem.1991.

Denny, J.B. (2006). Molecular mechanisms, biological actions, and neuropharmacology of the growth-associated protein GAP-43. Current neuropharmacology *4*, 293-304. https://doi.org/10.2174/157015906778520782.

Dezawa, M., Takahashi, I., Esaki, M., Takano, M., and Sawada, H. (2001). Sciatic nerve regeneration in rats induced by transplantation of *in vitro* differentiated bone-marrow stromal cells.

Discher, D.E., Janmey, P., and Wang, Y.-L. (2005). Tissue cells feel and respond to the stiffness of their substrate. Science (New York, N.Y.) *310*, 1139-1143. https://doi.org/10.1126/science.1116995.

Doddrell, R.D.S., Dun, X.-P., Moate, R.M., Jessen, K.R., Mirsky, R., and Parkinson, D.B. (2012). Regulation of Schwann cell differentiation and proliferation by the Pax-3 transcription factor. Glia *60*, 1269-1278. https://doi.org/10.1002/glia.22346.

Dong, Z., Brennan, A., Liu, N., Yarden, Y., Lefkowitz, G., Mirsky, R., and Jessen, K.R. (1995). Neu differentiation factor is a neuron-glia signal and regulates survival, proliferation, and maturation of rat schwann cell precursors. Neuron *15*, 585-596. https://doi.org/10.1016/0896-6273(95)90147-7.

Donnelly, C.J., Park, M., Spillane, M., Yoo, S., Pacheco, A., Gomes, C., Vuppalanchi, D., McDonald, M., Kim, H.H., and Merianda, T.T., et al. (2013). Axonally synthesized β-actin and GAP-43 proteins support distinct modes of axonal growth. J. Neurosci. *33*, 3311-3322. https://doi.org/10.1523/JNEUROSCI.1722-12.2013.

Driever, W., and Nüsslein-Volhard, C. (1988). The bicoid protein determines position in the Drosophila embryo in a concentration-dependent manner. Cell *54*, 95-104. https://doi.org/10.1016/0092-8674(88)90183-3.

Du, Z.-W., Chen, H., Liu, H., Lu, J., Qian, K., Huang, C.-L., Zhong, X., Fan, F., and Zhang, S.-C. (2015). Generation and expansion of highly pure motor neuron progenitors from human pluripotent stem cells. Nature Communications *6*, 6626. https://doi.org/10.1038/ncomms7626.

Duc, P., Vignes, M., Hugon, G., Sebban, A., Carnac, G., Malyshev, E., Charlot, B., and Rage, F. (2021). Human neuromuscular junction on micro-structured microfluidic devices implemented with a custom micro electrode array (MEA). Lab Chip *21*, 4223-4236. https://doi.org/10.1039/d1lc00497b.

Dupin, E., Calloni, G.W., Coelho-Aguiar, J.M., and Le Douarin, N.M. (2018). The issue of the multipotency of the neural crest cells. Developmental Biology. https://doi.org/10.1016/j.ydbio.2018.03.024.

Duval, K., Grover, H., Han, L.-H., Mou, Y., Pegoraro, A.F., Fredberg, J., and Chen, Z. (2017). Modeling Physiological Events in 2D vs. 3D Cell Culture. Physiology (Bethesda, Md.) *32*, 266-277. https://doi.org/10.1152/physiol.00036.2016.

Dyachuk, V., Furlan, A., Shahidi, M.K., Giovenco, M., Kaukua, N., Konstantinidou, C., Pachnis, V., Memic, F., Marklund, U., and Müller, T., et al. (2014). Neurodevelopment. Parasympathetic neurons originate from nerve-associated peripheral glial progenitors. Science (New York, N.Y.) *345*, 82-87. https://doi.org/10.1126/science.1253281.

Ebashi, S., Endo, M., and Otsuki, I. (1969). Control of muscle contraction. Quarterly reviews of biophysics *2*, 351-384. https://doi.org/10.1017/s0033583500001190.

Edmondson, R., Broglie, J.J., Adcock, A.F., and Yang, L. (2014). Three-dimensional cell culture systems and their applications in drug discovery and cell-based biosensors. Assay and drug development technologies *12*, 207-218. https://doi.org/10.1089/adt.2014.573.

Eldridge, C.F., Bunge, M.B., Bunge, R.P., and Wood, P.M. (1987). Differentiation of axon-related Schwann cells in vitro. I. Ascorbic acid regulates basal lamina assembly and myelin formation. The Journal of Cell Biology *105*, 1023-1034. https://doi.org/10.1083/jcb.105.2.1023.

El-Nachef, W.N., and Bronner, M.E. (2020). De novo enteric neurogenesis in post-embryonic zebrafish from Schwann cell precursors rather than resident cell types. Development (Cambridge, England) *147*. https://doi.org/10.1242/dev.186619.

Endo, Y., Osumi, N., and Wakamatsu, Y. (2002). Bimodal functions of Notch-mediated signaling are involved in neural crest formation during avian ectoderm development. Development *129*, 863-873. https://doi.org/10.1242/dev.129.4.863.

Entezari, M., Mozafari, M., Bakhtiyari, M., Moradi, F., Bagher, Z., and Soleimani, M. (2022). Three-dimensional-printed polycaprolactone/polypyrrole conducting scaffolds for differentiation of human olfactory ecto-mesenchymal stem cells into Schwann cell-like phenotypes and promotion of neurite outgrowth. Journal of biomedical materials research. Part A *110*, 1134-1146. https://doi.org/10.1002/jbm.a.37361.

Ericson, J., Morton, S., Kawakami, A., Roelink, H., and Jessell, T.M. (1996). Two critical periods of Sonic Hedgehog signaling required for the specification of motor neuron identity. Cell *87*, 661-673. https://doi.org/10.1016/s0092-8674(00)81386-0.

Ericson, J., Thor, S., Edlund, T., Jessell, T.M., and Yamada, T. (1992). Early stages of motor neuron differentiation revealed by expression of homeobox gene Islet-1. Science *256*, 1555-1560. https://doi.org/10.1126/science.1350865.

Eriksson, K.S., Zhang, S., Lin, L., Larivière, R.C., Julien, J.-P., and Mignot, E. (2008). The type III neurofilament peripherin is expressed in the tuberomammillary neurons of the mouse. BMC Neurosci *9*, 26. https://doi.org/10.1186/1471-2202-9-26.

Espinosa-Medina, I., Outin, E., Picard, C.A., Chettouh, Z., Dymecki, S., Consalez, G.G., Coppola, E., and Brunet, J.-F. (2014). Neurodevelopment. Parasympathetic ganglia derive from Schwann cell precursors. Science (New York, N.Y.) *345*, 87-90. https://doi.org/10.1126/science.1253286.

Etxaniz, U., Pérez-San Vicente, A., Gago-López, N., García-Dominguez, M., Iribar, H., Aduriz, A., Pérez-López, V., Burgoa, I., Irizar, H., and Muñoz-Culla, M., et al. (2014). Neural-competent cells of adult human dermis belong to the Schwann lineage. Stem Cell Reports *3*, 774-788. https://doi.org/10.1016/j.stemcr.2014.09.009.

Fahim, M.A., and Robbins, N. (1982). Ultrastructural studies of young and old mouse neuromuscular junctions. Journal of Neurocytology *11*, 641-656. https://doi.org/10.1007/BF01262429.

Fambrough, D.M. (1979). Control of acetylcholine receptors in skeletal muscle. Physiological reviews *59*, 165-227. https://doi.org/10.1152/physrev.1979.59.1.165.

Faravelli, I., Bucchia, M., Rinchetti, P., Nizzardo, M., Simone, C., Frattini, E., and Corti, S. (2014). Motor neuron derivation from human embryonic and induced pluripotent stem cells: experimental approaches and clinical perspectives. Stem Cell Res Ther *5*, 87. https://doi.org/10.1186/scrt476.

Faroni, A., Castelnovo, L.F., Procacci, P., Caffino, L., Fumagalli, F., Melfi, S., Gambarotta, G., Bettler, B., Wrabetz, L., and Magnaghi, V. (2014). Deletion of GABA-B receptor in Schwann cells regulates remak bundles and small nociceptive C-fibers. Glia *62*, 548-565. https://doi.org/10.1002/glia.22625.

Faustino Martins, J.-M., Fischer, C., Urzi, A., Vidal, R., Kunz, S., Ruffault, P.-L., Kabuss, L., Hube, I., Gazzerro, E., and Birchmeier, C., et al. (2020). Self-Organizing 3D Human Trunk Neuromuscular Organoids. Cell Stem Cell *26*, 172-186.e6. https://doi.org/10.1016/j.stem.2019.12.007.

Feltri, M.L., Poitelon, Y., and Previtali, S.C. (2016). How Schwann Cells Sort Axons: New Concepts. The Neuroscientist : a review journal bringing neurobiology, neurology and psychiatry *22*, 252-265. https://doi.org/10.1177/1073858415572361.

Feng, Z., and Ko, C.-P. (2008). The role of glial cells in the formation and maintenance of the neuromuscular junction. Annals of the New York Academy of Sciences *1132*, 19-28. https://doi.org/10.1196/annals.1405.016.

Fernandez-Valle, C., Gorman, D., Gomez, A.M., and Bunge, M.B. (1997). Actin plays a role in both changes in cell shape and gene-expression associated with Schwann cell myelination. The Journal of Neuroscience *17*, 241-250. https://doi.org/10.1523/JNEUROSCI.17-01-00241.1997.

Ferns, M.J., Campanelli, J.T., Hoch, W., Scheller, R.H., and Hall, Z. (1993). The ability of agrin to cluster AChRs depends on alternative splicing and on cell surface proteoglycans. Neuron *11*, 491-502. https://doi.org/10.1016/0896-6273(93)90153-I.

Fertuck, H.C., and Salpeter, M.M. (1976). Quantitation of junctional and extrajunctional acetylcholine receptors by electron microscope autoradiography after 125I-alpha-bungarotoxin binding at mouse neuromuscular junctions. The Journal of Cell Biology *69*, 144-158. https://doi.org/10.1083/jcb.69.1.144.

Fischbach, G.D. (1970). Synaptic potentials recorded in cell cultures of nerve and muscle. Science *169*, 1331-1333. https://doi.org/10.1126/science.169.3952.1331.

Fischer, L.R., Culver, D.G., Tennant, P., Davis, A.A., Wang, M., Castellano-Sanchez, A., Khan, J., Polak, M.A., and Glass, J.D. (2004). Amyotrophic lateral sclerosis is a distal axonopathy: evidence in mice and man. Experimental Neurology *185*, 232-240. https://doi.org/10.1016/j.expneurol.2003.10.004.

Flanagan-Steet, H., Fox, M.A., Meyer, D., and Sanes, J.R. (2005). Neuromuscular synapses can form in vivo by incorporation of initially aneural postsynaptic specializations. Development *132*, 4471-4481. https://doi.org/10.1242/dev.02044.

Fledrich, R., Kungl, T., Nave, K.-A., and Stassart, R.M. (2019). Axo-glial interdependence in peripheral nerve development. Development (Cambridge, England) *146*. https://doi.org/10.1242/dev.151704.

Fort, P., and Théveneau, E. (2014). PleiotRHOpic: Rho pathways are essential for all stages of Neural Crest development. Small GTPases *5*, e27975. https://doi.org/10.4161/sgtp.27975.

Fralish, Z., Lotz, E.M., Chavez, T., Khodabukus, A., and Bursac, N. (2021). Neuromuscular Development and Disease: Learning From in vitro and in vivo Models. Frontiers in cell and developmental biology *9*, 764732. https://doi.org/10.3389/fcell.2021.764732.

Francis, G.L. (2010). Albumin and mammalian cell culture: implications for biotechnology applications. Cytotechnology *62*, 1-16. https://doi.org/10.1007/s10616-010-9263-3.

Friede, R.L., Meier, T., and Diem, M. (1981). How is the exact length of an internode determined. Journal of the Neurological Sciences *50*, 217-228. https://doi.org/10.1016/0022-510x(81)90168-4.

Frisch, S.M., and Screaton, R.A. (2001). Anoikis mechanisms. Current Opinion in Cell Biology *13*, 555-562. https://doi.org/10.1016/S0955-0674(00)00251-9.

Frontera, W.R., and Ochala, J. (2015). Skeletal muscle: a brief review of structure and function. Calcified tissue international *96*, 183-195. https://doi.org/10.1007/s00223-014-9915-y.

Fukuta, M., Nakai, Y., Kirino, K., Nakagawa, M., Sekiguchi, K., Nagata, S., Matsumoto, Y., Yamamoto, T., Umeda, K., and Heike, T., et al. (2014). Derivation of mesenchymal stromal cells from pluripotent stem cells through a neural crest lineage using small molecule compounds with defined media. PLoS ONE *9*, e112291. https://doi.org/10.1371/journal.pone.0112291.

Furlan, A., and Adameyko, I. (2018). Schwann cell precursor: a neural crest cell in disguise? Developmental Biology *444 Suppl 1*, S25-S35. https://doi.org/10.1016/j.ydbio.2018.02.008.

Furlan, A., Dyachuk, V., Kastriti, M.E., Calvo-Enrique, L., Abdo, H., Hadjab, S., Chontorotzea, T., Akkuratova, N., Usoskin, D., and Kamenev, D., et al. (2017). Multipotent peripheral glial cells generate neuroendocrine cells of the adrenal medulla. Science (New York, N.Y.) *357*. https://doi.org/10.1126/science.aal3753.

Gao, L., Nath, S.C., Jiao, X., Zhou, R., Nishikawa, S., Krawetz, R., Li, X., and Rancourt, D.E. (2019). Post-Passage rock inhibition induces cytoskeletal aberrations and apoptosis in Human embryonic stem cells. Stem Cell Research *41*, 101641. https://doi.org/10.1016/j.scr.2019.101641.

Gao, S., Zheng, Y., Cai, Q., Wu, X., Yao, W., and Wang, J. (2015). Different methods for inducing adipose-derived stem cells to differentiate into Schwann-like cells. Archives of medical science : AMS *11*, 886-892. https://doi.org/10.5114/aoms.2015.53310.

Garratt, A.N., Voiculescu, O., Topilko, P., Charnay, P., and Birchmeier, C. (2000). A dual role of erbB2 in myelination and in expansion of the schwann cell precursor pool. The Journal of Cell Biology *148*, 1035-1046. https://doi.org/10.1083/jcb.148.5.1035.

Gautam, M., Noakes, P.G., Moscoso, L., Rupp, F., Scheller, R.H., Merlie, J.P., and Sanes, J.R. (1996). Defective neuromuscular synaptogenesis in agrin-deficient mutant mice. Cell *85*, 525-535. https://doi.org/10.1016/s0092-8674(00)81253-2.

Gautam, M., Noakes, P.G., Mudd, J., Nichol, M., Chu, G.C., Sanes, J.R., and Merlie, J.P. (1995). Failure of postsynaptic specialization to develop at neuromuscular junctions of rapsyn-deficient mice. Nature *377*, 232-236. https://doi.org/10.1038/377232a0.

Georgiou, J., and Charlton, M.P. (1999). Non-myelin-forming perisynaptic Schwann cells express protein zero and myelin-associated glycoprotein. Glia *27*, 101-109. https://doi.org/10.1002/(SICI)1098-1136(199908)27:2<101::AID-GLIA1>3.0.CO;2-H.

Georgiou, J., Robitaille, R., and Charlton, M.P. (1999). Muscarinic control of cytoskeleton in perisynaptic glia. J. Neurosci. *19*, 3836-3846. https://doi.org/10.1523/JNEUROSCI.19-10-03836.1999.

Georgiou, J., Robitaille, R., Trimble, W.S., and Charlton, M.P. (1994). Synaptic regulation of glial protein expression in vivo. Neuron *12*, 443-455. https://doi.org/10.1016/0896-6273(94)90284-4.

Gerber, D., Pereira, J.A., Gerber, J., Tan, G., Dimitrieva, S., Yángüez, E., and Suter, U. (2021). Transcriptional profiling of mouse peripheral nerves to the single-cell level to build a sciatic nerve ATlas (SNAT). eLife *10*. https://doi.org/10.7554/eLife.58591.

Gingras, M., Beaulieu, M.-M., Gagnon, V., Durham, H.D., and Berthod, F. (2008). In vitro study of axonal migration and myelination of motor neurons in a three-dimensional tissue-engineered model. Glia *56*, 354-364. https://doi.org/10.1002/glia.20617.

Girard, E., Bernard, V., Minic, J., Chatonnet, A., Krejci, E., and Molgó, J. (2007). Butyrylcholinesterase and the control of synaptic responses in acetylcholinesterase knockout mice. Life sciences *80*, 2380-2385. https://doi.org/10.1016/j.lfs.2007.03.011.

Glass, D.J., Bowen, D.C., Stitt, T.N., Radziejewski, C., Bruno, J., Ryan, T.E., Gies, D.R., Shah, S., Mattsson, K., and Burden, S.J., et al. (1996). Agrin acts via a MuSK receptor complex. Cell *85*, 513-523. https://doi.org/10.1016/s0092-8674(00)81252-0.

Gomez-Sanchez, J.A., Pilch, K.S., van der Lans, M., Fazal, S.V., Benito, C., Wagstaff, L.J., Mirsky, R., and Jessen, K.R. (2017). After Nerve Injury, Lineage Tracing Shows That Myelin and Remak Schwann Cells Elongate Extensively and Branch to Form Repair Schwann Cells, Which Shorten Radically on Remyelination. J. Neurosci. *37*, 9086-9099. https://doi.org/10.1523/JNEUROSCI.1453-17.2017.

Gould, T.W., Dominguez, B., Winter, F. de, Yeo, G.W., Liu, P., Sundararaman, B., Stark, T., Vu, A., Degen, J.L., and Lin, W., et al. (2019). Glial cells maintain synapses by inhibiting an activity-dependent retrograde protease signal. PLOS Genetics *15*, e1007948. https://doi.org/10.1371/journal.pgen.1007948.

Gouti, M., Tsakiridis, A., Wymeersch, F.J., Huang, Y., Kleinjung, J., Wilson, V., and Briscoe, J. (2014). In vitro generation of neuromesodermal progenitors reveals distinct roles for wnt signalling in the specification of spinal cord and paraxial mesoderm identity. PLoS biology *12*, e1001937. https://doi.org/10.1371/journal.pbio.1001937.

Grenier, K., Kao, J., and Diamandis, P. (2020). Three-dimensional modeling of human neurodegeneration: brain organoids coming of age. Mol Psychiatry *25*, 254-274. https://doi.org/10.1038/s41380-019-0500-7.

Griffin, J.W., and Thompson, W.J. (2008). Biology and pathology of nonmyelinating Schwann cells. Glia *56*, 1518-1531. https://doi.org/10.1002/glia.20778.

Grinspan, J.B., Marchionni, M.A., Reeves, M., Coulaloglou, M., and Scherer, S.S. (1996). Axonal interactions regulate Schwann cell apoptosis in developing peripheral nerve: neuregulin receptors and the role of neuregulins. The Journal of neuroscience : the official journal of the Society for Neuroscience *16*, 6107-6118.

Groves, A.K., and LaBonne, C. (2014). Setting appropriate boundaries: fate, patterning and competence at the neural plate border. Developmental Biology *389*, 2-12. https://doi.org/10.1016/j.ydbio.2013.11.027.

Guo, X., Badu-Mensah, A., Thomas, M.C., McAleer, C.W., and Hickman, J.J. (2020). Characterization of Functional Human Skeletal Myotubes and Neuromuscular Junction Derived-From the Same Induced Pluripotent Stem Cell Source. Bioengineering (Basel, Switzerland) *7*. https://doi.org/10.3390/bioengineering7040133.

Guo, X., Das, M., Rumsey, J., Gonzalez, M., Stancescu, M., and Hickman, J. (2010). Neuromuscular junction formation between human stem-cell-derived motoneurons and rat skeletal muscle in a defined system. Tissue engineering. Part C, Methods *16*, 1347-1355. https://doi.org/10.1089/ten.tec.2010.0040.

Guo, X., Gonzalez, M., Stancescu, M., Vandenburgh, H.H., and Hickman, J.J. (2011). Neuromuscular junction formation between human stem cell-derived motoneurons and human skeletal muscle in a defined system. Biomaterials *32*, 9602-9611. https://doi.org/10.1016/j.biomaterials.2011.09.014.

Hackland, J.O.S., Frith, T.J.R., Thompson, O., Marin Navarro, A., Garcia-Castro, M.I., Unger, C., and Andrews, P.W. (2017). Top-Down Inhibition of BMP Signaling Enables Robust Induction of hPSCs Into Neural Crest in Fully Defined, Xeno-free Conditions. Stem Cell Reports *9*, 1043-1052. https://doi.org/10.1016/j.stemcr.2017.08.008.

Happe, C.L., Tenerelli, K.P., Gromova, A.K., Kolb, F., and Engler, A.J. (2017). Mechanically patterned neuromuscular junctions-in-a-dish have improved functional maturation. MBoC *28*, 1950-1958. https://doi.org/10.1091/mbc.E17-01-0046.

Härönen, H., Zainul, Z., Tu, H., Naumenko, N., Sormunen, R., Miinalainen, I., Shakirzyanova, A., Oikarainen, T., Abdullin, A., and Martin, P., et al. (2017). Collagen XIII secures pre- and postsynaptic integrity of the neuromuscular synapse. Hum Mol Genet *26*, 2076-2090. https://doi.org/10.1093/hmg/ddx101.

Harrison, R. (1959). The outgrowth of the nerve fiber as a mode of protoplasmic movement. The Journal of experimental zoology *142*, 5-73. https://doi.org/10.1002/jez.1401420103.

Harty, B.L., and Monk, K.R. (2017). Unwrapping the unappreciated: recent progress in Remak Schwann cell biology. Current Opinion in Neurobiology *47*, 131-137. https://doi.org/10.1016/j.conb.2017.10.003.

Heredia, D.J., Feng, C.-Y., Agarwal, A., Nennecker, K., Hennig, G.W., and Gould, T.W. (2018). Postnatal Restriction of Activity-Induced Ca2+ Responses to Schwann Cells at the Neuromuscular Junction Are Caused by the Proximo-Distal Loss of Axonal Synaptic Vesicles during Development. J. Neurosci. *38*, 8650-8665. https://doi.org/10.1523/JNEUROSCI.0956-18.2018.

Hester, M.E., Murtha, M.J., Song, S., Rao, M., Miranda, C.J., Meyer, K., Tian, J., Boulting, G., Schaffer, D.V., and Zhu, M.X., et al. (2011). Rapid and efficient generation of functional motor neurons from human pluripotent stem cells using gene delivered transcription factor codes. Molecular Therapy: The Journal of the American Society of Gene Therapy *19*, 1905-1912. https://doi.org/10.1038/mt.2011.135.

Hindley, C.J., Condurat, A.L., Menon, V., Thomas, R., Azmitia, L.M., Davis, J.A., and Pruszak, J. (2016). The Hippo pathway member YAP enhances human neural crest cell fate and migration. Sci Rep *6*, 23208. https://doi.org/10.1038/srep23208.

Hörner, S.J., Couturier, N., Bruch, R., Koch, P., Hafner, M., and Rudolf, R. (2021). hiPSC-Derived Schwann Cells Influence Myogenic Differentiation in Neuromuscular Cocultures. Cells *10*. https://doi.org/10.3390/cells10123292.

Hörner, S.J., Couturier, N., Gueiber, D.C., Hafner, M., and Rudolf, R. (2022). Development and In Vitro Differentiation of Schwann Cells. Cells *11*. https://doi.org/10.3390/cells11233753.

Hosoyama, T., McGivern, J.V., van Dyke, J.M., Ebert, A.D., and Suzuki, M. (2014). Derivation of myogenic progenitors directly from human pluripotent stem cells using a sphere-based culture. STEM CELLS Translational Medicine *3*, 564-574. https://doi.org/10.5966/sctm.2013-0143.

Hu, B.-Y., and Zhang, S.-C. (2009). Differentiation of spinal motor neurons from pluripotent human stem cells. Nature protocols *4*, 1295-1304. https://doi.org/10.1038/nprot.2009.127.

Huang, C.-W., Huang, W.-C., Qiu, X., Da Fernandes Ferreira Silva, F., Wang, A., Patel, S., Nesti, L.J., Poo, M.-M., and Li, S. (2017). The Differentiation Stage of Transplanted Stem Cells Modulates Nerve Regeneration. Scientific Reports *7*, 17401. https://doi.org/10.1038/s41598-017-17043-4.

Huang, M., Miller, M.L., McHenry, L.K., Zheng, T., Zhen, Q., Ilkhanizadeh, S., Conklin, B.R., Bronner, M.E., and Weiss, W.A. (2016). Generating trunk neural crest from human pluripotent stem cells. Sci Rep *6*, 19727. https://doi.org/10.1038/srep19727.

Huang, Z., Powell, R., Phillips, J.B., and Haastert-Talini, K. (2020). Perspective on Schwann Cells Derived from Induced Pluripotent Stem Cells in Peripheral Nerve Tissue Engineering. Cells *9*. https://doi.org/10.3390/cells9112497.

Huff, T.C., Sant, D.W., Camarena, V., van Booven, D., Andrade, N.S., Mustafi, S., Monje, P.V., and Wang, G. (2021). Vitamin C regulates Schwann cell myelination by promoting DNA demethylation of pro-myelinating genes. Journal of Neurochemistry *157*, 1759-1773. https://doi.org/10.1111/jnc.15015.

Hughes, B.W., Kusner, L.L., and Kaminski, H.J. (2006). Molecular architecture of the neuromuscular junction. Muscle & Nerve *33*, 445-461. https://doi.org/10.1002/mus.20440.

Hyung, S., Yoon Lee, B., Park, J.-C., Kim, J., Hur, E.-M., and Francis Suh, J.-K. (2015). Coculture of Primary Motor Neurons and Schwann Cells as a Model for In Vitro Myelination. Scientific Reports *5*, 15122. https://doi.org/10.1038/srep15122.

Inoue, A., Setoguchi, K., Matsubara, Y., Okada, K., Sato, N., Iwakura, Y., Higuchi, O., and Yamanashi, Y. (2009). Dok-7 activates the muscle receptor kinase MuSK and shapes synapse formation. Science signaling *2*, ra7. https://doi.org/10.1126/scisignal.2000113.

Ionescu, A., Zahavi, E.E., Gradus, T., Ben-Yaakov, K., and Perlson, E. (2016). Compartmental microfluidic system for studying muscle-neuron communication and neuromuscular junction maintenance. European Journal of Cell Biology *95*, 69-88. https://doi.org/10.1016/j.ejcb.2015.11.004.

Jablonka-Shariff, A., Lu, C.-Y., Campbell, K., Monk, K.R., and Snyder-Warwick, A.K. (2020). Gpr126/Adgrg6 contributes to the terminal Schwann cell response at the neuromuscular junction following peripheral nerve injury. Glia *68*, 1182-1200. https://doi.org/10.1002/glia.23769.

Jacob, C. (2017). Chromatin-remodeling enzymes in control of Schwann cell development, maintenance and plasticity. Current Opinion in Neurobiology *47*, 24-30. https://doi.org/10.1016/j.conb.2017.08.007.

Jahromi, B.S., Robitaille, R., and Charlton, M.P. (1992). Transmitter release increases intracellular calcium in perisynaptic schwann cells in situ. Neuron *8*, 1069-1077. https://doi.org/10.1016/0896-6273(92)90128-z.

Jalal, S., Dastidar, S., and Tedesco, F.S. (2021). Advanced models of human skeletal muscle differentiation, development and disease: Three-dimensional cultures, organoids and beyond. Current Opinion in Cell Biology *73*, 92-104. https://doi.org/10.1016/j.ceb.2021.06.004.

James, D., and Tresman, R. (1968). De novo formation of neuro-muscular junctions in tissue culture. Nature *220*, 384-385. https://doi.org/10.1038/220384a0.

Jang, M., Cai, L., Udeani, G.O., Slowing, K.V., Thomas, C.F., Beecher, C.W., Fong, H.H., Farnsworth, N.R., Kinghorn, A.D., and Mehta, R.G., et al. (1997). Cancer chemopreventive activity of resveratrol, a natural product derived from grapes. Science *275*, 218-220. https://doi.org/10.1126/science.275.5297.218.

Jessen, K.R., Brennan, A., Morgan, L., Mirsky, R., Kent, A., Hashimoto, Y., and Gavrilovic, J. (1994). The schwann cell precursor and its fate: A study of cell death and differentiation during gliogenesis in rat embryonic nerves. Neuron *12*, 509-527. https://doi.org/10.1016/0896-6273(94)90209-7.

Jessen, K.R., and Mirsky, R. (2005). The origin and development of glial cells in peripheral nerves. Nature Reviews. Neuroscience *6*, 671-682. https://doi.org/10.1038/nrn1746.

Jessen, K.R., and Mirsky, R. (2016). The repair Schwann cell and its function in regenerating nerves. The Journal of Physiology *594*, 3521-3531. https://doi.org/10.1113/JP270874.

Jessen, K.R., and Mirsky, R. (2019). Schwann Cell Precursors; Multipotent Glial Cells in Embryonic Nerves. Frontiers in molecular neuroscience *12*, 69. https://doi.org/10.3389/fnmol.2019.00069.

Jessen, K.R., Mirsky, R., and Lloyd, A.C. (2015). Schwann Cells: Development and Role in Nerve Repair. Cold Spring Harbor Perspectives in Biology *7*. https://doi.org/10.1101/cshperspect.a020487.

Ji, Y., Hao, H., Reynolds, K., McMahon, M., and Zhou, C.J. (2019). Wnt Signaling in Neural Crest Ontogenesis and Oncogenesis. Cells *8*. https://doi.org/10.3390/cells8101173.

Jiang, B., Ou, W., Shamul, J.G., Chen, H., van Belleghem, S., Stewart, S., Liu, Z., Fisher, J.P., and He, X. (2022). Rock inhibitor may compromise human induced pluripotent stem cells for cardiac differentiation in 3D. Bioactive Materials *9*, 508-522. https://doi.org/10.1016/j.bioactmat.2021.07.013.

Jiang, L., Zhu, J.-K., Liu, X.-L., Xiang, P., Hu, J., and Yu, W.-H. (2008). Differentiation of rat adipose tissue-derived stem cells into Schwann-like cells in vitro. Neuroreport *19*, 1015-1019. https://doi.org/10.1097/WNR.0b013e3283040efc.

Jin, F., Dong, B., Georgiou, J., Jiang, Q., Zhang, J., Bharioke, A., Qiu, F., Lommel, S., Feltri, M.L., and Wrabetz, L., et al. (2011). N-WASp is required for Schwann cell cytoskeletal dynamics, normal myelin gene expression and peripheral nerve myelination. Development (Cambridge, England) *138*, 1329-1337. https://doi.org/10.1242/dev.058677.

Jöbsis, F.F., and O'Connor, M.J. (1966). Calcium release and reabsorption in the sartorius muscle of the toad. Biochemical and biophysical research communications *25*, 246-252. https://doi.org/10.1016/0006-291X(66)90588-2.

Jones, R.A., Harrison, C., Eaton, S.L., Llavero Hurtado, M., Graham, L.C., Alkhammash, L., Oladiran, O.A., Gale, A., Lamont, D.J., and Simpson, H., et al. (2017). Cellular and Molecular Anatomy of the Human Neuromuscular Junction. Cell Reports *21*, 2348-2356. https://doi.org/10.1016/j.celrep.2017.11.008.

Joseph, N.M., Mukouyama, Y., Mosher, J.T., Jaegle, M., Crone, S.A., Dormand, E.-L., Lee, K.-F., Meijer, D., Anderson, D.J., and Morrison, S.J. (2004). Neural crest stem cells undergo multilineage differentiation in developing peripheral nerves to generate endoneurial fibroblasts in addition to Schwann cells. Development *131*, 5599-5612. https://doi.org/10.1242/dev.01429.

Jung, N., Park, S., Choi, Y., Park, J.-W., Hong, Y.B., Park, H.H.C., Yu, Y., Kwak, G., Kim, H.S., and Ryu, K.-H., et al. (2016). Tonsil-Derived Mesenchymal Stem Cells Differentiate into a Schwann Cell Phenotype and Promote Peripheral Nerve Regeneration. International Journal of Molecular Sciences *17*. https://doi.org/10.3390/ijms17111867.

Kalcheim, C., and Kumar, D. (2017). Cell fate decisions during neural crest ontogeny. The International Journal of Developmental Biology *61*, 195-203. https://doi.org/10.1387/ijdb.160196ck.

Kang, H., Le Tian, Mikesh, M., Lichtman, J.W., and Thompson, W.J. (2014). Terminal Schwann cells participate in neuromuscular synapse remodeling during reinnervation following nerve injury. J. Neurosci. *34*, 6323-6333. https://doi.org/10.1523/JNEUROSCI.4673-13.2014.

Kastriti, M.E., and Adameyko, I. (2017). Specification, plasticity and evolutionary origin of peripheral glial cells. Current Opinion in Neurobiology *47*, 196-202. https://doi.org/10.1016/j.conb.2017.11.004.

Kastriti, M.E., Faure, L., Ahsen, D. von, Bouderlique, T.G., Boström, J., Solovieva, T., Jackson, C., Bronner, M., Meijer, D., and Hadjab, S., et al. (2022). Schwann cell precursors represent a neural crest-like state with biased multipotency. The EMBO journal, e108780. https://doi.org/10.15252/embj.2021108780.

Kastriti, M.E., Kameneva, P., Kamenev, D., Dyachuk, V., Furlan, A., Hampl, M., Memic, F., Marklund, U., Lallemend, F., and Hadjab, S., et al. (2019). Schwann Cell Precursors Generate the Majority of Chromaffin Cells in Zuckerkandl Organ and Some Sympathetic Neurons in Paraganglia. Front. Mol. Neurosci. *12*, 6. https://doi.org/10.3389/fnmol.2019.00006.

Kaufman, C.D., Liu, S.C., Cvetkovic, C., Lee, C.A., Naseri Kouzehgarani, G., Gillette, R., Bashir, R., and Gillette, M.U. (2020). Emergence of functional neuromuscular junctions in an engineered, multicellular spinal cord-muscle bioactuator. APL bioengineering *4*, 26104. https://doi.org/10.1063/1.5121440.

Kaukua, N., Shahidi, M.K., Konstantinidou, C., Dyachuk, V., Kaucka, M., Furlan, A., An, Z., Wang, L., Hultman, I., and Ahrlund-Richter, L., et al. (2014). Glial origin of mesenchymal stem cells in a tooth model system. Nature *513*, 551-554. https://doi.org/10.1038/nature13536.

Kengaku, M., Kawata, A., Kawashima, S., and Nakane, M. (1991). Role of fibronectin in the inhibitory effect of TGF-beta on choline acetyltransferase activity in co-cultures of spinal cord neurons and myotubes. Developmental Brain Research *61*, 281-284. https://doi.org/10.1016/0165-3806(91)90144-8.

Khan, M.M., Lustrino, D., Silveira, W.A., Wild, F., Straka, T., Issop, Y., O'Connor, E., Cox, D., Reischl, M., and Marquardt, T., et al. (2016). Sympathetic innervation controls homeostasis of neuromuscular junctions in health and disease. Proceedings of the National Academy of Sciences of the United States of America *113*, 746-750. https://doi.org/10.1073/pnas.1524272113.

Kidokoro, Y., Anderson, M.J., and Gruener, R. (1980). Changes in synaptic potential properties during acetylcholine receptor accumulation and neurospecific interactions in Xenopus nerve-muscle cell culture. Developmental Biology *78*, 464-483. https://doi.org/10.1016/0012-1606(80)90347-4.

Kim, H.-M., Noh, H.B., Lee, S.-H., Lee, K.-G., Chang, B., Cheong, E., Lee, C.J., and Hwang, D.-Y. (2021). Fine-tuning of dual-SMAD inhibition to differentiate human pluripotent stem cells into neural crest stem cells. Cell proliferation *54*, e13103. https://doi.org/10.1111/cpr.13103.

Kim, H.-S., Kim, J.Y., Song, C.L., Jeong, J.E., and Cho, Y.S. (2020). Directly induced human Schwann cell precursors as a valuable source of Schwann cells. Stem Cell Res Ther *11*, 257. https://doi.org/10.1186/s13287-020-01772-x.

Kim, H.-S., Lee, J., Lee, D.Y., Kim, Y.-D., Kim, J.Y., Lim, H.J., Lim, S., and Cho, Y.S. (2017). Schwann Cell Precursors from Human Pluripotent Stem Cells as a Potential Therapeutic Target for Myelin Repair. Stem Cell Reports *8*, 1714-1726. https://doi.org/10.1016/j.stemcr.2017.04.011.

Kim, K., Ossipova, O., and Sokol, S.Y. (2015). Neural crest specification by inhibition of the ROCK/Myosin II pathway. Stem Cells (Dayton, Ohio) *33*, 674-685. https://doi.org/10.1002/stem.1877.

Kim, N., Stiegler, A.L., Cameron, T.O., Hallock, P.T., Gomez, A.M., Huang, J.H., Hubbard, S.R., Dustin, M.L., and Burden, S.J. (2008). Lrp4 is a receptor for Agrin and forms a complex with MuSK. Cell *135*, 334-342. https://doi.org/10.1016/j.cell.2008.10.002.

Kingham, P.J., Kalbermatten, D.F., Mahay, D., Armstrong, S.J., Wiberg, M., and Terenghi, G. (2007). Adipose-derived stem cells differentiate into a Schwann cell phenotype and promote neurite outgrowth in vitro. Experimental Neurology *207*, 267-274. https://doi.org/10.1016/j.expneurol.2007.06.029.

Kioussi, C., Gross, M.K., and Gruss, P. (1995). Pax3: A paired domain gene as a regulator in PNS myelination. Neuron *15*, 553-562. https://doi.org/10.1016/0896-6273(95)90144-2.

Kitada, M., Murakami, T., Wakao, S., Li, G., and Dezawa, M. (2019). Direct conversion of adult human skin fibroblasts into functional Schwann cells that achieve robust recovery of the severed peripheral nerve in rats. Glia *67*, 950-966. https://doi.org/10.1002/glia.23582.

Ko, C.-P., and Robitaille, R. (2015). Perisynaptic Schwann Cells at the Neuromuscular Synapse: Adaptable, Multitasking Glial Cells. Cold Spring Harbor Perspectives in Biology *7*, a020503. https://doi.org/10.1101/cshperspect.a020503.

Kong, J.S., Huang, X., Choi, Y.-J., Yi, H.-G., Kang, J., Kim, S., Kim, J., Lee, H., Rim, Y.A., and Ju, J.H., et al. (2021). Promoting Long-Term Cultivation of Motor Neurons for 3D Neuromuscular Junction Formation of 3D In Vitro Using Central-Nervous-Tissue-Derived Bioink. Advanced healthcare materials *10*, e2100581. https://doi.org/10.1002/adhm.202100581.

Kraniak, J.M., Chalasani, A., Wallace, M.R., and Mattingly, R.R. (2018). Development of 3D culture models of plexiform neurofibroma and initial application for phenotypic characterization and drug screening. Experimental Neurology *299*, 289-298. https://doi.org/10.1016/j.expneurol.2017.10.012.

Krawetz, R.J., Li, X., and Rancourt, D.E. (2009). Human embryonic stem cells: caught between a ROCK inhibitor and a hard place. BioEssays : news and reviews in molecular, cellular and developmental biology *31*, 336-343. https://doi.org/10.1002/bies.200800157.

Kreitzer, F.R., Salomonis, N., Sheehan, A., Huang, M., Park, J.S., Spindler, M.J., Lizarraga, P., Weiss, W.A., So, P.-L., and Conklin, B.R. (2013). A robust method to derive functional neural crest cells from human pluripotent stem cells. American Journal of Stem Cells *2*, 119-131.

Kriebel, M.E., Hanna, R., and Muniak, C. (1986). Synaptic vesicle diameters and synaptic cleft widths at the mouse diaphragm in neonates and adults. Brain Research *392*, 19-29. https://doi.org/10.1016/0165-3806(86)90228-2.

Kumar, D., Nitzan, E., and Kalcheim, C. (2019). YAP promotes neural crest emigration through interactions with BMP and Wnt activities. Cell Communication and Signaling : CCS *17*, 69. https://doi.org/10.1186/s12964-019-0383-x.

Kurosawa, H. (2012). Application of Rho-associated protein kinase (ROCK) inhibitor to human pluripotent stem cells. Journal of bioscience and bioengineering *114*, 577-581. https://doi.org/10.1016/j.jbiosc.2012.07.013.

La Bierlein De Rosa, M., Sharma, A.D., Mallapragada, S.K., and Sakaguchi, D.S. (2017). Transdifferentiation of brain-derived neurotrophic factor (BDNF)-secreting mesenchymal stem cells significantly enhance BDNF secretion and Schwann cell marker proteins. Journal of bioscience and bioengineering *124*, 572-582. https://doi.org/10.1016/j.jbiosc.2017.05.014.

Lacazette, E., Le Calvez, S., Gajendran, N., and Brenner, H.R. (2003). A novel pathway for MuSK to induce key genes in neuromuscular synapse formation. The Journal of Cell Biology *161*, 727-736. https://doi.org/10.1083/jcb.200210156.

Lamotte, J.D. de, Roqueviere, S., Gautier, H., Raban, E., Bouré, C., Fonfria, E., Krupp, J., and Nicoleau, C. (2020). hiPSC-Derived Neurons Provide a Robust and Physiologically Relevant In Vitro Platform to Test Botulinum Neurotoxins. Frontiers in pharmacology *11*, 617867. https://doi.org/10.3389/fphar.2020.617867.

Lancaster, M.A., and Knoblich, J.A. (2014). Organogenesis in a dish: modeling development and disease using organoid technologies. Science (New York, N.Y.) *345*, 1247125. https://doi.org/10.1126/science.1247125.

Langhans, S.A. (2018). Three-Dimensional in Vitro Cell Culture Models in Drug Discovery and Drug Repositioning. Frontiers in pharmacology *9*, 6. https://doi.org/10.3389/fphar.2018.00006.

Latasa, M.-J., and Cosgaya, J.M. (2011). Regulation of Retinoid Receptors by Retinoic Acid and Axonal Contact in Schwann Cells. PLoS ONE *6*. https://doi.org/10.1371/journal.pone.0017023.

Latasa, M.-J., Ituero, M., Moran-Gonzalez, A., Aranda, A., and Cosgaya, J.M. (2010). Retinoic acid regulates myelin formation in the peripheral nervous system. Glia *58*, 1451-1464. https://doi.org/10.1002/glia.21020.

Latasa, M.-J., Jiménez-Lara, A.M., and Cosgaya, J.M. (2016). Retinoic acid regulates Schwann cell migration via NEDD9 induction by transcriptional and post-translational mechanisms. Biochimica et biophysica acta *1863*, 1510-1518. https://doi.org/10.1016/j.bbamcr.2016.04.009.

Le Douarin, N.M., and Teillet, M.-A.M. (1974). Experimental analysis of the migration and differentiation of neuroblasts of the autonomic nervous system and of neurectodermal mesenchymal derivatives, using a biological cell marking technique. Developmental Biology *41*, 162-184. https://doi.org/10.1016/0012-1606(74)90291-7.

Lee, G., Chambers, S.M., Tomishima, M.J., and Studer, L. (2010). Derivation of neural crest cells from human pluripotent stem cells. Nature protocols *5*, 688-701. https://doi.org/10.1038/nprot.2010.35.

Lee, G., Kim, H., Elkabetz, Y., Al Shamy, G., Panagiotakos, G., Barberi, T., Tabar, V., and Studer, L. (2007). Isolation and directed differentiation of neural crest stem cells derived from human embryonic stem cells. Nature Biotechnology *25*, 1468-1475. https://doi.org/10.1038/nbt1365.

Lee, H.-K., Velazquez Sanchez, C., Chen, M., Morin, P.J., Wells, J.M., Hanlon, E.B., and Xia, W. (2016). Three Dimensional Human Neuro-Spheroid Model of Alzheimer's Disease Based on Differentiated Induced Pluripotent Stem Cells. PLoS ONE *11*, e0163072. https://doi.org/10.1371/journal.pone.0163072.

Lee, S., Amici, S., Tavori, H., Zeng, W.M., Freeland, S., Fazio, S., and Notterpek, L. (2014). PMP22 is critical for actin-mediated cellular functions and for establishing lipid rafts. J. Neurosci. *34*, 16140-16152. https://doi.org/10.1523/JNEUROSCI.1908-14.2014.

Lee, Y.I., Mikesh, M., Smith, I., Rimer, M., and Thompson, W. (2011). Muscles in a mouse model of spinal muscular atrophy show profound defects in neuromuscular development even in the absence of failure in neuromuscular transmission or loss of motor neurons. Developmental Biology *356*, 432-444. https://doi.org/10.1016/j.ydbio.2011.05.667.

Lee, Y.I., Thompson, W.J., and Harlow, M.L. (2017). Schwann cells participate in synapse elimination at the developing neuromuscular junction. Current Opinion in Neurobiology *47*, 176-181. https://doi.org/10.1016/j.conb.2017.10.010.

Lehmann, H.C., and Höke, A. (2016). Use of engineered Schwann cells in peripheral neuropathy: Hopes and hazards. Brain Research *1638*, 97-104. https://doi.org/10.1016/j.brainres.2015.10.040.

Leimeroth, R., Lobsiger, C., Lüssi, A., Taylor, V., Suter, U., and Sommer, L. (2002). Membrane-bound neuregulin1 type III actively promotes Schwann cell differentiation of multipotent Progenitor cells. Developmental Biology *246*, 245-258. https://doi.org/10.1006/dbio.2002.0670.

Lemke, G.E., and Brockes, J.P. (1984). Identification and purification of glial growth factor. J. Neurosci. *4*, 75-83. https://doi.org/10.1523/JNEUROSCI.04-01-00075.1984.

Leung, A.W., Murdoch, B., Salem, A.F., Prasad, M.S., Gomez, G.A., and García-Castro, M.I. (2016). WNT/β-catenin signaling mediates human neural crest induction via a pre-neural border intermediate. Development (Cambridge, England) *143*, 398-410. https://doi.org/10.1242/dev.130849.

Li, L., Xiong, W.-C., and Mei, L. (2018). Neuromuscular Junction Formation, Aging, and Disorders. Annual review of physiology *80*, 159-188. https://doi.org/10.1146/annurev-physiol-022516-034255.

Li, W., Huang, L., Lin, W., Ke, Q., Chen, R., Lai, X., Wang, X., Zhang, J., Jiang, M., and Huang, W., et al. (2015). Engraftable neural crest stem cells derived from cynomolgus monkey embryonic stem cells. Biomaterials *39*, 75-84. https://doi.org/10.1016/j.biomaterials.2014.10.056.

Li, W., Sun, W., Zhang, Y., Wei, W., Ambasudhan, R., Xia, P., Talantova, M., Lin, T., Kim, J., and Wang, X., et al. (2011). Rapid induction and long-term self-renewal of primitive neural precursors from human embryonic stem cells by small molecule inhibitors. PNAS *108*, 8299-8304. https://doi.org/10.1073/pnas.1014041108.

Li, X., Meng, G., Krawetz, R., Liu, S., and Rancourt, D.E. (2008). The ROCK inhibitor Y-27632 enhances the survival rate of human embryonic stem cells following cryopreservation. Stem cells and development *17*, 1079-1085. https://doi.org/10.1089/scd.2007.0247.

Li, X.-J., Du, Z.-W., Zarnowska, E.D., Pankratz, M., Hansen, L.O., Pearce, R.A., and Zhang, S.-C. (2005). Specification of motoneurons from human embryonic stem cells. Nature Biotechnology *23*, 215-221. https://doi.org/10.1038/nbt1063.

Li, Y., Gonzalez, M.I., Meinkoth, J.L., Field, J., Kazanietz, M.G., and Tennekoon, G.I. (2003). Lysophosphatidic acid promotes survival and differentiation of rat Schwann cells. Journal of Biological Chemistry *278*, 9585-9591. https://doi.org/10.1074/jbc.M213244200.

Lin, C.-Y., Yoshida, M., Li, L.-T., Ikenaka, A., Oshima, S., Nakagawa, K., Sakurai, H., Matsui, E., Nakahata, T., and Saito, M.K. (2019). iPSC-derived functional human neuromuscular junctions model the pathophysiology of neuromuscular diseases. JCI Insight *4*. https://doi.org/10.1172/jci.insight.124299.

Lin, W., Burgess, R.W., Dominguez, B., Pfaff, S.L., Sanes, J.R., and Lee, K.F. (2001). Distinct roles of nerve and muscle in postsynaptic differentiation of the neuromuscular synapse. Nature *410*, 1057-1064. https://doi.org/10.1038/35074025.

Lin, W., Dominguez, B., Yang, J., Aryal, P., Brandon, E.P., Gage, F.H., and Lee, K.-F. (2005). Neurotransmitter acetylcholine negatively regulates neuromuscular synapse formation by a Cdk5-dependent mechanism. Neuron *46*, 569-579. https://doi.org/10.1016/j.neuron.2005.04.002.

Lin, W., Sanchez, H.B., Deerinck, T., Morris, J.K., Ellisman, M., and Lee, K.F. (2000). Aberrant development of motor axons and neuromuscular synapses in erbB2-deficient mice. Proceedings of the National Academy of Sciences of the United States of America *97*, 1299-1304. https://doi.org/10.1073/pnas.97.3.1299.

Lindgren, C.A., Newman, Z.L., Morford, J.J., Ryan, S.B., Battani, K.A., and Su, Z. (2013). Cyclooxygenase-2, prostaglandin E2 glycerol ester and nitric oxide are involved in muscarine-induced presynaptic enhancement at the vertebrate neuromuscular junction. The Journal of Physiology *591*, 4749-4764. https://doi.org/10.1113/jphysiol.2013.256727.

Liu, J.P., Laufer, E., and Jessell, T.M. (2001). Assigning the positional identity of spinal motor neurons: rostrocaudal patterning of Hox-c expression by FGFs, Gdf11, and retinoids. Neuron *32*, 997-1012. https://doi.org/10.1016/s0896-6273(01)00544-x.

Liu, Q., Spusta, S.C., Mi, R., Lassiter, R.N.T., Stark, M.R., Höke, A., Rao, M.S., and Zeng, X. (2012). Human neural crest stem cells derived from human ESCs and induced pluripotent stem cells: induction, maintenance, and differentiation into functional schwann cells. STEM CELLS Translational Medicine *1*, 266-278. https://doi.org/10.5966/sctm.2011-0042.

Liu, Y., Sugiura, Y., Chen, F., Lee, K.-F., Ye, Q., and Lin, W. (2019). Blocking skeletal muscle DHPRs/Ryr1 prevents neuromuscular synapse loss in mutant mice deficient in type III Neuregulin 1 (CRD-Nrg1). PLOS Genetics *15*, e1007857. https://doi.org/10.1371/journal.pgen.1007857.

Liu, Z., Jin, Y.-Q., Chen, L., Wang, Y., Yang, X., Cheng, J., Wu, W., Qi, Z., and Shen, Z. (2015). Specific marker expression and cell state of Schwann cells during culture in vitro. PLoS ONE *10*, e0123278. https://doi.org/10.1371/journal.pone.0123278.

Louit, A., Beaudet, M.-J., Gros-Louis, F., and Berthod, F. (2022). Tissue-engineered in vitro modeling of the impact of Schwann cells in amyotrophic lateral sclerosis. Biotechnology and bioengineering. https://doi.org/10.1002/bit.28083.

Lunn, J.S., Fishwick, K.J., Halley, P.A., and Storey, K.G. (2007). A spatial and temporal map of FGF/Erk1/2 activity and response repertoires in the early chick embryo. Developmental Biology *302*, 536-552. https://doi.org/10.1016/j.ydbio.2006.10.014.

Luttrell, S.M., Smith, A.S.T., and Mack, D.L. (2021). Creating stem cell-derived neuromuscular junctions in vitro. Muscle & Nerve. https://doi.org/10.1002/mus.27360.

Lynch, E., Peek, E., Reilly, M., FitzGibbons, C., Robertson, S., and Suzuki, M. (2021). Current Progress in the Creation, Characterization, and Application of Human Stem Cell-derived in Vitro Neuromuscular Junction Models. Stem cell reviews and reports. https://doi.org/10.1007/s12015-021-10201-2.

Ma, M.-S., Boddeke, E., and Copray, S. (2015). Pluripotent stem cells for Schwann cell engineering. Stem cell reviews and reports *11*, 205-218. https://doi.org/10.1007/s12015-014-9577-1.

Maden, M. (2007). Retinoic acid in the development, regeneration and maintenance of the nervous system. Nature Reviews. Neuroscience *8*, 755-765. https://doi.org/10.1038/nrn2212.

Maffioletti, S.M., Sarcar, S., Henderson, A.B.H., Mannhardt, I., Pinton, L., Moyle, L.A., Steele-Stallard, H., Cappellari, O., Wells, K.E., and Ferrari, G., et al. (2018). Three-Dimensional Human iPSC-Derived Artificial Skeletal Muscles Model Muscular Dystrophies and Enable Multilineage Tissue Engineering. Cell Reports *23*, 899-908. https://doi.org/10.1016/j.celrep.2018.03.091.

Maldonado, M., Luu, R.J., Ramos, M.E.P., and Nam, J. (2016). ROCK inhibitor primes human induced pluripotent stem cells to selectively differentiate towards mesendodermal lineage via epithelial-mesenchymal transition-like modulation. Stem Cell Research *17*, 222-227. https://doi.org/10.1016/j.scr.2016.07.009.

Manderfield, L.J., Aghajanian, H., Engleka, K.A., Lim, L.Y., Liu, F., Jain, R., Li, L., Olson, E.N., and Epstein, J.A. (2015). Hippo signaling is required for Notch-dependent smooth muscle differentiation of neural crest. Development (Cambridge, England) *142*, 2962-2971. https://doi.org/10.1242/dev.125807.

Marchant, L., Linker, C., Ruiz, P., Guerrero, N., and Mayor, R. (1998). The inductive properties of mesoderm suggest that the neural crest cells are specified by a BMP gradient. Developmental Biology *198*, 319-329. https://doi.org/10.1016/S0012-1606(98)80008-0.

Mars, T., Yu, K.J., Tang, X.M., Miranda, A.F., Grubic, Z., Cambi, F., and King, M.P. (2001). Differentiation of glial cells and motor neurons during the formation of neuromuscular junctions in cocultures of rat spinal cord explant and human muscle. The Journal of Comparative Neurology *438*, 239-251.

Martens, W., Sanen, K., Georgiou, M., Struys, T., Bronckaers, A., Ameloot, M., Phillips, J., and Lambrichts, I. (2014). Human dental pulp stem cells can differentiate into Schwann cells and promote and guide neurite outgrowth in an aligned tissue-engineered collagen construct in vitro. FASEB journal : official publication of the Federation of American Societies for Experimental Biology *28*, 1634-1643. https://doi.org/10.1096/fj.13-243980.

Martineau, É., Arbour, D., Vallée, J., and Robitaille, R. (2020). Properties of Glial Cell at the Neuromuscular Junction Are Incompatible with Synaptic Repair in the SOD1G37R ALS Mouse Model. J. Neurosci. *40*, 7759-7777. https://doi.org/10.1523/JNEUROSCI.1748-18.2020.

Martínez-Morales, P.L., Del Diez Corral, R., Olivera-Martínez, I., Quiroga, A.C., Das, R.M., Barbas, J.A., Storey, K.G., and Morales, A.V. (2011). FGF and retinoic acid activity gradients control the timing of neural crest cell emigration in the trunk. The Journal of Cell Biology *194*, 489-503. https://doi.org/10.1083/jcb.201011077.

Martyn, J.A.J., Fagerlund, M.J., and Eriksson, L.I. (2009). Basic principles of neuromuscular transmission. Anaesthesia *64 Suppl 1*, 1-9. https://doi.org/10.1111/j.1365-2044.2008.05865.x.

Massagué, J. (1998). TGF-beta signal transduction. Annual review of biochemistry *67*, 753-791. https://doi.org/10.1146/annurev.biochem.67.1.753.

Matsuse, D., Kitada, M., Kohama, M., Nishikawa, K., Makinoshima, H., Wakao, S., Fujiyoshi, Y., Heike, T., Nakahata, T., and Akutsu, H., et al. (2010). Human umbilical cord-derived mesenchymal stromal cells differentiate into functional Schwann cells that sustain peripheral nerve regeneration. Journal of neuropathology and experimental neurology *69*, 973-985. https://doi.org/10.1097/NEN.0b013e3181eff6dc.

Maury, Y., Côme, J., Piskorowski, R.A., Salah-Mohellibi, N., Chevaleyre, V., Peschanski, M., Martinat, C., and Nedelec, S. (2015). Combinatorial analysis of developmental cues efficiently converts human pluripotent stem cells into multiple neuronal subtypes. Nature Biotechnology *33*, 89-96. https://doi.org/10.1038/nbt.3049.

Mazaleyrat, K., Badja, C., Broucqsault, N., Chevalier, R., Laberthonnière, C., Dion, C., Baldasseroni, L., El-Yazidi, C., Thomas, M., and Bachelier, R., et al. (2020). Multilineage Differentiation for Formation of Innervated Skeletal Muscle Fibers from Healthy and Diseased Human Pluripotent Stem Cells. Cells *9*. https://doi.org/10.3390/cells9061531.

Mazzara, P.G., Massimino, L., Pellegatta, M., Ronchi, G., Ricca, A., Iannielli, A., Giannelli, S.G., Cursi, M., Cancellieri, C., and Sessa, A., et al. (2017). Two factor-based reprogramming of rodent and human fibroblasts into Schwann cells. Nature Communications *8*, 14088. https://doi.org/10.1038/ncomms14088.

McKenzie, I.A., Biernaskie, J., Toma, J.G., Midha, R., and Miller, F.D. (2006). Skin-derived precursors generate myelinating Schwann cells for the injured and dysmyelinated nervous system. The Journal of neuroscience : the official journal of the Society for Neuroscience *26*, 6651-6660. https://doi.org/10.1523/JNEUROSCI.1007-06.2006.

Means, J.C., Lopez, A.A., and Koulen, P. (2020). Resveratrol Protects Optic Nerve Head Astrocytes from Oxidative Stress-Induced Cell Death by Preventing Caspase-3 Activation, Tau Dephosphorylation at Ser422 and Formation of Misfolded Protein Aggregates. Cell Mol Neurobiol *40*, 911-926. https://doi.org/10.1007/s10571-019-00781-6.

Mehler, M.F., Mabie, P.C., Zhang, D., and Kessler, J.A. (1997). Bone morphogenetic proteins in the nervous system. Trends in Neurosciences *20*, 309-317. https://doi.org/10.1016/s0166-2236(96)01046-6.

Meier, C., Parmantier, E., Brennan, A., Mirsky, R., and Jessen, K.R. (1999). Developing Schwann Cells Acquire the Ability to Survive without Axons by Establishing an Autocrine Circuit Involving Insulin-Like Growth Factor, Neurotrophin-3, and Platelet-Derived Growth Factor-BB. J. Neurosci. *19*, 3847-3859. https://doi.org/10.1523/JNEUROSCI.19-10-03847.1999.

Melzer, W., Herrmann-Frank, A., and Lüttgau, H.C. (1995). The role of Ca2+ ions in excitation-contraction coupling of skeletal muscle fibres. Biochimica et biophysica acta *1241*, 59-116. https://doi.org/10.1016/0304-4157(94)00014-5.

Menendez, L., Yatskievych, T.A., Antin, P.B., and Dalton, S. (2011). Wnt signaling and a Smad pathway blockade direct the differentiation of human pluripotent stem cells to multipotent neural crest cells. Proceedings of the National Academy of Sciences of the United States of America *108*, 19240-19245. https://doi.org/10.1073/pnas.1113746108.

Metzler, E., Escobar, H., Sunaga-Franze, D.Y., Sauer, S., Diecke, S., and Spuler, S. (2022). Generation of hiPSC-Derived Skeletal Muscle Cells: Exploiting the Potential of Skeletal Muscle-Derived hiPSCs. Biomedicines *10*, 1204. https://doi.org/10.3390/biomedicines10051204.

Meyer, D., Yamaai, T., Garratt, A., Riethmacher-Sonnenberg, E., Kane, D., Theill, L.E., and Birchmeier, C. (1997). Isoform-specific expression and function of neuregulin. Development *124*, 3575-3586. https://doi.org/10.1242/dev.124.18.3575.

Mica, Y., Lee, G., Chambers, S.M., Tomishima, M.J., and Studer, L. (2013). Modeling neural crest induction, melanocyte specification, and disease-related pigmentation defects in hESCs and patient-specific iPSCs. Cell Reports *3*, 1140-1152. https://doi.org/10.1016/j.celrep.2013.03.025.

Milichko, V., and Dyachuk, V. (2020). Novel Glial Cell Functions: Extensive Potency, Stem Cell-Like Properties, and Participation in Regeneration and Transdifferentiation. Frontiers in cell and developmental biology *8*, 809. https://doi.org/10.3389/fcell.2020.00809.

Misgeld, T., Burgess, R.W., Lewis, R.M., Cunningham, J.M., Lichtman, J.W., and Sanes, J.R. (2002). Roles of Neurotransmitter in Synapse Formation. Neuron *36*, 635-648. https://doi.org/10.1016/S0896-6273(02)01020-6.

Misgeld, T., Kummer, T.T., Lichtman, J.W., and Sanes, J.R. (2005). Agrin promotes synaptic differentiation by counteracting an inhibitory effect of neurotransmitter. Proceedings of the National Academy of Sciences of the United States of America *102*, 11088-11093. https://doi.org/10.1073/pnas.0504806102.

Mishina, M., Takai, T., Imoto, K., Noda, M., Takahashi, T., Numa, S., Methfessel, C., and Sakmann, B. (1986). Molecular distinction between fetal and adult forms of muscle acetylcholine receptor. Nature *321*, 406-411. https://doi.org/10.1038/321406a0.

Mittaud, P., Marangi, P.A., Erb-Vögtli, S., and Fuhrer, C. (2001). Agrin-induced activation of acetylcholine receptor-bound Src family kinases requires Rapsyn and correlates with acetylcholine receptor clustering. Journal of Biological Chemistry *276*, 14505-14513. https://doi.org/10.1074/jbc.M007024200.

Monje, P.V. (2020a). Schwann Cell Cultures: Biology, Technology and Therapeutics. Cells *9*. https://doi.org/10.3390/cells9081848.

Monje, P.V. (2020b). The properties of human Schwann cells: Lessons from in vitro culture and transplantation studies. Glia *68*, 797-810. https://doi.org/10.1002/glia.23793.

Monje, P.V., Sant, D., and Wang, G. (2018). Phenotypic and Functional Characteristics of Human Schwann Cells as Revealed by Cell-Based Assays and RNA-SEQ. Mol Neurobiol *55*, 6637-6660. https://doi.org/10.1007/s12035-017-0837-3.

Monk, K.R., Feltri, M.L., and Taveggia, C. (2015). New insights on Schwann cell development. Glia *63*, 1376-1393. https://doi.org/10.1002/glia.22852.

Moransard, M., Borges, L.S., Willmann, R., Marangi, P.A., Brenner, H.R., Ferns, M.J., and Fuhrer, C. (2003). Agrin regulates rapsyn interaction with surface acetylcholine receptors, and this underlies cytoskeletal anchoring and clustering. Journal of Biological Chemistry *278*, 7350-7359. https://doi.org/10.1074/jbc.M210865200.

Morimoto, Y., Kato-Negishi, M., Onoe, H., and Takeuchi, S. (2013). Three-dimensional neuron-muscle constructs with neuromuscular junctions. Biomaterials *34*, 9413-9419. https://doi.org/10.1016/j.biomaterials.2013.08.062.

Morita, S., and Miyata, S. (2013). Synaptic localization of growth-associated protein 43 in cultured hippocampal neurons during synaptogenesis. Cell biochemistry and function *31*, 400-411. https://doi.org/10.1002/cbf.2914.

Morris, J.K., Lin, W., Hauser, C., Marchuk, Y., Getman, D., and Lee, K.F. (1999). Rescue of the cardiac defect in ErbB2 mutant mice reveals essential roles of ErbB2 in peripheral nervous system development. Neuron *23*, 273-283. https://doi.org/10.1016/s0896-6273(00)80779-5.

Morrison, S.J., Perez, S.E., Qiao, Z., Verdi, J.M., Hicks, C., Weinmaster, G., and Anderson, D.J. (2000). Transient Notch Activation Initiates an Irreversible Switch from Neurogenesis to Gliogenesis by Neural Crest Stem Cells. Cell *101*, 499-510. https://doi.org/10.1016/S0092-8674(00)80860-0.

Morrissey, T.K., Levi, A.D., Nuijens, A., Sliwkowski, M.X., and Bunge, R.P. (1995). Axon-induced mitogenesis of human Schwann cells involves heregulin and p185erbB2. Proceedings of the National Academy of Sciences of the United States of America *92*, 1431-1435. https://doi.org/10.1073/pnas.92.5.1431.

Mukherjee-Clavin, B., Mi, R., Kern, B., Choi, I.Y., Lim, H., Oh, Y., Lannon, B., Kim, K.J., Bell, S., and Hur, J.K., et al. (2019). Comparison of three congruent patient-specific cell types for the modelling of a human genetic Schwann-cell disorder. Nature biomedical engineering *3*, 571-582. https://doi.org/10.1038/s41551-019-0381-8.

Muller, Q., Beaudet, M.-J., Serres-Bérard, T. de, Bellenfant, S., Flacher, V., and Berthod, F. (2018). Development of an innervated tissue-engineered skin with human sensory neurons and Schwann cells differentiated from iPS cells. Acta Biomaterialia *82*, 93-101. https://doi.org/10.1016/j.actbio.2018.10.011.

Muppirala, A.N., Limbach, L.E., Bradford, E.F., and Petersen, S.C. (2021). Schwann cell development: From neural crest to myelin sheath. Wiley interdisciplinary reviews. Developmental biology *10*, e398. https://doi.org/10.1002/wdev.398.

Natarajan, A., Sethumadhavan, A., and Krishnan, U.M. (2019). Toward Building the Neuromuscular Junction: In Vitro Models To Study Synaptogenesis and Neurodegeneration. ACS omega *4*, 12969-12977. https://doi.org/10.1021/acsomega.9b00973.

Neve, A., Trüb, J., Saxena, S., and Schümperli, D. (2016). Central and peripheral defects in motor units of the diaphragm of spinal muscular atrophy mice. Molecular and Cellular Neurosciences *70*, 30-41. https://doi.org/10.1016/j.mcn.2015.11.007.

Newman, A.M., and Cooper, J.B. (2010). Lab-specific gene expression signatures in pluripotent stem cells. Cell Stem Cell *7*, 258-262. https://doi.org/10.1016/j.stem.2010.06.016.

Nishimune, H., Sanes, J.R., and Carlson, S.S. (2004). A synaptic laminin-calcium channel interaction organizes active zones in motor nerve terminals. Nature *432*, 580-587. https://doi.org/10.1038/nature03112.

Nitkin, R.M., Smith, M.A., Magill, C., Fallon, J.R., Yao, Y.M., Wallace, B.G., and McMahan, U.J. (1987). Identification of agrin, a synaptic organizing protein from Torpedo electric organ. The Journal of Cell Biology *105*, 2471-2478. https://doi.org/10.1083/jcb.105.6.2471.

Noisa, P., Lund, C., Kanduri, K., Lund, R., Lähdesmäki, H., Lahesmaa, R., Lundin, K., Chokechuwattanalert, H., Otonkoski, T., and Tuuri, T., et al. (2014). Notch signaling regulates the differentiation of neural crest from human pluripotent stem cells. Journal of Cell Science *127*, 2083-2094. https://doi.org/10.1242/jcs.145755.

Nordström, U., Jessell, T.M., and Edlund, T. (2002). Progressive induction of caudal neural character by graded Wnt signaling. Nature neuroscience *5*, 525-532. https://doi.org/10.1038/nn0602-854.

Noronha-Matos, J.B., Oliveira, L., Peixoto, A.R., Almeida, L., Castellão-Santana, L.M., Ambiel, C.R., Alves-do Prado, W., and Correia-de-Sá, P. (2020). Nicotinic α7 receptor-induced adenosine release from perisynaptic Schwann cells controls acetylcholine spillover from motor endplates. Journal of Neurochemistry *154*, 263-283. https://doi.org/10.1111/jnc.14975.

Ogawa, K., Nishinakamura, R., Iwamatsu, Y., Shimosato, D., and Niwa, H. (2006). Synergistic action of Wnt and LIF in maintaining pluripotency of mouse ES cells. Biochemical and biophysical research communications *343*, 159-166. https://doi.org/10.1016/j.bbrc.2006.02.127.

Ohgushi, M., Matsumura, M., Eiraku, M., Murakami, K., Aramaki, T., Nishiyama, A., Muguruma, K., Nakano, T., Suga, H., and Ueno, M., et al. (2010). Molecular pathway and cell state responsible for dissociation-induced apoptosis in human pluripotent stem cells. Cell Stem Cell *7*, 225-239. https://doi.org/10.1016/j.stem.2010.06.018.

Osafune, K., Caron, L., Borowiak, M., Martinez, R.J., Fitz-Gerald, C.S., Sato, Y., Cowan, C.A., Chien, K.R., and Melton, D.A. (2008). Marked differences in differentiation propensity among human embryonic stem cell lines. Nature Biotechnology *26*, 313-315. https://doi.org/10.1038/nbt1383.

Osaki, T., Uzel, S.G.M., and Kamm, R.D. (2018). Microphysiological 3D model of amyotrophic lateral sclerosis (ALS) from human iPS-derived muscle cells and optogenetic motor neurons. Science Advances *4*, eaat5847. https://doi.org/10.1126/sciadv.aat5847.

Osaki, T., Uzel, S.G.M., and Kamm, R.D. (2020). On-chip 3D neuromuscular model for drug screening and precision medicine in neuromuscular disease. Nature protocols *15*, 421-449. https://doi.org/10.1038/s41596-019-0248-1.

Overell, J.R., and Willison, H.J. (2005). Recent developments in Miller Fisher syndrome and related disorders. Current opinion in neurology *18*, 562-566. https://doi.org/10.1097/01.wco.0000173284.25581.2f.

Pan, S.-H., Zhao, N., Feng, X., Jie, Y., and Jin, Z.-B. (2021). Conversion of mouse embryonic fibroblasts into neural crest cells and functional corneal endothelia by defined small molecules. Science Advances *7*. https://doi.org/10.1126/sciadv.abg5749.

Park, H.S., Liu, S., McDonald, J., Thakor, N., and Yang, I.H. (2013). Neuromuscular junction in a microfluidic device. Conference proceedings: … Annual International Conference of the IEEE Engineering in Medicine and Biology Society. IEEE Engineering in Medicine and Biology Society. Annual Conference *2013*, 2833-2835. https://doi.org/10.1109/EMBC.2013.6610130.

Park, I.-H., Zhao, R., West, J.A., Yabuuchi, A., Huo, H., Ince, T.A., Lerou, P.H., Lensch, M.W., and Daley, G.Q. (2008). Reprogramming of human somatic cells to pluripotency with defined factors. Nature *451*, 141-146. https://doi.org/10.1038/nature06534.

Pașca, S.P. (2018). The rise of three-dimensional human brain cultures. Nature *553*, 437-445. https://doi.org/10.1038/nature25032.

Patani, R. (2016). Generating Diverse Spinal Motor Neuron Subtypes from Human Pluripotent Stem Cells. Stem Cells International *2016*. https://doi.org/10.1155/2016/1036974.

Patton, B.L., Cunningham, J.M., Thyboll, J., Kortesmaa, J., Westerblad, H., Edström, L., Tryggvason, K., and Sanes, J.R. (2001). Properly formed but improperly localized synaptic specializations in the absence of laminin alpha4. Nature neuroscience *4*, 597-604. https://doi.org/10.1038/88414.

Pease, S., Braghetta, P., Gearing, D., Grail, D., and Williams, R.L. (1990). Isolation of embryonic stem (ES) cells in media supplemented with recombinant leukemia inhibitory factor (LIF). Developmental Biology *141*, 344-352. https://doi.org/10.1016/0012-1606(90)90390-5.

Peltz, L., Gomez, J., Marquez, M., Alencastro, F., Atashpanjeh, N., Quang, T., Bach, T., and Zhao, Y. (2012). Resveratrol exerts dosage and duration dependent effect on human mesenchymal stem cell development. PLoS ONE *7*, e37162. https://doi.org/10.1371/journal.pone.0037162.

Personius, K.E., and Sawyer, R.P. (2005). Terminal Schwann cell structure is altered in diaphragm of mdx mice. Muscle & Nerve *32*, 656-663. https://doi.org/10.1002/mus.20405.

Peterson, E.R., Crain, S.M., and Murray, M.R. (1965). Differentiation and prolonged maintenance of bioelectrically active spinal cord cultures (rat, chick and human). Zeitschrift fur Zellforschung und mikroskopische Anatomie (Vienna, Austria : 1948) *66*, 130-154. https://doi.org/10.1007/BF00339322.

Petrov, K.A., Girard, E., Nikitashina, A.D., Colasante, C., Bernard, V., Nurullin, L., Leroy, J., Samigullin, D., Colak, O., and Nikolsky, E., et al. (2014). Schwann cells sense and control acetylcholine spillover at the neuromuscular junction by α7 nicotinic receptors and butyrylcholinesterase. J. Neurosci. *34*, 11870-11883. https://doi.org/10.1523/JNEUROSCI.0329-14.2014.

Picchiarelli, G., Demestre, M., Zuko, A., Been, M., Higelin, J., Dieterlé, S., Goy, M.-A., Mallik, M., Sellier, C., and Scekic-Zahirovic, J., et al. (2019). FUS-mediated regulation of acetylcholine receptor transcription at neuromuscular junctions is compromised in amyotrophic lateral sclerosis. Nat Neurosci *22*, 1793-1805. https://doi.org/10.1038/s41593-019-0498-9.

Pinard, A., Lévesque, S., Vallée, J., and Robitaille, R. (2003). Glutamatergic modulation of synaptic plasticity at a PNS vertebrate cholinergic synapse. European Journal of Neuroscience *18*, 3241-3250. https://doi.org/10.1111/j.1460-9568.2003.03028.x.

Pinchot, S.N., Jaskula-Sztul, R., Ning, L., Peters, N.R., Cook, M.R., Kunnimalaiyaan, M., and Chen, H. (2010). Identification and Validation of Notch Pathway Activating Compounds through a Novel High-Throughput Screening Method. Cancer *117*, 1386-1398. https://doi.org/10.1002/cncr.25652.

Piovesana, R., Faroni, A., Tata, A.M., and Reid, A.J. (2020). Functional Characterization of Muscarinic Receptors in Human Schwann Cells. International Journal of Molecular Sciences *21*. https://doi.org/10.3390/ijms21186666.

Pla, P., and Monsoro-Burq, A.H. (2018). The neural border: Induction, specification and maturation of the territory that generates neural crest cells. Developmental Biology *444 Suppl 1*, S36-S46. https://doi.org/10.1016/j.ydbio.2018.05.018.

Podder, A.K., Mohamed, M.A., Tseropoulos, G., Nasiri, B., and Andreadis, S.T. (2022). Engineering Nanofiber Scaffolds with Biomimetic Cues for Differentiation of Skin-Derived Neural Crest-like Stem Cells to Schwann Cells. International Journal of Molecular Sciences *23*. https://doi.org/10.3390/ijms231810834.

Pomp, O., Brokhman, I., Ziegler, L., Almog, M., Korngreen, A., Tavian, M., and Goldstein, R.S. (2008). PA6-induced human embryonic stem cell-derived neurospheres: a new source of human peripheral sensory neurons and neural crest cells. Brain Research *1230*, 50-60. https://doi.org/10.1016/j.brainres.2008.07.029.

Portier, M.M., Escurat, M., Landon, F., Djabali, K., and Bousquet, O. (1993). Peripherin and neurofilaments: expression and role during neural development. Comptes rendus de l'Academie des sciences. Serie III, Sciences de la vie *316*, 1124-1140.

Prasad, M.S., Charney, R.M., and García-Castro, M.I. (2019). Specification and formation of the neural crest: Perspectives on lineage segregation. Genesis (New York, N.Y. : 2000) *57*, e23276. https://doi.org/10.1002/dvg.23276.

Procacci, P., Ballabio, M., Castelnovo, L.F., Mantovani, C., and Magnaghi, V. (2012). GABA-B receptors in the PNS have a role in Schwann cells differentiation? Frontiers in Cellular Neuroscience *6*, 68. https://doi.org/10.3389/fncel.2012.00068.

Purves, D., Augustine, G.J., Fitzpatrick, D., Katz, L.C., LaMantia, A.-S., McNamara, J.O., and Williams, S.M. (2001). Neuroscience. 2nd edition (Sinauer Associates).

Puttonen, K.A., Ruponen, M., Naumenko, N., Hovatta, O.H., Tavi, P., and Koistinaho, J. (2015). Generation of Functional Neuromuscular Junctions from Human Pluripotent Stem Cell Lines. Frontiers in Cellular Neuroscience *9*. https://doi.org/10.3389/fncel.2015.00473.

Qu, Q., Li, D., Louis, K.R., Li, X., Yang, H., Sun, Q., Crandall, S.R., Tsang, S., Zhou, J., and Cox, C.L., et al. (2014). High-efficiency motor neuron differentiation from human pluripotent stem cells and the function of Islet-1. Nature Communications *5*, 3449. https://doi.org/10.1038/ncomms4449.

Raffa, P., Easler, M., and Urciuolo, A. (2022). Three-dimensional in vitro models of neuromuscular tissue. Neural Regeneration Research *17*, 759-766. https://doi.org/10.4103/1673-5374.322447.

Ragancokova, D., Jahn, K., Kotsiari, A., Schlesinger, F., Haastert, K., Stangel, M., Petri, S., and Krampfl, K. (2009). Analysis of neuroprotective effects of valproic acid on primary motor neurons in monoculture or co-cultures with astrocytes or Schwann cells. Cell Mol Neurobiol *29*, 1037-1043. https://doi.org/10.1007/s10571-009-9393-3.

Ranvier, L.A. (1878). Lecons sur l'Histologie du Systeme Nerveux, par ML Ranvier, recueillies par M (Paris: F. Savy).

Razavi, S., Ahmadi, N., Kazemi, M., Mardani, M., and Esfandiari, E. (2012). Efficient transdifferentiation of human adipose-derived stem cells into Schwann-like cells: A promise for treatment of demyelinating diseases. Advanced biomedical research *1*, 12. https://doi.org/10.4103/2277-9175.96067.

Reddy, L.V., Koirala, S., Sugiura, Y., Herrera, A.A., and Ko, C.P. (2003). Glial cells maintain synaptic structure and function and promote development of the neuromuscular junction in vivo. Neuron *40*, 563-580. https://doi.org/10.1016/s0896-6273(03)00682-2.

Reed, C.B., Feltri, M.L., and Wilson, E.R. (2021). Peripheral glia diversity. Journal of anatomy. https://doi.org/10.1111/joa.13484.

Reist, N.E., and Smith, S.J. (1992). Neurally evoked calcium transients in terminal Schwann cells at the neuromuscular junction. Proceedings of the National Academy of Sciences of the United States of America *89*, 7625-7629. https://doi.org/10.1073/pnas.89.16.7625.

Rekler, D., and Kalcheim, C. (2022). Completion of neural crest cell production and emigration is regulated by retinoic-acid-dependent inhibition of BMP signaling. eLife *11*. https://doi.org/10.7554/eLife.72723.

Remak, R. (1838). Observationes anatomicae et microscopicae de systematis nervosi structura. (Berlin).

Rider, C.C., and Mulloy, B. (2010). Bone morphogenetic protein and growth differentiation factor cytokine families and their protein antagonists. Biochemical Journal *429*, 1-12. https://doi.org/10.1042/BJ20100305.

Ridgway, E.B., and Ashley, C.C. (1967). Calcium transients in single muscle fibers. Biochemical and biophysical research communications *29*, 229-234. https://doi.org/10.1016/0006-291x(67)90592-x.

Riethmacher, D., Sonnenberg-Riethmacher, E., Brinkmann, V., Yamaai, T., Lewin, G.R., and Birchmeier, C. (1997). Severe neuropathies in mice with targeted mutations in the ErbB3 receptor. Nature *389*, 725-730. https://doi.org/10.1038/39593.

Rimington, R.P., Fleming, J.W., Capel, A.J., Wheeler, P.C., and Lewis, M.P. (2021). Bioengineered model of the human motor unit with physiologically functional neuromuscular junctions. Sci Rep *11*, 11695. https://doi.org/10.1038/s41598-021-91203-5.

Rinwa, P., Calvo-Enrique, L., Zhang, M.-D., Nyengaard, J.R., Karlsson, P., and Ernfors, P. (2021). Demise of nociceptive Schwann cells causes nerve retraction and pain hyperalgesia. Pain *162*, 1816-1827. https://doi.org/10.1097/j.pain.0000000000002169.

Robitaille, R. (1995). Purinergic receptors and their activation by endogenous purines at perisynaptic glial cells of the frog neuromuscular junction. J. Neurosci. *15*, 7121-7131. https://doi.org/10.1523/JNEUROSCI.15-11-07121.1995.

Rochon, D., Rousse, I., and Robitaille, R. (2001). Synapse–Glia Interactions at the Mammalian Neuromuscular Junction. J. Neurosci. *21*, 3819-3829. https://doi.org/10.1523/JNEUROSCI.21-11-03819.2001.

Rodrigues, A.C.Z., Messi, M.L., Wang, Z.-M., Abba, M.C., Pereyra, A., Birbrair, A., Zhang, T., O'Meara, M., Kwan, P., and Lopez, E.I.S., et al. (2018). The Sympathetic Nervous System Regulates Skeletal Muscle Motor

Innervation and Acetylcholine Receptor Stability. Acta Physiologica (Oxford, England), e13195. https://doi.org/10.1111/apha.13195.

Rodrigues, A.Z.C., Wang, Z.-M., Messi, M.L., and Delbono, O. (2019). Sympathomimetics regulate neuromuscular junction transmission through TRPV1, P/Q- and N-type Ca2+ channels. Molecular and Cellular Neurosciences *95*, 59-70. https://doi.org/10.1016/j.mcn.2019.01.007.

Rogers, R.S., and Nishimune, H. (2017). THE ROLE OF LAMININS IN THE ORGANIZATION AND FUNCTION OF NEUROMUSCULAR JUNCTIONS. Matrix biology : journal of the International Society for Matrix Biology *57-58*, 86-105. https://doi.org/10.1016/j.matbio.2016.08.008.

Rosso, G., Liashkovich, I., Young, P., Röhr, D., and Shahin, V. (2017). Schwann cells and neurite outgrowth from embryonic dorsal root ganglions are highly mechanosensitive. Nanomedicine : nanotechnology, biology, and medicine *13*, 493-501. https://doi.org/10.1016/j.nano.2016.06.011.

Roth, T.M., Ramamurthy, P., Ebisu, F., Lisak, R.P., Bealmear, B.M., and Barald, K.F. (2007). A mouse embryonic stem cell model of Schwann cell differentiation for studies of the role of neurofibromatosis type 1 in Schwann cell development and tumor formation. Glia *55*, 1123-1133. https://doi.org/10.1002/glia.20534.

Rothstein, M., Bhattacharya, D., and Simoes-Costa, M. (2018). The molecular basis of neural crest axial identity. Developmental Biology *444 Suppl 1*, S170-S180. https://doi.org/10.1016/j.ydbio.2018.07.026.

Rudolf, R., Khan, M.M., Lustrino, D., Labeit, S., Kettelhut, I.C., and Navegantes, L.C.C. (2013). Alterations of cAMP-dependent signaling in dystrophic skeletal muscle. Frontiers in physiology *4*, 290. https://doi.org/10.3389/fphys.2013.00290.

Ruegg, M.A., and Bixby, J.L. (1998). Agrin orchestrates synaptic differentiation at the vertebrate neuromuscular junction. Trends in Neurosciences *21*, 22-27. https://doi.org/10.1016/s0166-2236(97)01154-5.

Safaeinejad, Z., Kazeminasab, F., Kiani-Esfahani, A., Ghaedi, K., and Nasr-Esfahani, M.H. (2018). Multi-effects of Resveratrol on stem cell characteristics: Effective dose, time, cell culture conditions and cell type-specific responses of stem cells to Resveratrol. European Journal of Medicinal Chemistry *155*, 651-657. https://doi.org/10.1016/j.ejmech.2018.06.037.

Sakuma, K., and Yamaguchi, A. (2011). The recent understanding of the neurotrophin's role in skeletal muscle adaptation. Journal of Biomedicine and Biotechnology *2011*, 201696. https://doi.org/10.1155/2011/201696.

Sances, S., Bruijn, L.I., Chandran, S., Eggan, K., Ho, R., Klim, J.R., Livesey, M.R., Lowry, E., Macklis, J.D., and Rushton, D., et al. (2016). Modeling ALS with motor neurons derived from human induced pluripotent stem cells. Nat Neurosci *19*, 542-553. https://doi.org/10.1038/nn.4273.

Sanes, J.R., and Lichtman, J.W. (1999). Development of the vertebrate neuromuscular junction. Annual Review of Neuroscience *22*, 389-442. https://doi.org/10.1146/annurev.neuro.22.1.389.

Santhanam, N., Kumanchik, L., Guo, X., Sommerhage, F., Cai, Y., Jackson, M., Martin, C., Saad, G., McAleer, C.W., and Wang, Y., et al. (2018). Stem cell derived phenotypic human neuromuscular junction model for dose response evaluation of therapeutics. Biomaterials *166*, 64-78. https://doi.org/10.1016/j.biomaterials.2018.02.047.

Santosa, K.B., Keane, A.M., Jablonka-Shariff, A., Vannucci, B., and Snyder-Warwick, A.K. (2018). Clinical relevance of terminal Schwann cells: An overlooked component of the neuromuscular junction. Journal of neuroscience research *96*, 1125-1135. https://doi.org/10.1002/jnr.24231.

Saulite, L., Vavers, E., Zvejniece, L., Dambrova, M., and Riekstina, U. (2018). The Differentiation of Skin Mesenchymal Stem Cells Towards a Schwann Cell Phenotype: Impact of Sigma-1 Receptor Activation. Molecular neurobiology *55*, 2840-2850. https://doi.org/10.1007/s12035-017-0511-9.

Schaefers, C., Rothmiller, S., Thiermann, H., Rein, T., and Schmidt, A. (2022). The Efficiency of Direct Maturation: the Comparison of Two hiPSC Differentiation Approaches into Motor Neurons. Stem Cells International *2022*, 1320950. https://doi.org/10.1155/2022/1320950.

Scherr, T., Streule, K., Bartschat, A., Böhland, M., Stegmaier, J., Reischl, M., Orian-Rousseau, V., and Mikut, R. (2020). BeadNet: deep learning-based bead detection and counting in low-resolution microscopy images. Bioinformatics *36*, 4668-4670. https://doi.org/10.1093/bioinformatics/btaa594.

Schindelin, J., Arganda-Carreras, I., Frise, E., Kaynig, V., Longair, M., Pietzsch, T., Preibisch, S., Rueden, C., Saalfeld, S., and Schmid, B., et al. (2012). Fiji: an open-source platform for biological-image analysis. Nat Methods *9*, 676-682. https://doi.org/10.1038/nmeth.2019.

Schwann, T. (1839). Mikroskopische Untersuchungen über die Übereinstimmung in der Struktur und dem Wachsthum der Thiere und Pflanzen (Berlin: Sander, Berlin, Germany).

Seilheimer, B., Persohn, E., and Schachner, M. (1989). Antibodies to the L1 adhesion molecule inhibit Schwann cell ensheathment of neurons in vitro. J Cell Biol *109*, 3095-3103. https://doi.org/10.1083/jcb.109.6.3095.

Sela-Donenfeld, D., and Kalcheim, C. (1999). Regulation of the onset of neural crest migration by coordinated activity of BMP4 and Noggin in the dorsal neural tube. Development *126*, 4749-4762.

Shah, N.M., Marchionni, M.A., Isaacs, I., Stroobant, P., and Anderson, P.J. (1994). Glial growth factor restricts mammalian neural crest stem cells to a glial fate. Cell *77*, 349-360. https://doi.org/10.1016/0092-8674(94)90150-3.

Shea, G.K.H., Tsui, A.Y.P., Chan, Y.S., and Shum, D.K.Y. (2010). Bone marrow-derived Schwann cells achieve fate commitment—a prerequisite for remyelination therapy. Experimental Neurology *224*, 448-458. https://doi.org/10.1016/j.expneurol.2010.05.005.

Shen, C., Cheng, W., Yu, P., Wang, L., Zhou, L., Zeng, L., and Yang, Q. (2016). Resveratrol pretreatment attenuates injury and promotes proliferation of neural stem cells following oxygen-glucose deprivation/reoxygenation by upregulating the expression of Nrf2, HO-1 and NQO1 in vitro. Molecular medicine reports *14*, 3646-3654. https://doi.org/10.3892/mmr.2016.5670.

Shi, L., Huang, L., He, R., Huang, W., Wang, H., Lai, X., Zou, Z., Sun, J., Ke, Q., and Zheng, M., et al. (2018). Modeling the Pathogenesis of Charcot-Marie-Tooth Disease Type 1A Using Patient-Specific iPSCs. Stem Cell Reports *10*, 120-133. https://doi.org/10.1016/j.stemcr.2017.11.013.

Shimada, Y., Fischman, D.A., and Moscona, A.A. (1969). Formation of neuromuscular junctions in embryonic cell cultures. Proceedings of the National Academy of Sciences of the United States of America *62*, 715-721. https://doi.org/10.1073/pnas.62.3.715.

Shimizu, K., Kassai, H., Kamei, Y., Yamamoto, K., Nagashima, T., Maekawa, T., Akiyama, H., and Honda, H. (2022). Alignment of Skeletal Muscle Cells Facilitates Acetylcholine Receptor Clustering and Neuromuscular Junction Formation with Co-Cultured Human iPSC-Derived Motor Neurons. Cells *11*. https://doi.org/10.3390/cells11233760.

Shimizu, S., Kitada, M., Ishikawa, H., Itokazu, Y., Wakao, S., and Dezawa, M. (2007). Peripheral nerve regeneration by the in vitro differentiated-human bone marrow stromal cells with Schwann cell property. Biochemical and biophysical research communications *359*, 915-920. https://doi.org/10.1016/j.bbrc.2007.05.212.

Simões-Costa, M., and Bronner, M.E. (2015). Establishing neural crest identity: a gene regulatory recipe. Development *142*, 242-257. https://doi.org/10.1242/dev.105445.

Singh, T., and Vazquez, M. (2019). Time-Dependent Addition of Neuronal and Schwann Cells Increase Myotube Viability and Length in an In Vitro Tri-culture Model of the Neuromuscular Junction. Regen. Eng. Transl. Med. *22*, 389. https://doi.org/10.1007/s40883-019-00095-5.

Singh Roy, N., Nakano, T., Xuing, L., Kang, J., Nedergaard, M., and Goldman, S.A. (2005). Enhancer-specified GFP-based FACS purification of human spinal motor neurons from embryonic stem cells. Experimental Neurology *196*, 224-234. https://doi.org/10.1016/j.expneurol.2005.06.021.

Smith, A., Long, C.J., Pirozzi, K., and Hickman, J.J. (2013a). A functional system for high-content screening of neuromuscular junctions in vitro. Technology *1*, 37-48. https://doi.org/10.1142/S2339547813500015.

Smith, A.S.T., Passey, S.L., Martin, N.R.W., Player, D.J., Mudera, V., Greensmith, L., and Lewis, M.P. (2016). Creating Interactions between Tissue-Engineered Skeletal Muscle and the Peripheral Nervous System. Cells, Tissues, Organs *202*, 143-158. https://doi.org/10.1159/000443634.

Smith, D.O. (1991). Sources of adenosine released during neuromuscular transmission in the rat. The Journal of Physiology *432*, 343-354. https://doi.org/10.1113/jphysiol.1991.sp018388.

Smith, I.W., Mikesh, M., Lee, Y.I., and Thompson, W.J. (2013b). Terminal Schwann cells participate in the competition underlying neuromuscular synapse elimination. J. Neurosci. *33*, 17724-17736. https://doi.org/10.1523/JNEUROSCI.3339-13.2013.

Smith, S.J., Wilson, M., Ward, J.H., Rahman, C.V., Peet, A.C., Macarthur, D.C., Rose, F.R.A.J., Grundy, R.G., and Rahman, R. (2012). Recapitulation of tumor heterogeneity and molecular signatures in a 3D brain cancer model with decreased sensitivity to histone deacetylase inhibition. PLoS ONE *7*, e52335. https://doi.org/10.1371/journal.pone.0052335.

Snyder-Warwick, A.K., Satoh, A., Santosa, K.B., Imai, S., and Jablonka-Shariff, A. (2018). Hypothalamic Sirt1 protects terminal Schwann cells and neuromuscular junctions from age-related morphological changes. Aging Cell *17*. https://doi.org/10.1111/acel.12776.

Soliman, E., Bianchi, F., Sleigh, J.N., George, J.H., Cader, M.Z., Cui, Z., and Ye, H. (2018). Engineered method for directional growth of muscle sheets on electrospun fibers. Journal of Biomedical Materials Research Part A *106*, 1165-1176. https://doi.org/10.1002/jbm.a.36312.

Solovieva, T., and Bronner, M. (2021). Schwann cell precursors: Where they come from and where they go. Cells & development *166*, 203686. https://doi.org/10.1016/j.cdev.2021.203686.

Southam, K.A., King, A.E., Blizzard, C.A., McCormack, G.H., and Dickson, T.C. (2013). Microfluidic primary culture model of the lower motor neuron-neuromuscular junction circuit. Journal of Neuroscience Methods *218*, 164-169. https://doi.org/10.1016/j.jneumeth.2013.06.002.

Stegmaier, J., Otte, J.C., Kobitski, A., Bartschat, A., Garcia, A., Nienhaus, G.U., Strähle, U., and Mikut, R. (2014). Fast segmentation of stained nuclei in terabyte-scale, time resolved 3D microscopy image stacks. PLoS ONE *9*, e90036. https://doi.org/10.1371/journal.pone.0090036.

Steinbeck, J.A., Jaiswal, M.K., Calder, E.L., Kishinevsky, S., Weishaupt, A., Toyka, K.V., Goldstein, P.A., and Studer, L. (2016). Functional Connectivity under Optogenetic Control Allows Modeling of Human Neuromuscular Disease. Cell Stem Cell *18*, 134-143. https://doi.org/10.1016/j.stem.2015.10.002.

Stemple, D.L., and Anderson, D.J. (1992). Isolation of a stem cell for neurons and glia from the mammalian neural crest. Cell *71*, 973-985. https://doi.org/10.1016/0092-8674(92)90393-Q.

Steventon, B., Araya, C., Linker, C., Kuriyama, S., and Mayor, R. (2009). Differential requirements of BMP and Wnt signalling during gastrulation and neurulation define two steps in neural crest induction. Development *136*, 771-779. https://doi.org/10.1242/dev.029017.

Stewart, H.J., Morgan, L., Jessen, K.R., and Mirsky, R. (1993). Changes in DNA synthesis rate in the Schwann cell lineage in vivo are correlated with the precursor—Schwann cell transition and myelination. The European journal of neuroscience *5*, 1136-1144. https://doi.org/10.1111/j.1460-9568.1993.tb00968.x.

Stierli, S., Napoli, I., White, I.J., Cattin, A.-L., Monteza Cabrejos, A., Garcia Calavia, N., Malong, L., Ribeiro, S., Nihouarn, J., and Williams, R., et al. (2018). The regulation of the homeostasis and regeneration of peripheral nerve is distinct from the CNS and independent of a stem cell population. Development (Cambridge, England) *145*. https://doi.org/10.1242/dev.170316.

Straka, T., Vita, V., Prokshi, K., Hörner, S.J., Khan, M.M., Pirazzini, M., Williams, M.P.I., Hafner, M., Zaglia, T., and Rudolf, R. (2018). Postnatal Development and Distribution of Sympathetic Innervation in Mouse Skeletal Muscle. International Journal of Molecular Sciences *19*. https://doi.org/10.3390/ijms19071935.

Strickland, J.B., Davis-Anderson, K., Micheva-Viteva, S., Twary, S., Iyer, R., Harris, J.F., and Solomon, E.A. (2022). Optimization of Application-Driven Development of In Vitro Neuromuscular Junction Models. Tissue engineering. Part B, Reviews. https://doi.org/10.1089/ten.TEB.2021.0204.

Suazo, I., Vega, J.A., García-Mesa, Y., García-Piqueras, J., García-Suárez, O., and Cobo, T. (2022). The Lamellar Cells of Vertebrate Meissner and Pacinian Corpuscles: Development, Characterization, and Functions. Frontiers in Neuroscience *16*, 790130. https://doi.org/10.3389/fnins.2022.790130.

Sugiura, Y., and Lin, W. (2011). Neuron-glia interactions: the roles of Schwann cells in neuromuscular synapse formation and function. Bioscience reports *31*, 295-302. https://doi.org/10.1042/BSR20100107.

Syroid, D.E., Maycox, P.R., Burrola, P.G., Liu, N., Wen, D., Lee, K.F., Lemke, G., and Kilpatrick, T.J. (1996). Cell death in the Schwann cell lineage and its regulation by neuregulin. Proceedings of the National Academy of Sciences of the United States of America *93*, 9229-9234. https://doi.org/10.1073/pnas.93.17.9229.

Takahashi, K., Tanabe, K., Ohnuki, M., Narita, M., Ichisaka, T., Tomoda, K., and Yamanaka, S. (2007). Induction of pluripotent stem cells from adult human fibroblasts by defined factors. Cell *131*, 861-872. https://doi.org/10.1016/j.cell.2007.11.019.

Takahashi, K., and Yamanaka, S. (2006). Induction of pluripotent stem cells from mouse embryonic and adult fibroblast cultures by defined factors. Cell *126*, 663-676. https://doi.org/10.1016/j.cell.2006.07.024.

Tanabe, Y., William, C., and Jessell, T.M. (1998). Specification of motor neuron identity by the MNR2 homeodomain protein. Cell *95*, 67-80. https://doi.org/10.1016/s0092-8674(00)81783-3.

Tang, Y., Liu, L., Li, J., Yu, L., Severino, F.P.U., Wang, L., Shi, J., Tu, X., Torre, V., and Chen, Y. (2016). Effective motor neuron differentiation of hiPSCs on a patch made of crosslinked monolayer gelatin nanofibers. J. Mater. Chem. B *4*, 3305-3312. https://doi.org/10.1039/C6TB00351F.

Tasdemir-Yilmaz, O.E., Druckenbrod, N.R., Olukoya, O.O., Dong, W., Yung, A.R., Bastille, I., Pazyra-Murphy, M.F., Sitko, A.A., Hale, E.B., and Vigneau, S., et al. (2021). Diversity of developing peripheral glia revealed by single-cell RNA sequencing. Developmental cell *56*, 2516-2535.e8. https://doi.org/10.1016/j.devcel.2021.08.005.

Taveggia, C., Zanazzi, G., Petrylak, A., Yano, H., Rosenbluth, J., Einheber, S., Xu, X., Esper, R.M., Loeb, J.A., and Shrager, P., et al. (2005). Neuregulin-1 type III determines the ensheathment fate of axons. Neuron *47*, 681-694. https://doi.org/10.1016/j.neuron.2005.08.017.

Tchieu, J., Zimmer, B., Fattahi, F., Amin, S., Zeltner, N., Chen, S., and Studer, L. (2017). A Modular Platform for Differentiation of Human PSCs into All Major Ectodermal Lineages. Cell Stem Cell *21*, 399-410.e7. https://doi.org/10.1016/j.stem.2017.08.015.

Thoma, E.C., Merkl, C., Heckel, T., Haab, R., Knoflach, F., Nowaczyk, C., Flint, N., Jagasia, R., Jensen Zoffmann, S., and Truong, H.H., et al. (2014). Chemical conversion of human fibroblasts into functional Schwann cells. Stem Cell Reports *3*, 539-547. https://doi.org/10.1016/j.stemcr.2014.07.014.

Thompson, D.M., and Buettner, H.M. (2006). Neurite Outgrowth is Directed by Schwann Cell Alignment in the Absence of Other Guidance Cues. Ann Biomed Eng *34*, 669-676. https://doi.org/10.1007/s10439-005-9053-9.

Thomson, S.R., Wishart, T.M., Patani, R., Chandran, S., and Gillingwater, T.H. (2012). Using induced pluripotent stem cells (iPSC) to model human neuromuscular connectivity: promise or reality? Journal of anatomy *220*, 122-130. https://doi.org/10.1111/j.1469-7580.2011.01459.x.

Tiegs, O. (1953). Innervation of voluntary muscle. Physiological reviews *33*, 90-144. https://doi.org/10.1152/physrev.1953.33.1.90.

Tintignac, L.A., Brenner, H.-R., and Rüegg, M.A. (2015). Mechanisms Regulating Neuromuscular Junction Development and Function and Causes of Muscle Wasting. Physiological reviews *95*, 809-852. https://doi.org/10.1152/physrev.00033.2014.

Todd, K.J., Auld, D.S., and Robitaille, R. (2007). Neurotrophins modulate neuron-glia interactions at a vertebrate synapse. The European journal of neuroscience *25*, 1287-1296. https://doi.org/10.1111/j.1460-9568.2007.05385.x.

Todd, K.J., Darabid, H., and Robitaille, R. (2010). Perisynaptic glia discriminate patterns of motor nerve activity and influence plasticity at the neuromuscular junction. The Journal of neuroscience : the official journal of the Society for Neuroscience *30*, 11870-11882. https://doi.org/10.1523/JNEUROSCI.3165-10.2010.

Tomita, K., Madura, T., Sakai, Y., Yano, K., Terenghi, G., and Hosokawa, K. (2013). Glial differentiation of human adipose-derived stem cells: implications for cell-based transplantation therapy. Neuroscience *236*, 55-65. https://doi.org/10.1016/j.neuroscience.2012.12.066.

Tribulo, C., Aybar, M.J., Nguyen, V.H., Mullins, M.C., and Mayor, R. (2003). Regulation of Msx genes by a Bmp gradient is essential for neural crest specification. Development *130*, 6441-6452. https://doi.org/10.1242/dev.00878.

Turing, A.M. (1952). The chemical basis of morphogenesis. Phil. Trans. R. Soc. Lond. B *237*, 37-72. https://doi.org/10.1098/rstb.1952.0012.

Uesaka, T., Nagashimada, M., and Enomoto, H. (2015). Neuronal Differentiation in Schwann Cell Lineage Underlies Postnatal Neurogenesis in the Enteric Nervous System. J. Neurosci. *35*, 9879-9888. https://doi.org/10.1523/JNEUROSCI.1239-15.2015.

Uesaka, T., Okamoto, M., Nagashimada, M., Tsuda, Y., Kihara, M., Kiyonari, H., and Enomoto, H. (2021). Enhanced enteric neurogenesis by Schwann cell precursors in mouse models of Hirschsprung disease. Glia *69*, 2575-2590. https://doi.org/10.1002/glia.24059.

Ullian, E.M., Harris, B.T., Wu, A., Chan, J.R., and Barres, B.A. (2004). Schwann cells and astrocytes induce synapse formation by spinal motor neurons in culture. Molecular and Cellular Neurosciences *25*, 241-251. https://doi.org/10.1016/j.mcn.2003.10.011.

Umbach, J.A., Adams, K.L., Gundersen, C.B., and Novitch, B.G. (2012). Functional neuromuscular junctions formed by embryonic stem cell-derived motor neurons. PLoS ONE *7*, e36049. https://doi.org/10.1371/journal.pone.0036049.

Undamatla, J., and Szaro, B.G. (2001). Differential expression and localization of neuronal intermediate filament proteins within newly developing neurites in dissociated cultures of Xenopus laevis embryonic spinal cord. Cell motility and the cytoskeleton *49*, 16-32. https://doi.org/10.1002/cm.1017.

Urciuolo, A., Serena, E., Ghua, R., Zatti, S., Giomo, M., Mattei, N., Vetralla, M., Selmin, G., Luni, C., and Vitulo, N., et al. (2020). Engineering a 3D in vitro model of human skeletal muscle at the single fiber scale. PLoS ONE *15*, e0232081. https://doi.org/10.1371/journal.pone.0232081.

Uzel, S.G.M., Platt, R.J., Subramanian, V., Pearl, T.M., Rowlands, C.J., Chan, V., Boyer, L.A., So, P.T.C., and Kamm, R.D. (2016). Microfluidic device for the formation of optically excitable, three-dimensional, compartmentalized motor units. Science Advances *2*. https://doi.org/10.1126/sciadv.1501429.

van der Wal, E., Herrero-Hernandez, P., Wan, R., Broeders, M., in ’t Groen, Stijn L.M., van Gestel, T.J., van IJcken, W.F., Cheung, T.H., van der Ploeg, Ans T., and Schaaf, G.J., et al. (2018). Large-Scale Expansion of Human iPSC-Derived Skeletal Muscle Cells for Disease Modeling and Cell-Based Therapeutic Strategies. Stem Cell Reports *10*, 1975-1990. https://doi.org/10.1016/j.stemcr.2018.04.002.

VanSaun, M., Herrera, A.A., and Werle, M.J. (2003). Structural alterations at the neuromuscular junctions of matrix metalloproteinase 3 null mutant mice. Journal of Neurocytology *32*, 1129-1142. https://doi.org/10.1023/B:NEUR.0000021907.68461.9c.

VanSaun, M., Humburg, B.C., Arnett, M.G., Pence, M., and Werle, M.J. (2007). Activation of Matrix Metalloproteinase-3 is altered at the frog neuromuscular junction following changes in synaptic activity. Developmental neurobiology *67*, 1488-1497. https://doi.org/10.1002/dneu.20523.

VanSaun, M., and Werle, M.J. (2000). Matrix metalloproteinase-3 removes agrin from synaptic basal lamina. Journal of neurobiology *43*, 140-149.

Varga, I., and Mravec, B. (2015). Chapter 8 - Nerve Fiber Types. In Nerves and Nerve Injuries, R.S. Tubbs, E. Rizk, M.M. Shoja, M. Loukas, N. Barbaro and R.J. Spinner, eds. (San Diego: Academic Press [Imprint]; Elsevier Science & Technology Books), pp. 107–113.

Véga, C., Martiel, J.-L., Drouhault, D., Burckhart, M.-F., and Coles, J.A. (2003). Uptake of locally applied deoxyglucose, glucose and lactate by axons and Schwann cells of rat vagus nerve. The Journal of Physiology *546*, 551-564. https://doi.org/10.1113/jphysiol.2002.029751.

Velasquez, J.T., St John, J.A., Nazareth, L., and Ekberg, J.A.K. (2018). Schwann cell lamellipodia regulate cell-cell interactions and phagocytosis. Molecular and Cellular Neurosciences *88*, 189-200. https://doi.org/10.1016/j.mcn.2018.01.001.

Verma, S., Khurana, S., Vats, A., Sahu, B., Ganguly, N.K., Chakraborti, P., Gourie-Devi, M., and Taneja, V. (2022). Neuromuscular Junction Dysfunction in Amyotrophic Lateral Sclerosis. Mol Neurobiol *59*, 1502-1527. https://doi.org/10.1007/s12035-021-02658-6.

Vernardis, S.I., Terzoudis, K., Panoskaltsis, N., and Mantalaris, A. (2017). Human embryonic and induced pluripotent stem cells maintain phenotype but alter their metabolism after exposure to ROCK inhibitor. Scientific Reports *7*, 42138. https://doi.org/10.1038/srep42138.

Vila, O.F., Chavez, M., Ma, S.P., Yeager, K., Zholudeva, L.V., Colón-Mercado, J.M., Qu, Y., Nash, T.R., Lai, C., and Feliciano, C.M., et al. (2021). Bioengineered optogenetic model of human neuromuscular junction. Biomaterials *276*, 121033. https://doi.org/10.1016/j.biomaterials.2021.121033.

Vila, O.F., Qu, Y., and Vunjak-Novakovic, G. (2020). In vitro models of neuromuscular junctions and their potential for novel drug discovery and development. Expert opinion on drug discovery *15*, 307-317. https://doi.org/10.1080/17460441.2020.1700225.

Vila, O.F., Uzel, S.G.M., Ma, S.P., Williams, D., Pak, J., Kamm, R.D., and Vunjak-Novakovic, G. (2019). Quantification of human neuromuscular function through optogenetics. Theranostics *9*, 1232-1246. https://doi.org/10.7150/thno.25735.

Villanueva, S., Glavic, A., Ruiz, P., and Mayor, R. (2002). Posteriorization by FGF, Wnt, and retinoic acid is required for neural crest induction. Developmental Biology *241*, 289-301. https://doi.org/10.1006/dbio.2001.0485.

Vilmont, V., Cadot, B., Ouanounou, G., and Gomes, E.R. (2016). A system for studying mechanisms of neuromuscular junction development and maintenance. Development (Cambridge, England) *143*, 2464-2477. https://doi.org/10.1242/dev.130278.

Virchow, R. (1858). Die Cellularpathologie in ihrer Begründung auf physiologische und pathologische Gewebelehre (Berlin: Hirschwald).

Wakao, S., Hayashi, T., Kitada, M., Kohama, M., Matsue, D., Teramoto, N., Ose, T., Itokazu, Y., Koshino, K., and Watabe, H., et al. (2010). Long-term observation of auto-cell transplantation in non-human primate reveals safety and efficiency of bone marrow stromal cell-derived Schwann cells in peripheral nerve regeneration. Experimental Neurology *223*, 537-547. https://doi.org/10.1016/j.expneurol.2010.01.022.

Wakao, S., Matsuse, D., and Dezawa, M. (2014). Mesenchymal stem cells as a source of Schwann cells: their anticipated use in peripheral nerve regeneration. Cells, Tissues, Organs *200*, 31-41. https://doi.org/10.1159/000368188.

Walker, A., Su, H., Conti, M.A., Harb, N., Adelstein, R.S., and Sato, N. (2010). Non-muscle myosin II regulates survival threshold of pluripotent stem cells. Nature Communications *1*, 71. https://doi.org/10.1038/ncomms1074.

Walsh, M.K., and Lichtman, J.W. (2003). In vivo time-lapse imaging of synaptic takeover associated with naturally occurring synapse elimination. Neuron *37*, 67-73. https://doi.org/10.1016/s0896-6273(02)01142-x.

Wang, P.-Y., Thissen, H., and Tsai, W.-B. (2012a). The roles of RGD and grooved topography in the adhesion, morphology, and differentiation of C2C12 skeletal myoblasts. Biotechnology and bioengineering *109*, 2104-2115. https://doi.org/10.1002/bit.24452.

Wang, Y., Teng, H.-L., and Huang, Z. (2012b). Intrinsic migratory properties of cultured Schwann cells based on single-cell migration assay. PLOS ONE *7*, e51824. https://doi.org/10.1371/journal.pone.0051824.

Wang, Y., Wei, T., Wang, Q., Zhang, C., Li, K., and Deng, J. (2022). Resveratrol's neural protective effects for the injured embryoid body and cerebral organoid. BMC Pharmacol Toxicol *23*, 47. https://doi.org/10.1186/s40360-022-00593-3.

Wanner, I.B., Guerra, N.K., Mahoney, J., Kumar, A., Wood, P.M., Mirsky, R., and Jessen, K.R. (2006). Role of N-cadherin in Schwann cell precursors of growing nerves. Glia *54*, 439-459. https://doi.org/10.1002/glia.20390.

Wanner, I.B., and Wood, P.M. (2002). N-Cadherin Mediates Axon-Aligned Process Growth and Cell–Cell Interaction in Rat Schwann Cells. The Journal of Neuroscience: The Official Journal of the Society for Neuroscience *22*, 4066-4079. https://doi.org/10.1523/JNEUROSCI.22-10-04066.2002.

Watanabe, K., Ueno, M., Kamiya, D., Nishiyama, A., Matsumura, M., Wataya, T., Takahashi, J.B., Nishikawa, S., Nishikawa, S., and Muguruma, K., et al. (2007). A ROCK inhibitor permits survival of dissociated human embryonic stem cells. Nature Biotechnology *25*, 681-686. https://doi.org/10.1038/nbt1310.

Weis, J., Fine, S.M., David, C., Savarirayan, S., and Sanes, J.R. (1991). Integration site-dependent expression of a transgene reveals specialized features of cells associated with neuromuscular junctions. The Journal of Cell Biology *113*, 1385-1397. https://doi.org/10.1083/jcb.113.6.1385.

Weiss, T., Taschner-Mandl, S., Bileck, A., Slany, A., Kromp, F., Rifatbegovic, F., Frech, C., Windhager, R., Kitzinger, H., and Tzou, C.-H., et al. (2016). Proteomics and transcriptomics of peripheral nerve tissue and cells unravel new aspects of the human Schwann cell repair phenotype. Glia 64, 2133-2153. https://doi.org/10.1002/glia.23045.

Wichterle, H., Lieberam, I., Porter, J.A., and Jessell, T.M. (2002). Directed differentiation of embryonic stem cells into motor neurons. Cell *110*, 385-397. https://doi.org/10.1016/S0092-8674(02)00835-8.

Wiszniak, S., and Schwarz, Q. (2019). Notch signalling defines dorsal root ganglia neuroglial fate choice during early neural crest cell migration. BMC Neuroscience *20*, 21. https://doi.org/10.1186/s12868-019-0501-0.

Woldeyesus, M.T., Britsch, S., Riethmacher, D., Xu, L., Sonnenberg-Riethmacher, E., Abou-Rebyeh, F., Harvey, R., Caroni, P., and Birchmeier, C. (1999). Peripheral nervous system defects in erbB2 mutants following genetic rescue of heart development. Genes & Development *13*, 2538-2548. https://doi.org/10.1101/gad.13.19.2538.

Wolpowitz, D., Mason, T.B., Dietrich, P., Mendelsohn, M., Talmage, D.A., and Role, L.W. (2000). Cysteine-rich domain isoforms of the neuregulin-1 gene are required for maintenance of peripheral synapses. Neuron *25*, 79-91. https://doi.org/10.1016/s0896-6273(00)80873-9.

Wood, S.J., and Slater, C.R. (2001). Safety factor at the neuromuscular junction. Progress in neurobiology *64*, 393-429. https://doi.org/10.1016/s0301-0082(00)00055-1.

Woodhoo, A., Alonso, M.B.D., Droggiti, A., Turmaine, M., D'Antonio, M., Parkinson, D.B., Wilton, D.K., Al-Shawi, R., Simons, P., and Shen, J., et al. (2009). Notch controls embryonic Schwann cell differentiation, postnatal myelination and adult plasticity. Nat Neurosci *12*, 839-847. https://doi.org/10.1038/nn.2323.

Wrana, J.L. (2000). Regulation of Smad activity. Cell *100*, 189-192. https://doi.org/10.1016/s0092-8674(00)81556-1.

Wu, H., Xiong, W.C., and Mei, L. (2010). To build a synapse: signaling pathways in neuromuscular junction assembly. Development (Cambridge, England) *137*, 1017-1033. https://doi.org/10.1242/dev.038711.

Xie, M., Kamenev, D., Kaucka, M., Kastriti, M.E., Zhou, B., Artemov, A.V., Storer, M., Fried, K., Adameyko, I., and Dyachuk, V., et al. (2019). Schwann cell precursors contribute to skeletal formation during embryonic development in mice and zebrafish. PNAS *116*, 15068-15073. https://doi.org/10.1073/pnas.1900038116.

Xie, S., Lu, F., Han, J., Tao, K., Wang, H., Simental, A., Hu, D., and Yang, H. (2017). Efficient generation of functional Schwann cells from adipose-derived stem cells in defined conditions. Cell cycle (Georgetown, Tex.) *16*, 841-851. https://doi.org/10.1080/15384101.2017.1304328.

Xing, G., Xiong, W.-C., and Mei, L. (2020). Rapsyn as a signaling and scaffolding molecule in neuromuscular junction formation and maintenance. Neuroscience Letters *731*, 135013. https://doi.org/10.1016/j.neulet.2020.135013.

Xu, Y., Liu, Z., Liu, L., Zhao, C., Xiong, F., Zhou, C., Li, Y., Shan, Y., Peng, F., and Zhang, C. (2008). Neurospheres from rat adipose-derived stem cells could be induced into functional Schwann cell-like cells in vitro. BMC Neuroscience *9*, 21. https://doi.org/10.1186/1471-2202-9-21.

Yaffe, D., and Saxel, O. (1977). Serial passaging and differentiation of myogenic cells isolated from dystrophic mouse muscle. Nature *270*, 725-727. https://doi.org/10.1038/270725a0.

Yamamoto, K., Yamaoka, N., Imaizumi, Y., Nagashima, T., Furutani, T., Ito, T., Okada, Y., Honda, H., and Shimizu, K. (2021). Development of a human neuromuscular tissue-on-a-chip model on a 24-well-plate-format compartmentalized microfluidic device. Lab Chip *21*, 1897-1907. https://doi.org/10.1039/D1LC00048A.

Yang, J.-F., Cao, G., Koirala, S., Reddy, L.V., and Ko, C.-P. (2001). Schwann Cells Express Active Agrin and Enhance Aggregation of Acetylcholine Receptors on Muscle Fibers. The Journal of Neuroscience: The Official Journal of the Society for Neuroscience *21*, 9572-9584. https://doi.org/10.1523/JNEUROSCI.21-24-09572.2001.

Yi, H., Xie, B., Liu, B., Wang, X., Xu, L., Liu, J., Li, M., Zhong, X., and Peng, F. (2018). Derivation and Identification of Motor Neurons from Human Urine-Derived Induced Pluripotent Stem Cells. Stem Cells International *2018*, 3628578. https://doi.org/10.1155/2018/3628578.

Yim, A.K.Y., Wang, P.L., Bermingham, J.R., Hackett, A., Strickland, A., Miller, T.M., Ly, C., Mitra, R.D., and Milbrandt, J. (2022). Disentangling glial diversity in peripheral nerves at single-nuclei resolution. Nat Neurosci *25*, 238-251. https://doi.org/10.1038/s41593-021-01005-1.

Yoshida, M., Kitaoka, S., Egawa, N., Yamane, M., Ikeda, R., Tsukita, K., Amano, N., Watanabe, A., Morimoto, M., and Takahashi, J., et al. (2015). Modeling the Early Phenotype at the Neuromuscular Junction of Spinal Muscular Atrophy Using Patient-Derived iPSCs. Stem Cell Reports *4*, 561-568. https://doi.org/10.1016/j.stemcr.2015.02.010.

Yoshioka, K., Ito, A., Kawabe, Y., and Kamihira, M. (2020). Novel neuromuscular junction model in 2D and 3D myotubes co-cultured with induced pluripotent stem cell-derived motor neurons. Journal of bioscience and bioengineering *129*, 486-493. https://doi.org/10.1016/j.jbiosc.2019.10.004.

Young, P., Nie, J., Wang, X., McGlade, C.J., Rich, M.M., and Feng, G. (2005). LNX1 is a perisynaptic Schwann cell specific E3 ubiquitin ligase that interacts with ErbB2. Molecular and Cellular Neurosciences *30*, 238-248. https://doi.org/10.1016/j.mcn.2005.07.015.

Zelada, D., Bermedo-García, F., Collao, N., and Henríquez, J.P. (2021). Motor function recovery: deciphering a regenerative niche at the neuromuscular synapse. Biological reviews of the Cambridge Philosophical Society *96*, 752-766. https://doi.org/10.1111/brv.12675.

Zhang, B., Luo, S., Wang, Q., Suzuki, T., Xiong, W.C., and Mei, L. (2008). LRP4 serves as a coreceptor of agrin. Neuron *60*, 285-297. https://doi.org/10.1016/j.neuron.2008.10.006.

Zhang, D., Pekkanen-Mattila, M., Shahsavani, M., Falk, A., Teixeira, A.I., and Herland, A. (2014a). A 3D Alzheimer's disease culture model and the induction of P21-activated kinase mediated sensing in iPSC derived neurons. Biomaterials *35*, 1420-1428. https://doi.org/10.1016/j.biomaterials.2013.11.028.

Zhang, H.-T., Cheng, H.-Y., Zhang, L., Fan, J., Chen, Y.-Z., Jiang, X.-D., and Xu, R.-X. (2009). Umbilical cord blood cell-derived neurospheres differentiate into Schwann-like cells. Neuroreport *20*, 354-359. https://doi.org/10.1097/WNR.0b013e328323d74c.

Zhang, J., Chen, J., Xu, C., Yang, J., Guo, Q., Hu, Q., and Jiang, H. (2014b). Resveratrol inhibits phenotypic switching of neointimal vascular smooth muscle cells after balloon injury through blockade of Notch pathway. Journal of cardiovascular pharmacology *63*, 233-239. https://doi.org/10.1097/FJC.0000000000000040.

Zhang, S., Botchway, B.O.A., Zhang, Y., and Liu, X. (2019). Resveratrol can inhibit Notch signaling pathway to improve spinal cord injury. Annals of anatomy = Anatomischer Anzeiger : official organ of the Anatomische Gesellschaft *223*, 100-107. https://doi.org/10.1016/j.aanat.2019.01.015.

Zhao, X., Le, T.P., Erhardt, S., Findley, T.O., and Wang, J. (2021). Hippo-Yap Pathway Orchestrates Neural Crest Ontogenesis. Frontiers in cell and developmental biology *9*. https://doi.org/10.3389/fcell.2021.706623.

Ziegler, L., Grigoryan, S., Yang, I.H., Thakor, N.V., and Goldstein, R.S. (2011). Efficient generation of schwann cells from human embryonic stem cell-derived neurospheres. Stem cell reviews and reports *7*, 394-403. https://doi.org/10.1007/s12015-010-9198-2.

6 APPENDIX

6.1 Publications

Parts of the work contained in this thesis have been published in a peer-reviewed, indexed scientific journal:

Hörner, S.J., Couturier, N., Bruch, R., Koch, P., Hafner, M., and Rudolf, R. (2021). hiPSC-Derived Schwann Cells Influence Myogenic Differentiation in Neuromuscular Cocultures. Cells 10. https://doi.org/10.3390/cells10123292.

Hörner, S.J., Couturier, N., Gueiber, D.C., Hafner, M., and Rudolf, R. (2022). Development and In Vitro Differentiation of Schwann Cells. Cells 11. https://doi.org/10.3390/cells11233753.

6.2 Statement on contributions, copyright and self-plagiarism

I, Sarah Hörner, hereby confirm that this thesis and the data presented therein is the result of my own independent work. Contributions by other persons have been clearly indicated and are listed in summary in the following Table. No other sources than those indicated have been used. All Figures were created by myself. Some of those have been based on Figures previously published in the articles listed above, this is indicated and referenced accordingly in the respective Figure legends, and the original Figures were also created by myself.

Table 12: Contributions from other persons

Contributor	Section	Contribution
Bruch, Roman	2.4	Establishment of analysis workflows and partly analyzed data for the quantifications of marker protein expression and cell elongation using the Bead-Net software and TWANG algorithm as described in sections 2.4.1 and 2.4.2.
	3.1.5	Data shown in Table 9, Table 10, and Figure 3-17 was produced jointly with the methods described above
Couturier, Nathalie	2.1.9	Preparation of C2C12 cells for bioinks, preparation and culture of C2C12 spheroids
	3.2	Preparation of C2C12 myoblast culture for one of three experiments described in Section 3.2.2, data shown in Figure 3-26B was produced jointly (cell culture and immunostaining)

Grob, Madleine (supervised Master thesis)	2.1.8	Design and execution of test experiments with magnets to immobilize Scaffolene strips
	3.2.2	Preparation of C2C12 myoblast culture for one of three experiments described
Gueiber, Daniele (supervised Bachelor thesis and student assistant)	2.1.9	Generation of stl files and g-codes for 3D-printing, generation of schematic pictures of CAD designs shown in Figure 2-5, operation of bioprinters, preparation of prints not including cells
	3.2.3	Preparation of prints not including cells, generation of CAD files, generation of CAD model images shown in Figure 3-25C and Figure 3-26A+C